Paulo A. Gameiro

ON THE REPROGRAMMING OF THE KREBS CYCLE IN HYPOXIC AND *VHL*-DEFICIENT CANCER CELLS

Supervisors:
Professor Gregory Stephanopoulos
Professor Rui de Carvalho

Doctoral thesis in Biochemistry, specialty Bioenergetics, supervised by Professor Gregory Stephanopoulos and by Professor Rui de Carvalho, and submitted to Department of Life Sciences, Faculty of Sciences and Technology of University of Coimbra.

September, 2013

Memorandum: This doctoral thesis was equally supervised by Professor Othon Iliopoulos, at Massachusetts General Hospital (MGH), Cancer Center, in Boston. University of Coimbra does not acknowledge three PhD supervisors.

Memorando: Esta tese doutoral foi igualmente orientada pelo Professor Othon Iliopoulos, no Massachusetts General Hospital (MGH), Cancer Center, em Boston. A Universidade de Coimbra não reconhece três orientadores de doutoramento.

FCTUC FACULDADE DE CIÊNCIAS E TECNOLOGIA UNIVERSIDADE DE COIMBRA

Massachusetts Institute of Technology

MASSACHUSETTS GENERAL HOSPITAL
CANCER CENTER

This page was intentionally left blank

The scientific studies presented in this doctoral thesis are the result of a collaboration between Massachusetts Institute of Technology (MIT), Department of Chemical Engineering, under the supervision of Professor Gregory Stephanopoulos, and Massachusetts General Hospital (MGH), Cancer Center, under the supervision of Professor Othon Iliopoulos. The financial support was provided by National Institutes of Health (NIH) grant R01 DK075850 (in the Stephanopoulos Lab), by NIGH grant R01 CA122591, the MGH Proton Beam Federal Share Project, and an Astra-Zeneca Award (in the Iliopoulos Lab). At the Center for Neuroscience and Cell Biology (CNC), University of Coimbra, Professor Rui de Carvalho supervised the thesis proposal, provided academic support, and is the supervisor of this doctoral thesis at the home institution. The Portuguese financial support was provided by FEDER/COMPETE, CNC (PTDC/EBB-EBI/115810/2009). The scholarship granted to the candidate was funded by Fundação para a Ciência e Tecnologia (FCT), reference number SRFH/BD/45928/2008.

Governo da República Portuguesa

This page was intentionally left blank

ON THE REPROGRAMMING OF THE KREBS CYCLE IN HYPOXIC AND *VHL*-DEFICIENT CANCER CELLS

by

Paulo A. Gameiro

Doctoral thesis in Biochemistry, specialty Bioenergetics, supervised by Professor Gregory Stephanopoulos and by Professor Rui de Carvalho, and submitted to Department of Life Sciences, Faculty of Sciences and Technology of University of Coimbra.

September, 2013

SUMMARY

Cancer cells reprogram their metabolism to support efficient macromolecule synthesis and proliferate within disparate microenvironments, in particular hypoxia. It has been acknowledged for many years that cancer cells rewire their metabolism as if they were exposed to hypoxia. This metabolic reprogramming entails an increased glucose uptake, a high glycolytic flux and ample lactate production, which mitigates glucose catabolism in the Krebs cycle. During the last decade, cancer biologists have demonstrated that cancer cells harboring specific oncogenic alterations also rely on a glutamine-maintained Krebs cycle to support aberrant growth. These studies were primarily focused on the oncogene Myc, and the role of other oncogenes and tumor suppressors in regulating glutamine metabolism remained unexplored until recently. Indeed, cells must produce new DNA, lipids and proteins before division, and the Krebs cycle provides many of the precursors necessary for these anabolic processes, including acetyl-CoA (for fatty acid synthesis) and aspartate (for pyrimidine synthesis). Therefore, it is not entirely surprising that cancer cells strive to maintain a functional Krebs cycle. However, the knowledge on glutamine catabolism, its regulation and significance in hypoxic and cancer cells was limited. In this doctoral thesis, we sought to elucidate the biosynthetic role of glutamine so as to understand the metabolic plasticity of hypoxic and “pseudohypoxic” cancer cells.

We identified reductive carboxylation (RC) from glutamine as a major pathway for lipid synthesis under hypoxia. Acetyl-CoA is the precursor for lipid synthesis and is generated from glucose-derived pyruvate in well-oxygenated cells. Cells exposed to hypoxia redirect glucose carbons away from the Krebs cycle and acetyl-CoA synthesis, making it unclear how hypoxic cells maintain *de novo*

lipogenesis. Using ^{13}C isotopic tracers and mass spectrometry (MS) analyses, we showed that mammalian cells under hypoxia conditions rely on RC of α-ketoglutarate by isocitrate dehydrogenase 1 (IDH1) to maintain *de novo* lipid synthesis. Renal cell carcinoma (RCC) cells deficient in the von Hippel–Lindau tumor suppressor (*VHL*) preferentially used RC for lipid synthesis even at normal oxygen levels.

HIF- 1α/2α are transcription factors that mediate cellular adaptations to hypoxia, and *VHL*-deficient cells exhibit HIF-1α/2α expression regardless of oxygen supply. To investigate the role of HIF and the signaling underlying reductive carboxylation, we introduced into RCC cells a series of tumor-associated *VHL* mutations that differ in their ability to inactivate HIF, and showed that HIF is strictly necessary to promote RC for *de novo* lipogenesis. Expression of a HIF-2α mutant was sufficient to induce RC and lipogenesis from glutamine in *VHL*-reconstituted RCC cells. We also demonstrated *in vivo* RC activity in *VHL*-deficient tumors growing as xenografts in mice, and showed that *VHL*-deficient cells are selectively sensitive to glutamine deprivation *in vitro and in vivo*.

RC is a NADPH-dependent reaction, wherein NADPH donates the hydride ion (H^-) that reduces α-ketoglutarate into isocitrate. In this context, the source(s) of NADPH contributing to RC have not been investigated. To this end, we evaluated the contribution of NADPH generated in mitochondria by the enzyme nicotinamide nucleotide transhydrogenase (NNT). NNT resides in the inner membrane of the mitochondrion and transhydrogenates NADH into NADPH. We showed that knockdown of NNT inhibits the contribution of RC to the Krebs cycle in SkMel5 and 786-O RCC cells, whereas overexpression of NNT was sufficient to stimulate this pathway. These observations were supported by an impairment of the NAD(P)H / $NAD(P)^+$ ratios.

Finally, we investigated the role of HIF expression in regulating pyrimidine biosynthesis from glutamine in RCC cells. Glutamine can also be used in the Krebs cycle to generate aspartate - the carbon source for pyrimidine synthesis. Using ^{13}C tracers, we showed that *VHL*-deficient RCC cells rely on RC-derived aspartate to maintain *de novo* pyrimidine synthesis. Inhibiting glutaminase (GLS) depleted the levels of pyrimidine intermediates in *VHL*-deficient cells but not in *VHL*-reconstituted cells, which utilized glucose oxidation to fuel the aspartate pool. Inhibiting both the *de novo* and salvage pyrimidine synthesis pathways selectively inhibited the growth of *VHL*-deficient cells, whereas addition of nucleosides partially rescued the growth effect.

In this doctoral thesis, we have elucidated the reprogramming of the Krebs cycle in hypoxic and *VHL*-deficient cancer cells. Ultimately, these findings classify reductive carboxylation as a survival mechanism to maintain biosynthesis, and suggest that targeting the pleiotropic glutamine-to-biomass signature of HIF expression with glutaminase inhibitors may be a viable therapeutic strategy for *VHL*-deficient tumors.

RESUMO

As células cancerígenas reprogramam o seu metabolismo para manterem a síntese de macromoléculas e proliferarem em ambientes díspares, em particular hipoxia. Há muitos anos que têm vindo a ser reconhecido que as células cancerígenas restruturam o seu metabolismo como se estivessem expostas a condições de hipoxia. Esta reprogramação metabólica envolve um aumento da captação de glucose, uma elevação do fluxo glicolítico e ampla produção de lactato, o que reduz o catabolismo de glucose no ciclo de Krebs. Durante a última década, biólogos do cancro têm demonstrado que células cancerígenas contendo mutações oncogénicas específicas também dependem de glutamina para manter a atividade do ciclo de Krebs, e suportar uma proliferação aberrante. Estes estudos foram principalmente focados no oncogene Myc, e o papel de outros oncogenes e supressores de tumor na regulação do metabolismo da glutamina tem permanecido inexplorado até recentemente. Efetivamente, as células têm de produzir novo DNA, lípidos e proteínas para que possam dividir-se, e o ciclo de Krebs produz muitos dos precursores necessários para estes processos anabólicos, incluindo acetyl-CoA (para a síntese de ácidos gordos) e aspartato (para a síntese de pirimidinas). Desta forma, não é totalmente surpreendente que as células cancerígenas se esforcem para manter um ciclo de Krebs funcional. Contudo, o conhecimento é limitado no que toca ao metabolismo da glutamina, da sua regulação e significância em células cancerígenas e hipóxicas. Nesta dissertação doutoral, nós procurámos elucidar o papel biossintético da glutamina de forma a compreender a plasticidade metabólica de células cancerígenas hipóxicas e pseudo-hipóxicas.

Nós identificámos a carboxilação redutiva (CR), a partir de glutamina, com a via principal para a síntese de lípidos em condições de hipoxia. Acetyl-CoA é o precursor para a síntese de lípidos e, em condições normais de oxigénio, é gerado a partir de piruvato vindo da glucose. Contudo, as células expostas a hipoxia inibem o fluxo de carbonos da glucose para o ciclo de Krebs e acetyl-CoA, surgindo a questão de como a lipogénese *de novo* poderá ser mantida em células em hipoxia. Usando marcadores isotópicos de carbono 13 e análises de espectrometria de massa, nós mostrámos que linhas celulares humanas em condições de hipoxia dependem da conversão de α-cetoglutarato em isocitrato (carboxilação redutiva, CR), mediada pela isocitrato desidrogenase 1 (IDH1), para manter a lipogénese *de novo*. Além disso, as células de carcinoma renal (CCR) que são deficientes no supressor de tumor von Hippel-Lindau (*VHL*) também dependem da reação CR para a síntese de lípidos mesmo a condições normais de oxigénio.

Os HIF-1α/2α são fatores de transcrição que medeiam adaptações celular a hipoxia, e as células deficientes em *VHL* expressam HIF-1α/2α constitutivamente; isto é, independentemente da

disponibilidade de oxigénio. Para investigar o papel do HIF e da sinalização subjacente à carboxilação redutiva, nós introduzimos várias proteínas mutantes de VHL em células CCR (deficientes em *VHL*) que diferem na sua capacidade de inativar HIF, e mostrámos que HIF é estritamente necessário para estimular a reação CR para a lipogénese *de novo.* A expressão de uma proteína HIF-2α mutante foi suficiente para induzir CR em células CCR previamente reconstituídas com a proteína VHL funcional. Nós demonstrámos que a carboxilação redutiva está ativa *in vivo* em tumores deficientes em *VHL* crescidos como xenógrafos em ratinhos, e mostrámos que as células deficientes em *VHL* são seletivamente sensíveis à privação de glutamina em condições *in vitro* e *in vivo*.

A carboxilação redutiva é uma reação que depende de NADPH, onde este doa o anião hidreto (H^-) que reduz o α-cetoglutarato em isocitrato. Neste contexto, a(s) fonte(s) de NADPH que contribuem para a reação CR não for investigadas anteriormente. Para tal, nós avaliámos a contribuição de NADPH mitocondrial gerado pela enzima nicotinamida nucleótido transidrogenase (NNT). NNT reside na membrana interna da mitocôndria e converte NADH em NADPH. Nós mostrámos que a diminuição da expressão de NNT em células SkMel5 e 786-O inibe a contribuição da carboxilação redutiva para a atividade do ciclo de Krebs, enquanto a sobre-expressão de NNT foi suficiente para estimular esta via. Estas observações foram suportadas por alterações nos rácios de NAD(P)H / $NAD(P)^+$.

Finalmente, nós investigámos o papel do HIF em células CCR na regulação da biossíntese de pirimidinas a partir de glutamina. A glutamina pode ser usada no ciclo de Krebs para gerar aspartato – a fonte de carbono para a síntese de pirimidinas. Usando marcadores de carbono 13, nós mostrámos que células CCR deficientes em *VHL* dependem do aspartato produzido pela carboxilação redutiva para manter a síntese de pirimidinas *de novo*. A inibição da glutaminase (GLS) reduziu os níveis intermediários das pirimidinas em células deficientes em *VHL* mas não em células reconstituídas com *VHL* funcional, sendo que as últimas utilizaram a oxidação de glucose mais eficientemente para alimentar a produção de aspartato. A dupla inibição das vias *de novo* e de reciclagem da síntese de pirimidinas inibiu seletivamente o crescimento das células deficientes em *VHL*, enquanto a adição de nucleósidos ao meio de cultura resgatou este efeito no crescimento celular.

Nesta dissertação doutoral, nós elucidámos a reprogramação do ciclo de Krebs em células cancerígenas deficientes em *VHL* e em hipoxia. Em última instância, estes resultados classificam a carboxilação redutiva como um mecanismo de sobrevivência celular para a manutenção de biossíntese, e sugerem que a utilização de inibidores da GLS para suprimir esta via pleiotrópica de glutamina-para-biomassa (dependente de HIF) poderá ser uma estratégia terapêutica viável para tumores deficientes em *VHL*.

Keywords

Cancer Metabolism,
Glutaminase,
Glutamine,
Hypoxia-Inducible Factors (HIFs),
Isocitrate Dehydrogenase,
Isotopic Tracers,
Kidney Cancer,
Krebs Cycle,
Lipogenesis,
NADPH,
Nicotinamide Nucleotide Transhydrogenase (NNT),
Pyrimidine Biosynthesis,
Reductive Carboxylation,
VHL,
Warburg Effect

Palavras-Chave

Biossíntese de Pirimidinas,
Cancro do Rim,
Carboxilação Redutiva,
Ciclo de Krebs,
Efeito Warburg,
Fatores Induzíveis for Hipoxia (HIFs),
Glutaminase,
Glutamina,
Isocitrato Desidrogenase,
Lipogénese,
Marcadores Isotópicos,
Metabolismo do Cancro,
NADPH,
Nicotinamida Nucleótido Transidrogenase (NNT),
VHL

This page was intentionally left blank

To Marguerita

and

To my family

This page was intentionally left blank

Acknowledgments

This is probably the most important page of this PhD thesis and by far the most gratifying to write. A hard one too. It is axiomatic but I want to emphasize that all my acknowledgments are an accurate tribute to those who helped me scientifically throughout the last four years and six months of my doctoral training. Without their help, I am firmly sure that I would not have a PhD thesis, not one that I would write at the moment. Because I learned so much from others, it becomes hard to look at this PhD thesis as my accomplishment. My accomplishment is to share these doctoral results with my mentors, Marguerita and friends, and that there is biological significance to this work.

I would like to thank Rui de Carvalho, my supervisor in Portugal, for accepting me as a PhD student, for helping me on my interests in metabolism, and for finding the best lab to pursue my naïve ideas – the Stephanopoulos Lab.

I would like to thank Greg Stephanopoulos for being my supervisor and accepting me in his lab. I say accepting me in his lab because, as a Visiting Student at MIT, it took me a while to grasp the philosophy of the lab, and interacting with Greg taught me how to perform at MIT. I thank Greg for the scientific discussions – these helped me develop a quantitative reasoning and think properly about numbers. This did shape my understanding of things, and it will help me in the future. Greg is very operative with his words, and that also contributed to me being more efficient, an aspect that always has room for improvement. Greg is a great scientist.

I want to mention that my appreciation to Othon's guidance should not detract my other acknowledgments. The plain truth is that I don´t think we would have published the Cell Metabolism paper if it weren´t for Othon´s consistent support, and I would still be struggling in other things. I would not be in the US right now, and my PhD would have turned out differently. I thank Othon for helping me be a scientist. Thanks to Othon, I learned the concept of biological significance and how to design *the* experiment that will address *the* question. He is a great scientist and *apparently* even better doctor. I

could continue but I decided to have a two page acknowledgment section. Oh, I should just thank Othon for saving my relationship with Marguerita (Ana for most).

I would like to thank Christian Metallo. He was crucial in the beginning of my PhD; he taught me metabolic flux analysis and many experimental approaches. We worked together on the reductive carboxylation and hypoxia journey (Chapter III), and we had great brainstorming sessions. Christian is now an assistant professor in the Bioengineering Department at University of California, in San Diego, and I wish him all the best. Joanne Kelleher is a great biochemist. She is the kind of scientist everyone would like to have around to discuss science; she just knows a lot about theory in biochemistry. Thanks Joanne for the scientific guidance, for giving me good papers to read, and for the book gift on metabolic regulation.

I would like to thank Pilar López-Larrubia and Rocio Pérez-Carro. Pilar is our great collaborator in Spain, and performed NMR analysis for the work in Chapter IV. She is an outstanding NMR spectroscopist, and her work was absolutely critical for this PhD thesis. She was the first person seeing reductive carboxylation activity in our *VHL*-deficient tumors *in vivo*; how awesome is that? Thanks so much for collaborating with us Pilar. Thanks, Rocio. Without your mice skills, we would not have done it either.

Last and far from least comes Marguerita. She knows me better than me. This ought not to be a love declaration. As you will see in a moment, Marguerita has to be in the acknowledgements big time. Marguerita, I must write about you because your patience with my anxieties is just so pleasingly reassuring! Without your magnificent social skills, I would not have been careful enough to carry on at specific moments of my PhD. Marguerita expresses her contribution to this PhD thesis even at the official level. She conducted the *in vivo* growth experiments of Chapter IV, and many others that I do not show here. She intellectually contributed to this work and, on top of that, she is the love of my life.

Contents

List of Figures and Tables

"The greater danger for most of us is not that our aim is too high and we miss it,
but that it is too low and we reach it."

Michelangelo

This page was intentionally left blank

Chapter 1

1. Introduction

I.1. Motivation

The metabolism of cancer cells reflects their function – unrestricted growth – which differs from normal counterpart cells. Every mammalian cell must consume nutrients to fulfill the following requirements of survival: i) production of adenosine 5´-triphosphate (ATP) to drive unfavorable reactions, ii) production of metabolic precursors for macromolecule turnover, and iii) maintenance of the redox state. Yet, a dividing cell needs to duplicate itself and, therefore, to produce an excess of macromolecules (biomass) while keeping pace with the aforementioned bioenergetic needs. As such, cancer cells undergo fundamental changes in their metabolism to support biomass synthesis, adapt to limited nutrient resources, and to compete (successfully) for these supplies with surrounding normal cells. Primed by the seminal work of the biochemist Otto Warburg in the 1920s, scientists have long observed that virtually all cancer cells exhibit an increased demand for glucose when compared to normal cells (Gatenby and Gillies, 2004). Importantly, the recognition that cancer cells exhibit an increased glucose uptake led to the implementation of the ^{18}F – deoxyglucose positron-emission tomography (PET) imaging tool to diagnose tumors. The PET scan monitors glucose uptake by tissues in the body and is used in the clinic to detect cancers and predict response to treatment (Ben-Haim and Ell, 2009), being one example of how to exploit the glucose avidity of tumors. In addition, it is now established that cancer cells also increase their demand for other nutrients, in particular glutamine. Glutamine is an abundant extracellular nutrient, being traditionally viewed as a nitrogen transporter and a non-essential aminoacid (NEAA). The classical studies of Newsholme, Brand, Wagner and others challenged the aforementioned view reporting that fast proliferating and transformed cells exhibit a high rate of glutamine utilization when compared to slow proliferating and primary cells (Brand, 1985; Neermann and Wagner, 1996; Newsholme et al., 1985a, 1985b). Ultimately, mammalian cells must use glutamine-derived nitrogens for the synthesis of DNA bases but, as discussed herein, glutamine has also emerged as a tumor nutrient and significant carbon source for the proliferation of cancer cells.

The era of oncogenes/tumor suppressors and the cancer genome revolution taught us that cancer arises from mutational events that affect core signal transduction pathways regulating cell survival and growth (Vogelstein et al., 2013). However, it is becoming recognized that many of the oncogenic signals that confer growth advantage and malignancy ultimately affect metabolic pathways of cell growth (Levine and Puzio-Kuter, 2010; McKnight, 2010). This knowledge has shifted attention towards metabolic pathways, stimulating research on the metabolism of cancer cells and how it can be targeted therapeutically. Over the last 15 years, landmark studies have elucidated how growth signals, oncogenes/tumor suppressors and environmental cues (such as hypoxia) not only regulate glucose and glutamine uptake but also determine the intracellular fate of these nutrients in cancer cells (Cairns et al., 2011; DeBerardinis and Thompson, 2012). This means that, in addition to increasing the overall consumption of glucose and glutamine, cancer cells also reprogram their metabolism to catabolize these nutrients via specific pathways. It is in this sense that *metabolic reprogramming* of cancer cells is referred herein. As detailed below, the mechanistic connection between oncogenic signals and metabolism warrants a thorough study of metabolism that may lead to viable therapies. While targeting nutrient uptake to inhibit cancer cell growth may significantly affect the growth of normal cells, the concept of targeting intermediary metabolism (and more specifically, metabolic *branch points*) is more clinically appealing on the grounds that specific fluxes may be dispensable for normal cells. This was the resilient motivation of the present doctoral thesis; the aim was to identify metabolic vulnerabilities of cancer cells that can be targeted therapeutically.

Figure I-1 illustrates the metabolic outcome of targeting a specific metabolic branch point versus nutrient uptake or, in general terms, a linear pathway. Let us assume a normal cell consumes 4 nutrient units to synthesize the products 1 and 2 via pathway A, whereas a cancer cell consumes 8 nutrient units to synthesize the same biomass products, and let us assume cell growth depends linearly on nutrient consumption. Hence, the cancer cell exhibits a two-fold higher flux through pathway A than the normal cell and, thereby, grows twice as fast. Downstream of pathway A, the normal cell catabolizes

the 4 nutrients units equally via pathways B and C, whereas a cancer cell preferentially relies on C. Inhibiting 50% of the flux through pathway A will decrease the overall consumption of 2 nutrient units in the normal cell and 4 nutrient units in the cancer cell. While the two-fold difference is a win for inhibiting nutrient consumption in the cancer cell, both the normal and the cancer cell are affected by 50% in their overall nutrient consumption (ΔN) and growth. Therefore, the therapeutic effect is 1. In contrast, inhibiting 50% of pathway C will decrease the consumption of 1 nutrient unit in the normal cell and 3 nutrient units in the cancer cell. While this represents a three-fold effect in nutrient consumption, it also translates into a therapeutic effect of 1.5, since the normal cell does not rely on pathway C to the same extent as the cancer cell. Varying the conditions of this example will lead to different outcomes, but the principle holds in that targeting specific metabolic alterations of cancer cells bears theoretical advantages. As described in Chapter 2, studying cellular metabolism requires the use of stable isotopes to identify what metabolic reactions are activated or inhibited in cancer cells.

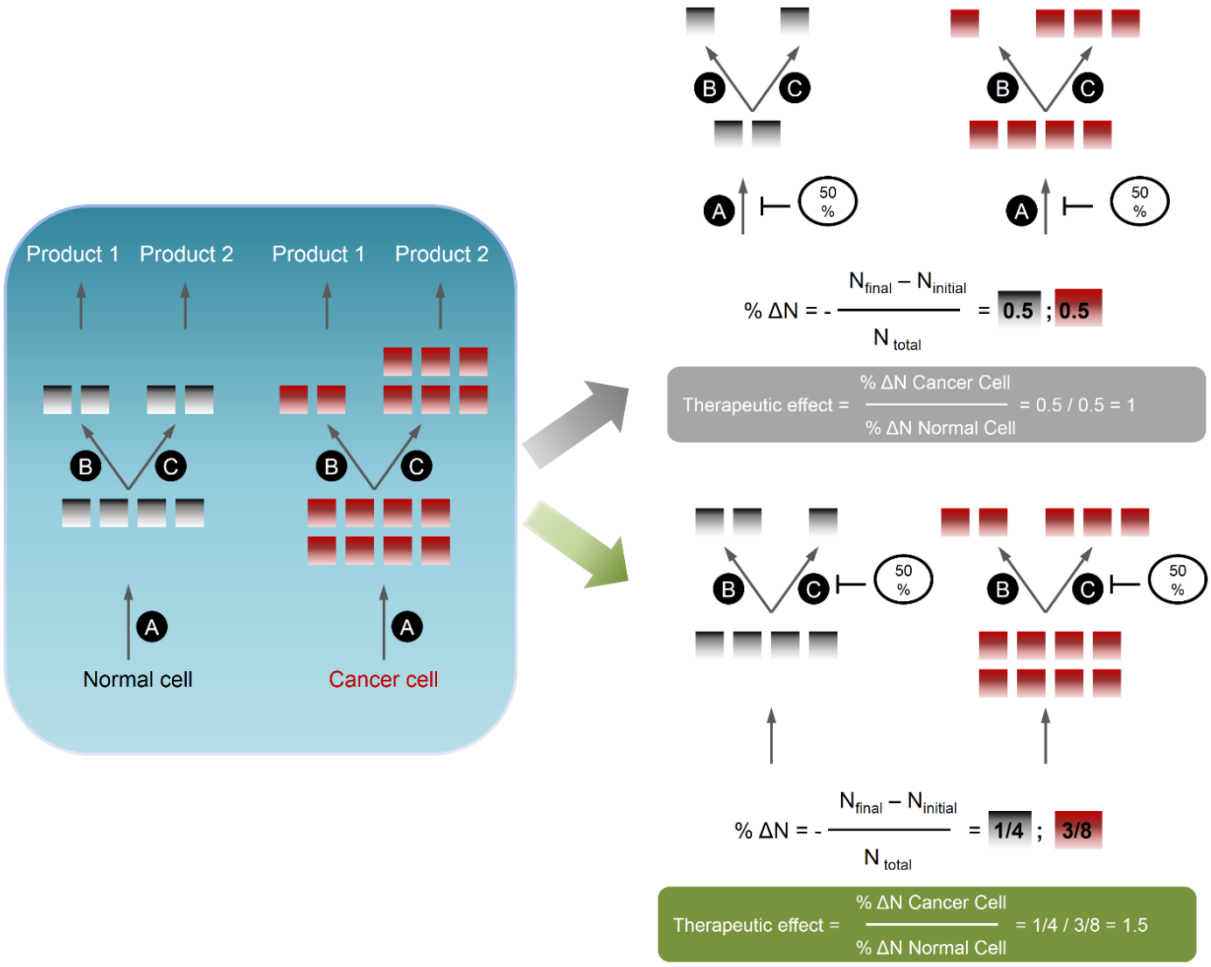

Figure I-1. Therapeutic Efficacy of Targeting a Linear Versus a Branched Pathway

The left diagram illustrates a simple metabolic network for the production of biomass from metabolic precursors or nutrients. Products 1 and 2 are synthesized from four nutrient units (black squares) in the normal cell and eight nutrient units (red squares) in the cancer cell. The metabolic network is comprised by pathways A, B and C. The right diagrams show the effect on nutrient consumption (ΔN) and the therapeutic effect by inhibiting 50% of activity in pathway A (top) or pathway C (bottom).

I.2. The Warburg Effect

One of the metabolic hallmarks of cancer cells is the activation of glycolysis and lactate production even in the presence of adequate oxygen. This seminal discovery was made by Otto Warburg in the 1920s. Warburg and co-workers used a homemade reaction vessel to measure CO_2 production (as readout of lactate production from bicarbonate-containing buffer) and O_2 consumption (as readout of

respiration) in tumor and normal tissue slices. Surprisingly, he observed that respiration rates were similar between tumor and normal tissues, but that tumor tissues exhibited high lactate production even in the presence of adequate oxygen; that is, oxygen availability was unable to prevent lactate production (a reverse Pasteur effect). Later in 1927, Warburg directly measured arterial and venous plasma levels of glucose and lactate in Jensen's sarcomas implanted in rats and compared these levels with those of healthy organs. The difference between venous and arterial levels was an indication of glucose consumption and lactate production, and Warburg observed that tumors consumed, on average, 70 mg of glucose and secreted 46 mg of lactic acid whereas healthy organs consumed about 7 times less glucose and did not exhibit net lactate secretion into the blood (Warburg et al., 1927). These findings set the *aerobic glycolysis* paradigm that cancer cells convert most of the glucose (at least 66%) to lactic acid even under the presence of oxygen – the Warburg effect [for a review on the work of Otto Warburg, see (Koppenol et al., 2011)].

The conversion of glucose to pyruvate – glycolysis – is a universal metabolic pathway that occurs in all kingdoms of life, from microorganisms to superior eukaryotes (Boiteux and Hess, 1981; Dandekar et al., 1999). Glucose-derived pyruvate has two major fates in the cell – conversion to lactate in the cytosol (via lactate dehydrogenase, LDH) or to acetyl-Coenzyme A (AcCoA) in the mitochondrion (via pyruvate dehydrogenase, PDH). Under aerobic conditions, a normal mammalian cell converts most of the pyruvate to AcCoA and catabolizes it through the tri-carboxylic acid (TCA) or Krebs cycle, transferring reducing equivalents (the hydride ion H^-) from the Krebs cycle intermediates to nicotinamide adenine dinucleotide (NAD^+) via NADH-linked dehydrogenases. In turn, the reduced NAD^+ (i.e., NADH) donates the electrons to the respiratory electron transport chain (ETC), which transfers the electrons to molecular oxygen through oxidation-reduction reactions that are coupled to ATP synthesis, under the energy conservation rules of the chemiosmotic model (Brand and Murphy, 1987; Mitchell, 1979). Upon a switch to low oxygen conditions (hypoxia), ETC-mediated ATP synthesis is inhibited and cells switch to anaerobic glycolysis, reducing pyruvate to lactate to recycle the NAD^+

necessary for the subsequent glycolytic cycles (Brand and Murphy, 1987; Hardie, 2000). In contrast, cancer cells heavily rely on glycolysis and divert most of the pyruvate to lactate production both in normoxia and hypoxia. Hence, the Warburg effect was the first evidence that cancer cells *reprogram* their metabolism to rely on specific metabolic fluxes (Figure I-2).

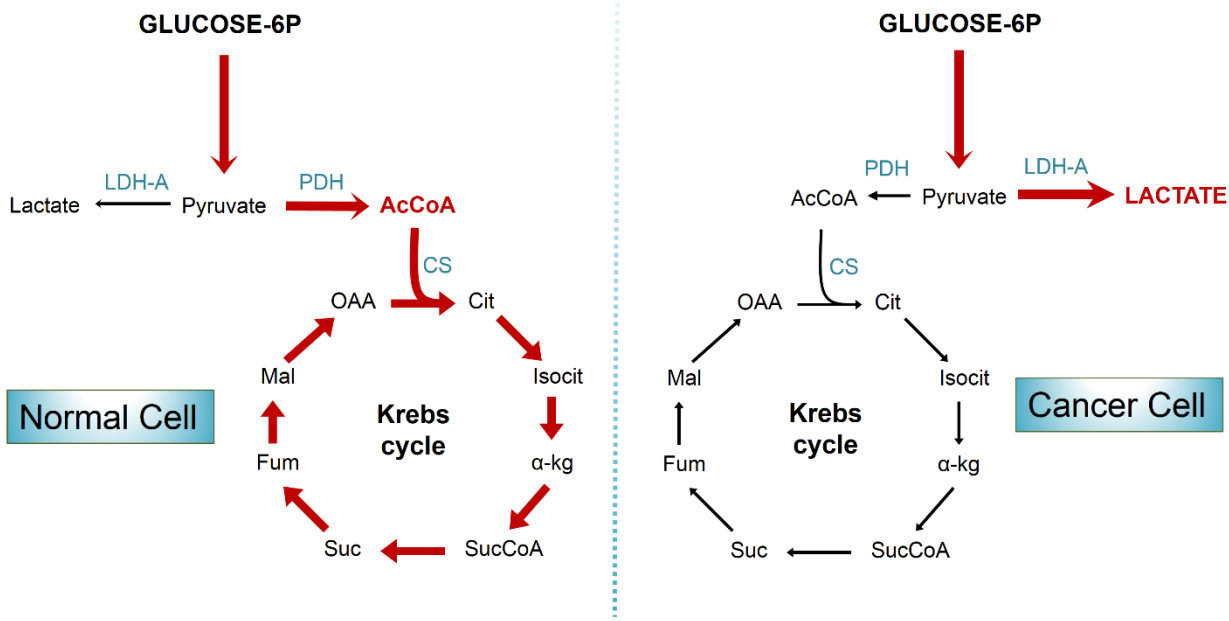

Figure I-2. The Warburg Effect

Left: Under normal oxygen conditions, a normal cell catabolizes most of the pyruvate through pyruvate dehydrogenase (PDH), producing acetyl-CoA (AcCoA) for the Krebs cycle (left). A cancer cell diverts most of the pyruvate to lactate through lactate dehydrogenase A (LDH-A), even under normal oxygen conditions (right). The lines thickness is proportional to the activity of the correspondent reactions. CS, citrate synthase.

I.3. Molecular Mechanisms Underlying the Warburg Effect

3.1. Hypoxia-inducible Factors (HIFs)

Low oxygen (<3-4%), or hypoxia, is a hallmark of most solid tumors and it selects for cancer cells that can adapt their metabolism to nutrient-limited conditions (Gatenby and Gillies, 2004; Pouysségur et al., 2006). Typically, mammalian cells respond and adapt to changes in O_2 availability by regulating the activity of hypoxia-inducible factors (HIFs). The transcription factors hypoxia-inducible factors 1α and 2α (HIF-1α, HIF-2α) are master regulators of the hypoxic program, stimulating anaerobic glycolysis and angiogenesis when oxygen becomes limited (Gordan and Simon, 2007; Semenza, 2010). In well-oxygenated cells, the HIF-α subunit (1α or 2α) is rapidly hydroxylated by O_2-dependent prolyl hydroxylases (PHDs) and recognized by the Von Hippel-Lindau protein (pVHL), a component of the E3-ubiquitin ligase complex that targets HIF-α for degradation in the proteasome (Ivan et al., 2001; Jaakkola et al., 2001). Upon hypoxia, the PHDs activity is inhibited and the HIF-1α (or HIF-2α) subunit becomes stabilized, it translocates to the nucleus and dimerizes with the HIF-1β partner to induce a transcriptional program that mitigates O_2 consumption [for a review, see (Kim et al., 2003)]. The HIF transcriptional program inhibits the rate of oxidative phosphorylation (OXPHOS) and increases the expression of glucose transporters, glycolytic enzymes, lactate dehydrogenase A (LDH-A) and pyruvate dehydrogrenase kinase 1 (PDK1), which inhibits PDH and reroutes pyruvate away from the mitochondria towards lactate production (Ebert et al., 1996; Firth et al., 1994; Kim et al., 2006; Papandreou et al., 2006). As a result, HIF expression enforces anaerobic glucose metabolism, and this metabolic reprogramming is necessary for the survival and growth of hypoxic cells (Lum et al., 2007; Pouysségur et al., 2006). In addition to HIF stabilization, the hypoxia signaling also impinges on mRNA translation, protein turnover, microRNAs and chromatin modifications, and some of these processes are regulated in a HIF-independent manner (Kulshreshtha et al., 2007; Melvin and Rocha, 2012; Wouters and Koritzinsky, 2008). Together, these evidences illustrate the pleiotropic effects of hypoxia

and the critical role of HIF on the metabolic response to low oxygen conditions. But HIF *should* be inactive in normoxia.

Otto Warburg was criticized over many years for hypothesizing later in his career that mitochondrial respiration was damaged in cancer cells, because O_2 availability was unable to prevent lactate production in cancer cells (Warburg, 1956). The criticism was largely due to lack of evidence of mitochondrial defects/mutations associated with bioenergetics defects [for a review on mitochondria and cancer, see (Wallace, 2012)]. Today, we know that germline, loss of function mutations in the Krebs cycle enzyme fumarate hydratase (FH) predisposes individuals to leiomyomas and renal cell cancer (RCC), whereas mutations in succinate dehydrogenase (SDH) cause hereditary paragangliomas and phaeochromocytomas, strongly suggesting that these enzymes act as tumor suppressors (Baysal et al., 2000; Guzy et al., 2008; Kaelin Jr., 2009; Semenza, 2010). Conversely, gain of function mutations in the isocitrate dehydrogenase 1 (IDH1) and 2 (IDH2) have also been found in a subset of gliomas, acute myeloid leukemia (AML) and other malignancies and can lead to the production of the putative oncometabolite R(-)-2-hydroxyglutarate (2HG) (Dang et al., 2010; Ward et al., 2010; Yan et al., 2009). Importantly, mutations in FH and SDH lead to the accumulation of fumarate and succinate, respectively, which can inhibit PHDs and stabilize HIF-1α subunits even under normoxia conditions –pseudohypoxia – thereby providing a mechanistic link between mitochondrial dysfunction, HIF and cancer metabolism (Isaacs et al., 2005; Pollard et al., 2005; Selak et al., 2005). A more prominent example of cancer-associated mutations linked to HIF stabilization in normoxia is the disruption of the pVHL-HIF interaction. The pVHL protein is an established tumor suppressor because of its ability to degrade HIF (Iliopoulos et al., 1995; Kondo et al., 2002), being inactivated in the majority (approximately 60-70%) of sporadic clear-cell renal cell carcinomas (RCC) (Iliopoulos, 2006). Thus, *VHL*-deficient RCC cells are the *sine qua non* of a Warburg-like system, exhibiting constitutive HIF-1α and/or HIF-2α activity irrespective of oxygen availability (Kim et al., 2003). Indeed, HIF-1α is necessary and sufficient to promote glycolysis and lactate production in *VHL*-deficient RCC cells (Hu et al., 2003),

demonstrating the definite role of HIF transcription factors in contributing to the Warburg effect (Semenza, 2007). Of note, Warburg observed that cancer and normal cells exhibit similar OXPHOS rates, but HIF expression should rather decrease OXPHOS activity and O_2 consumption. In this regard, Warburg performed his manometer experiments in the presence of ample oxygen, excess glucose, and with the thickness of the tissue slices being limited to <400μm (to prevent hypoxia). On one hand, it is possible that HIF was active in the original tumor setting, but the experimental conditions of Warburg's (which were optimized to prevent hypoxia) could have led to HIF degradation and offset putative differences on oxygen consumption between tumor and normal tissues. Conversely, Warburg's observations also raise the hypothesis that additional oncogenic alterations may contribute to the aerobic glycolysis phenotype in a HIF-independent manner. Indeed, additional genetic abnormalities can independently stimulate aerobic glycolysis, as described below. Yet, some of these oncogenic signals also intersect HIF signaling, promoting a glycolytic program that is required for unrestricted proliferation.

3.2. The Oncogenes Myc, Akt and the PKM2 Switch

During the last 20 years, efforts in cancer biology have revealed many of the molecular mechanisms underlying the Warburg effect in cancer cells [for two reviews on regulation of cancer metabolism, see (Cairns et al., 2011; Koppenol et al., 2011)]. One of the first evidences that oncogenes can affect energy metabolism was the report that the oncogene Ras stimulates glucose transport and that Scr phosphorylates glycolytic enzymes and lactate dehydrogenase in transformed fibroblasts (Cooper et al., 1984; Flier et al., 1987). Later, Chi Dang and colleagues demonstrated the first mechanistic connection between an oncogene and aerobic glycolysis, showing that the oncogenic transcription factor Myc trans-activates the promoter of lactate dehydrogenase A (LDHA), increasing its expression and lactate production under normal oxygen conditions (Shim et al., 1997). The authors also showed that the induction of LDHA expression was necessary for MYC-mediated transformation, and later

studies extended these findings showing that Myc activates most of the glycolytic enzymes including glucose transporters [see the mini review (Gordan et al., 2007). Myc and HIF share many of the glycolytic targets, but their role on glucose metabolism differs in that Myc expression can stimulate glycolysis under normoxia, whereas HIF requires hypoxia or “abnormal” stabilization under normoxia. There is evidence of cross-talk between HIF and Myc function (Gordan et al., 2007), and this interplay will come into context later in this thesis.

The Ras and phosphatidylinositide 3-kinase (PI3K) pathway is one of the most commonly altered signaling pathways in cancer (Shaw and Cantley, 2006). Mutations in receptor tyrosine kinases (RTKs), in the Ras oncogene, in the PI3K complex or in the tumor suppressor PTEN can lead the constitutive activation of the Akt kinase, which phosphorylates downstream targets that activate the expression of glucose transporters (GLUTs), hexokinase 2, phosphofructokinase 1 (PFK1) and 2 (PFK2). Activation of the PI3K-Akt pathway is sufficient to stimulate aerobic glycolysis and renders Akt-expressing cells sensitive to glucose withdrawal (Elstrom et al., 2004). In addition, Akt phosphorylates and inhibits the tuberous sclerosis 2 (TSC2), thereby activating the mammalian target of rapamycin (mTOR). The mTOR kinase is a key sensor of nutrient availability, integrating growth signals and environmental cues so as to mediate biosynthesis when nutrients are abundant. When activated, the mTOR signaling increases mRNA translation, ribosomal biogenesis; it stimulates lipid synthesis and the pentose phosphate pathway (PPP). Moreover, mTOR can stimulate the glycolytic flux by activating the translation of HIF-1α. Although mTOR is inhibited under hypoxic conditions (Brugarolas et al., 2004), there is evidence that constitutive activation of mTOR signaling in tumors and mouse embryo fibroblasts (MEF) leads to the accumulation of HIF under normoxia (Brugarolas et al., 2003; Shackelford et al., 2009). For an overview of mTOR and growth control and metabolism, see Figure 3 in (Laplante and Sabatini, 2012).

The explanation for the Warburg effect was to a certain extent rekindled by the discovery that metabolic enzymes themselves can be isoform selected to support aerobic glycolysis. The pyruvate

kinase (PK) enzyme converts phosphoenolpyruvate (PEP) to pyruvate and it has two splice variants, PKM1 (expressed in most adult tissues) and PKM2 (expressed during embryonic development) (Sybille Mazurek et al., 2005). Christofk *et al.* reported that cancer cells selectively express the pyruvate kinase isoform M2 (PKM2) whereas normal cells express the isoform M1 (PKM1), and demonstrated that the PKM1-PKM2 switch was necessary for the Warburg effect and tumor growth (Christofk et al., 2008b). The oncogene Myc induces the splicing factors that produce M2, further supporting its role in mediating aerobic glycolysis(David et al., 2010). Furthermore, PKM2 is regulated by protein kinase signaling, wherein it is directly phosphorylated and inhibited by growth factor receptors (Hitosugi et al., 2009) and its activity is also decreased upon binding to phosphotyrosine residues (Christofk et al., 2008a). Paradoxically, phosphotyrosine -mediated inhibition of PKM2 is required for cell growth. Moreover, PKM2 has a lower activity than PKM1, but PKM2-expressing cells exhibit higher lactate production than PKM1-expressing cells. In light of this conundrum, strong evidences now suggest that low PKM2 activity promotes the accumulation of upstream glycolytic intermediates to fuel serine synthesis in cancer cells (Chaneton et al., 2012; Ye et al., 2012). In fact, the serine and glycine synthesis pathways have been shown to be necessary for the rapid, aggressive growth of cancer cells (Jain et al., 2012; Possemato et al., 2011; Zhang et al., 2012). Conversely, other studies have deciphered the lactate paradox in PKM2 expressing cells. It was reported that PEP can serve as a phosphate donor to phosphorylate phosphoglycerate mutase (PGAM1), in which case PEP is converted to pyruvate in a PKM2 and ATP-independent manner (Vander Heiden et al., 2010). Here, the authors proposed that the combined action of PKM2 and phosphorylated PGAM1 allow high rates of PEP-to-pyruvate conversion in PKM2-expressing cells. Importantly, Luo *et al.* later showed that HIF-1 directly binds to the promoter of PKM2, which in turn interacts with HIF-1α subunits and increase its transcriptional activity (Luo et al., 2011). This positive feedback loop underlines the cooperation between PKM2 and HIF to stimulate both glycolysis and lactate production under normoxia. The role of lactate in cancer also goes beyond its action in NAD^+ recycling. Compelling evidences suggest that the lactate produced in hypoxic and HIF-

expressing cells can fuel oxidative metabolism in oxygenated tumor cells, while others have hypothesized that lactate production may serve as a selective pressure in the tumor microenvironment to promote tumor invasion (Gatenby and Gillies, 2004; Sonveaux et al., 2008) . Together, these studies established that oncogenic alterations – activation of Myc, Akt and the switch to PKM2 – are intertwined with HIF signaling to support a glycolytic program necessary for cancer cell growth.

I.4. Cancer Cell Growth and the Need for Glutamine Metabolism

The classical studies of Newsholme, Brand, Wagner and others initially showed that activated lymphocytes and cancer cells exhibit a high rate of glutamine utilization when compared to slow proliferating and primary cells (Brand, 1985; Neermann and Wagner, 1996; Newsholme et al., 1985a, 1985b). Ultimately, glutamine is required for progression through the cell cycle and proliferation, as glutamine-derived nitrogens are strictly necessary for purine and pyrimidine synthesis (Colombo et al., 2011; Gaglio et al., 2009). However, recent studies in cancer biology have shown that cancer cells require glutamine-derived carbons to fuel the Krebs cycle and sustain rapid proliferation in response to growth signals, oncogene activation and loss of tumor suppressors (Ben-Sahra et al., 2013; DeBerardinis et al., 2007; Le et al., 2012; Mitsuishi et al., 2012; Robitaille et al., 2013; Son et al., 2013; Wang et al., 2010a; Wise et al., 2008; Yang et al., 2009). In retrospect, mammalian cells must produce new DNA, lipids and proteins before division, and the Krebs cycle provides many of the precursors necessary for these biosynthetic processes (figure I-3) (DeBerardinis et al., 2008). Therefore, the switch to a glutamine-maintained Krebs cycle in glycolytic cancer cells supports an efficient carbon flux for nucleotide, lipids and non-essential amino acid biosynthesis, as well as NADPH production for redox maintenance [see the following reviews on glutamine metabolism in cancer cells (Dang, 2009a; DeBerardinis and Cheng, 2009; Kaelin et al., 2010; Wise and Thompson, 2010)]. One of the major oncogenic mechanisms of glutamine addiction is the activation of Myc in cancer cells. As an established oncogene, Myc stimulates mitochondrial biogenesis, and increases the expression of

glutaminase 1 (GLS1) through the repression of the micro RNA miR-23a/b (Dang, 2009b). A consequence of the Myc-mediated transcriptional program is the activation of glutamine oxidation in the Krebs cycle – the glutaminolysis pathway, which renders glioblastoma cells highly dependent on glutamine to proliferate (Wise et al., 2008). The requirement for a functional Krebs cycle can be also evidenced by the essential role of pyruvate carboxylase in supporting the growth of glioblastoma cells in the absence of glutamine (Cheng et al., 2011). This notion also calls for the mechanisms that rewire cancer cells to depend either on glucose- and/or glutamine-derived carbons to fuel specific metabolic pathways. In fact, it has been shown that glucose uptake and glutamine uptake are coupled through the hexosamine biosynthetic pathway and the Mondo-A transcriptional program (Kaadige et al., 2009; Wellen et al., 2010), which suggests that cancer cells *must* coordinate glucose and glutamine utilization in central carbon metabolism to support proliferation.

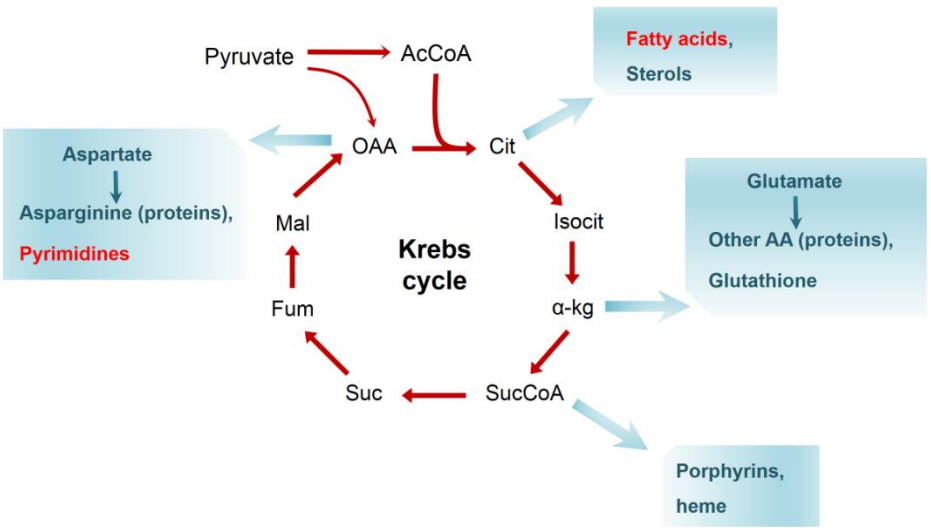

Figure I-3. The Role of the Krebs Cycle in Anabolism

The diagram shows the biosynthetic fate of the Krebs cycle intermediates. The anabolic products studied in this doctoral thesis are shown in red.

AcCoA is a major precursor for lipid synthesis and protein acetylation, being generated from glucose-derived pyruvate through mitochondrial metabolism and the ATP-dependent citrate lyase (ACLY) reaction in the cytosol. In 2005, the team of Craig Thompson reported that inhibition of ACLY impairs lipid synthesis and tumor growth (Hatzivassiliou et al., 2005). The authors hypothesized that cancer cells rely on a truncated version of the Krebs cycle, wherein the glucose-derived citrate in the mitochondria is exported to the cytosol and converted to AcCoA and oxaloacetate (via ACLY) for lipid synthesis. The cytosolic oxaloacetate is reduced to malate and recycled back to the mitochondrion, completing the cycle. Later, it was shown that the significance of ACLY in cancer cells extends the biosynthetic fate of AcCoA, as evidenced by the role of ACLY-derived AcCoA in maintaining histone acetylation in response to growth factors (Wellen et al., 2009). For clarity, these findings may seem incompatible with the Warburg effect, but the conventional understanding was that the remaining glucose-derived pyruvate (not converted to lactate) was critical to maintain *de novo* lipogenesis through the action of ACLY. However, this hypothesis implies that enough pyruvate is *allowed* to be diverted towards mitochondrial citrate for lipid synthesis in cancer cells. As we shall see herein, this does not hold for *true* Warburg-like or hypoxic cells.

I.5. The Scientific Questions Addressed Herein

Hypoxic cells and, by extension, *true* Warburg-like cells convert glucose to lactate at near-maximum theoretical levels, which raises the question of how the Krebs cycle is supplied with AcCoA to support lipogenesis. In this context, the catabolism of glutamine under hypoxia or “pseudohypoxic” conditions is not understood, and this was a fundamental question of this doctoral thesis. Here, we show that cells under hypoxic conditions primarily utilize glutamine to generate citrate and lipids through reductive carboxylation of α-ketoglutarate by isocitrate dehydrogenase (IDH1). Glutamine can contribute to lipogenic AcCoA through two distinct pathways. Glutamine-derived α-ketoglutarate can be oxidatively metabolized in the Krebs cycle and generate pyruvate from malic enzyme (glutaminolysis),

which in turn can be converted to AcCoA. Alternatively, cells can reductively carboxylate α-ketoglutarate to generate isocitrate/citrate (reductive carboxylation, RC). Here, we labeled cancer and non-transformed human-derived cell lines with ^{13}C isotopic tracers which specifically trace the contribution of glutaminolysis, RC and glucose oxidation to lipogenic AcCoA. We show that hypoxic cells almost exclusively reply on glutamine-derived RC to produce *de novo* fatty acids (Metallo et al., 2012). In parallel, other groups also showed that cells under hypoxic conditions or defective mitochondria primarily utilize glutamine to generate citrate and lipids through RC by IDH1 or IDH2 (Mullen et al., 2011; Scott et al., 2011; Wise et al., 2011), corroborating our findings that glutamine is a major substrate for *de novo* lipogenesis upon hypoxia.

Given the role of HIF-1α/2α in the cellular response to hypoxia, we hypothesized that HIF is the critical regulator of RC. HIF can be directly activated by loss of the VHL tumor suppressor, and *VHL*-deficient RCC cells exhibit constitutive HIF expression even under normal oxygen conditions (a pseudohypoxia state). We show that *VHL*-deficient cells also rely on RC for lipid synthesis even under normoxia, and metabolic profiling of two isogenic clones that differ in pVHL expression (WT8 and PRC3) suggest that reintroduction of wild-type VHL can restore glucose utilization for lipogenesis (Metallo et al., 2012). The *VHL* tumor suppressor protein (pVHL) has been reported to have several functions other than the well-studied targeting of HIF. Specifically, it has been reported that pVHL regulates the large subunit of RNA polymerase (Pol) II (Mikhaylova et al., 2008), p53 (Roe et al., 2006), and the Wnt signaling regulator Jade-1. VHL has also been implicated in regulation of NF-kB signaling, tubulin polymerization, cilia biogenesis, and proper assembly of extracellular fibronectin (Chitalia et al., 2008; Kim et al., 2003; Ohh et al., 1998; Thoma et al., 2007; Yang et al., 2007). Hypoxia inactivates the α-ketoglutarate-dependent HIF prolyl hydroxylases (PHDs), leading to stabilization of HIF. In addition to this well-established function, oxygen availability regulates other signaling processes including mTOR signaling, the unfolded protein response (Wouters and Koritzinsky, 2008), the expression of microRNAs that regulate mRNA translation (Chan et al., 2009; Kulshreshtha et al., 2007),

and the activity of a larger family of α-ketoglutarate dependent cellular oxygenases that lead to posttranslational modification of chromatin modifiers (Melvin and Rocha, 2012). It is therefore conceivable that the effect of hypoxia on RC that we report may be mediated by signaling mechanisms independent of the disruption of the pVHL-HIF interaction. Thus, we sought to elucidate the signaling mechanisms underlying RC induction by hypoxia and loss-of-*VHL*. We (1) demonstrate that HIF is necessary and sufficient to promote RC, (2) provide insights into the molecular mechanisms that link HIF to RC, (3) detect RC activity in human *VHL*-deficient RCC cells growing as tumors in nude mice, (4) provide evidence that the reductive phenotype of *VHL*-deficient cells renders them sensitive to glutamine restriction *in vitro*, and (5) show that inhibition of glutaminase suppresses the growth of *VHL*-deficient xenograft tumors (Gameiro et al., 2013a).

Reductive carboxylation by IDH enzymes is a NADPH-dependent reaction, wherein NADPH donates the hydride ion (H^-) that reduces α-ketoglutarate into isocitrate (Dalziel and Londesborough, 1968; Leonardi et al., 2012; Siebert et al., 1957). However, we observe that HIF expression does not increase NADPH levels, which raises the question of how IDH1 and IDH2 are supplied with NADPH to catalyze the reverse reaction. In particular, the source(s) of NADPH for RC in the mitochondrion (by IDH2) have not been investigated. The enzyme nicotinamide nucleotide transhydrogenase (NNT), residing in the inner membrane of the mitochondrion, catalyzes the transfer of hydride ion equivalents (H^-) from NADH to NADPH using the proton gradient: ($xH_{out} \rightarrow xH_{in}$) as follows: $NADH + NADP^+ + xH_{(out)} \rightarrow NAD^+ + NADPH + xH_{(in)}$. NNT is regarded as a major source of NADPH in the mitochondrion and reduced glutathione (Rydström, 2006; Sheeran et al., 2010; Yin et al., 2012). It is therefore conceivable that NNT activity generates the NADPH necessary for the RC reaction in the mitochondrion, a hypothesis that has been speculated before (Sazanov and Jackson, 1994), but has never been experimentally tested. Using ^{13}C isotopic tracers, we show that NNT contributes to RC in the mitochondrion and regulates glucose and glutamine utilization in the Krebs cycle (Gameiro et al., 2013b).

In addition to being a source of lipogenic AcCoA, glutamine can also be used in the Krebs cycle to generate aspartate, which is the carbon source for pyrimidine synthesis. Given the role of HIF-1α/2α in regulating glutamine metabolism, we hypothesized that loss of *VHL* would affect pyrimidine synthesis in RCC cells. Using ^{13}C and ^{15}N glutamine tracers, we show that *VHL*-deficient RCC cells utilize RC-derived aspartate to maintain *de novo* pyrimidine synthesis. Inhibiting the utilization of glutamine-carbons compromises *de novo* pyrimidine synthesis in *VHL*-deficient cells but not in *VHL*-reconstituted cells, which can utilize glucose oxidation to maintain aspartate synthesis. We also provide evidences that the contribution of the salvage pathway for pyrimidine synthesis is altered upon loss of *VHL*, and that this phenotype can be targeted to selectively inhibit the growth of *VHL*-deficient cells (*in preparation*).

In my doctoral work, I also participated in studies investigating how other oncogenes and tumor suppressors affect glutamine metabolism. Specifically, we observe that oncogenic K-Ras also increases glutamine utilization in the Krebs cycle of transformed fibroblasts (Gaglio et al., 2011), whereas loss of the tumor suppressor Rb changes nucleotide levels and reprograms glutamine metabolism to maintain glutathione synthesis in flies and human cancer cells (Nicolay et al., 2013).

In this thesis, we i) identify reductive carboxylation (RC) as the main pathway of lipid synthesis in hypoxic and *VHL*-deficient RCC cells, ii) elucidate the role of HIF in promoting RC and the biological significance of the reductive phenotype in *VHL*-deficient RCC cells, iii) determine the contribution of NNT-derived NADPH for the RC reaction, iv) demonstrate the regulation of pyrimidine synthesis by HIF in RCC cells, and iv) explore the role of other oncogenic signals in regulating glutamine utilization in the Krebs cycle. Taken together, these observations lay the ground for metabolism-based therapeutic strategies for targeting glutamine catabolism in HIF-driven tumors (such as RCC) and possibly the hypoxic compartment of solid tumors in general.

"The first key to success is the ability to apply your physical and mental energies to one problem without growing weary."

Thomas Edison

This page was intentionally left blank

Chapter II

II. Experimental Procedures

Chapter II describes Isotopic Methods partially reviewed in the book chapter:

Gameiro PA, Metallo CM, Stephanopoulos G. (2012). Systems-level analysis of cancer metabolism. In Systems Metabolic Engineering (Chapter 11), (**Springer**)

II.1. Isotopic Methods

1.1. Stable isotopes, Mass spectrometry and Technical terminology

Heavy stable isotopes are the most practical means of tracing and quantifying intracellular metabolism, wherein isotope-labeled substrates (i.e., *tracers*) are catabolized through enzyme-mediated reactions in the metabolic network. Provided that knowledge of atom transitions is available, the metabolic fate of these tracers can be exploited to quantify the activity of metabolic reactions. Specifically, the degree of isotopic enrichment in metabolic intermediates and products will inform on the contribution (or *relative flux*) of different reactions (that catabolize the tracer) to the formation of metabolites of interest. In conjugation with substrate uptake and product secretion rates, the isotopic enrichment of metabolites can be further used to estimate *absolute fluxes* (in mol per cell per time unit) using Metabolic Flux Analysis (MFA), as described below. A metabolic flux captures multiple levels of cellular regulation, including protein expression, metabolite concentrations, posttranslational modifications and allosteric regulation; hence, it represents a powerful metric to evaluate cellular activity. Herein, we used ^{13}C-labeled glucose and glutamine tracers and mass spectrometry (MS) to study intermediary metabolism in the Krebs cycle, and macromolecule biosynthesis.

Mass spectrometry–based studies are carried out by coupling a separation technique to a mass analyzer through different ionization interfaces. Here, we primarily used gas chromatography – mass spectrometry (GC-MS), in which metabolites in a complex mixture (cellular extract) are separated in a column coupled to a MS detection system that generates ions through electron impact (EI). A fragmentation pattern specific to the metabolite structure is produced, and a mass spectrum is recorded where fragments are sorted based on their mass-to-charge ratio (m/z). GC-MS offers high chromatographic resolution and sensitivity for amino and organic acids, which comprise a significant part of the molecules in central carbon metabolism. GC-MS analysis requires that the metabolites are either volatile or rendered volatile by derivatization. Here, we performed silylation via tert-butyldimethylsilylation (TBDMS), which is an established method to reduce the polarity of amino and

organic acids through an anhydrous reaction that forms ester derivatives. For information on MS approaches, protocols, chemical derivatization and ^{13}C isotopic tracers for the metabolic profiling of cancer cells, please see (Griffin and Shockcor, 2004; Halket et al., 2005; Walther et al., 2012; Yuan et al., 2012).

Mass spectrometry detects molecules that differ in mass, as determined by *mass isotopomers*. The measured mass isotopomers may comprise molecules that differ in their isotopic composition. For example, glutamine labeled with either one ^{15}N or ^{13}C atom are detected by MS as the same mass isotopomer. The mass spectrum of a heavy isotope-enriched molecule is comprised by a set of mass isotopomer distributions (MIDs) (each one corresponding to a single molecular fragment), which distinguish populations of molecules that have a different number of neutrons. Although no positional enrichment is directly measured by MS, it is often possible to retrieve such information via analysis of the molecular fragmentation (Christensen and Nielsen, 1999; Dauner and Sauer, 2000). Mass isotopomers of a molecular fragment are generally represented by the mass *m* plus the number of non-abundant isotopes. The fraction mass 0 (or M0, notation used in this work) denotes the mass of molecules comprised by atoms of the most common isotope present naturally. The increase in mass (M1, M2, M3, etc) refers to molecules enriched with the correspondent number of heavy isotopes from the tracer or from natural abundance (e.g., 1.1% for ^{13}C). The MID pattern of a metabolite readily indicates the abundance of each mass isotopomer relative to the total, representing a readout of activity of the different reactions metabolizing the tracer.

A complication associated with MID patterns is the natural abundance of ^{13}C, ^{2}H, ^{17}O, ^{18}O, ^{15}N and ^{29}Si atoms, among others. In isotopic studies using TBDMS, the natural abundance of atoms in the derivatization group significantly contributes to the isotopic enrichment of the analyte, so measured MIDs need to be corrected for the naturally labeled atoms that are not derived from the tracer. Glutamine labeled with ^{13}C in the five carbons ([U-$^{13}C_5$] glutamine, in which “U” denotes uniformly) was used in this work and will be used as example. When A549 cells (a human lung carcinoma line) are

labeled with 99% [U-$^{13}C_5$] glutamine, prior to correction MID depicts a percent enrichment of M5 glutamine of approximately 60% which is a consequence of abundant M6 and M7 fractions in the population of molecules. Here, we used a correction method executed within Matlab (Mathworks), which is adapted from Fernandez' et al. (Fernandez et al., 1996). As seen in figure II-1, the corrected MID closely resembles that expected of the original tracer, with M5 comprising approximately 90% of the intracellular glutamine.

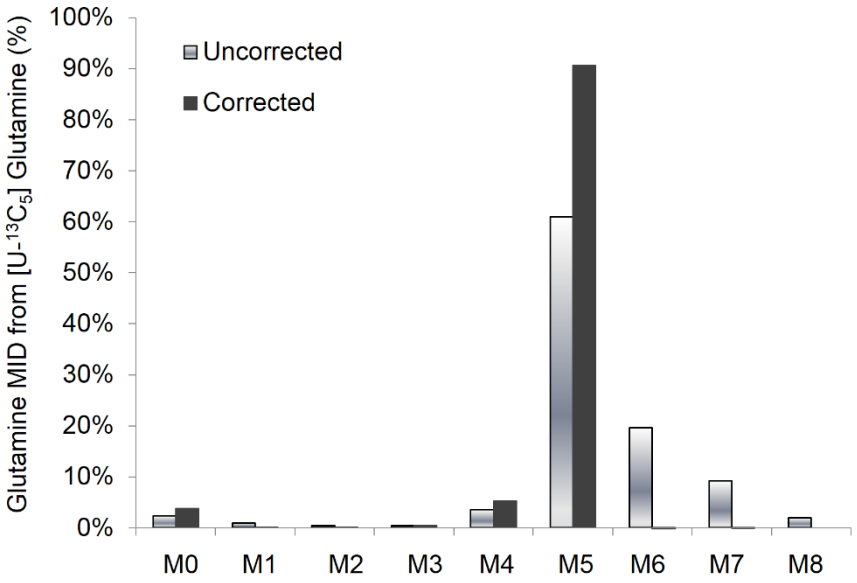

Figure II-1. Mass Isotopomer Distribution (MID) of Glutamine

Mass isotopomer distribution (MID) of intracellular glutamine in A549 cells cultured with [U-$^{13}C_5$] (99%) glutamine. The glutamine MID was obtained by GC-MS analysis of the cell extract. Metabolites were derivatized with TBDMS, which generates a glutamine fragment of 431 m/z (M0). An in-house algorithm corrected for the natural abundance of C, H, O, N, P, Si, S and F atoms.

1.2. Choice of ^{13}C isotopic tracers

The experimental design is critical to obtain the desired metabolic information from isotopic labeling studies. In particular, the choice of tracer limits the range of possible measured MIDs and therefore strongly influences the quality of the data. A wide collection of stable isotopes is now available, and

several studies have been conducted to test the effectiveness of different ^{13}C tracers to determine specific fluxes in mammalian cells (Metallo et al., 2009; Walther et al., 2012). Here, we used different ^{13}C-labeled glucose and glutamine tracers to probe the activity of specific reactions in central carbon metabolism, as described below.

To trace glucose catabolism, we used uniformly ^{13}C labeled glucose ([U-$^{13}C_6$] glucose), glucose labeled with ^{13}C in carbon 3 ([3-$^{13}C_1$] glucose), and glucose simultaneously labeled with ^{13}C in carbons 1 and 2 ([1,2-$^{13}C_2$] glucose). The [U-$^{13}C_6$] glucose tracer transfers *two* ^{13}C atoms to Krebs cycle metabolites via pyruvate dehydrogenase (PDH), whereas pyruvate carboxylase (PC) activity incorporates *three* ^{13}C atoms in oxaloacetate, which then propagate to other Krebs cycle metabolites. Therefore, the formation of M2 and M3 mass isotopomers are associated with PDH and PC activity, respectively, whereas M5 citrate, M4 α-ketoglutarate, and M4 glutamate isotopomers reflect the overall contribution of glucose carbons via PDH, PC and/or continued Krebs cycle (Figure II-2). AcCoA molecules originating from [U-$^{13}C_6$] glucose are fully labeled, and the labeled fatty acids (we used palmitate as a readout) are represented by M2, M4, M6, M8, M10, M12, M14, and M16 mass isotopomers. The [3-$^{13}C_1$] glucose isotope was used to trace the specific contribution of glucose-derived anaplerosis, in which the ^{13}C in carbon 1 (C1) of pyruvate is either retained in oxaloacetate via PC or lost as CO_2 through PDH. The [1,2-$^{13}C_2$] glucose tracer was used in Chapter V to probe flux split ratios into the pentose phosphate pathway (PPP) versus anaerobic glycolysis; the oxidative decarboxylation of 6-phosphogluconate into D-ribulose 5-phosphate (oxidative PPP) ultimately produces singly ^{13}C-labeled glyceraldehyde 3-phosphate (GAP), while glycolysis forms M2 GAP. Therefore, the relative activity of these two pathways can be ascertained by the MIDs of the downstream metabolites pyruvate and lactate, in specific through analysis of the M2 to M1 ratio (Vizan et al., 2005).

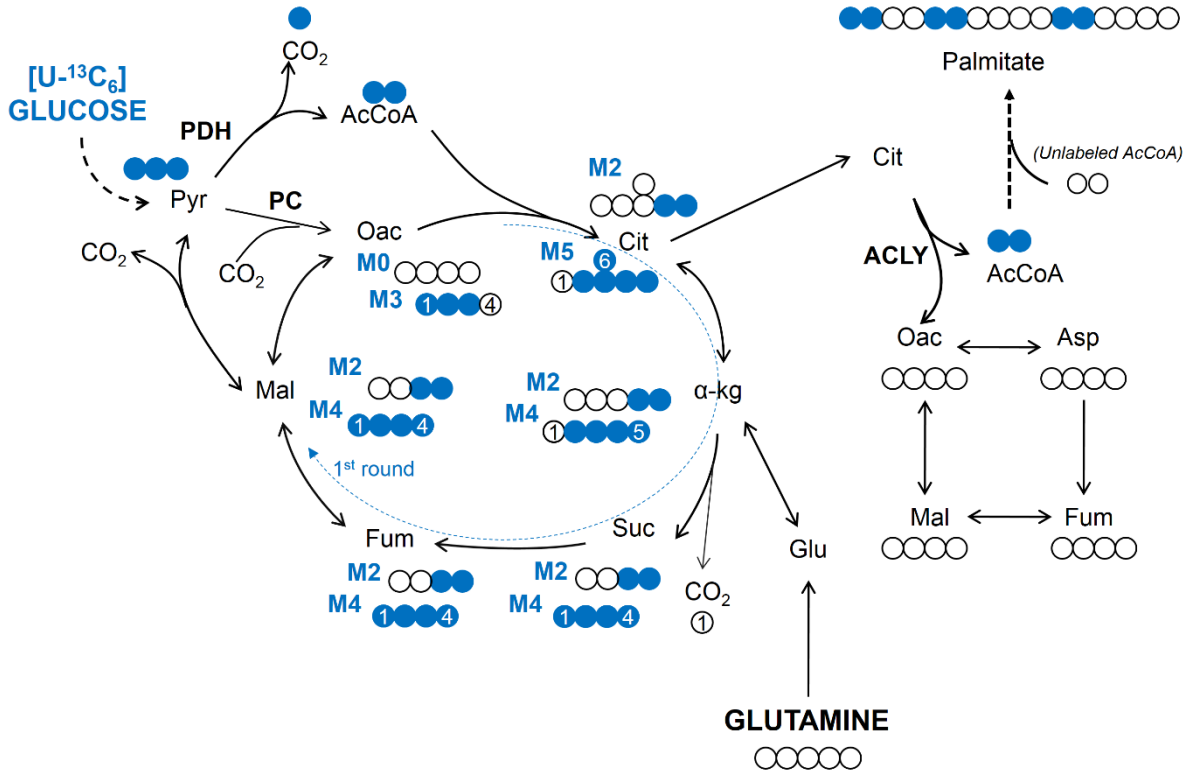

Figure II-2. Carbon Atom Transition Map for [U-$^{13}C_6$] Glucose

The map illustrates the fate of [U-$^{13}C_6$] glucose in the Krebs cycle and palmitate (carbon atoms are represented by circles). The [U-$^{13}C_6$] glucose-derived isotopic label (blue circles) are retained in the Krebs cycle, transferring two ^{13}C atoms to citrate (M2 Cit), α-ketoglutarate (M2 α-kg), succinate (M2 Suc), fumarate (M2 Fum), and malate (M2 Mal) via pyruvate dehydrogenase, or *three* ^{13}C atoms to oxaloacetate (M3 Oac) via pyruvate carboxylase (PC). The condensation of PC-derived Oac with fully labeled acetyl-CoA (M2 AcCoA) forms M5 Cit, M4 α-kg, M4 Suc, M4 Fum and M4 Mal. Other possible combinations between labeled/unlabeled Oac and acetyl-CoA are not shown. Labeling patterns arising from molecular symmetry, some unlabeled intermediates and cellular compartments are omitted for simplicity. The first round of the Krebs cycle is illustrated, and positional labeling is depicted for relevant metabolites.

To trace glutamine catabolism in the Krebs cycle, we used uniformly ^{13}C labeled glutamine ([U-$^{13}C_5$] glutamine) and [1-$^{13}C_1$] glutamine. The [U-$^{13}C_5$] glutamine tracer transfers *four* ^{13}C atoms to the Krebs cycle intermediates through oxidation (forward Krebs cycle) whereas it incorporates *five* ^{13}C

atoms in citrate through reductive carboxylation (RC), generating M5 citrate, M3 oxaloacetate, M3 aspartate, M3 malate and M3 fumarate. AcCoA molecules originating from [U-$^{13}C_5$] glutamine are fully labeled. Therefore, [U-$^{13}C_5$] glutamine traces the overall contribution of glutamine (via RC and glutaminolysis) to lipid synthesis (Figure II-3). Of note, since the glutaminolytic pathway generates M3 pyruvate from [U-$^{13}C_5$] glutamine (via mitochondrial malic enzyme), M5 citrate can in principle be formed via condensation of glutaminolysis-derived AcCoA (M2 AcCoA) with M3 oxaloacetate (not depicted in Figure II-3). Thus, the M5 citrate from [U-$^{13}C_5$] glutamine can be an ambiguous readout of RC activity in cells that heavily rely on complete glutaminolysis (glutamine-to-pyruvate conversion).

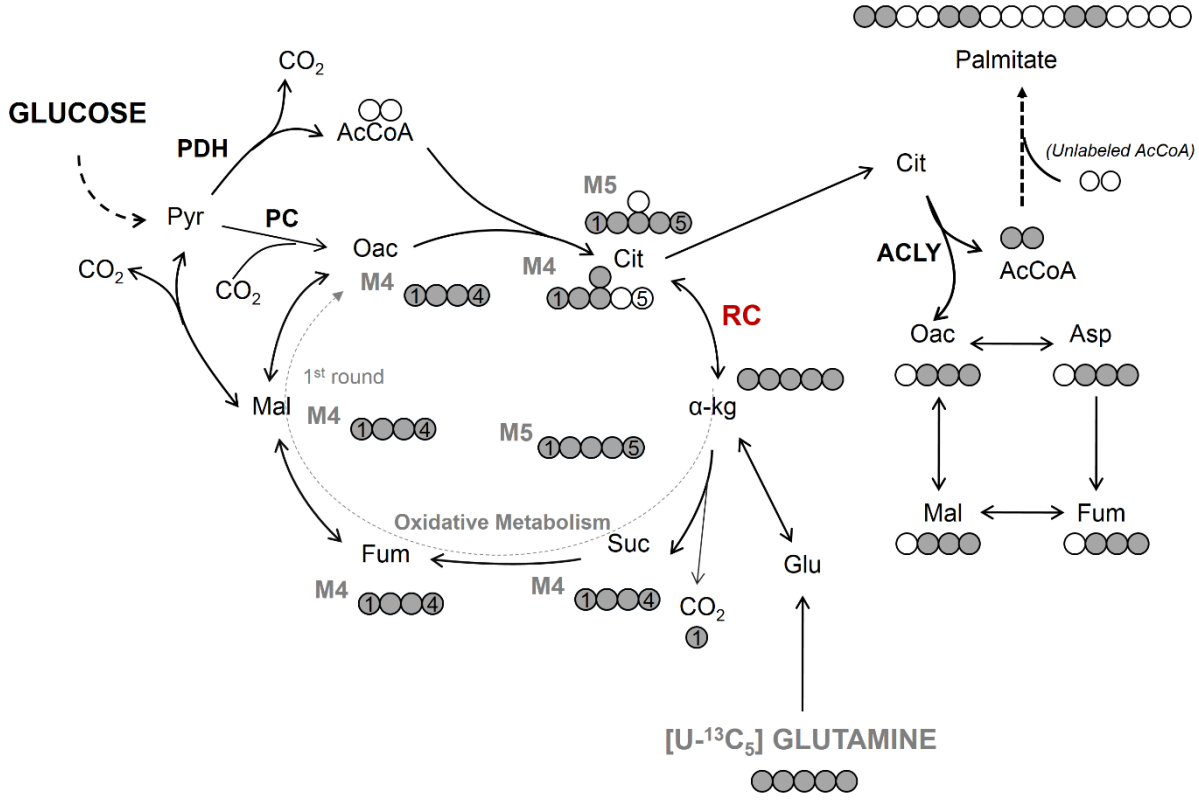

Figure II-3. Carbon Atom Transition Map for [U-$^{13}C_5$] Glutamine

The map illustrates the fate of [U-$^{13}C_5$] glutamine in the Krebs cycle and palmitate (carbon atoms are represented by circles). Mass isotopomers generated by reductive carboxylation (RC) include M5 citrate (Cit), M3 oxaloacetate (Oac), M3 aspartate (Asp), M3 malate (Mal), and M3 fumarate (Fum). Mass isotopomers generated by oxidative metabolism include M4 Cit, M4 succinate (Suc), M4 Fum and M4 Oac. Both RC and complete glutaminolysis (not shown) generate fully labeled acetyl-CoA (M2 AcCoA). For simplicity, labeling patterns arising from molecular symmetry and cellular compartments are not shown. The first round of the Krebs cycle is illustrated, and positional labeling is depicted for relevant metabolites.

To specifically trace the contribution of RC to the Krebs cycle, we used [1-$^{13}C_1$] glutamine, in which the ^{13}C labeled carbon is lost during oxidation of α-ketoglutarate, but it is retained in citrate through RC activity and transferred to metabolites downstream of the ACLY reaction (Figure II-4). To trace the contribution of RC to lipid synthesis, we used [5-$^{13}C_1$] glutamine because the [1-$^{13}C_1$] glutamine-derived isotopic label cannot be incorporated in AcCoA through RC. [5-$^{13}C_1$] glutamine transfers one ^{13}C atom to AcCoA and fatty acids through RC *only*. Although the [5-$^{13}C_1$] glutamine-derived isotopic label is transferred to Krebs cycle metabolites oxidatively, it cannot be incorporated into citrate as carbons 5 or 6 (which comprise the AcCoA carbon skeleton of citrate – see the AcCoA moiety highlighted by dashed circles in Figure II-4). Consequently, [5-$^{13}C_1$] glutamine is specific to trace the RC-to-lipid flux.

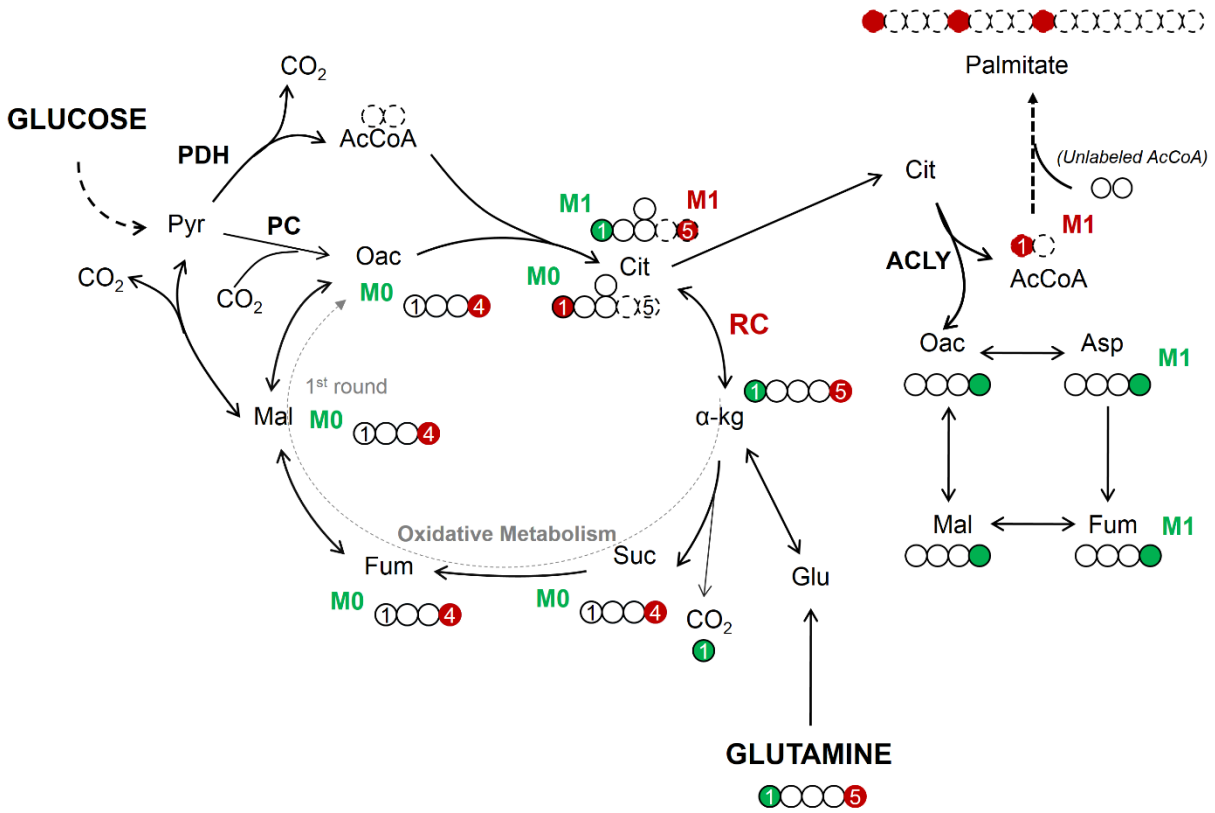

Figure II-4. Carbon Atom Transition Map for [1-$^{13}C_1$] Glutamine and [5-$^{13}C_1$] Glutamine

The map illustrates the fate of [1-$^{13}C_1$] and [5-$^{13}C_1$] glutamine used to trace the *reductive* Krebs cycle in this work (carbon atoms are represented by circles). The [1-$^{13}C_1$] glutamine-derived isotopic label (green circle) is lost during oxidation of α-ketoglutarate, but it is retained during the reductive Krebs cycle and transferred to citrate and downstream metabolites. [5-$^{13}C_1$] glutamine-derived isotopic label (red) is incorporated into acetyl-CoA (AcCoA) and fatty acids through reductive carboxylation *only*; isotopic label from [5-$^{13}C_1$] glutamine cannot be transferred to fatty acids through oxidative Krebs cycle. Metabolites containing the AcCoA carbon skeleton are highlighted by dashed circles. For simplicity, labeling patterns arising from molecular symmetry and cellular compartments are not shown. Positional labeling is depicted for relevant metabolites only.

1.3. Metabolic Flux Analysis (MFA)

Computational estimation of fluxes and their associated 95% confidence intervals was accomplished using the metabolic elementary unit (EMU) framework – based software *Metran* executed in Matlab (Mathworks) as previously described (Antoniewicz et al., 2007, 2006). Briefly, mass isotopomer distributions (MIDs) for each metabolite are simulated using initial "guess" flux vectors, the substrate labeling information (in this case, [1-$^{13}C_1$] glutamine and [U-$^{13}C_6$] glucose datasets) and a stoichiometric matrix outlined by the reaction network and atom transitions. The simulated MIDs are compared with measured MIDs (obtained by GC-MS analysis) and the flux vector is iteratively adjusted by minimizing the residuals between simulated and measured MIDs. Upon obtaining an accepted fit, the sensitivities of the simulated MIDs are extracted to determine 95% confidence intervals associated with each flux estimate. The flux estimations and confidence intervals were subject to the following assumptions:

1. Cellular metabolism and isotopic labeling are at steady-state. Cells were labeled for 24 hours with either ^{13}C glutamine or ^{13}C glucose tracers. We confirmed that the metabolite labeling from glutamine does not change significantly after approximately 12-18 hours, allowing for an acceptable assumption of pseudo steady-state. This is exemplified in Figure II-5 for vector-only (pBABE) and *VHL*-reconstituted UMRC2 cells, cultured in the presence of [U-$^{13}C_5$] glutamine for different periods of time.

2. Dissolved CO_2 exchanges freely with gaseous CO_2 such that unlabeled CO_2 is available for use in carboxylation reactions. Thus, we did not balance the CO_2 production and consumption in our MFA.

3. Fatty acid oxidation and protein turnover are negligible relative to glucose and glutamine consumption. Thus, we did not consider these fluxes in our MFA.

4. Two separate compartments of pyruvate are assumed to exist, with cytosolic pyruvate (primarily glucose-derived) used to generate lactate and mitochondrial pyruvate (derived from Krebs cycle metabolites) used for alanine synthesis. These compartments are exchangeable and required to fit the differential labeling observed in lactate and alanine.

5. Fumarate and succinate are symmetric metabolites, and a dilution pool of unlabeled succinate is assumed to exist. Isotopic enrichment of succinate pools from tracers is often observed to be decreased when compared to other Krebs cycle metabolites. Inclusion of a "dilution flux" to succinate pool was required to fit the differential labeling observed in succinate when compared to other Krebs cycle metabolites. The measured succinate is comprised of both pools (metabolically active and dilution compartment).

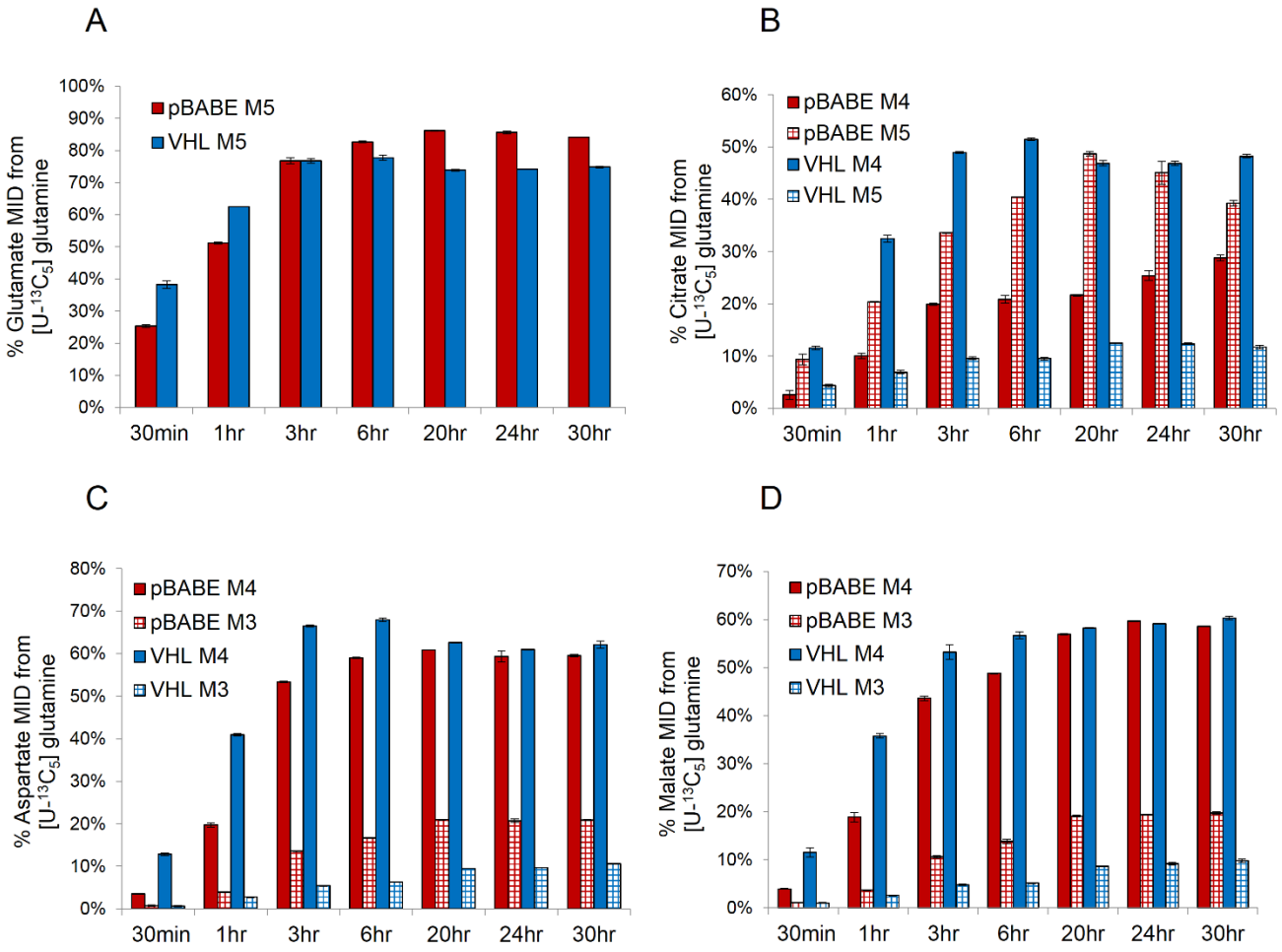

Figure II-5. Time-Course Labeling of UMRC2 Cell Lines from [U-$^{13}C_5$] Glutamine

Vector-only (pBABE) and *VHL*-reconstituted cells were cultured in the presence of [U-$^{13}C_5$] glutamine for different periods of time. The percent ^{13}C enrichment of (A) glutamate, (B) citrate, (C) aspartate, and (D) malate is shown for isotopomer readouts of glutamine incorporation (M5 glutamate), reductive carboxylation (M5 citrate, M3, aspartate and M3 malate) and oxidative Krebs cycle (M4 citrate, M4 aspartate and M4 malate).

1.4. Isotopomer Spectral Analysis (ISA)

The principle of ISA was initially developed by Joanne Kelleher and colleagues to quantify *de novo* synthesis of fatty acids using ^{13}C acetate tracers (Kelleher and Masterson, 1992; Kharroubi et al., 1992). ISA provides a general framework to measure the contribution of different sources to the precursor pool (e.g., acetyl-CoA) of a given product (e.g., palmitate); it requires the biochemistry to follow the polymerization principle, with monomeric subunits (the precursors) condensing into a polymer (the product). There are two dimensionless parameters that are determined by the ISA approach: D is the fractional contribution of ^{13}C-enriched atoms of the tracer versus endogenous pathways (1-D) as sources of the precursor (lipogenic AcCoA); g(t) indicates the fraction of newly synthesized product in the sample (e.g. palmitate) (Figure II-6). The ISA assumes that the precursor mixture rapidly achieves metabolic and isotopic steady-state during the incubation with the tracer. A key component of the ISA model is that the sampled product is not required to attain isotopic steady-state. The ISA model uses equations to calculate the probability of the appearance of each mass isotopomer (M0, M1, M2, etc) in palmitate, based on test values for D and g(t) (Kelleher and Masterson, 1992; Yoo et al., 2004). These probabilities are compared with the actual fractional abundance obtained for each palmitate mass isotopomer (the MID obtained by GC-MS) and a fitting procedure outputs a best estimate for D and g(t). Here, we performed ISA using the software *Metran* and estimated the percent contribution to lipogenic AcCoA (D value) and the percent *de novo* lipogenesis (g(t) value), together with their associated confidence intervals.

For calculation of the absolute *de novo* lipogenic flux (in pmol of palmitate per cell per hour), the quantity of newly synthesized palmitate was determined by multiplying the percentage of *de novo* lipogenesis (g(t) value) by the total cellular palmitate. Palmitate was quantitated by GC/MS using a tri-heptadecanoin (C17) internal standard. The absolute flux of a given substrate (e.g. glutamine) to palmitate was calculated by multiplying the percent contribution to lipogenic AcCoA (the D value) by the amount of newly synthesized palmitate and dividing by the integral viable cell density over the course of the experiment (this absolute flux quantification was used in Chapter III).

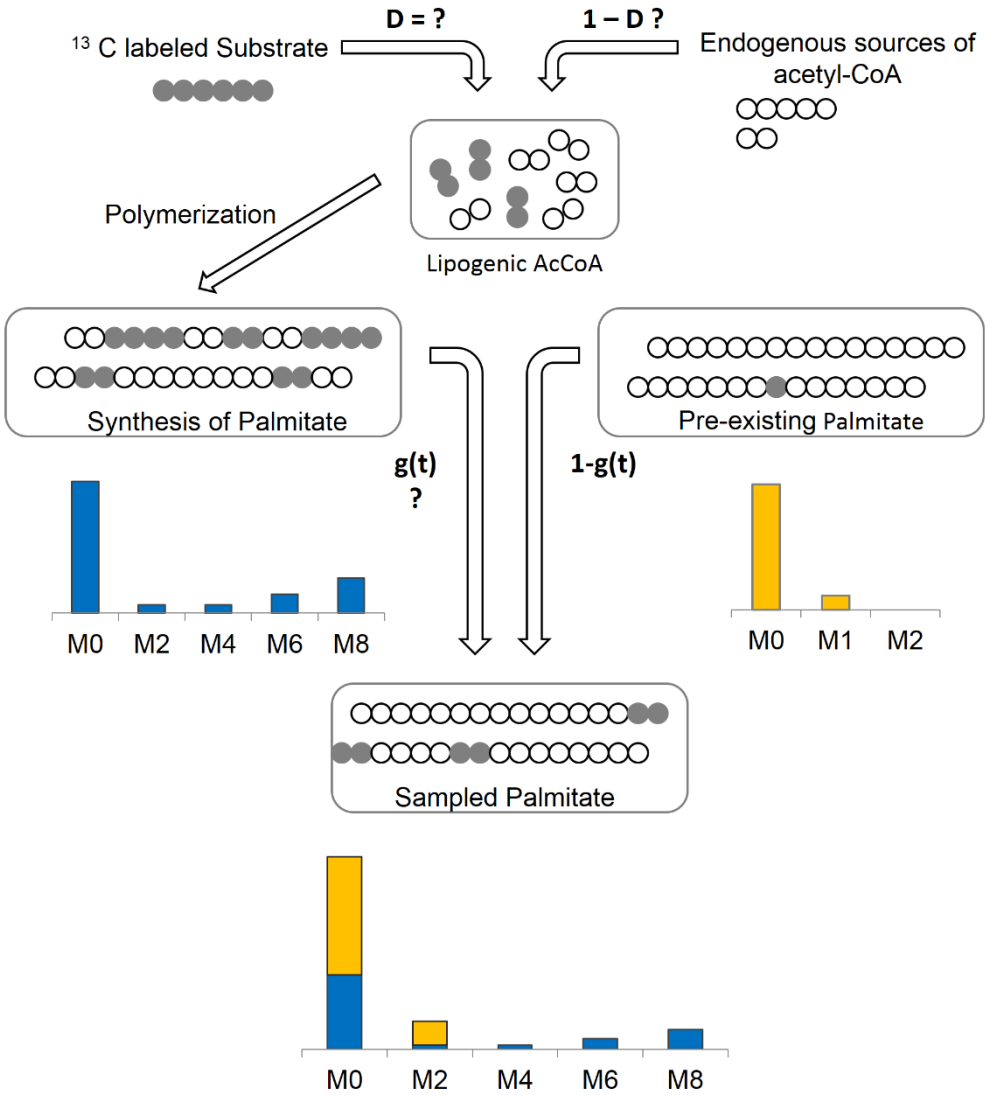

Figure II-6. The Isotopomer Spectral Analysis (ISA) Method

A ^{13}C-labeled glucose tracer is used to trace the glucose-to-lipid flux. The glucose-derived ^{13}C atoms and endogenous sources (e.g. acetate, glutamine) contribute to the pool of lipogenic acetyl-CoA (AcCoA). The D parameter indicates the unknown fractional contribution (or relative flux) of the glucose tracer to lipogenic AcCoA. During the incubation with the tracer, palmitate is synthesized from 8 molecules of AcCoA. The newly synthesized palmitate mixes with an existing pool of palmitate (prior to tracer addition) and the fraction of *de novo* palmitate synthesis after a period t is g(t). Each bar graph represents the palmitate mass isotopomer distribution (MID). Pre-existing palmitate has a significant M1 enrichment due to natural abundance. The parameters D and g(t) are estimated by fitting the predicted to the measured MID in the sampled palmitate.

II.2. Metabolite Analysis of Cellular Medium

For MFA, absolute flux estimates in pmol/cell/hour were obtained using glucose/glutamine uptake and lactate/glutamate secretion rates. Cells were seeded in 6 well plates at low density in basal DMEM (Sigma), spent medium collected at the end of a 72 hours growth period (in triplicate) and glucose, lactate, glutamine, and glutamate concentrations were measured using a Yellow Springs Instruments (YSI) 7100. Cell number was determined using a hemocytometer. The specific growth rate (μ) was estimated through regression of equation 1. The uptake/secretion rates were calculated using the normalized consumption/secretion coefficient (Δn/ΔX) which is multiplied by the estimated specific growth rate (μ), according to equation 2, in which Δn is the measured finite difference of moles consumed/produced, ΔX is the difference in cell density (cells/cm^2), and v is the specific uptake/secretion flux.

$$Ln\,(X) = Ln\,(X_0) + \mu t \qquad (1)$$

$$v = \mu \frac{\Delta n}{\Delta X} \qquad (2)$$

II.3. Polar Metabolites / Fatty-Acids Extraction and GC-MS Analysis

At the conclusion of labeling, metabolic activity was quenched with 0.4ml -80ºC methanol. An equal volume of distilled H_2O was added, cells were detached by pipette-scraping the plate and extracts were obtained by adding 0.8ml of -20ºC chloroform. Samples were centrifuged at 12,000rpm for10 min at 4ºC. For polar metabolite analysis, the aqueous phase (top) was collected and evaporated under airflow or using a vacuum centrifuge. Dried metabolites were dissolved in 30μl of 2% methoxyamine hydrochloride (Mox) in pyridine (Pierce), at 37°C for 1.5 hours, and derivatized by adding 45μl of N-methyl-N-(tert-butyldimethylsilyl)trifluoroacetamide (MBTSTFA) + 1% tert-butyldimethylchlorosilane (TBDMCS; Pierce) at 55-60°C for 1 hour. For ISA experiments, the chloroform phase containing the

non-polar metabolites (bottom) was collected and evaporated. Fatty acid methyl esters (FAMEs) were obtained by dissolving and reacting the dried chloroform fractions in either 50–100 µl of Methyl-8 reagent (Pierce) and incubating at 60ºC for 1hour, or in 500µl of 2% (v/v) H_2SO_4:methanol at 55-60ºC for 2 hours. After transesterification using method ii), FAMEs were isolated by adding 400µl of hexane and 100µl of saturated NaCl. The hexane phase was transferred to a new tube for evaporation under airflow. Dried FAMEs were dissolved in 50µl of hexane prior to injection on the GC-MS. GC-MS analysis was performed using an Agilent 6890 GC equipped with a 30m DB-35MS capillary column interfaced to an Agilent 5975B MS operating under electron impact (EI) ionization at 70 eV. One µl of sample was injected in splitless mode at 270°C, using helium as the carrier gas at a flow rate of 1 $ml.min^{-1}$. For measurement of polar metabolites, the GC oven temperature was held at 100°C for 3 min and increased to 300°C at 3.5°$C.min^{-1}$. For analysis of FAMEs, the initial GC oven temperature was 100ºC, then increased to 200ºC at 20°$C.min^{-1}$, to 230°C at 5°$C.min^{-1}$, and finally to 300C at 20°$C.min^{-1}$, at which held for 2.5min. The MS source and quadrupole were held at 230°C and 150°C, respectively, and the detector was operated in scanning mode, recording mass-to-charge-ratio spectra in the range of 100 – 605 *m/z*.

II.4. DNA Extraction and GC-MS Analysis

At the conclusion of the labeling period, cells were detached by trypsinization and centrifuged at 1,200 RPM for 5min. The supernatant was aspirated and the DNA isolated from the cell pellet using a DNeasy Blood & Tissue column (Qiagen). Column elution was performed with 100µl of DNAse-free water and the DNA concentration determined using a Nanodrop instrument (Thermo scientific). To hydrolyze the DNA into individual free bases, 200µl of 88% formic acid were added to the DNA-containing tubes, the solution (formic acid: H_2O, 2:1) transferred to a vacuum hydrolysis tubes (Thermo scientific) for hydrolysis at 140ºC for 1hr. Optimization experiments showed that no significant gain of GM-MS signal was obtained by extending the hydrolysis time. The hydrolyzed DNA was evaporated

under air-flow. Similarly to the polar metabolites, the free bases were derivatized using Mox and MBTSTFA + 1% TBDMCS, as previously described for the GC-MS analysis of nucleotide bases (O'Donoghue et al., 1994). The derivatization volume was adjusted so as to obtain a final DNA concentration of either 50ng/µl or 100ng/µl, based on the previous Nanodrop quantification. For the GC-MS analysis, either 1µl (of 100ng/µl) or 2µl (of 50ng/µl) sample was injected in splitless mode at 270°C, using helium as the carrier gas at a flow rate of 1 $ml.min^{-1}$. The GC-MS parameters were as described above for the polar metabolites; the GC oven temperature ramp was slightly modified to allow a better separation of late elution free bases, in particular adenine and guanine.

II.5. Cell Culture and Metabolic Labeling

All cell lines were obtained from ATCC, tested for mycoplasma, cultured in 5% CO_2 incubators and maintained in DMEM (GIBCO BRL) containing 10% FBS (Hyclone) supplemented with penicillin-streptomycin (Invitrogen). PRC3 and WT8 were described before (Iliopoulos et al., 1995). The VC3 glioma cell line was provided by T. Lautenschlaeger, MDA-MB-231 and HCT116 cell lines were provided by F. Chiaradonna, MRC5 cells were provided by S. Lippard, SN12C, ACHN and 786-O cells were provided by K. Courtney and L. Cantley, MCF10A cells were provided by J. Brugge. Neonatal epithelial kidney (NEK) cells were derived from transgenic mice engineered to harbor UBCcreER; Rosa 26 lox-stop-lox HIF1dPA or UBCcreER; Rosa 26 lox-stop-lox HIF2dPA or UBCcreER as control. NEK cell were cultured in DMEM/F12 medium supplemented with insulin-transferrin-selenium (Invitrogen 41400-045) and EGF (Gemini Bio300-110). Hypoxic culture was conducted by either i) feeding a custom mixture of 1% O_2, 5% CO_2 and 94% N_2 to a standard incubator controlled at 5% CO_2, or ii) using an hypoxia incubator (ESPEC, BNP-210). In some experiments, HEPES (Mediatech) was added to the culture medium at 20mM to maintain pH between normoxic and hypoxic cultures. The internal gas content was monitored using Fyrite gas analysers (Bacharach) for CO_2 and O_2. O_2 levels were confirmed at 1–3% during hypoxic culture. For isotopic labeling experiments, cells were seeded in 6

well plates and cultured with glucose- and glutamine-free DMEM (basal DMEM, Sigma, D5030), containing 10% dialyzed FBS (Hyclone), supplemented with 25mM naturally labeled glucose and the appropriate ^{13}C glutamine tracer, or with the appropriate ^{13}C glucose tracer (25mM) and 4mM naturally labeled glutamine, except in Chapter VI. In Chapter VI, all experiments were conducted using the basal DMEM supplemented with 10mM glucose and 2mM glutamine. We confirmed that these concentrations do not affect the growth rate of our cell lines and better reflect physiological conditions. [U-$^{13}C_5$] glutamine, [5-$^{13}C_1$] glutamine, [1-$^{13}C_1$] glutamine, [U-$^{13}C_6$] glucose, [3-$^{13}C_1$] glucose and [1,2-$^{13}C_2$] glucose were obtained from Cambridge Isotope Labs. For polar metabolite analyses, metabolic labeling was conducted for 24 hours. Labelling of fatty acids for ISA was conducted over 3–5 days of culture in an excess of tracer medium (3ml per well in a six-well plate) to prevent nutrient depletion. Labeling of biomass DNA was conducted for 8 days, wherein cell culture splitting was necessary to allow continuous labeling of growing cells during the entire time course.

II.6. Cell Viability Assays

Cells were cultured in basal DMEM supplemented with 25mM glucose, 1mM glutamine and 10% dialyzed FBS except in Chapter VI, in which the basal DMEM was supplemented with 10mM glucose, 2mM glutamine and 10% dialyzed FBS. Cells were cultured in either six- or twelve-well plates over 3 days with the appropriate medium, until confluence was reached in the control wells. In Chapter IV, cell number was determined manually and viability by trypan blue exclusion. In Chapters V and VI, cell viability was assayed by crystal violet staining. In brief, the medium was aspirated, and cells were fixed with a 6.25% glutaraldehyde solution for 10min. The fixating solution was aspirated and the wells rinsed twice with distillated H_20, stained with a 0.1% crystal violet solution for 40min and thoroughly rinsed with H_2O. Quantification of cell viability was determined by the absorbance of crystal violet-retaining cells at 595 nm.

II.7. Plasmids, Transfections and Generation of Cell Lines

In Chapter III, stable polyclonal cell populations with decreased IDH1 and IDH2 expression were generated by lentiviral-mediated shRNA expression. pLKO.1 lentiviral vectors targeting IDH1 had shRNA sequences of CCGGGCTGCTTGCATTAAAGGTTTACTCGAGTAAACCTTTAATGCAAGCAGCTTTTT (IDH1a; TRCN0000027298) and CCGGCGAATCATTTGGGAATTGATTCTCGAGAATCAATTCCCAAATGATTCGTTTTT (IDH1b; TRCN0000027289); IDH2 had shRNA sequence CCGGGTGGACATCCAGCTAAAGTATCTCGAGATACTTTAGCTGGATGTCCACTTTTT (TRCN0000027225). For controls, either non-targeting control shRNA (SHC002; Sigma) or pLKO.1 scrambled control vector34 (Addgene) were used. Cells were selected with 2 $\mu g.ml^{-1}$ puromycin. In Chapter IV, pBABE puro plasmids expressing HA-VHL mutants Y98H, Y98N, Y112H, Y112N, L188V and pBABE hygro plasmid expressing HA-HIF2α p-a were purchased from Addgene**.** EE-VHL were constructed by PCR amplification of wild type VHL with oligos forward 5'-GCGCGGATCCGCCACCATGGAATACATGCCCATGGAAATGCCCCGGAGGGCGGAG-3' and reverse 5'-GCGCGAATTCAATCTCCCATCCGTTGATGTGCAATG-3'. PCR product was restricted with BamHI and EcoRI and ligated into pBABE puro vector. Plasmids encoding shRNA targeting PDK1 (CCAGGGTGTGATTGAATACAA and GATCAGTGAATGCTTGTGAAA), ACLY (CGAGGACTTGTACTTCACCTA, GCCTCAAGATACTATACATTT and GCCTAAGTACTCTTGCCAGTT) and luciferase as control were obtained from the Broad TRC library available at Massachusets General Hospital (MGH). In Chapter V, stable polyclonal cell populations of Sk-Mel5 and 786-O cells with decreased NNT expression were generated by infection with lentiviral particles containing NNT-targeting pLKO.1 lentiviral vectors that had shRNA sequences of 5'-CCGGCCCTATGGTTAATCCAACATTCTCGAGAATGTTGGATTAACCATAGGGTTTTT-3' (NNTA; TRCN0000028541, Sigma) and 5'-

CCGGCGAGAAGCTAATAGCATTATTCTCGAGAATAATGCTATTAGCTTCTCGTTTTT-3' (NNTD; TRCN0000028507, Sigma). We used a non-targeting control shRNA sequence of CCGGCAACAAGATGAAGAGCACCAACTCGAGTTGGTGCTCTTCATCTTGTTGTTTTT (scramble control; SHC002, Sigma) as control. Cells were selected with 2 μg.ml^{-1} puromycin. For the exogenous expression of NNT, Sk-Mel5 cells were transfected with a pCMV6-Entry vector containing a full length cDNA clone of NNT (RC224002; OriGene) together with TurboFectin 8 transfection reagent (OriGene). A polyclonal population was generated by selecting the SkMel5 cells with 0.75 mg.ml^{-1} neomycin (G418) for 2–3 weeks. For all experiments with genetically-engineering cell lines, cells were selected for at least two passages before initiating tracer and flux experiments. Suitable lentiviral or retroviral-packaging plasmids were co-transfected with each of the targeting or control vectors into HEK293T cells, and supernatants containing lentiviruses or retroviruses were collected after 48-72hrs, filtered, and used for infection.

II.8. Determination of NAD(P)$^+$/NAD(P)H ratios

Cellular NAD(P)$^+$/NAD(P)H levels were assayed using a fluorescence-based assay kit, according to the manufacturer's instructions (Cell Technology). Standard deviations of mean (SEM) of ratios were calculated using a first-order Taylor approximation of averaged ratios obtained from triplicate measurements. One representative experiment was shown. In Chapter IV, the NADP$^+$/NADPH ratio was also determined employing the method developed in Krebs lab, as described therein (Veech et al., 1969). In brief, the isocitrate dehydrogenase (IDH) equilibrium (equation 3) was used to determine the ratio of NADP$^+$/NADPH. The equilibrium concentrations of the oxidized (α-ketoglutarate) and reduced (isocitrate/citrate) metabolites of the associated NAD(P)-linked dehydrogenase were measured to determine the correspondent ratios of *free* dinucleotides. Cells were rinsed twice with 2ml PBS before extraction to eliminate the contribution of extracellular metabolites. Ratios were obtained from individualized metabolite measurements in the same GC-MS injection. In Chapter V, Cellular

NAD(P)H/NAD(P)$^+$ ratios were also measured by LC-MS, employing a methanol extraction, as described previously (Yuan et al., 2012).

$$\frac{[\alpha-\text{ketoglutarate}]\,[CO2]\,[NADPH]}{[\text{Isocitrate}][NADP+]} = \text{K (IDH)} = 1.17\ \text{M} \quad (3)$$

II.9. Western Blotting

Proteins were extracted and immune-blotted as described before (Zimmer et al., 2008). Cells were rinsed twice with ice-cold PBS and lysed for 30min using RIPA buffer supplemented with protease inhibitors. Cell were scraped, clarified by centrifugation at 12,000rpm for 10min, and the proteins were resolved in SDS-PAGE gels, transferred to PVDF membrane (Bio-Rad), and detected using the following antibodies: anti-IDH1 (Santa Cruz Biotechnology or Cell Signaling), anti-IDH2 (Abcam or Novus Biologicals), rabbit polyclonal anti-HIF-1α (BD Biosciences), rabbit polyclonal anti-HIF-2α (Novus NB100-122), anti-VHL (IG32), anti-GLUT1 (Alpha Diagnostics), anti-GLS (Abnova), anti-GLUD1 (Novus Biologicals), anti-ACLY (Cell Signaling), anti-PDK1 (Cell Signaling), anti-NNT (Invitrogen), anti-Actin (Neo-markers, or Novus Biologicals), and anti-tubulin (Sigma). For some immune-blotting experiments (Chapter V), proteins were extracted with a 2-5% SDS solution to maximize lysis of mitochondrial proteins (e.g., NNT). Cells were then scraped, and proteins denatured at 95 °C for 10 min. Cell lysates were clarified by centrifugation. Proteins were detected using the appropriate horseradish-peroxidase-conjugated secondary antibodies (anti-mouse, anti-rabbit or anti-goat) and chemiluminescence.

II.10. Animal Studies

All protocols conformed to institutional regulation. We tested *VHL*-deficient RCC 786-O, UMRC2 and UMRC3 cells and chose the latter as xenograft models based on the growth aggressiveness *in vivo*. 5 x 10^6 UMRC3 cells were injected subcutaneously into the right flank of nu/nu mice. When tumors reached 100 mm^3, BPTES (12.5mg/kg) or vehicle control (1.5 % DMSO in 1M Tris, pH 8) was administered intraperitoneally (Chapter IV). 5 x 10^6 knockdown and control SkMel5 cells were injected subcutaneously in the left and right flank of nu/nu mice, respectively. At day 20, animals were sacrificed by cervical dislocation, and tumors were collected and weighed (Chapter V). The tumor volumes were calculated as length [mm] x $width^2$ [mm^2] x 0.5. For *in vivo* ^{13}C labeling studies (Chapter IV), UMRC3 cells were injected in both flanks of nu/nu mice. ^{13}C labeling infusions were begun when tumors reached an external diameter of 1-1.5 cm. Animals (n=3) were infused with [1-$^{13}C_1$] glutamine, as previously described(Marin-Valencia et al., 2012). In brief, a bolus of 0.28 $mg.g^{-1}$ bodyweight (300 µl) was administrated over 1 min and followed by a continuous infusion of 0.005$mg.g^{-1}.min^{-1}$ at 450 $µl.h^{-1}$ during 0.5, 1, 2 or 6 hours. Non-infused animals were used as controls for further analysis. At the end of indicated infusion times, blood was collected from the heart and animals sacrificed by cervical dislocation. Tumors and kidneys were quickly dissected, weighted, frozen in liquid nitrogen and stored at -80 ºC. Tumors weighted between 1.124 ± 0.136 g (mean ± SEM). Tumors from one flank were used for NMR analysis and extracted as previously described (Cerdan et al., 1990). Tumors and kidneys from the other flank were used for GC-MS analysis and metabolites extracted as previously described (Wu et al., 2008).

II.11. ^{13}C NMR Spectroscopy

High-resolution proton-decoupled ^{13}C NMR spectra of tumor extracts were obtained at 11.7 T (125.13 Hz, 25ºC, pH = 7.2) in a Bruker AVANCE 500WB NMR spectrometer using a commercial (5 mm) triple-resonance probe (^{1}H, ^{13}C, ^{2}H) optimized for direct ^{13}C detection. The acquisition conditions were: 30º flip angle, 30 kHz spectral width, 3s relaxation delay, and 1.09s acquisition time. Proton decoupling was gated during all acquisition using a broad-band composite pulse decoupling sequence, and chemical shifts were calibrated with dioxane (0.1 % vol/vol, 67.4 ppm). Resonance assignments were based on literature values and internal standards. Spectra deconvolution was performed using the software MestRec-C 4.8.6.0. (Mestrelab Research S.L.). ^{13}C NMR resonance areas were normalized relative to the dioxane resonance area used as internal reference.

II.12. Statistical Analysis

For MFA and ISA results, error bars represent 95% confidence intervals. In all other experiments, error bars represent SEM unless otherwise noted. Statistical significance was determined using two-tailed Student's t test, unless otherwise noted. *$p < 0.05$, **$p < 0.001$.

"Science progresses funeral by funeral."

Max Planck

This page was intentionally left blank

Chapter III

III. Reductive Carboxylation by IDH1 mediates lipogenesis under hypoxia

Chapter III presents doctoral work published in a peer-reviewed scientific journal:

Metallo CM, Gameiro PA, Bell EL, Mattaini KR, Yang J, Hiller K, Jewell CM, Johnson ZR, Irvine DJ, Guarente L, Kelleher JK, Vander Heiden MG, Iliopoulos O*, Stephanopoulos G*. (2012). Reductive glutamine metabolism by IDH1 mediates lipogenesis under hypoxia. ***Nature*** 481, 380-4.

*Corresponding authors.

III.1. ABSTRACT

Mammalian cells must consume glucose and glutamine to support biosynthetic processes necessary for growth. Acetyl coenzyme A (AcCoA) is a major precursor for lipid synthesis and is, conventionally, generated from glucose-derived pyruvate through the citrate shuttle and ATP citrate lyase (ACLY) in the cytosol. However, cancer cells and, more pronouncedly, those exposed to hypoxia convert most of the glucose to lactate, directing glucose carbons away from the Krebs cycle and lipid synthesis. Although it is recognized that cancer cells rely on glutamine-dependent anaplerosis to maintain a functional Krebs cycle, the regulation of glutamine utilization in hypoxic conditions is not understood. Specifically, it is unclear how hypoxic cells can maintain *de novo* lipogenesis, since glutamine oxidation in the Krebs cycle can replenish the four-carbon intermediates but not AcCoA. Alternatively, glutamine-derived α-ketoglutarate can be reductively carboxylated by isocitrate dehydrogenase 1 (IDH1) or 2 (IDH2) to generate citrate (reductive carboxylation), and recent studies have indicated that the IDH reaction is highly reversible. Here we show that human cells exposed to hypoxia conditions rely almost exclusively on reductive carboxylation by IDH1 to support *de novo* lipogenesis. Furthermore, renal cell lines deficient in the von Hippel–Lindau tumor suppressor protein (pVHL) that constitutively express the hypoxia-inducible factors (HIFs) preferentially use reductive carboxylation for lipid biosynthesis even at normal oxygen levels. These results identify RC as the major pathway lipid synthesis under hypoxia, and warrant further investigation on the HIF signaling and molecular mechanisms underlying the reductive phenotype under hypoxia.

While cancer cells shift towards a glycolytic metabolism (Semenza, 2010), glutamine-derived carbons are required for a functional Krebs cycle, cell cycle progression and proliferation (Wise and Thompson, 2010). More pronouncedly, low oxygen conditions (hypoxia) lead to the stabilization of the hypoxia-inducible factors (HIF-1α and/or HIF-2α), shunting most of the pyruvate away from the Krebs cycle and Acetyl-CoA (AcCoA) synthesis (Denko, 2008; Gordan and Simon, 2007). This prompted us to

understand how hypoxic and perhaps true Warburg-like cells reprogram their glutamine utilization to maintain macromolecule synthesis, in specific lipogenesis. Glutamine is catabolized into glutamate, which can be converted to α-ketoglutarate (α-kg) either in the cytosol or mitochondria. Glutamine-derived α-kg can contribute carbon to lipogenic AcCoA through two distinct pathways: i) α-kg can be oxidized in the Krebs cycle and generate pyruvate (via malic enzyme) (DeBerardinis et al., 2007), which can be converted to lipogenic AcCoA by the mitochondrial pyruvate dehydrogenase (PDH), or ii) α-kg can be reductively carboxylated by the NADPH-dependent isocitrate dehydrogenase enzyme 1 (IDH1) or 2 (IDH2) to generate isocitrate – the reductive carboxylation (RC) pathway. ^{13}C isotopic studies have reported that RC contributes to *de novo* lipogenesis in brown adipocytes (Yoo et al., 2004, 2008), and it has been shown that the IDH reaction is highly reversible in cancer cells (Metallo et al., 2009; Ward et al., 2010). Here, we sought to elucidate the biosynthetic role of glutamine under hypoxia conditions, and show that hypoxia renders mammalian cells reliant on glutamine-derived RC to produce approximately 70-80% of *de novo* fatty-acids.

III.2. RESULTS

Reductive Carboxylation Is Active in Cancer Cell Lines and the Major Route of Glutamine-Derived Lipids

We observed that the A549 lung carcinoma cell line exhibited an increased glutamine uptake at approximately 1% oxygen (hypoxia) when compared to 21% oxygen (normoxia), while glutamate secretion remained unchanged (Figure III-1A). This suggested that hypoxic cells may exhibit an increased demand for glutamine-carbons to support biosynthesis. Glucose consumption and lactate secretion rates were also elevated in hypoxia when compared to normoxia conditions, as expected upon a HIF-mediated switch to anaerobic metabolism. First, to investigate the biosynthetic role of glutamine under normoxia, we cultured several human-derived cancer cell lines in the presence of ^{13}C glutamine tracers for several days and compared their contribution to the formation of fatty-acids by gas chromatography-mass spectrometry (GC-MS). To trace which pathway cells use to metabolize

glutamine carbon into lipids we used either [5-$^{13}C_1$] glutamine or [U-$^{13}C_5$] glutamine which transfers ^{13}C atoms to fatty-acids via RC or all pathways (glutaminolysis and RC), respectively [see Chapter II for atom transition map]. As shown in Figure III-1B, Sk-Mel5 melanoma cells incorporate the ^{13}C isotopic label from both [5-$^{13}C_1$] glutamine and [U-$^{13}C_5$] glutamine into palmitate, with little difference observed between the two tracers. To quantify the specific contribution of glutamine to lipid synthesis through RC or all pathways, we performed isotopomer spectral analysis (ISA), as described in Chapter II. In all cell lines tested, including those derived from lung, mammary, colon and squamous cell carcinoma as well as melanoma, glioblastoma and leukemia, [5-$^{13}C_1$] glutamine and [U-$^{13}C_5$] glutamine labeled approximately 15-25% of the *de novo* synthesized lipids and little difference was observed between the two tracers (Figure III-1C). This indicates that RC is the major pathway for glutamine-derived lipids, and that glutaminolysis is negligible in contributing to *de novo* lipogenesis. To confirm the RC activity in the Krebs cycle, we cultured some of the cell lines in the presence of [1-$^{13}C_1$] glutamine for 24 hours under normoxia, wherein one ^{13}C atom is transferred to Krebs cycle metabolites through RC but not through glutamine oxidation (glutaminolysis) [See Chapter II]. The cell lines tested significantly incorporated label from [1-$^{13}C_1$] glutamine in citrate and metabolites downstream of the irreversible ACLY thereby showing active RC activity in the Krebs cycle, as determined by the percent M1 enrichment in the metabolite pools (Figure III-1D). The glutaminolysis pathway is also an important means of glutamine catabolism and can be characterized by quantifying the contribution of glutamine carbon to lactate. Consistent with the literature (DeBerardinis et al., 2007), glutamine-derived ^{13}C label from [U-$^{13}C_5$]glutamine was also detected in lactate, and the percentage of M3 lactate was higher in glioma cells (Figure III-1E). These observations show that RC is active in several cancer cell lines and is the major route of glutamine utilization for lipid synthesis (over glutamine oxidation) in cultured cells.

Next, we sought to test which isoenzyme(s) are responsible for the RC activity. Mammalian cells express three IDH enzymes encoded by separate genes: IDH1 (cytosolic, $NADP^+$-dependent), IDH2 (mitochondrial, $NADP^+$-dependent) and the multi-subunit enzyme IDH3 (mitochondrial, NAD^+-

dependent). IDH3 is allosterically regulated and is thought to operate in the oxidative direction. The $NADP^+$-dependent isozymes are capable of catalyzing the RC reaction; however, the specific enzyme responsible for this flux is not definitively known (Dalziel and Londesborough, 1968; Siebert et al., 1957). As measurements of metabolite pools in subcellular compartments and labeling therein cannot yet be reliably obtained, we used RNA interference to knockdown expression of IDH1 and IDH2 selectively in A549 cells (Figure III 1-F). Using the percent M1 labeling from of [1-$^{13}C_1$] glutamine as a readout, we measured a significant and robust decrease in RC activity when IDH1 messenger RNA (mRNA) was targeted using short hairpin RNAs (shRNAs) (Figure III-1G). These changes were consistent with results using [U-$^{13}C_5$] glutamine and reproduced using several cell lines (data not shown). Finally, we employed ^{13}C metabolic flux analysis (MFA) to determine absolute fluxes in control and IDH1-knocked down A549 cells, using [U-$^{13}C_5$] glutamine (MFA is described in Chapter II). The fitted data showed that reductive IDH flux is significantly decreased in IDH1-knocked down when compared to control cells (Figure III-1H), and this change was the primary alteration observed in the network (data not shown). These results suggest that IDH1 contributes to the RC flux observed in A549 cells. We confirmed that IDH1 is indeed capable of converting NADPH, α-kg and CO_2 to isocitrate and $NADP^+$ by enzymatic analysis using a recombinant IDH1 protein (data not shown). The proliferation rate of A549 and other cell lines with IDH1 knockdown was impaired (Figure III-1I and data not shown), indicating that reductive metabolism of glutamine in the cytosol may be necessary for robust growth. In contrast to our results with IDH1 shRNAs, we detected no significant change in reductive flux when targeting IDH2 mRNA in A549, MDA-MB-231 and HCT116 cells (data not shown). Although IDH2 may promote RC in some tissues or conditions, these results are consistent with the proposed role of IDH2 as an oxidative Krebs cycle enzyme (Hartong et al., 2008). Together, these findings show that i) several cancer cell lines exhibit active RC by IDH1 *in vitro,* ii) reductive glutamine metabolism (via RC) is the primary pathway through which glutamine carbons are converted to lipids in cultured cells iii) the RC pathway contributes to approximately 20% of *de novo* lipogenesis under normoxia.

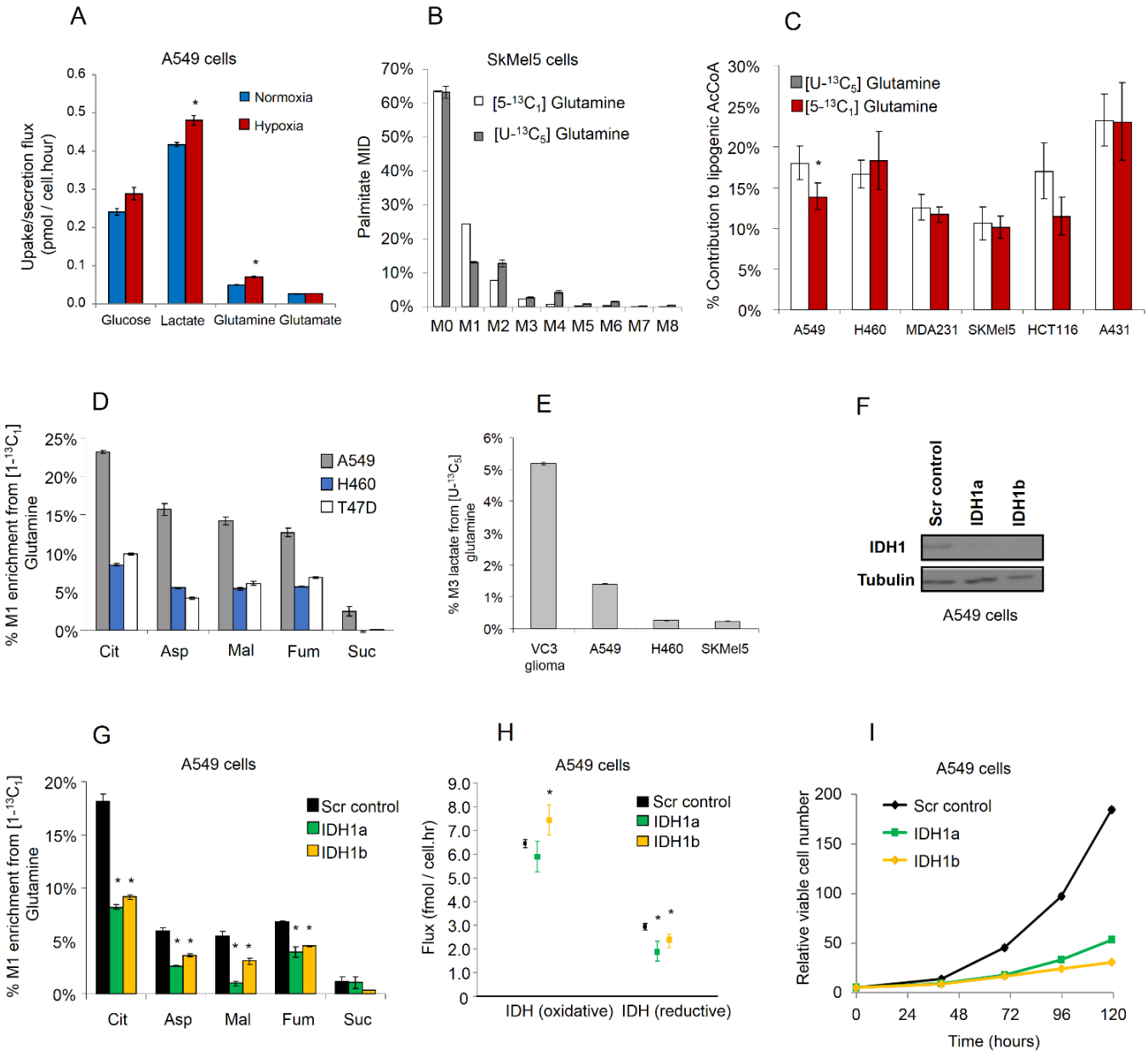
A
A549 cells
Upake/secretion flux (pmol / cell.hour)
Normoxia
Hypoxia
Glucose
Lactate
Glutamine
Glutamate
B
SkMel5 cells
Palmitate MID
[5-13C1] Glutamine
[U-13C5] Glutamine
M0 M1 M2 M3 M4 M5 M6 M7 M8
C
% Contribution to lipogenic AcCoA
[U-13C5] Glutamine
[5-13C1] Glutamine
A549
H460
MDA231
SKMel5
HCT116
A431
D
% M1 enrichment from [1-13C1] Glutamine
A549
H460
T47D
Cit
Asp
Mal
Fum
Suc
E
% M3 lactate from [U-13C3] glutamine
VC3 glioma
A549
H460
SKMel5
F
Scr control
IDH1a
IDH1b
IDH1
Tubulin
A549 cells
G
A549 cells
% M1 enrichment from [1-13C1] Glutamine
Scr control
IDH1a
IDH1b
Cit
Asp
Mal
Fum
Suc
H
A549 cells
Flux (fmol / cell.hr)
Scr control
IDH1a
IDH1b
IDH (oxidative)
IDH (reductive)
I
A549 cells
Relative viable cell number
Scr control
IDH1a
IDH1b
Time (hours)

Figure III-1. Reductive Carboxylation Is the Primary Pathway of Glutamine Conversion to Lipids

(A) Cell-specific uptake and secretion of glucose/glutamine and lactate/glutamate. Metabolite levels were measured at the start and end of culture and normalized to the integral viable cell density to calculate fluxes. (B) Mass Isotopomer Distribution (MID) of biomass-extracted palmitate in SkMel5 cells cultured for 3 days in the presence of either [U-$^{13}C_5$] glutamine or [5-$^{13}C_1$] glutamine. (C) Specific contribution of [U-$^{13}C_5$] glutamine or [5-$^{13}C_1$] glutamine to lipogenic AcCoA in the indicated cell lines, determined by isotopomer spectral analysis (ISA). (D) Evidence for reductive carboxylation activity in A549, H460 and T47D cells using [1-$^{13}C_1$] glutamine, determined by the % M1 label in metabolite pools. (E) Glutaminolysis activity in the indicated cancer cell lines. (F) Expression levels of IDH1 in A549-derived cell lines, as indicated. (G) Relative contribution of reductive carboxylation in the panel of A549 cell lines, using the [1-$^{13}C_1$] glutamine tracer. (H) IDH flux estimates from ^{13}C metabolic flux analysis (MFA) model in control or IDH1-knocked down A549 cells cultured with [U-$^{13}C_5$] glutamine. (I) Cell proliferation of the panel of A549 cell lines. Statistical significance compares hypoxia to normoxia conditions in (A), [5-$^{13}C_1$] glutamine to [U-$^{13}C_5$] glutamine in (C), and IDH1-knocked down to control cells in (G), (H). Error bars represent 95% confidence intervals in panels (C), (H). Cit, citrate; Asp, aspartate; Mal, malate; Fum, fumarate; Suc, succinate; IDH, isocitrate dehydrogenase; Scr, scramble.

Reductive Carboxylation Is the Primary Pathway for *De Novo* Lipogenesis under Hypoxia Conditions

To test the contribution of RC activity in hypoxia, we cultured A549 in the presence of [1-$^{13}C_1$] glutamine for 24 hours and measured the percent of ^{13}C enrichment in the pools of Krebs cycle metabolites. We observed a significant increase in the contribution of RC to the Krebs cycle in A549 cells cultured under hypoxia, and the IDH1 knockdown decreased its activity in both normoxia and hypoxia (Figure III-2A). Because glucose is typically the primary carbon source for lipid synthesis, we sought to test the effect of hypoxia on the contribution of glucose oxidation versus RC (from glutamine) to fatty-acid synthesis. To this end, we cultured A549 cells for several days in the presence of either [U-$^{13}C_6$] glucose or [5-$^{13}C_1$] glutamine under normoxia or hypoxia conditions. Strikingly, we observed a marked change in the fatty-acid labeling patterns from both substrates (Figure III-2B, 2C). A549 cells preferentially used glucose for palmitate synthesis under normoxic conditions. In contrast, palmitate produced under hypoxia was primarily synthesized from glutamine through the reductive pathway. In fact, RC accounted for approximately 80% of the carbon used for *de novo* lipogenesis in A549 cells

growing under hypoxia whereas the contribution of [U-$^{13}C_6$] glucose to fatty-acid synthesis was dramatically decreased in this condition, as quantified by isotopomer spectral analysis (ISA) (Figure III-2D). Although proliferation rates and relative *de novo* lipogenesis were lower under hypoxia (data not shown and Figure III-2E), the absolute flux of reductive glutamine metabolism to palmitate synthesis was significantly increased in hypoxic cultures (Figure III-2F). Knocking down IDH1 also mitigated the use of RC for lipogenesis under hypoxia (Figure III-2G). Together, these findings show that hypoxia switches the substrate preference from glucose to glutamine-derived carbons to support approximately 70-80% of *de novo* lipogenesis. We therefore hypothesized that hypoxia increases the glutamine dependency to support proliferation. Indeed, we found that hypoxic cells were more sensitive to glutamine withdrawal than cells grown under normoxia conditions (Figure III-2H). Of note, the reductive carboxylation switch under hypoxia is not a cell line specific phenomenon, and a similar reductive phenotype was observed in all cancer cell lines from different tissues, including lung carcinoma (H1299), osteosarcoma (143B), colorectal carcinoma (HCT116), breast adenocarcinoma (MDA MB-231), melanoma (SkMel5) and also non-transformed cells such as MRC5 cells and T lymphocytes (Figure III-I and data not shown).

Hypoxia Promotes Reductive Carboxylation by Inhibiting the Pyruvate Dehydrogenase Flux

To gain insight into the mechanisms controlling this switch to reductive glutamine metabolism, we analyzed changes in the labeling and abundances of Krebs cycle metabolites in cells grown under hypoxia. Hypoxia leads to the stabilization of HIF-1α, which activates glycolytic enzymes, lactate dehydrogenase A (LDH-A) and pyruvate dehydrogenase kinase 1 (PDK1). Thus, HIF activation promotes a glycolytic program that shunts pyruvate away from the mitochondrion and towards lactate production. We observed a significant decrease in relative contribution of pyruvate dehydrogenase (PDH) complex in the lung carcinoma A549 cell line and non-transformed lung MRC5 cells grown under hypoxia, as determined by the percent M2 enrichment in Krebs cycle metabolites from [U-$^{13}C_6$] glucose

(Figure III-3A). In addition, we observed that the citrate pool became depleted in hypoxic when compared to normoxic cells (Figure III-3B). Conversely, using the [1-$^{13}C_1$] glutamine tracer, we observed a dramatic increase in the contribution of RC to the Krebs cycle in hypoxic MRC5 cells (Figure III-3C), consistent with our previous results showing the lipogenic switch to RC under hypoxia. Given the marked reduction in the PDH activity observed in hypoxia, we hypothesized that the RC switch in hypoxia is driven by a low PDH flux in the Krebs cycle. We tested the ability of dichloroacetate (DCA) to restore PDH activity and mitigate the contribution of reductive metabolism to lipogenesis. DCA inhibits pyruvate dehydrogenase kinase (PDK1) (Bonnet et al., 2007), which is a known HIF-1α target that phosphorylates and inhibits PDH. Although DCA treatment had no observable effect on glucose and glutamine utilization under normoxia, it restored glucose oxidation in the Krebs cycle (Figure III-3D) and inhibited the contribution of RC to lipogenic AcCoA in hypoxic A549 cells (Figure III-3E). These observations show that hypoxia coordinates glucose oxidation (inhibiting it) and RC (activating it) to maintain *de novo* lipogenesis, and raise the hypothesis that hypoxic-mediated low PDH flux may stimulate the RC flux through a mass action effect. However, further studies are warranted in understanding whether modulation of the PDH flux and citrate levels by hypoxia or “pseudo-hypoxia” promote the RC flux through mass-action kinetics.

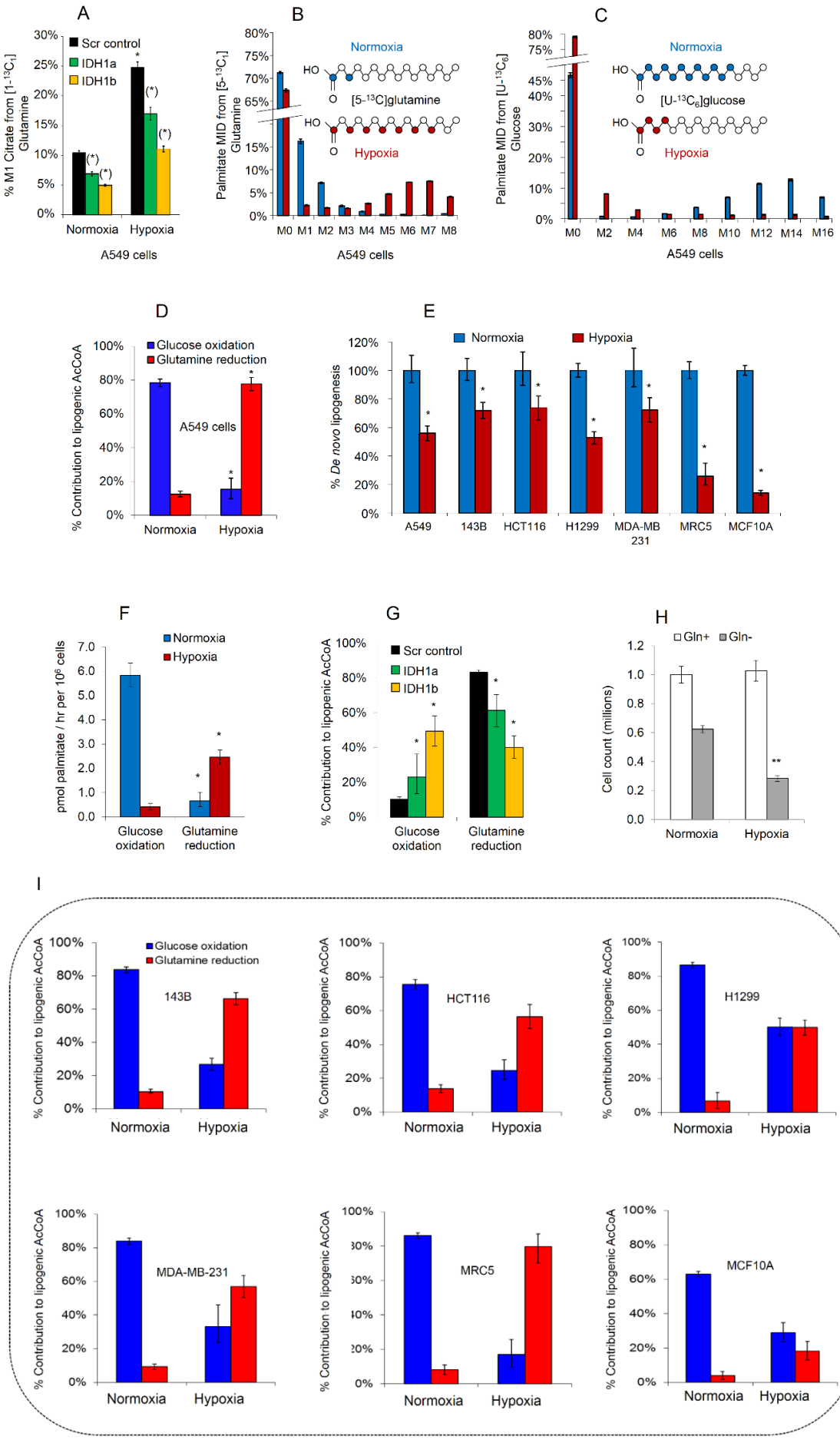
A
% M1 Citrate from [1-13C1] Glutamine
Scr control
IDH1a
IDH1b
Normoxia
Hypoxia
A549 cells
B
Palmitate MID from [5-13C1] Glutamine
Normoxia
[5-13C]glutamine
Hypoxia
M0 M1 M2 M3 M4 M5 M6 M7 M8
A549 cells
C
Palmitate MID from [U-13C6] Glucose
Normoxia
[U-13C6]glucose
Hypoxia
M0 M2 M4 M6 M8 M10 M12 M14 M16
A549 cells
D
% Contribution to lipogenic AcCoA
Glucose oxidation
Glutamine reduction
A549 cells
Normoxia Hypoxia
E
% De novo lipogenesis
Normoxia
Hypoxia
A549 143B HCT116 H1299 MDA-MB 231 MRC5 MCF10A
F
pmol palmitate / hr per 10^6 cells
Normoxia
Hypoxia
Glucose oxidation
Glutamine reduction
G
% Contribution to lipogenic AcCoA
Scr control
IDH1a
IDH1b
Glucose oxidation
Glutamine reduction
H
Gln+ Gln-
Cell count (millions)
Normoxia Hypoxia
I
% Contribution to lipogenic AcCoA
Glucose oxidation
Glutamine reduction
143B
HCT116
H1299
MDA-MB-231
MRC5
MCF10A
Normoxia Hypoxia

Figure III-2. Hypoxia Reprograms Cells to Rely on Reductive Carboxylation for De Novo Lipogenesis

(A) Effect of hypoxia on the relative contribution of reductive carboxylation (RC) in control and IDH1-knocked down A549 cells. (B and C) ^{13}C Labeling of palmitate extracts from A549 cells cultured under normoxia or hypoxia with [5-$^{13}C_1$] glutamine (B) or [U-$^{13}C_6$] glucose (C). Similar results were observed in myristate, oleate and stearate pools (not shown). (D) Specific contribution of glucose oxidation ([U-$^{13}C_6$] glucose) or glutamine reduction ([5-$^{13}C_1$] glutamine) to lipogenic AcCoA in A549 cells under normoxia and hypoxia, determined by isotopomer spectral analysis (ISA). (E) Specific rates of *de novo* lipogenesis determined via ISA modeling as described in the experimental procedures. g(t) values were normalized to those of normoxic culture and normalized by palmitate abundances in order to account for differences in cell growth/number. (F) Absolute contribution (flux) of [U-$^{13}C_6$] glucose and [5-$^{13}C_1$] glutamine to palmitate in A549 cells, determined by multiplying the specific contribution determined in (D) by the palmitate abundance in normoxia/hypoxia. (G) Effect of IDH1 knockdown on the relative contribution of glucose oxidation and glutamine reduction to palmitate in A549 cells cultured under hypoxia conditions. (H) Huh7 cell proliferation after 4 days in the presence or absence of glutamine. Statistical significance compares hypoxia to normoxia conditions in (D), (E), (F), (H), IDH1-knocked down to control cells in (G) (asterisk in parenthesis in (A) indicates comparison between control and IDH1-knocked down cells). (I) ISA analysis to determine the contribution of glucose oxidation and glutamine reduction to lipogenic AcCoA in different cell lines Note that MCF10A cells were cultured in DMEM/F12 basal medium with 5% horse serum that was not dialyzed. Therefore unlabeled glutamine, glutamate, and proline were present an potentially dilute the contribution of [5-$^{13}C_1$] glutamine to lipids. Error bars represent 95% confidence intervals in panels (D), (E), (F), (G), (I). IDH, isocitrate dehydrogenase; Scr, scramble.

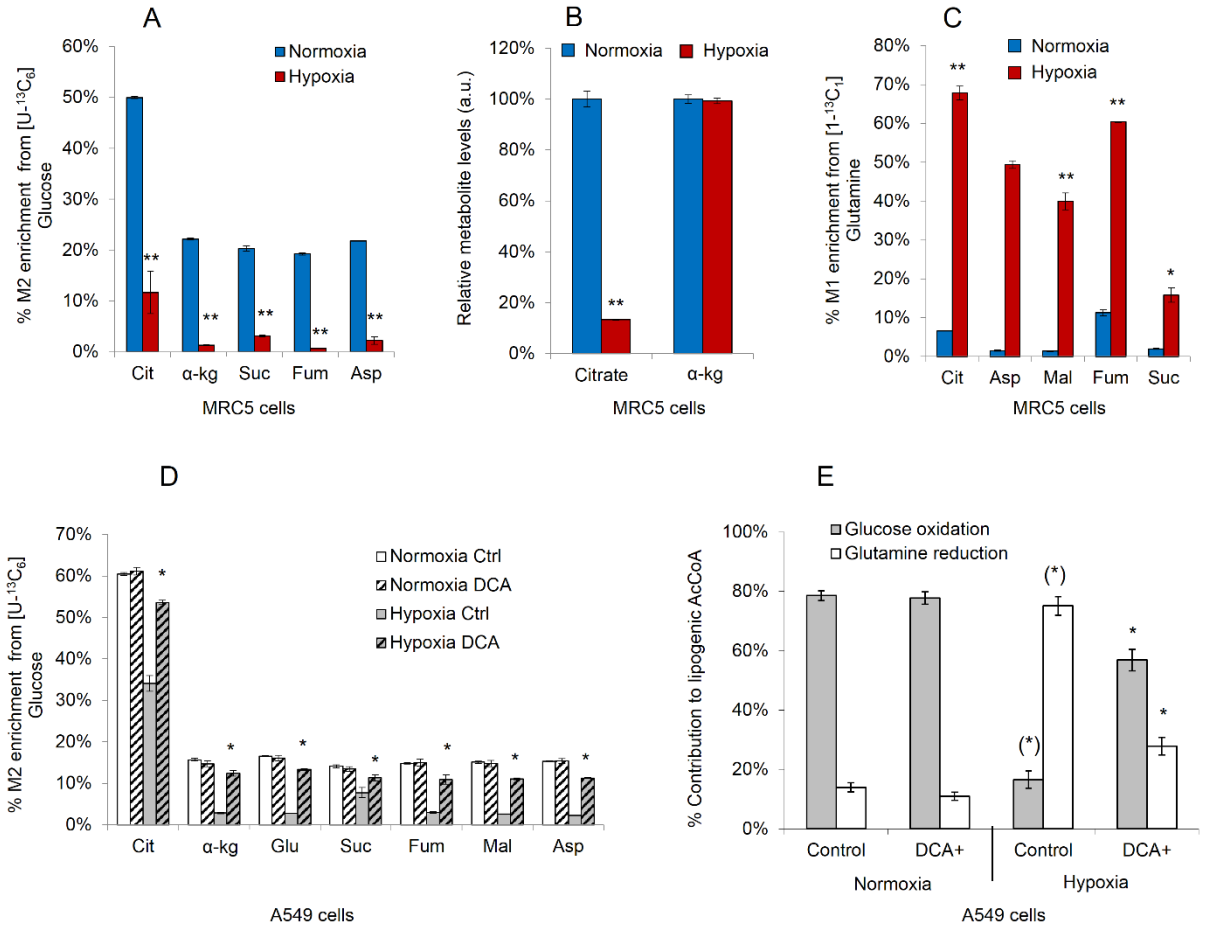

Figure III.23. Evidence for Regulation of Reductive Carboxylation by the PDH Flux under Hypoxia

MRC5 and A549 cells were cultured under normoxia or hypoxia for 3 days in the presence of either [U-$^{13}C_6$] glucose or [1-$^{13}C_1$] glutamine (A) Relative contribution of glucose oxidation in the Krebs cycle in MRC5 cells, as determined by the percent M2 enrichment from [U-$^{13}C_6$] glucose (see experimental procedures for atom transition map). (B) Relative abundance of citrate and α-ketoglutarate pools in normoxic and hypoxic MRC5 cells (C) Relative contribution of reductive carboxylation to the formation of Krebs cycle metabolites in normoxic and hypoxic MRC5 cells, determined by percent M1 enrichment from [1-$^{13}C_1$] glutamine. (D) Relative contribution of glucose oxidation in the Krebs cycle in A549 cells cultured with or without dichloroacetate (DCA) (5mM) under normoxia and hypoxia. (E) Specific contribution of glucose oxidation and glutamine reduction to lipogenic AcCoA in A549 cells cultured with or without 5mM DCA, determined by isotopomer spectral analysis (ISA). Statistical significance compares hypoxia to normoxia conditions in (A), (B), (C), DCA-treated to untreated cells under hypoxia in (D), (E) (asterisk in parenthesis in (E) indicates comparison between hypoxia and normoxia). Error bars represent 95% confidence intervals in panels (E). Cit, citrate; α-kg, α-ketoglutarate; Glu, glutamate; Suc, succinate; Fum, fumarate; Mal, malate; Asp, aspartate.

Loss of *VHL* Renders Renal Cancer Cells Reliant on RC for *De Novo* Lipogenesis Even Under Normoxia

The von Hippel–Lindau tumor suppressor protein (pVHL) is frequently lost in renal cell carcinoma (RCC) and results in a state of "pseudohypoxia", in which HIF signaling is activated even at normal oxygen levels (Figure III-4A) (Kim et al., 2003). To investigate the role of the VHL-HIF pathway in promoting the lipogenic switch to reductive carboxylation (RC), we labeled *VHL*-deficient RCC cells with either [U-$^{13}C_6$] glucose or [5-$^{13}C_1$] glutamine and performed ISA. Remarkably, *VHL*-deficient RCC cell lines preferentially used glutamine-derived RC for lipogenesis even under normal oxygen conditions, whereas those expressing wild-type (WT) *VHL* behaved similarly to other carcinoma cell lines (Figure III-4B). To test if pVHL expression is necessary to suppress RC, we metabolically labeled two isogenic clones that differ in pVHL expression (WT8 and PRC3 cells), derived from the 786-O RCC cell line (Iliopoulos et al., 1995). Indeed, expression of wild-type VHL (WT8 cells) resulted in a switch back to oxidative glucose metabolism as the source of carbon for lipid synthesis under normoxia (Figure III-4C). Furthermore, knocking down HIF-2α (Figure III-4D, 4E) partially inhibited RC and restored the contribution of glucose oxidation for lipid synthesis in *VHL*-deficient 786-O cells. These observations suggest that HIF is necessary to mediate RC under hypoxic or "pseudo-hypoxic" (VHL loss) conditions.

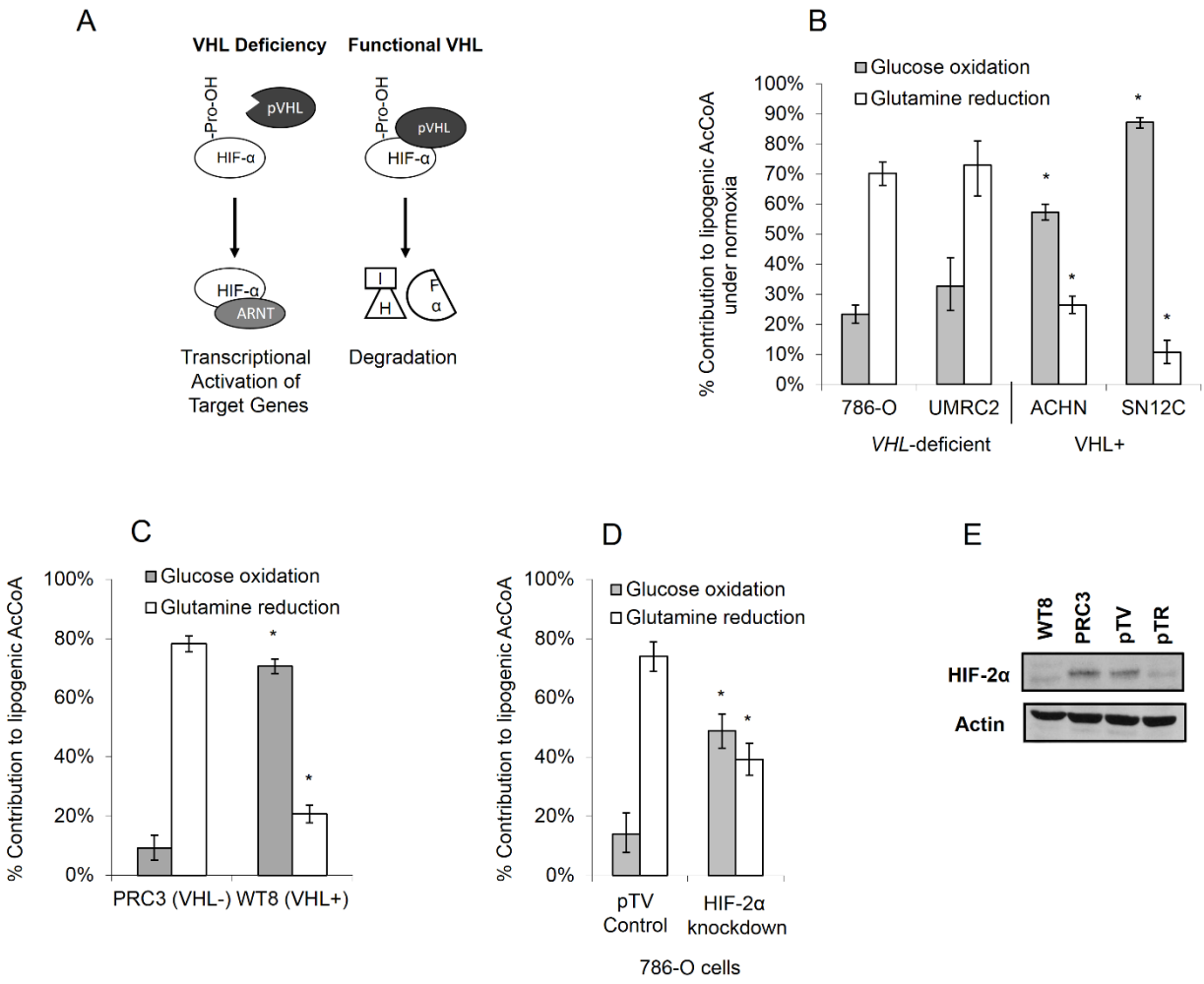

Figure III-4. Evidence for the Reductive Carboxylation Switch in Renal Cancer Cells Even under Normoxia

(A) Schematic of stabilized HIF-2α expression under normoxia conditions. (B-D). Specific contribution of glucose oxidation ([U-$^{13}C_6$] glucose) and glutamine reduction ([5-$^{13}C_1$] glutamine) to lipogenesis in renal cell carcinoma (RCC) lines (B), PRC3 (VHL-/-) and WT8 (VHL+/+) isogenic cells derived from the 786-O RCC line (C) and vector control (pTV) or HIF-2α knocked down (pTR) cells derived from 786-O RCC line (D), determined by the isotopomer spectral analysis (ISA) model. (E) Expression levels of HIF-2α in the panel of RCC cell lines used. Statistical significance compares *VHL*-positive to *VHL*-negative cells in (B), VHL-reconstituted to VHL-negative cells in (C), and HIF-2α knockdown to control 786-O cells. Error bars represent 95% confidence intervals in (B), (C), (D).

III.3. DISCUSSION

Here, we sought to investigate how hypoxia regulates central carbon metabolism. One on hand, the HIF-mediated glycolytic switch ensures that glucose-derived pyruvate is diverted towards lactate production; on the other, this must be reconcilable with a functional Krebs cycle and availability of AcCoA for lipid synthesis. Our ^{13}C isotopic studies showed that reductive carboxylation (RC) is a major pathway for *de novo* lipid synthesis under hypoxia, which represents a bona-fide switch in central carbon metabolism.

Theoretically, IDH1 and IDH2 are the NADPH-dependent isoenzymes capable of catalyzing the reductive conversion of α-kg into isocitrate. Our data provided evidence that RC in A549 and 143B cells involves IDH1-mediated catalysis in the cytoplasm. However, given the almost exclusive use of RC for lipogenesis under hypoxia, a redundant or contributing role of mitochondrial IDH2 in this pathway is probable. In fact, parallel studies reporting the RC switch under hypoxia show that IDH2 can contribute to the RC activity in glioma cells, RCC cells deficient in fumarate hydratase (FH) and cells with deficient mitochondria (Mullen et al., 2011; Wise et al., 2011). Thus, it is possible that the IDH isoenzyme responsible for RC depends on the cellular context or redox state.

Our ^{13}C isotopic studies showed that the RC-to-lipid switch also occurs in normal, non-transformed cells under hypoxia, suggesting that the reductive phenotype is specific to hypoxia and HIF. However, oxygen availability regulates a large family of α-ketoglutarate (α-kg) dependent cellular oxygenases, that regulate histone and DNA modifications (Melvin and Rocha, 2012). Although our observations suggested that HIF is required, at least in part, for the activation of RC, it is conceivable that additional hypoxia-associated changes may also promote RC in a HIF-independent manner. In this context, it is also unclear whether HIF is sufficient per se to promote RC, and we wished to further investigate the molecular mechanisms underlying the RC activation under hypoxia.

Our data showed that renal cancer carcinoma (RCC) cell lines deficient in the *VHL* tumor suppressor also rely on RC to produce approximately 80% of *de novo* fatty-acids even under normoxia.

This suggests that reductive glutamine utilization may be, not only associated with hypoxia, but also linked to specific cancer cells, in this case *VHL*-deficient RCC cells that exhibit constitute HIF expression. Indeed, the metabolic profiling of PRC3/WT8 cells suggested that wild-type *VHL* can restore glucose utilization for lipid synthesis. Also, knocking-down HIF-2α led to a partial suppression of RC in *VHL*-deficient RCC cells (Figure III-4D). However, since the VHL tumor suppressor protein (pVHL) has HIF-independent functions [see Chapter I], further studies are necessary to test whether the VHL-HIF interaction is strictly required to modulate the RC activity in RCC cells. Our findings also raised the possibility that *VHL*-deficient cells may be sensitive to glutamine deprivation, which may have therapeutic implications.

Myc has an established role in regulating glutamine catabolism, in particular glutaminolysis (Wise et al., 2008). This metabolic reprogramming provides an effective, glucose-independent means of fueling the Krebs cycle (Le et al., 2012) and potentially generating AcCoA for biosynthesis. This brings attention to signaling mechanisms by which cells divert α-kg to either oxidative Krebs cycle or RC. In this regard, there is evidence of differential cross-talk between HIF isoforms and myc function. Stabilization of HIF1α in hypoxia inhibits the interaction of myc with its transcriptional cofactors, whereas HIF-2α promotes cell cycle progression by enhancing myc function (Gordan et al., 2007). In this work, we did not investigate the specific role of HIF-1α and/or HIF-2α in activating RC, and *myc* amplifications may add to this complexity and promote glutaminolysis or RC, depending on their partnering with HIF-1α or HIF-2α correspondingly.

Hypoxia can be viewed as a hallmark of the tumor microenvironment, which leads to a HIF-dependent glycolytic program (Denko, 2008). Since glucose is delivered to cells through the vasculature, it may be limited in microenvironments with decreased oxygen availability (Gatenby and Gillies, 2004). The reductive metabolism of amino acids for lipid synthesis may therefore allow cells to conserve glucose for production of ribose and other biosynthetic precursors (for example, one carbon pool, hexosamines) that are not typically generated from other nutrients. Thus, activation of RC may

allow cells to distribute available nutrients more efficiently in poorly vascularized microenvironments. Our results added to the understanding of cellular plasticity in hypoxic environments.

This page was intentionally left blank

"To guarantee success, act as if it were impossible to fail."

Dorothea Brande

This page was intentionally left blank

Chapter IV

IV. In Vivo HIF-Mediated Reductive Carboxylation Is Regulated by Citrate Levels and Sensitizes VHL-Deficient Cells to Glutamine Deprivation

Chapter IV presents doctoral work published in a peer-reviewed scientific journal:

Gameiro PA, Yang J, Metelo AM, Pérez-Carro R, Baker R, Wang Z, Arreola A, Rathmell WK, Olumi A, López-Larrubia P, Stephanopoulos G, Iliopoulos O. (2013). In Vivo HIF-Mediated Reductive Carboxylation Is Regulated by Citrate Levels and Sensitizes VHL-Deficient Cells to Glutamine Deprivation*. ***Cell Metabolism*** 17, 372-85.

*This article was commented in Nature Reviews Cancer [Metabolism: Glutamine connections] and Cancer Discovery [Research Watch: Metabolism].

IV.1. ABSTRACT

We previously showed that hypoxic and *VHL*-deficient renal cell carcinoma (RCC) cells rely on glutamine to generate citrate and lipids through reductive carboxylation (RC) of α-ketoglutarate. Hypoxia Inducible Factors 1α/2α (HIF-1α / 2α) are stabilized and mediate critical cellular responses to hypoxia, with *VHL*-deficient cells exhibiting constitute HIF-1α/2α expression regardless of oxygen availability. To provide insights into the role of HIF and the molecular mechanisms underlying RC, we introduced into *VHL*-deficient RCC cells a series of tumor-associated *VHL* mutations that differ in their ability to inactivate HIF. Here, we show that reintroduction of either wild type or HIF-inactivating *VHL* mutants inhibits RC and lipogenesis from glutamine. In contrast, reintroduction of *VHL* mutants with attenuated or lost HIF inactivating properties failed to inhibit this pathway. Expression of a HIF-2α mutant was sufficient to induce RC and lipogenesis from glutamine in *VHL*-reconstituted RCC cells. Furthermore, HIF expression drastically reduced intracellular citrate levels under normoxia. Feeding *VHL*-deficient RCC cells with acetate or citrate or knocking down PDK-1 and ACLY restored citrate levels and suppressed RC. These data suggest that HIF-induced low intracellular citrate levels promote the reductive flux by mass action kinetics on the IDH reaction. Using [1-$^{13}C_1$] glutamine, we demonstrated *in vivo* RC activity in *VHL*-deficient tumors growing as xenografts in mice. Lastly, HIF rendered *VHL*-deficient cells sensitive to glutamine deprivation *in vitro*, and systemic administration of glutaminase inhibitors suppressed the growth of RCC cells as mice xenografts.

As introduced in Chapter I, “Warburg-like” or hypoxic cells mitigate glucose catabolism in the Krebs cycle. We and others demonstrated that cells under hypoxic conditions utilize glutamine to generate citrate and lipids through reductive carboxylation (RC) of α-ketoglutarate by isocitrate dehydrogenase 1 (IDH1) or 2 (IDH2) [See Chapter III and (Metallo et al., 2012; Mullen et al., 2011; Scott et al., 2011; Wise et al., 2011)].

Thus far, the mechanisms by which hypoxia promotes RC are under debate. As detailed in Chapter I, the *VHL* tumor suppressor protein (pVHL) exhibits several functions that are HIF-independent. In addition, while hypoxia inhibits the α-ketoglutarate (α-kg) dependent HIF prolyl hydroxylases (PHDs) and leads to HIF stabilization, oxygen availability also regulates other α-ketoglutarate dependent cellular oxygenases that mediate posttranslational modification of several substrates [See Chapter I]. Thus, it is conceivable that the effect of hypoxia or loss of *VHL* on RC activity that we reported in Chapter III may be mediated by signaling mechanisms independent of HIF. In addition, it is unclear whether HIF is sufficient to promote RC under normoxia conditions. Here, we demonstrate that the pVHL-HIF interaction is strictly necessary to modulate RC activity and that HIF is sufficient to promote the reductive pathway through a mass-action effect on citrate levels. Furthermore, we provide evidences for the biological significance of RC.

IV.2. RESULTS

Functional Interaction between pVHL and HIF Is Necessary to Inhibit RC

To test whether the inhibition of reductive carboxylation (RC) by pVHL requires its ability to bind and inactivate the alpha regulatory subunit of HIF, we tested a panel of VHL germline mutations that are linked to different clinical phenotypes of the *VHL* disease and differ in their affinity to bind HIF. Missense germline type 2A *VHL* mutations confer a low risk for RCC to their carrier individuals and retain an attenuated HIF binding and regulatory activity. In contrast, type 2B mutations, which are defective in HIF binding and regulation, confer a high risk for RCC. On the other hand, type 2C *VHL* germline mutations are associated with an increased risk of pheochromocytomas, but not RCC, and they retain the ability to bind and inactivate HIF in a manner similar to wild-type protein, an observation that suggests that type 2C mutations inactivate HIF-independent function(s) of pVHL (Li et al., 2007).

We infected *VHL*-deficient human UMRC2 renal carcinoma cells with retroviruses and generated polyclonal cell populations expressing wild-type pVHL or type 2A (Y112H), type 2B (Y98N, Y112N),

and type 2C (L188V) pVHL mutants. First, we confirmed that expression of HIF-1α/HIF-2α and their downstream target GLUT1 were downregulated in cells expressing wild-type pVHL or type 2C mutant protein (Figure IV-1A). The effect of type 2A pVHL mutations appeared intermediate between wild-type and type 2B mutations regarding GLUT1 (Figure IV-1A, GLUT1 lane).

To profile the metabolic phenotype of the engineered cell lines, we labeled the cells with either [U-$^{13}C_6$] glucose or [1-$^{13}C_1$] glutamine and determined the incorporation of each tracer in Krebs cycle metabolites using gas chromatography-mass spectrometry (GC-MS) (Figure IV-1B, see also Chapter II for complete atom transition map). Reintroduction of wild-type pVHL or type 2C pVHL mutant suppressed the contribution of RC from glutamine (Figure IV-1C), as determined by the degree of labeled carbon (M1 enrichment) of the indicated metabolites (Figure IV-1B, green circles). Conversely, type 2B mutants (Y112N/Y98N, which are defective in HIF inactivation) exhibited active RC to a level comparable to *VHL*-deficient control cells. We observed a concurrent regulation in glucose metabolism in the different *VHL* mutants. Reintroduction of wild-type or type 2C pVHL mutant, which can meditate HIF-α destruction, stimulated glucose oxidation via pyruvate dehydrogenase (PDH), as determined by the degree of ^{13}C-labeled Krebs cycle metabolites (M2 enrichment) (Figures IV-1D and IV-1E). In contrast, reintroduction of an HIF nonbinding Type 2B pVHL mutant failed to stimulate glucose oxidation, resembling the phenotype observed in *VHL*-deficient cells (Figures IV-1D and IV-1E). Additional evidence for the overall glucose utilization was obtained from the enrichment of M3 isotopomers using [U-$^{13}C_6$] glucose (Supplemental Figure S1A), which shows a lower contribution of glucose-derived carbons to the Krebs cycle in *VHL*-deficient RCC cells (via pyruvate carboxylase and/or continued Krebs cycling).

To test the effect of HIF activation on the overall glutamine incorporation in the Krebs cycle, we labeled an isogenic pair of *VHL*-deficient and *VHL*-reconstituted UMRC2 cells with [U-$^{13}C_5$] glutamine, which generates M4 fumarate, M4 malate, M4 aspartate, and M4 citrate mass isotopomers through glutamine oxidation (see Chapter II). As seen in Supplemental figure S1B, *VHL*-deficient/*VHL*-positive

UMRC2 cells exhibited a similar enrichment of M4 fumarate, M4 malate, and M4 asparate (but not citrate) showing that *VHL*-deficient cells up-regulate RC without compromising oxidative metabolism from glutamine. Next, we tested whether HIF inactivation by pVHL is necessary to regulate the reductive utilization of glutamine for lipogenesis. To this end, we traced the relative incorporation of [U-$^{13}C_6$] glucose or [5-$^{13}C_1$] glutamine into palmitate. Labeled carbon derived from [5-$^{13}C_1$] glutamine can be incorporated into fatty acids exclusively through RC, and the labeled carbon cannot be transferred to palmitate through the oxidative Krebs cycle (Figure IV-1B, red carbons). Tracer incorporation from [5-$^{13}C_1$] glutamine occurs in the one carbon (C1) of AcCoA, which results in labeling of palmitate at M1, M2, M3, M4, M5, M6, M7, and M8 mass isotopomers. In contrast, lipogenic AcCoA molecules originating from [U-$^{13}C_6$] glucose are fully labeled, and the labeled palmitate is represented by M2, M4, M6, M8, M10, M12, M14, and M16 mass isotopomers. *VHL*-deficient control cells and cells expressing pVHL type 2B mutants exhibited high palmitate labeling from the [5-$^{13}C_1$] glutamine; conversely, reintroduction of wild-type or type 2C pVHL mutant (L188V) resulted in high labeling from [U-$^{13}C_6$] glucose (Figures IV-2A and IV-2B, box inserts highlight the heavier mass isotopomers).

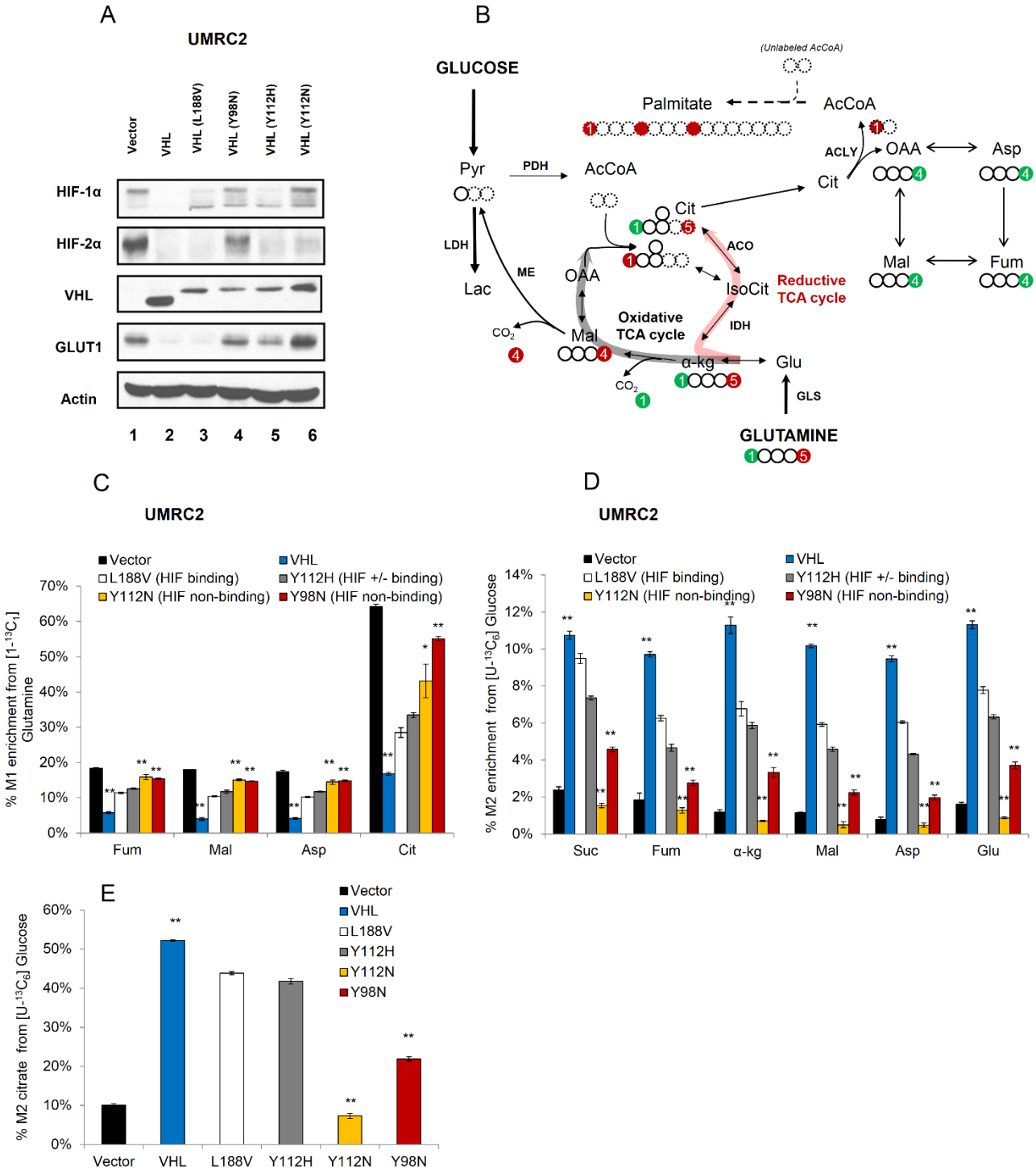
A
UMRC2
Vector
VHL
VHL (L188V)
VHL (Y98N)
VHL (Y112H)
VHL (Y112N)
HIF-1α
HIF-2α
VHL
GLUT1
Actin
1 2 3 4 5 6
B
GLUCOSE
(Unlabeled AcCoA)
Palmitate
AcCoA
ACLY
OAA
Asp
Cit
Pyr
PDH
AcCoA
Cit
LDH
ACO
ME
OAA
Lac
IsoCit
Reductive TCA cycle
Oxidative TCA cycle
IDH
Mal
Fum
CO2
α-kg
Glu
GLS
GLUTAMINE
C
UMRC2
Vector
VHL
L188V (HIF binding)
Y112H (HIF +/- binding)
Y112N (HIF non-binding)
Y98N (HIF non-binding)
% M1 enrichment from [1-13C1] Glutamine
Fum
Mal
Asp
Cit
D
UMRC2
% M2 enrichment from [U-13C6] Glucose
Suc
Fum
α-kg
Mal
Asp
Glu
E
% M2 citrate from [U-13C6] Glucose
Vector
VHL
L188V
Y112H
Y112N
Y98N

Figure IV-1. HIF Inactivation Is Necessary for Downregulation of Reductive Carboxylation by pVHL

(A) Expression of HIF-1α, HIF-2α, and their target protein GLUT1 in UMRC2-derived cell lines, as indicated. (B) Carbon atom transition map: the fate of [1-$^{13}C_1$] and [5-$^{13}C_1$] glutamine used to trace reductive carboxylation in this work (carbon atoms are represented by circles). The [1-$^{13}C_1$] (green circle) and [5-$^{13}C_1$] (red circle) glutamine-derived isotopic labels are retained during the reductive Krebs cycle (bold red pathway). Metabolites containing the AcCoA carbon skeleton are highlighted by dashed circles. (C) Relative contribution of reductive carboxylation. (D and E) Relative contribution of glucose oxidation to the carbons of indicated metabolites (D) and citrate (E). Student's t test compared *VHL*-reconstituted to vector-only or to *VHL* mutants (Y98N/Y112N). Pyr, pyruvate; Lac, lactate; AcCoA, acetyl-CoA, Cit, citrate; IsoCit, isocitrate; α-kg, α-ketoglutarate; Suc, succinate; Fum, fumarate; Mal, malate; OAA, oxaloacetate; Asp, aspartate; Glu, glutamate; PDH, pyruvate dehydrogenase; ME, malic enzyme; IDH, isocitrate dehydrogenase enzymes; ACO, aconitase enzymes; ACLY, ATP-citrate lyase; GLS, glutaminase.

Next, to determine the specific contribution from glucose oxidation or glutamine reduction to lipogenic AcCoA, we performed isotopomer spectral analysis (ISA) of palmitate labeling patterns. ISA indicates that wild-type pVHL or pVHL L188V mutant-reconstituted UMRC2 cells relied mainly on glucose oxidation to produce lipogenic AcCoA, while UMRC2 cells reconstituted with a pVHL mutant defective in HIF inactivation (Y112N or Y98N) primarily employed RC. Upon disruption of the pVHL-HIF interaction, glutamine becomes the preferred substrate for lipogenesis, supplying 70%–80% of the lipogenic AcCoA (Figure IV-2C). This is not a cell-line-specific phenomenon, but it applies to *VHL*-deficient human RCC cells in general; the same changes are observed in 786-O cells reconstituted with wild-type pVHL or mutant pVHL or infected with vector only as control (Supplemental Figure S2). Type 2A pVHL mutants (Y112H, which retain partial HIF binding) confer an intermediate reductive phenotype between wild-type VHL (which inactivates HIF) and type 2B pVHL mutants (which are totally defective in HIF regulation) as seen in Figures IV-1 and IV-2. Taken together, these data demonstrate that the ability of pVHL to regulate reductive carboxylation and lipogenesis from glutamine tracks genetically with its ability to bind and degrade HIF, at least in RCC cells.

HIF Is Sufficient to Induce RC from Glutamine in RCC Cells

To test the hypothesis that HIF-2α is sufficient to promote RC from glutamine, we expressed a pVHL-insensitive HIF-2α mutant (HIF-2α P405A/P531A, marked as HIF-2α P-A) in *VHL*-reconstituted 786-O cells (Figure IV-3). HIF-2α P-A is constitutively expressed in this polyclonal cell population, despite the reintroduction of wild-type VHL, reflecting a pseudohypoxia condition (Figure IV-3A). We confirmed that this mutant is transcriptionally active by assaying for the expression of its targets genes GLUT1, LDHA, HK1, EGLN, HIG2, and VEGF (Figures IV-3B and S3A). As shown in Figure IV-3C, reintroduction of wild-type VHL into 786-O cells suppressed RC, whereas the expression of the constitutively active HIF-2α mutant was sufficient to stimulate this reaction, restoring the M1 enrichment of Krebs cycle metabolites observed in *VHL*-deficient 786-O cells. Expression of HIF-2α P-A also led to a concomitant decrease in glucose oxidation, corroborating the metabolic alterations observed in glutamine metabolism (Figures IV-3D and IV-3E). Additional evidence of the HIF-2α regulation on the reductive phenotype was obtained with [U-$^{13}C_5$] glutamine, which generates M5 citrate, M3 fumarate, M3 malate, and M3 aspartate through RC (Figure IV-3F).

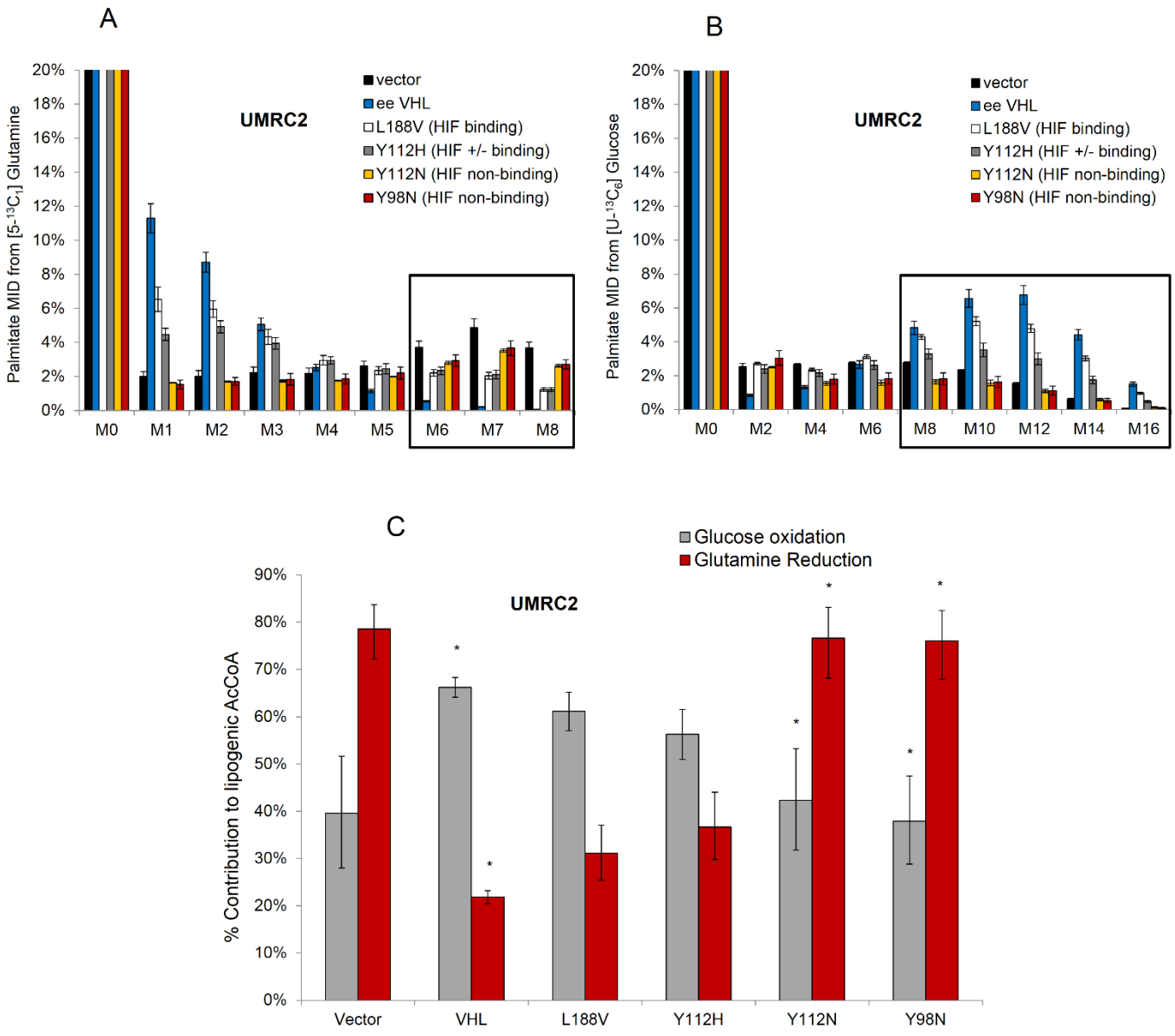

Figure IV-2. HIF Inactivation Is Necessary for Downregulation of Reductive Lipogenesis by pVHL

(A and B) VHL-deficient UMRC2 cells were cultured for 3 days in the presence of either [U-$^{13}C_6$] glucose or [5-$^{13}C_1$] glutamine. Mass isotopomer distributions (MIDs) of biomass-extracted palmitate in parental cells reconstituted with empty vector control (vector), wild-type EE-VHL, or HA-VHL mutants and labeled with [5-$^{13}C_1$] glutamine (A) or [U-$^{13}C_6$] glucose (B). Note: M0 equals 70%–80%; scale shown up to 20%. (C) Specific contribution to lipogenic acetyl-CoA as estimated by the ISA method. Statistical significance compared *VHL*-reconstituted to vector-only or to *VHL* mutants (Y98N/Y112N). Error bars represent 95% confidence intervals in (C).

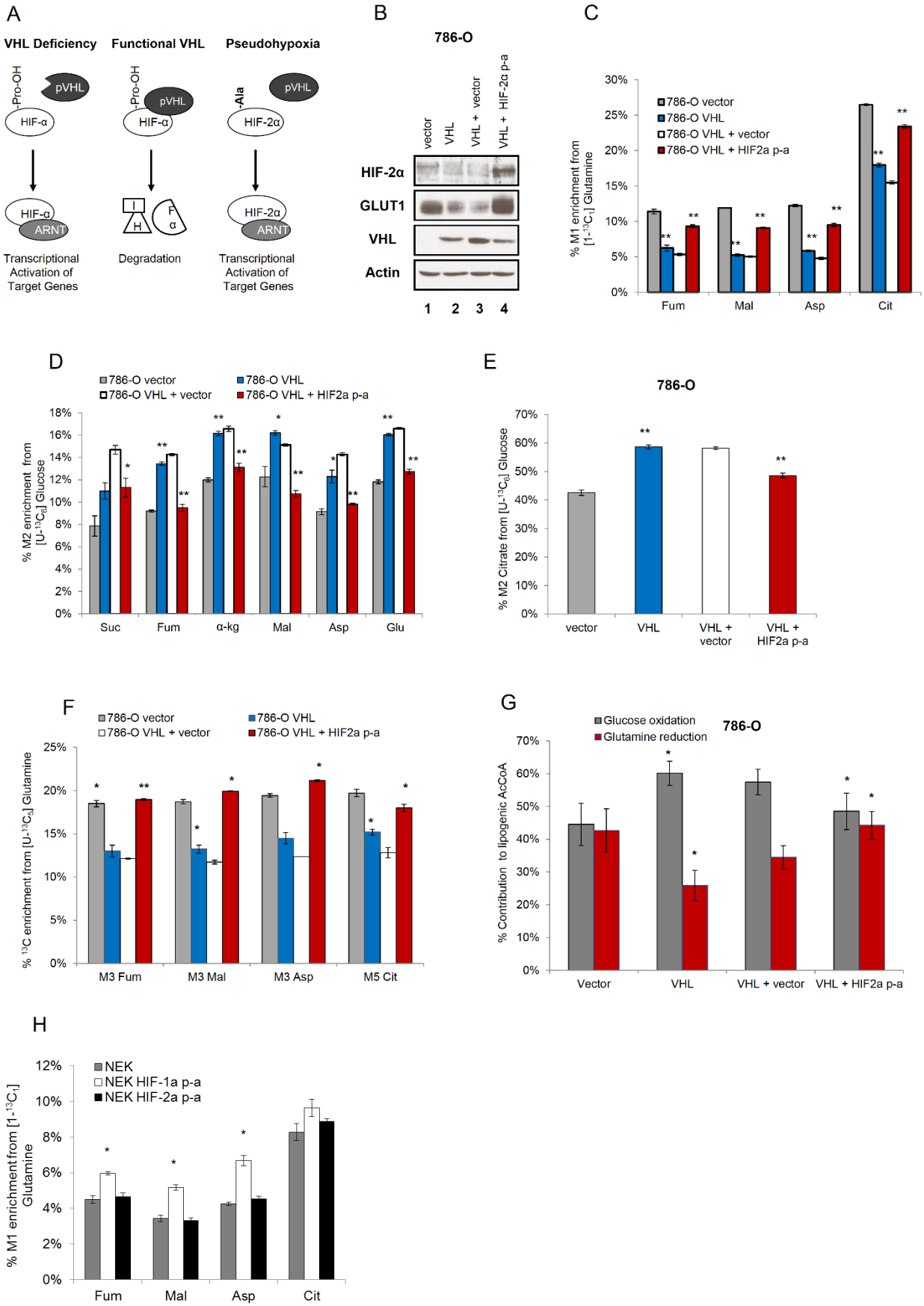
A
VHL Deficiency
Functional VHL
Pseudohypoxia
-Pro-OH
pVHL
HIF-α
ARNT
Transcriptional Activation of Target Genes
Degradation
-Ala
HIF-2α
B
786-O
vector
VHL
VHL + vector
VHL + HIF-2α p-a
HIF-2α
GLUT1
VHL
Actin
1 2 3 4
C
786-O vector
786-O VHL
786-O VHL + vector
786-O VHL + HIF2a p-a
% M1 enrichment from [1-13C1] Glutamine
Fum
Mal
Asp
Cit
D
% M2 enrichment from [U-13C6] Glucose
Suc
Fum
α-kg
Mal
Asp
Glu
E
786-O
% M2 Citrate from [U-13C6] Glucose
vector
VHL
VHL + vector
VHL + HIF2a p-a
F
% 13C enrichment from [U-13C3] Glutamine
M3 Fum
M3 Mal
M3 Asp
M5 Cit
G
Glucose oxidation
Glutamine reduction
786-O
% Contribution to lipogenic AcCoA
Vector
VHL
VHL + vector
VHL + HIF2a p-a
H
NEK
NEK HIF-1a p-a
NEK HIF-2a p-a
% M1 enrichment from [1-13C1] Glutamine
Fum
Mal
Asp
Cit

Figure IV-3. Expression of HIF-2α Is Sufficient to Induce Reductive Carboxylation and Lipogenesis from Glutamine in RCC Cells

(A) Schematic of stabilized HIF-2α expression under normoxia conditions. (B) Expression of pVHL, HIF-2α, and its target protein GLUT1 in 786-O-derived cells, as indicated. (C) Relative contributions of reductive carboxylation. (D and E) Relative contribution of glucose oxidation to the carbons of indicated metabolites (D) and citrate (E). (F) Evidence for induction of reductive carboxylation by HIF-2α P-A using [U-$^{13}C_5$] glutamine. Student's t test compared *VHL*-reconstituted or mutant HIF-2α-expressing cells to corresponding controls. (G) ISA results showing the specific contribution of glucose oxidation and glutamine reduction to lipogenic acetyl-CoA. (H) Regulation of reductive carboxylation in neonatal epithelial kidney cells (NEK) by mouse HIF1α p-a and HIF2α p-a paralogues, induced for 72 hours. Student's *t*-test compared wild type EE-VHL, mutant HIF2α pa, or inducible HIF-1α/2α expressing cells to corresponding control cells in (C), (D), (E), (F), (H), and statistical significance in (G) indicates comparison between *VHL*-reconstituted to vector-only or to *VHL* mutants (Y98N/Y112N). Error bars denote 95% confidence intervals in (G). Suc, succinate; Fum, fumarate; α-kg, α-ketoglutarate; Mal, malate; Asp, aspartate; Glu, glutamate; Cit, citrate.

Next, we tested whether *VHL*-independent HIF-2α expression was sufficient not only to stimulate RC in the Krebs cycle but also to switch the substrate preference for lipogenesis from glucose to glutamine. Expression of HIF-2α P-A in 786-O cells phenocopied the loss-of-*VHL* with regards to glutamine reduction for lipogenesis (Figure IV-3G), suggesting that HIF-2α can induce the glutamine-to-lipid pathway in RCC cells per se. Although reintroduction of wild-type VHL restored glucose oxidation in UMRC2 and UMRC3 cells, HIF-2α P-A expression did not measurably affect the contribution of each substrate to the Krebs cycle or lipid synthesis in these RCC cells (Figure S3B-S3I). UMRC2 and UMRC3 cells endogenously express both HIF-1α and HIF-2α, whereas 786-O cells exclusively express HIF-2α. There is compelling evidence suggesting, at least in RCC cells, that HIF-α isoforms have overlapping –but also distinct – functions and their roles in regulating bioenergetics processes remain an area of active investigation. Overall, HIF-1α has an antiproliferative effect, and its expression *in vitro* leads to rapid death of RCC cells while HIF-2α promotes tumor growth (Keith et al., 2012; Raval et al., 2005). Because of this, we were not able to stably express the HIF-1α P-A mutant in cells that endogenously express HIF-2α only. To get insights into the role of HIF-α paralogs in promoting RC, we used

mouse neonatal epithelial kidney (NEK) cells and selectively induced the expression of mouse HIF-1α or HIF-2α P-A in normoxia. Expressing HIF-1α P-A activated RC, consistent with our observation in cancer cell lines. In this model, HIF-2α P-A did not affect the contribution of this reaction to any of the Krebs cycle metabolites, at least in the condition studied (Figure IV-3H). Thus, it is possible that the induction of RC by HIF-1α or HIF-2α is species- or cell type-specific. Alternatively, there may be a redundant role of the paralogs, and/or one may adapt the control of the metabolic program in the absence of the other paralog.

Metabolic Flux Analysis Show Net Reversion of the IDH Flux upon HIF Activation

To determine absolute fluxes in RCC cells, we employed ^{13}C metabolic flux analysis (MFA), as described in Chapter II. Herein, we performed MFA using a combined model of [U-$^{13}C_6$] glucose and [1-$^{13}C_1$] glutamine tracer data sets from the 786-O derived isogenic clones PRC3 (VHL-/-) / WT8 (VHL+) cells, which show a robust metabolic regulation by reintroduction of pVHL. To this end, we first determined specific glucose/glutamine consumption and lactate/glutamate secretion rates. As expected, PRC3 exhibited increased glucose consumption and lactate production when compared to WT8 counterparts (Figure IV-4A). While PRC3 exhibited both higher glutamine consumption and glutamate production rates than WT8 (Figure IV-4A), the net carbon influx was higher in PRC3 cells (Figure IV-4B). Importantly, the fitted data show that the flux of citrate to α-ketoglutarate was *negative* in PRC3 cells (Figure IV-4C). This indicates that the net (forward plus reverse) flux of isocitrate dehydrogenase and aconitase (IDH + ACO) is toward citrate production. The exchange flux was also higher in PRC3 than WT8 cells, whereas the PDH flux was lower in PRC3 cells. In agreement with the tracer data, these MFA results strongly suggest that the reverse IDH + ACO fluxes surpass the forward flux in *VHL*-deficient cells. The estimated ATP citrate lyase (ACLY) flux was also lower in PRC3 than in WT8 cells. Furthermore, the malate dehydrogenase (MDH) flux was negative, reflecting a net conversion of oxaloacetate into malate in *VHL*-deficient cells (Figure IV-4C). This indicates an increased flux through the reductive pathway downstream of IDH, ACO, and ACLY. Additionally, some

Krebs cycle flux estimates downstream of α-ketoglutarate were not significantly different between PRC3 and WT8 (Table IV-1). This shows that *VHL*-deficient cells maintain glutamine oxidation while upregulating reductive carboxylation (see also Figure S1B). This finding is in agreement with the higher glutamine uptake observed in *VHL*-deficient cells. Table IV-1 shows the metabolic network and complete MFA estimates. Similar MFA results were obtained in *VHL*-deficient vector versus *VHL*-reconstituted UMRC2 cells (data not shown). Together, the MFA data show that HIF expression reverses the net IDH flux, perhaps to compensate for a deficient citrate production due to inhibition of PDH.

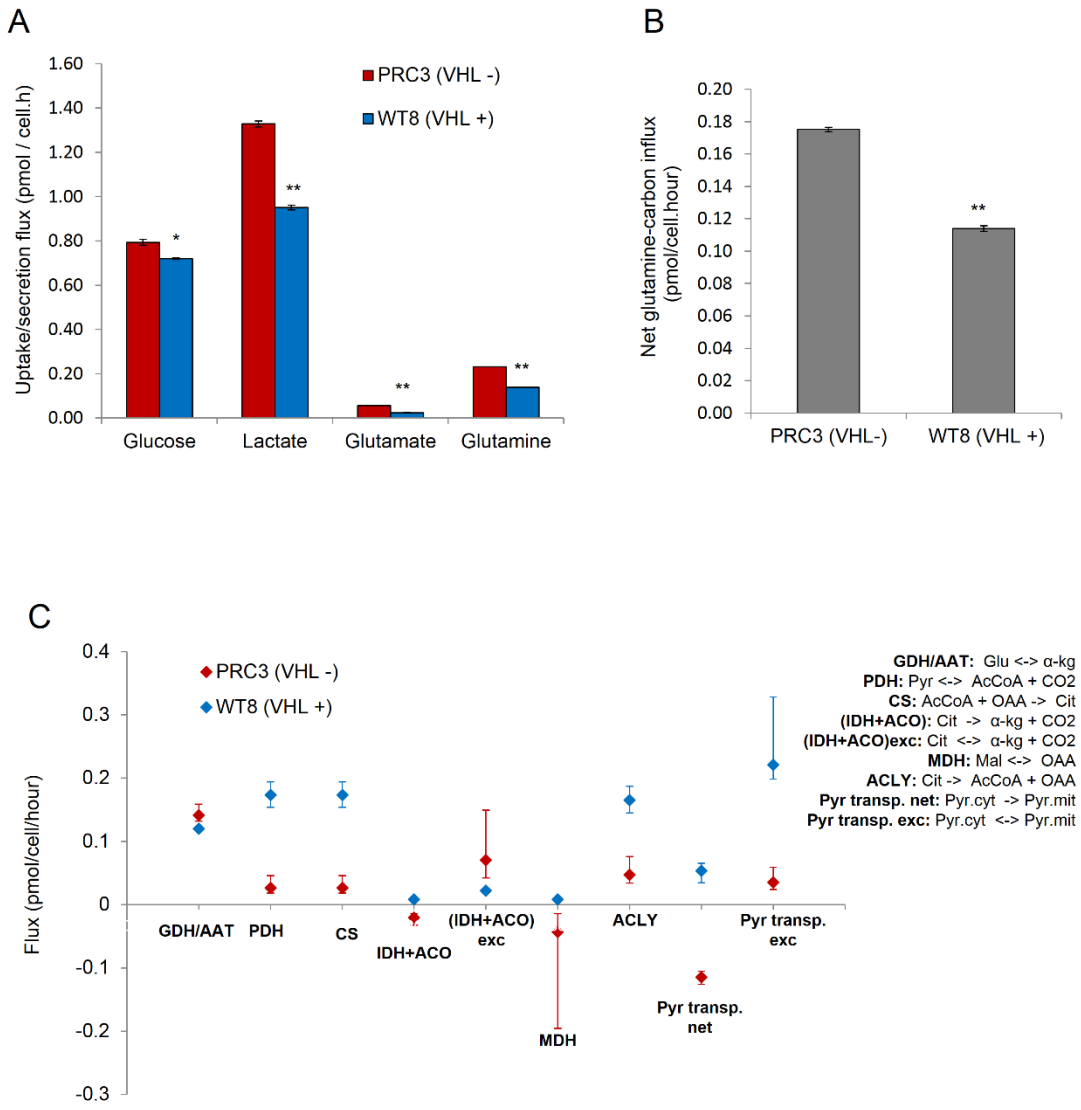

Figure IV-4. Metabolic Flux Analysis of *VHL*-Deficient and *VHL*-Reconstituted RCC Cells

(A) Extracellular fluxes (Glucose and Glutamine uptake, Glutamate and Lactate secretion) in PRC3 (VHL-/-) and WT8 (VHL+) isogenic cells. (B) Net influx of glutamine-derived carbons determined by the difference between glutamine uptake and glutamate secretion. (C) Flux estimates from combined [U-$^{13}C_6$] glucose / [1-$^{13}C_1$] glutamine MFA model. Student's t test compared WT8 to PRC3 cells in (A), (B). Error bars denote 95% confidence intervals in (C). GDH, glutamate dehydrogenase; AAT, aspartate aminotransferase; PDH, pyruvate dehydrogenase; CS, citrate synthase; IDH, isocitrate dehydrogenase; ACO, aconitase; MDH, malate dehydrogenase; ACLY, ATP-citrate lyase; Pyr transp, pyruvate transport between cytosol and mitochondria.

Table IV-1. Determined Fluxes and their 95% Confidence Intervals for PRC3/WT8 Estimated from MFA Model Using [U-$^{13}C_6$] Glucose and [1-$^{13}C_1$] Glutamine Tracer Datasets

Reaction	PRC3 (VHL-)			WT8 (VHL+)		
	Flux pmol/cell/hour	95% Confidence Intervals		Flux pmol/cell/hour	95% Confidence Intervals	
		Lower	Upper		Lower	Upper
Glycolysis	0.79	0.78	0.81	0.72	0.71	0.73
Glc.x → G6P	0.79	0.43	0.81	-0.59	-0.67	0.33
G6P → F6P	0.00	0.00	Inf	0.04	0.00	Inf
G6P ↔ F6P	0.79	0.67	0.81	0.28	0.26	0.32
F6P→DHAP + GAP	0.79	0.67	0.81	0.28	0.26	0.32
DHAP→ GAP	0.47	0.00	Inf	0.00	0.00	Inf
DHAP ↔ GAP	1.58	1.46	1.62	1.01	0.98	1.02
GAP→3PG	0.00	0.00	Inf	0.37	0.00	Inf
GAP ↔ 3PG	1.58	1.46	1.62	1.01	0.98	1.02
3PG → Pyr.c	1.37	1.33	1.41	0.95	0.93	0.97
Pyr.c ↔ Lac	0.87	0.00	Inf	0.21	0.00	Inf
Lac → Lac.x	1.37	1.33	1.41	0.95	0.93	0.97
Pentose Phosphate Pathway						
G6P → P5P + CO2	0.00	0.00	0.36	1.31	0.39	1.40
P5P + P5P → S7P + GAP	0.00	0.00	0.12	0.44	0.13	0.47
P5P + P5P ↔ S7P + GAP	2.55	0.00	Inf	1.10E+04	0.00E+00	Inf
S7P + GAP → F6P + E4P	0.00	0.00	0.12	0.44	0.13	0.47
S7P + GAP ↔ F6P + E4P	0.28	0.00	Inf	0.70	0.00	Inf
P5P + E4P → F6P + GAP	0.00	0.00	0.12	0.44	0.13	0.47
P5P + E4P ↔ F6P + GAP	1.97	0.00	Inf	2.28	0.00	Inf
Anaplerotic reactions						
Pyr.m + CO2 → Oac	0.02	0.00	0.16	0.00	0.00	0.02
Mal → Pyr.m + CO2	0.16	0.13	0.32	0.12	0.12	0.12
Mal ↔ Pyr.m + CO2	0.05	0.00	0.16	0.01	0.01	0.02
Glu → α-kg	0.14	0.13	0.16	0.12	0.12	0.12
Glu ↔ α-kg	10.62	0.63	Inf	1.43E+05	3.07E+00	Inf
Oac → Asp	0.00	0.00	0.00	0.00	0.00	0.00
Oac ↔ Asp	0.32	0.00	Inf	0.47	0.00	Inf
Krebs cycle						
Pyr.m →AcCoA.m + CO2	0.03	0.02	0.05	0.17	0.15	0.19
AcCoA.m + Oac → Cit	0.03	0.02	0.05	0.17	0.15	0.19
Cit → α-kg + CO2	-0.02	-0.03	-0.01	0.01	0.01	0.01
Cit ↔ α-kg + CO2	0.07	0.04	0.15	0.02	0.02	0.03
α-kg → Suc + CO2	0.12	0.11	0.13	0.13	0.12	0.13
Suc → Fum	0.12	0.11	0.13	0.13	0.12	0.13
Suc ↔ Fum	0.01	0.00	0.03	0.00	0.00	0.03
Fum → Mal	0.12	0.11	0.13	0.13	0.12	0.13
Fum ↔ Mal	2.08	0.68	Inf	1.07	0.38	Inf
Mal → Oac	-0.04	-0.20	-0.01	0.01	0.01	0.01
Mal ↔ Oac	1.63E+02	9.54E-	Inf	2.21E+04	8.77E-01	Inf
Cit → AcCoA.c + Oac	0.05	0.03	0.08	0.17	0.14	0.19
AcCoA.c → Palm	0.05	0.03	0.08	0.17	0.14	0.19
Glutamine metabolism						
Pyr.c → Ala	0.00	0.00	0.00	0.00	0.00	0.00
Pyr.c ↔ Ala	4.23	0.00	Inf	0.96	0.00	Inf
Gln.x → Gln	0.19	0.18	0.21	0.14	0.14	0.14
Gln → Glu	0.19	0.18	0.21	0.14	0.14	0.14
Glu →Glu.x	0.05	0.05	0.06	0.02	0.02	0.02
Mixing/Dilution						
Pyr.c → Pyr.m	-0.11	-0.13	-0.11	0.05	0.03	0.07
Pyr.c ↔ Pyr.m	0.04	0.02	0.06	0.22	0.20	0.33
Pyr.c → Pyr.mnt	0.33	0.19	0.38	0.00	0.00	0.35
Pyr.m → Pyr.mnt	0.00	0.00	0.00	0.00	0.00	0.00

HIF Activation Promotes RC by Lowering Citrate Levels

In support of the existing literature, our MFA data showed that HIF inhibits the absolute pyruvate dehydrogenase (PDH) flux (Kim et al., 2006; Papandreou et al., 2006). We observed that citrate levels were depleted in *VHL*-deficient UMRC2 cells (Figure IV-5A), with the citrate-to-α-kg ratio being equally decreased in the *VHL*-deficient and HIF-2α P-A-expressing RCC cell lines (Figure IV-5B and S4A). We hypothesized that low citrate levels are key in promoting reductive carboxylation (RC) through mass action. To test if the mechanism by which HIF promotes RC lies in its ability to reduce citrate levels, we restored the intracellular pools of citrate, hoping to suppress RC in the Krebs cycle. First, we knocked down the HIF target PDK-1 (Figure IV-5C) and observed a decreased contribution of RC to the Krebs cycle in *VHL*-deficient PRC3 cells (Figure IV-5D). Similarly, knocking down the ATP citrate lyase enzyme (Figure IV-5E) inhibited RC in PRC3 cells (relative contribution of RC in Figure IV-5F, total contribution of RC in Figure S4B). Next, we labeled *VHL*-deficient and *VHL*-reconstituted UMRC2 cells with [1-$^{13}C_1$] glutamine and supplemented the medium with 1 mM and 4 mM acetate. Addition of acetate decreased the relative (Figure IV-5G) and total contribution (Figure IV-5H) of RC in *VHL*-deficient cells, with minimal effects observed in the *VHL*-reconstituted counterparts. The M1 enrichment informs on RC for the formation of Krebs cycle metabolites. The absence of a major effect of acetate on the minimal RC of *VHL*-reconstituted cells is consistent with the observation that addition of acetate to these cells did not increase the intracellular citrate levels significantly (Figures IV-5I and S4C). In contrast, addition of acetate to *VHL*-deficient cells led to a significant increase in their citrate levels (Figures IV-5I and S4C) (to a level similar to the one observed in *VHL*-positive cells) as well as significant inhibition of RC. To pinpoint the metabolic route of the acetate-to-citrate flux, we labeled the control and ACLY knockdown PRC3 cells with [U-$^{13}C_2$] acetate and observed an increased percentage of M2 citrate under ACLY knockdown conditions (Supplemental Figure S4D), suggesting that the acetate rescue of citrate levels in *VHL*-deficient cells probably occurs through condensation with

oxaloacetate via citrate synthase rather than through the reversibility of ACLY. We confirmed that acetate can serve as a lipogenic source in the pair of PRC3/WT8 cells (Supplemental Figure S4E). We also cultured PRC3/WT8 cells with [5-$^{13}C_1$] glutamine in the presence of acetate at natural abundance enrichment levels. In line with the previous observations, the contribution of glutamine reduction to lipogenic acetyl-CoA was decreased under the presence of acetate (Supplemental Figure S4F). Next, we directly supplemented the medium with citrate and rinsed the cells thoroughly with PBS before extraction to ensure measurement of the intracellular metabolite. Addition of 8 mM citrate decreased the M1 enrichment of citrate in *VHL*-deficient UMRC2 cells to half but, in contrast to acetate, did have a moderate effect on the minimal RC observed in *VHL*-reconstituted cells (Figure IV-5J). Interestingly the level of M1 fumarate, M1 aspartate, and M1 malate were unaffected. One could expect the addition of unlabeled citrate to decrease, by definition, the percent enrichment of M1 citrate, regardless of its putative effect on RC. To control for this effect of exogenous citrate on the total formation of RC-derived citrate, we labeled the cells with [1-$^{13}C_1$] glutamine and [U-$^{13}C_6$] citrate and subtracted the total M6 citrate ions (which are exogenous and not metabolically generated by the cell) from the total citrate ions and calculated the total contribution of RC using the formula % M1 x (total ions – % M6 x total ions). Likewise, exogenous citrate significantly decreased the total contribution of RC in the *VHL*-deficient UMRC2 cells but also had a moderate effect in the RC observed in *VHL*-reconstituted cells (Figure IV-5K). This differential effect between acetate and citrate on RC is consistent with and supports our hypothesis that endogenous citrate levels regulate RC by mass action. Addition of citrate in the medium, in contrast to acetate, led to an increase in the citrate-to-α-ketoglutarate ratio (Figure IV-5L) and absolute citrate levels (Supplemental Figure S4H) not only in *VHL*-deficient but also *VHL*-reconstituted cells. The ability of exogenous citrate, but not acetate, to also affect RC in *VHL*-reconstituted cells may be explained by compartmentalization differences or by allosteric inhibition of citrate synthase (Williamson and Cooper, 1980); that is, the ability of acetate to raise the intracellular levels of citrate may be limited in (*VHL*-reconstituted) cells that exhibit high endogenous levels of

citrate. Whatever the mechanism, the results imply that increasing the pools of intracellular citrate has a direct biochemical effect in cells with regards to their reliance on RC. Finally, we assayed the transcript and protein levels of enzymes involved in the reductive utilization of glutamine and did not observe significant differences between *VHL*-deficient and *VHL*-reconstituted UMRC2 cells (Supplemental Figures S4I and S4J), suggesting that HIF does not promote RC by direct transactivation of these enzymes. The IDH1/IDH2 equilibrium is defined as follows:

$$\frac{[\alpha - \text{ketoglutarate}]\,[\text{NADPH}]\,[\text{CO2}]}{[\text{Isocitrate}][\text{NADP}+]} = \text{K (IDH)}$$

Therefore, we sought to investigate whether HIF could affect the driving force of the IDH reaction by also enhancing NADPH production. We did not observe a significant alteration of the $NADP^+$/NADPH ratio between *VHL*-deficient and *VHL*-positive cells in the cell lysate (Supplemental Figure S4K). Yet, we determined the ratio of the free dinucleotides using the measured ratios of suitable oxidized (α-ketoglutarate) and reduced (isocitrate/citrate) metabolites that are linked to the NADP-dependent IDH enzymes. The determined ratios (Supplemental Figure S4L) are in close agreement with the values initially reported by the Krebs lab (Veech et al., 1969) and showed that HIF-expressing UMRC2 cells exhibit a higher $NADP^+$/NADPH ratio. Collectively, these data strongly suggest that HIF-regulated citrate levels modulate the reductive flux to maintain adequate lipogenesis.

Reductive Carboxylation from Glutamine is Detectable *in vivo*

VHL-deficient RCC cells rely on reductive carboxylation (RC) for lipid synthesis, potentially suggesting that this reaction can contribute to tumor growth. RC is known to occur in bacteria and in the brown adipose tissue (Yoo et al., 2004, 2008) and more recently described in cancer cell lines (see Chapter III and references therein), but whether it occurs *in vivo* in other tissues of vertebrates or in actual tumors is not known. We sought to determine the activity of RC in tumors derived from *VHL*-

deficient UMRC3 cells growing as subcutaneous xenografts in nude mice. We infused several tumor-bearing mice with [1-$^{13}C_1$] glutamine (see Experimental Procedures in Chapter II) and analyzed the citrate enrichment in tumor extracts by high-resolution ^{13}C Nuclear Magnetic Resonance (NMR) spectroscopy and GC-MS (Figure IV-6). [1-$^{13}C_1$] glutamine will transfer carbon to citrate only through RC, so the mere detection of ^{13}C enrichment in citrate will indicate that this reaction is active *in vivo*. In order to attain maximal ^{13}C enrichment of citrate, we carried out a time course infusion of [1-$^{13}C_1$] glutamine and attained an isotopic-steady state of ^{13}C glutamine enrichment in the tumor (Figure IV-6A). We also analyzed the ^{13}C glutamine enrichment in the plasma at the earliest and latest infusion points and observed similar ^{13}C enrichment after 6 hr. As seen in Figure IV-6B, we detected ^{13}C enriched citrate in the tumor within 30 min, with RC accounting for 4% of citrate production after 6hr of infusion (Figure IV-6B). Notably, the steady-state ^{13}C glutamine enrichment in the tumor was 30% (Figure IV-6A), indicating that the reductive flux accounts for at least 12% of citrate production in *VHL*-deficient tumors under these experimental conditions. The kidney cortex is reported to be relatively hypoxic (Zhong et al., 1998).Thus, we analyzed the ^{13}C citrate enrichment in kidney extracts in parallel and showed that RC is also active in this organ (Figure IV-6B). The steady-state ^{13}C enrichment of glutamine was also established in the normal kidney, but it was higher (Figure IV-6B), indicating an overall lower contribution of RC in the kidney when compared to the tumor. Despite the steady-state ^{13}C enrichment of the glutamine precursor, the percentage of M1 citrate appeared to increase overtime in the tumor, whereas it reached a plateau in the normal kidneys and plasma. Importantly, there was no evidence that RC appears in the tumor in a delayed fashion compared to plasma or kidney, strongly suggesting that RC occurs in the tumor xenografts. Concordant results were obtained by ^{13}C NMR spectroscopy (Figures IV-6C and IV-6D) in which ^{13}C enrichment was observed in tumor extracts after 6hr of infusion, and no signal was detected in the carboxyl group region in control mice (Figure IV-6C). These results indicate that RC occurs *in vivo*, at least in *VHL*-deficient tumors.

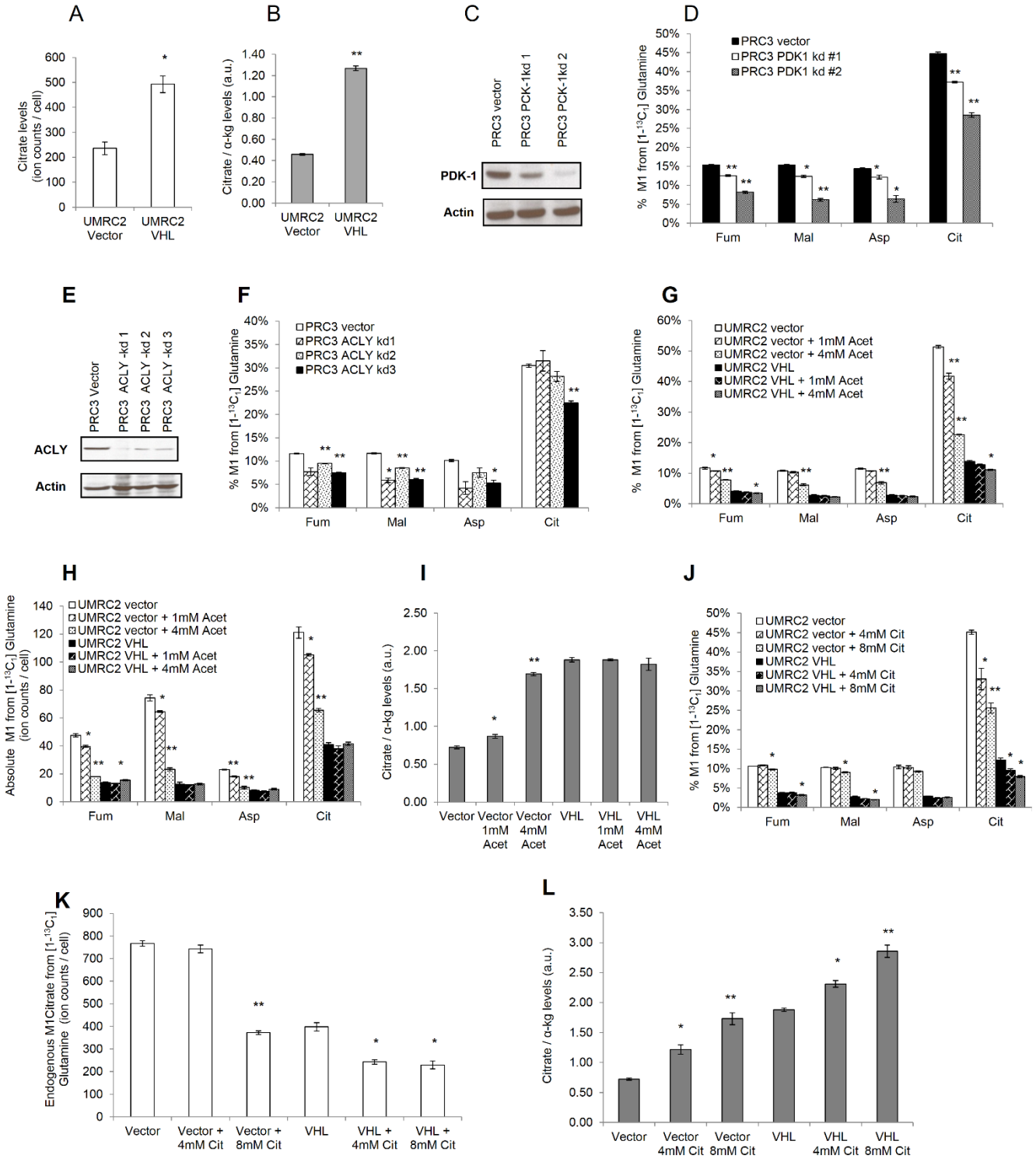
A
Citrate levels (ion counts / cell)
UMRC2 Vector
UMRC2 VHL
B
Citrate / α-kg levels (a.u.)
UMRC2 Vector
UMRC2 VHL
C
PRC3 vector
PRC3 PCK-1kd 1
PRC3 PCK-1kd 2
PDK-1
Actin
D
PRC3 vector
PRC3 PDK1 kd #1
PRC3 PDK1 kd #2
% M1 from [1-13C1] Glutamine
Fum
Mal
Asp
Cit
E
PRC3 Vector
PRC3 ACLY -kd 1
PRC3 ACLY -kd 2
PRC3 ACLY -kd 3
ACLY
Actin
F
PRC3 vector
PRC3 ACLY kd1
PRC3 ACLY kd2
PRC3 ACLY kd3
% M1 from [1-13C1] Glutamine
Fum
Mal
Asp
Cit
G
UMRC2 vector
UMRC2 vector + 1mM Acet
UMRC2 vector + 4mM Acet
UMRC2 VHL
UMRC2 VHL + 1mM Acet
UMRC2 VHL + 4mM Acet
% M1 from [1-13C1] Glutamine
Fum
Mal
Asp
Cit
H
UMRC2 vector
UMRC2 vector + 1mM Acet
UMRC2 vector + 4mM Acet
UMRC2 VHL
UMRC2 VHL + 1mM Acet
UMRC2 VHL + 4mM Acet
Absolute M1 from [1-13C1] Glutamine (ion counts / cell)
Fum
Mal
Asp
Cit
I
Citrate / α-kg levels (a.u.)
Vector
Vector 1mM Acet
Vector 4mM Acet
VHL
VHL 1mM Acet
VHL 4mM Acet
J
UMRC2 vector
UMRC2 vector + 4mM Cit
UMRC2 vector + 8mM Cit
UMRC2 VHL
UMRC2 VHL + 4mM Cit
UMRC2 VHL + 8mM Cit
% M1 from [1-13C1] Glutamine
Fum
Mal
Asp
Cit
K
Endogenous M1Citrate from [1-13C1] Glutamine (ion counts / cell)
Vector
Vector + 4mM Cit
Vector + 8mM Cit
VHL
VHL + 4mM Cit
VHL + 8mM Cit
L
Citrate / α-kg levels (a.u.)
Vector
Vector 4mM Cit
Vector 8mM Cit
VHL
VHL 4mM Cit
VHL 8mM Cit

Figure IV-5. Regulation of HIF-Mediated Reductive Carboxylation by Citrate Levels

(A and B) Citrate ion counts (A) and citrate-to-α-ketoglutarate ratio (B) in RCC cells. (C) Validation of PDK-1 knockdown in *VHL*-deficient PRC3 cells. (D) Relative contribution of reductive carboxylation to the Krebs cycle under PDK-1 knockdown conditions. (E) Validation of ACLY knockdown in PRC3 cells. (F) Effect of ACLY knockdown on the relative contribution of reductive carboxylation. (G and H) Effect of acetate and citrate on the activity of reductive carboxylation in *VHL*-deficient/*VHL*-reconstituted UMRC2 cells. Acetate suppresses the relative (G) and total (H) contribution of reductive carboxylation in *VHL*-deficient UMRC2 cells (I) Rescue of citrate-to-α-ketoglutarate ratio by acetate addition. (J and K) Exogenous citrate suppresses the relative (J) and total (K) contribution of reductive carboxylation in *VHL*-deficient UMRC2 cells. (L) Rescue of citrate-to-α-ketoglutarate ratio by exogenous citrate in (K). Student's *t*-test compared *VHL*-reconstituted to *VHL*-deficient cells (for A and B), and acetate/citrate-treated, or ACLY/PDK-1 knocked-down cells to correspondent controls. ACLY, ATP-citrate lyase; PDK-1, pyruvate dehydrogenase kinase.

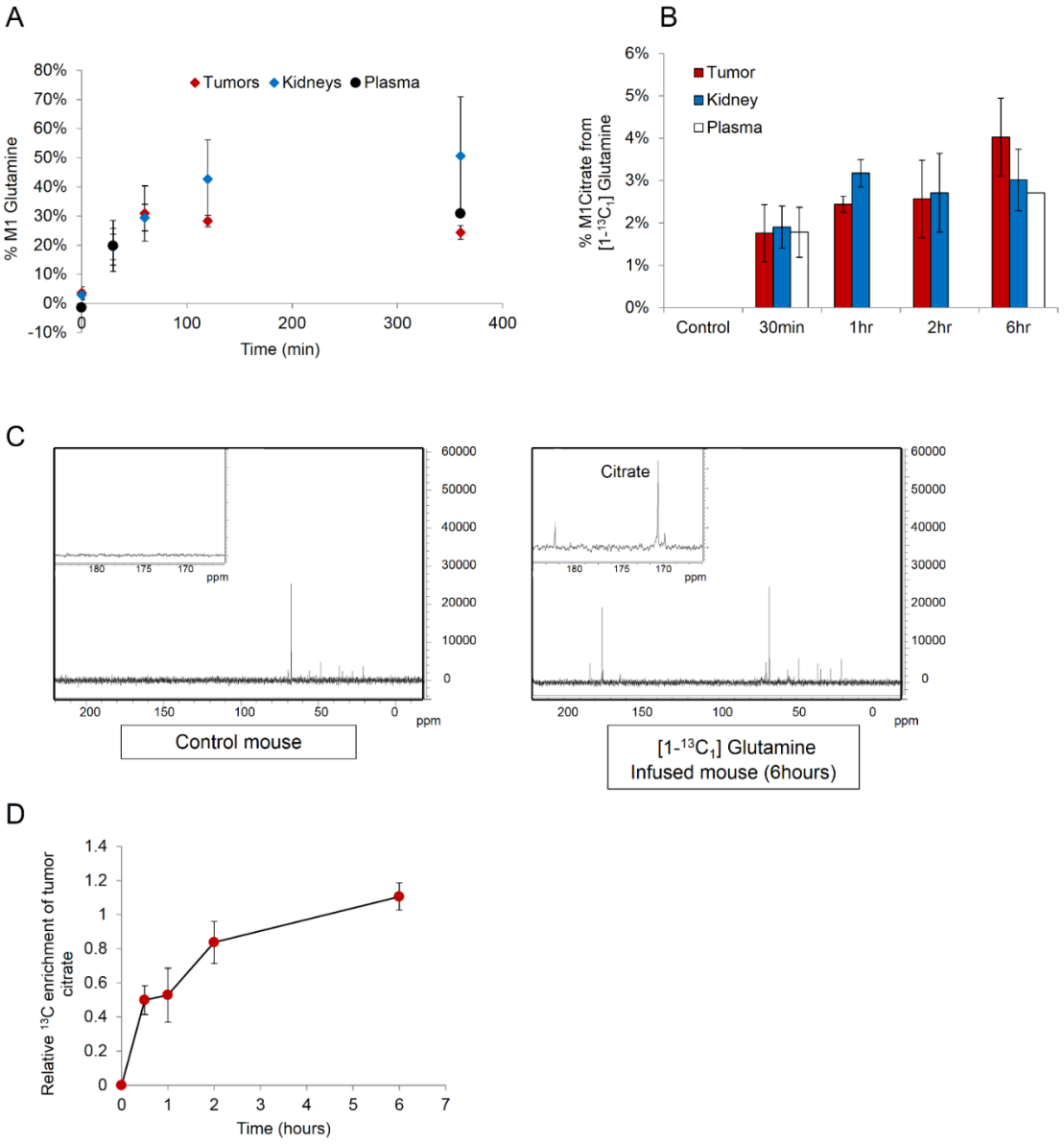

Figure IV-6. Evidence for Reductive Carboxylation Activity *In Vivo*

(A) Time course of ^{13}C enrichment (%) of glutamine in tumor, normal kidney, and plasma extracts during infusion with [1-$^{13}C_1$] glutamine (n = 3 per time point). ^{13}C enrichment at time zero was determined using control non-infused mice. (B) Percent M1 citrate in the different tissues as determined by GC-MS analysis. (C) High-resolution ^{13}C NMR spectra showing ^{13}C enrichment of carboxylic groups in tumor extracts of a [1-$^{13}C_1$] glutamine-infused mouse when compared to a control mouse. (D) NMR analysis of ^{13}C enrichment in tumor citrate during the time course of infusion determined by deconvolution of the carboxyl group signals. The area of the citrate signal was divided by tumor weight and normalized to the dioxane signal.

Loss of *VHL* Renders RCC Cells Sensitive to Glutamine Deprivation

Renal cell carcinoma (RCC) cells engaged in reductive carboxylation (RC) from glutamine to produce citrate, and this reaction was active in *VHL*-deficient RCC xenograft tumors. We therefore hypothesized that *VHL* deficiency results in cell addiction to glutamine for proliferation. We treated the isogenic clones PRC3 (*VHL*-deficient cells) and WT8 (*VHL*-reconstituted cells) with the glutaminase inhibitor 968 (Wang et al., 2010a). *VHL*-deficient PRC3 cells were more sensitive to treatment with 968, compared to the *VHL*-reconstituted WT8 cells (Figure IV-7A). To confirm that this is not only a cell-line-specific phenomenon, we also cultured UMRC2 cells in the presence of 968 or diluent control and showed selective sensitivity of *VHL*-deficient cells (Figure IV-7B). To test if the selective sensitivity of *VHL*-deficient cells to glutaminase inhibitors is linked, at least in part, to defective carbon supply, we asked whether cell proliferation could be rescued by anaplerotic substrates. Supplementing the cultured medium with a cell-permeable form of the substrate α-ketoglutarate or acetate, we rescued *VHL*-deficient cells from treatment with 968 (Figure IV-7C). The selective sensitivity and rescue by anaplerotic and lipogenic substrates was also corroborated in 786-O cells (Figure IV-7D). We observed a similar growth-inhibitory phenotype in *VHL*-deficient UMRC2 cells using a different glutaminase inhibitor (BPTES), confirming the sensitivity to glutamine deprivation under *VHL*-deficient conditions (Figure IV-7E). Glutamine addiction of *VHL*-deficient cells is not an *in vitro*-only phenomenon. Systemic administration of the glutaminase inhibitor BPTES suppressed the growth of *VHL*-deficient UMRC3 cells as tumors in nude mice (Figure IV-7F). In summary, our findings show that HIF is necessary and sufficient to promote RC from glutamine. By inhibiting glucose oxidation in the Krebs cycle and reducing citrate levels, HIF shifts the IDH reaction toward RC to support citrate production and lipogenesis. The reductive flux is active *in vivo*, fuels tumor growth, and can potentially be targeted pharmacologically (Figure IV-7G).

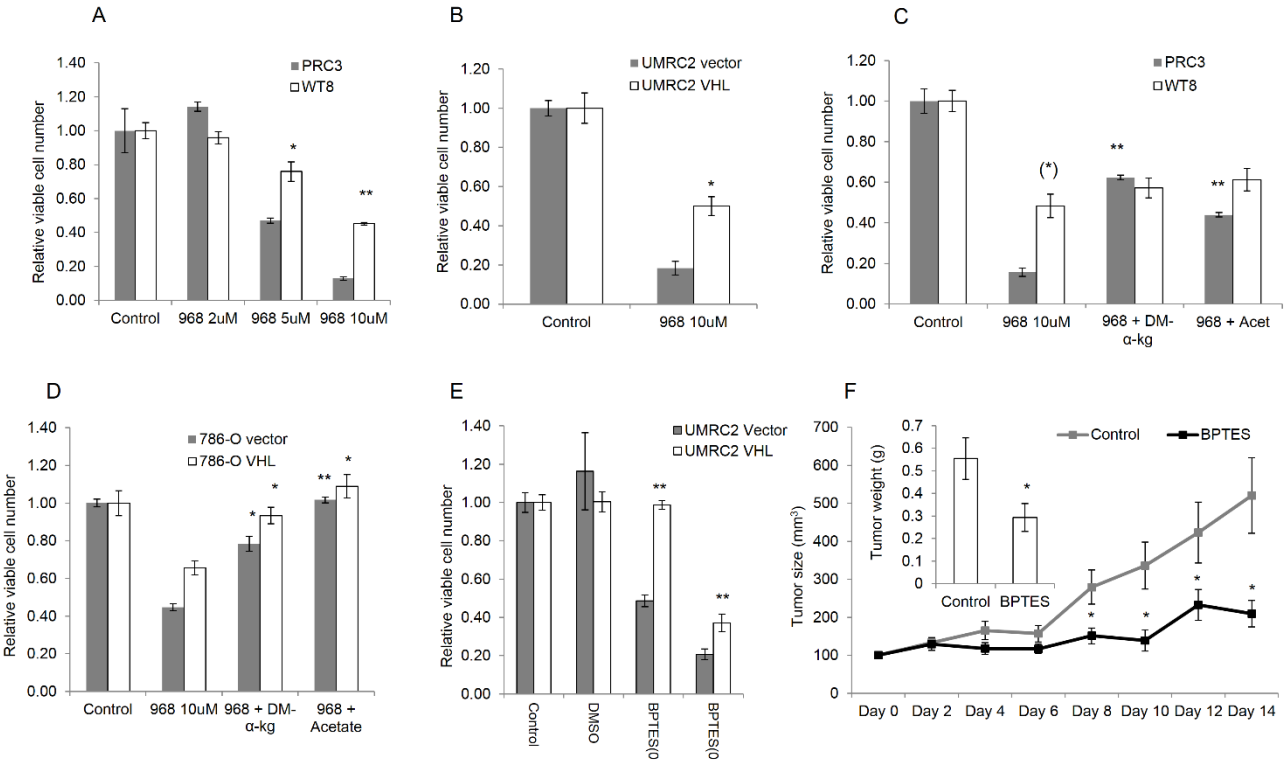
A
Relative viable cell number
PRC3
WT8
Control
968 2uM
968 5uM
968 10uM
B
Relative viable cell number
UMRC2 vector
UMRC2 VHL
Control
968 10uM
C
Relative viable cell number
PRC3
WT8
Control
968 10uM
968 + DM-α-kg
968 + Acet
D
Relative viable cell number
786-O vector
786-O VHL
Control
968 10uM
968 + DM-α-kg
968 + Acetate
E
Relative viable cell number
UMRC2 Vector
UMRC2 VHL
Control
DMSO
BPTES/0
BPTES/5
F
Tumor size (mm³)
Tumor weight (g)
Control
BPTES
Day 0
Day 2
Day 4
Day 6
Day 8
Day 10
Day 12
Day 14

G

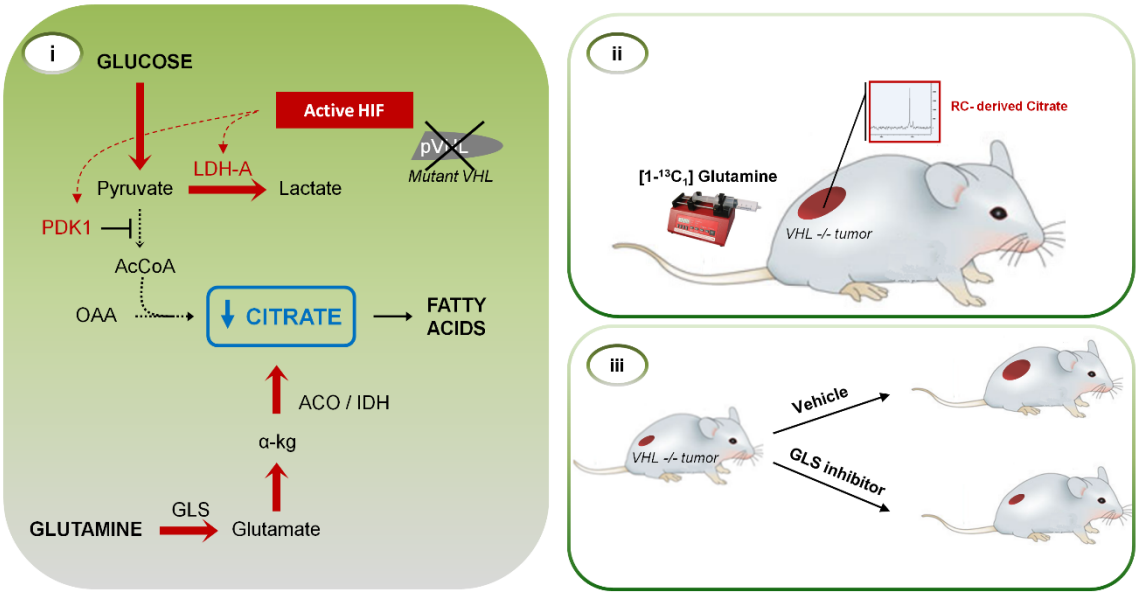
i
GLUCOSE
Active HIF
pVHL
Mutant VHL
LDH-A
Pyruvate
Lactate
PDK1
AcCoA
OAA
CITRATE
FATTY ACIDS
ACO / IDH
α-kg
GLUTAMINE
GLS
Glutamate
ii
RC- derived Citrate
[1-13C1] Glutamine
VHL -/- tumor
iii
VHL -/- tumor
Vehicle
GLS inhibitor

Figure IV-7. *VHL*-Deficient Cells and Tumors Are Sensitive to Glutamine Deprivation

(A–E) Cell proliferation is normalized to the corresponding cell type grown in 1 mM glutamine-containing medium. Effect of treatment with glutaminase (GLS) inhibitor 968 in PRC3/WT8 (A) and UMRC2 cells (B). Rescue of GLS inhibition with dimethyl α-ketoglutarate (DM-α-kg; 4 mM) or acetate (4 mM) in PRC3/WT8 clonal cells (C) and polyclonal 786-O cells (D). Effect of GLS inhibitor BPTES in UMRC2 cells (E). (F) GLS inhibitor BPTES suppresses growth of human UMRC3 RCC cells as xenografts in nu/nu mice. When the tumors reached 100mm^3, injections with BPTES or vehicle control were carried out daily for 14 days (n = 12). BPTES treatment decreases tumor size and mass (see insert). Student's t test compares *VHL*-reconstituted cells to control cells in (A), (B), and (E) and DM-α-kg or acetate-rescued cells to correspondent control cells treated with 968 only in (C) and (D) (asterisk in parenthesis indicates comparison between *VHL*-reconstituted to control cells). Student's t test compares control to BPTES-treated mice in (F). (G) Summary of the regulation of reductive carboxylation by HIF and its biological significance *in vivo*. GLS, glutaminase.

IV.3. DISCUSSION

Here, we provided mechanistic insights that link HIF to RC. First, we demonstrated that polyclonal reconstitution of *VHL* in several human *VHL*-deficient RCC cell lines inhibited RC and restored glucose oxidation. Second, the *VHL* mutational analysis demonstrated that the ability of pVHL to mitigate reductive lipogenesis is mediated by HIF and is not the outcome of previously reported, HIF-independent pVHL function(s). Third, to prove our hypothesis we showed that constitutive expression of a *VHL*-independent HIF mutant was sufficient to phenocopy the reductive phenotype observed in *VHL*-deficient cells. In addition, we showed that RC is not a mere *in vitro* phenomenon, but it can be detected *in vivo* in human tumors growing as mouse xenografts. Lastly, treatment of *VHL*-deficient human xenografts with glutaminase inhibitors led to suppression of their growth as tumors.

In this work, we also examined the mechanism(s) by which HIF promotes RC. It is established that hypoxic induction of HIF transactivates several enzymes involved in glucose uptake and glycolysis, including GLUT1, hexokinase, phosphofructokinase, and aldolase (Iyer et al., 1998). In addition, HIF directly binds to the promoter of, and transactivates, PKM2, pyruvate dehydrogenase kinase 1 (PDK1) and lactate dehydrogenase A (LDHA) (Ebert et al., 1996; Firth et al., 1994; Kim et al., 2006; Luo et al.,

2011; Papandreou et al., 2006). This orchestrated upregulation of several enzymes ensures the diversion of pyruvate to lactate production. This raised the hypothesis that RC may be triggered by a deficient pyruvate oxidation in the mitochondrion and the subsequent reduction in citrate levels. Our MFA analysis indicated a significantly lower absolute pyruvate dehydrogenase (PDH) flux and net conversion of α-ketoglutarate into citrate upon HIF activation. The ATP citrate lyase flux was lower in *VHL*-deficient cells when compared to the *VHL*-positive counterparts, which supports our previous observations that *de novo*

lipogenesis is decreased under hypoxia conditions (Metallo et al., 2012). Indeed, HIF expression, either by loss of *VHL* or normoxic induction of HIF-2α P-A, reduced citrate levels. Conversely, administration of exogenous citrate or acetate in *VHL*-deficient cells restored the low citrate levels to the levels encountered in *VHL*-replete cells and inhibited RC. Exogenous administration of acetate or citrate had a mild effect in *VHL*-positive cells. In the case of either cell type, the magnitude of changes in RC reflected the degree of changes in intracellular citrate levels. These observations show that fluctuations in citrate levels by HIF modulate, at least in part, the flux of the reverse IDH reaction. This finding underlines the compensatory role of RC in maintaining an adequate flux for lipogenesis under HIF-activated conditions.

In addition to the role of HIF in regulating RC through citrate, we examined whether HIF directly regulates enzymes along the reductive Krebs cycle pathway (see Figure IV-1B). We did not observe changes in the transcript or protein levels of GLS, GDH, IDH1, IDH2, ACO1, or ATP citrate lyase between *VHL*-deficient and *VHL*-reconstituted UMRC2 cells. This is in line with previous studies that did not identify any of these enzymes as transcriptional targets of HIF-1α or HIF-2α (Mole et al., 2009; Ortiz-Barahona et al., 2010; Schödel et al., 2011; Wenger et al., 2005). Nevertheless, it is conceivable that HIF may affect the activity of these enzymes through regulation of cofactor availability or posttranslational modification of the enzymes. For example, the reverse IDH reaction requires NADPH, as allosteric cofactor (Dalziel and Londesborough, 1968; Leonardi et al., 2012) and HIF-mediated

changes in NADPH levels may indirectly influence IDH activity. In our studies we did not observe increased NADPH levels in *VHL*-deficient cells when compared to the *VHL*-positive counterparts, which is in agreement with existing literature showing that HIF-1α activates NADPH oxidase and hypoxia limits NADPH production (Diebold et al., 2010; Tribble and Jones, 1990). These data suggest that the mass-action effect of HIF toward RC is not accounted for by an increase in NADPH production. Other signaling pathways may regulate RC through NADPH availability, and the source(s) of NADPH contributing to RC in the cytosol/mitochondrion are under investigation. For example, the mitochondrial enzyme nicotinamide nucleotide transhydrogenase (NNT) transfers reducing equivalents from NADH to NADPH and has been hypothesized to contribute to RC by IDH2 (Sazanov and Jackson, 1994).This hypothesis raises the possibility that NADPH-producing reactions may regulate the RC flux in a HIF-independent manner. This topic will be the focus of Chapter V.

In addition, posttranslational modifications of the enzymes involved in RC may be influenced by hypoxia and/or HIF expression indirectly. For example, aconitase (ACO1) activity is reportedly regulated by hypoxia through iron-sulfur cluster modifications and phosphorylation (Chan et al., 2009; Rouault, 2006), and AcCoA is a required substrate for protein acetylation, which regulates major cellular functions including central carbon metabolism (Wang et al., 2010b; Zhao et al., 2010). Thus, it is conceivable that HIF contributes to these modifications and therefore influences the activity of glutamine-metabolizing enzymes at the posttranslational level.

Our current work showed that HIF-2α is sufficient to induce the reductive program in RCC cells that express only the HIF-2α paralog, while mouse NEK cells appeared to use HIF-1α preferentially to promote RC. Together with the evidence that HIF-1α and HIF-2α may have opposite roles in tumor growth (Keith et al., 2012; Maranchie et al., 2002; Raval et al., 2005), it is possible that the cellular context dictates which paralog activates RC. It is also possible that HIF-2α adopts the RC regulatory function of HIF-1α upon deletion of the latter in RCC cells. Further studies are warranted in understanding the relative role of HIF-α paralogs in regulating RC in different cell types.

Finally, the selective sensitivity to glutaminase inhibitors exhibited by *VHL*-deficient cells, together with the observed RC activity *in vivo*, strongly suggests that reductive glutamine metabolism may fuel tumor growth. Investigating whether the reductive flux correlates with tumor hypoxia and/or contributes to the actual cell survival under low oxygen conditions is warranted. Together, our findings underscore the biological significance of reductive carboxylation in *VHL*-deficient RCC cells.

IV.4. Supplemental Information

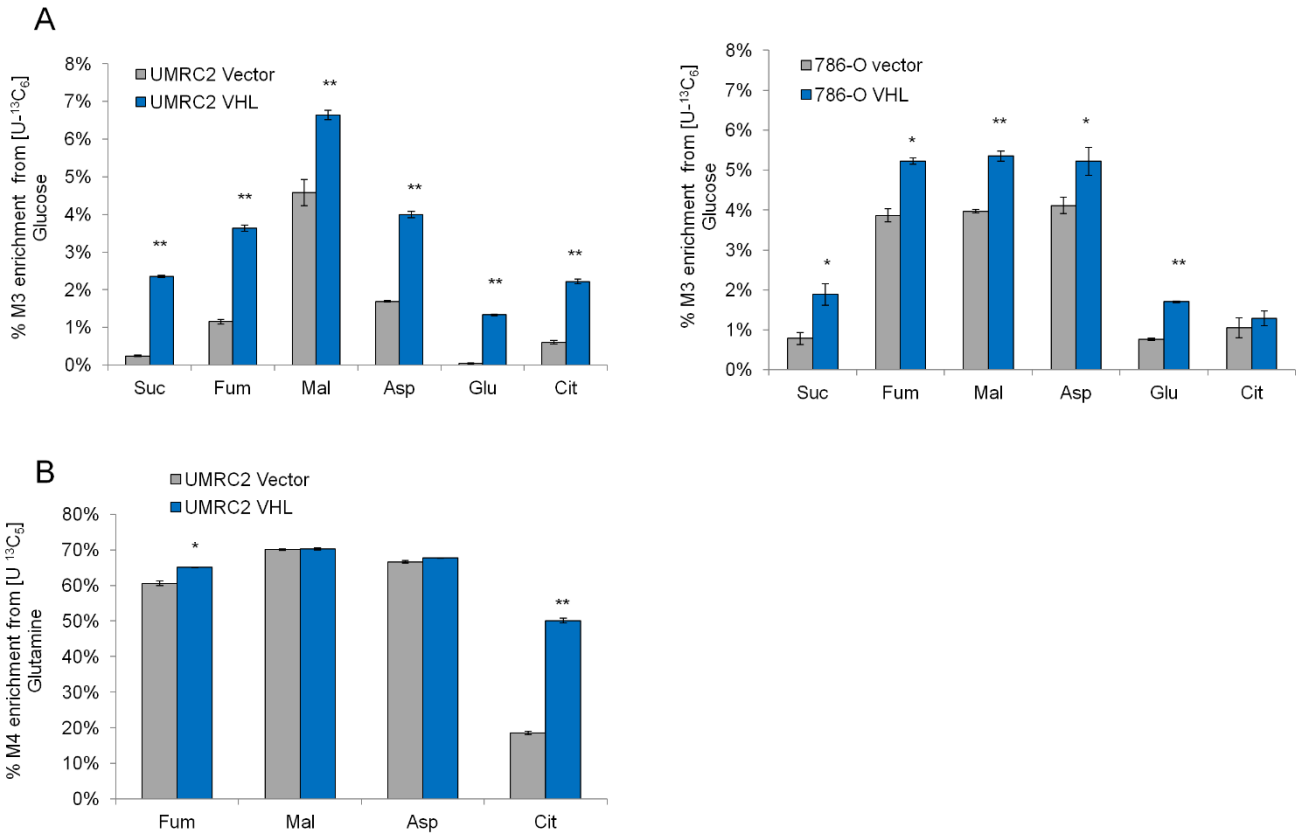

Supplementary Figure IV-S1. Evidence for Regulation of Glucose and Glutamine Utilization by pVHL in RCC Cells, Related to Figure IV-1.

(A) Contribution of pyruvate carboxylation and (B) glutamine oxidation to the Krebs cycle in RCC cells. Student's t-test compared *VHL*-reconstituted to vector-only RCC cells.

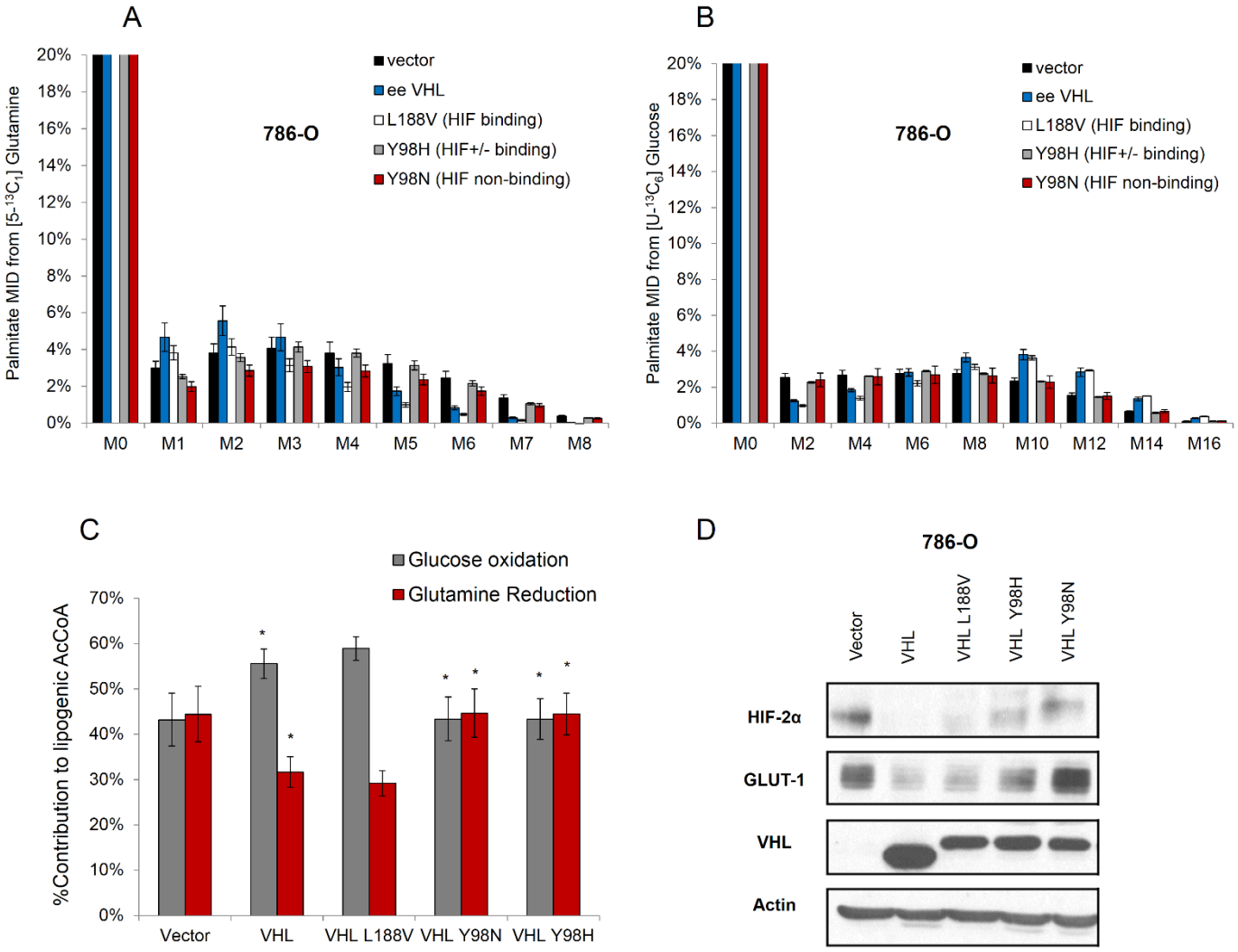
A
Palmitate MID from [5-13C1] Glutamine
786-O
vector
ee VHL
L188V (HIF binding)
Y98H (HIF+/- binding)
Y98N (HIF non-binding)
M0 M1 M2 M3 M4 M5 M6 M7 M8
B
Palmitate MID from [U-13C6] Glucose
786-O
M0 M2 M4 M6 M8 M10 M12 M14 M16
C
Glucose oxidation
Glutamine Reduction
%Contribution to lipogenic AcCoA
Vector VHL VHL L188V VHL Y98N VHL Y98H
D
786-O
Vector VHL VHL L188V VHL Y98H VHL Y98N
HIF-2α
GLUT-1
VHL
Actin

Supplementary Figure IV-S2. Regulation of Reductive Lipogenesis by the pVHL-HIF Interaction in 786-O Cells, Related to Figure IV-2.

The panel of mutant 786-O cells was cultured for 2-3 days with [5-$^{13}C_1$] glutamine or [U-$^{13}C_6$] glucose. (A-B) Mass isotopomer distributions (MIDs) of palmitate in 786-O cells labeled with [5-$^{13}C_1$] glutamine (A) or [U-$^{13}C_6$] glucose (B). (C) Specific contribution from glucose oxidation and glutamine reduction to lipogenic AcCoA in a panel of 786-O-derived cell lines, using the ISA method (D) HIF-2α, VHL and GLUT1 protein levels in vector-only, VHL-reconstituted and VHL mutant 786-O cells. Statistical significance compared VHL-reconstituted to vector-only or to VHL mutants (Y98N/Y98H). Error bars represent 95% confidence intervals in (C).

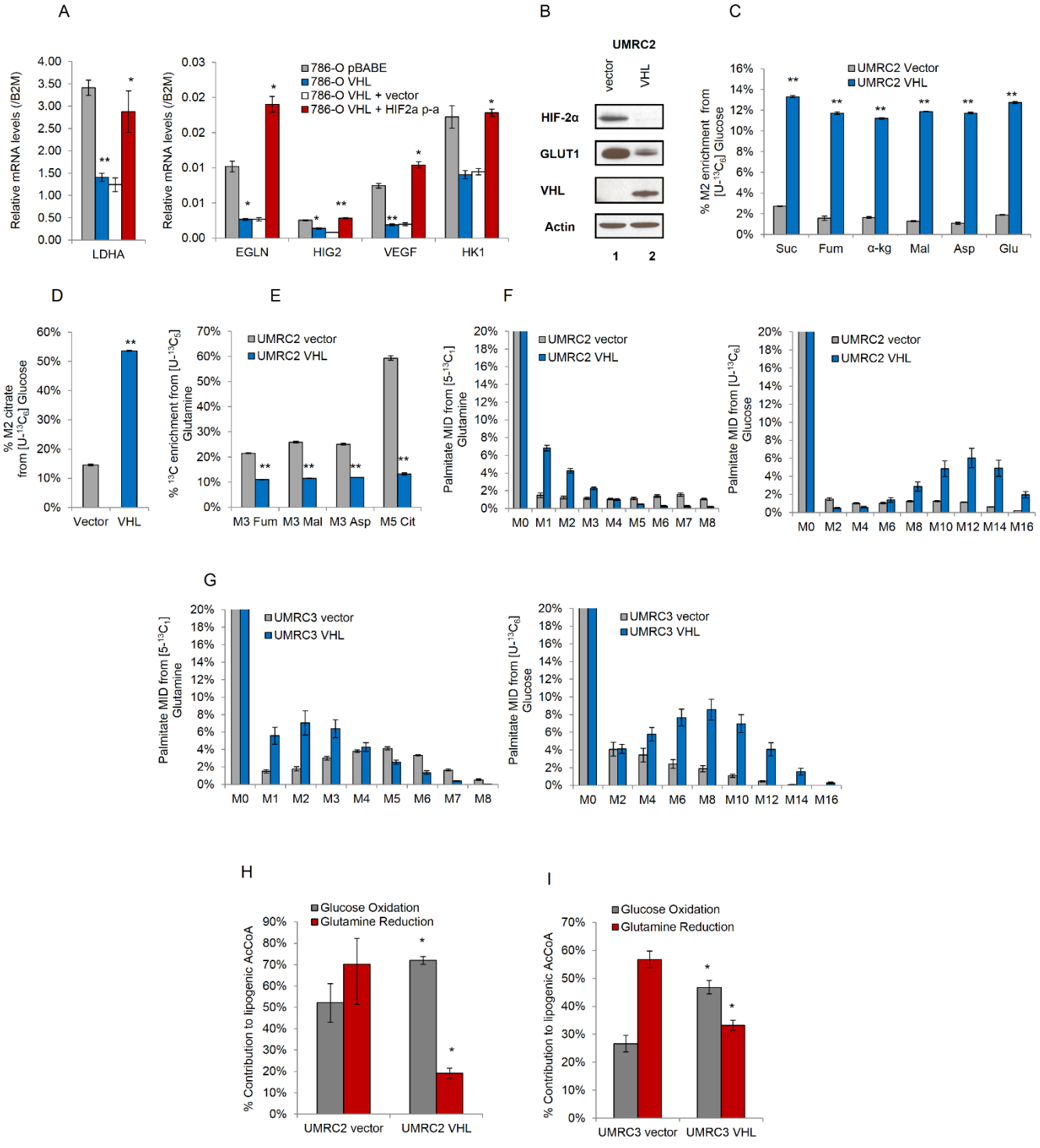
A
Relative mRNA levels (/B2M)
LDHA
786-O pBABE
786-O VHL
786-O VHL + vector
786-O VHL + HIF2a p-a
EGLN
HIG2
VEGF
HK1
B
UMRC2
vector
VHL
HIF-2α
GLUT1
VHL
Actin
1
2
C
% M2 enrichment from [U-13C6] Glucose
UMRC2 Vector
UMRC2 VHL
Suc
Fum
α-kg
Mal
Asp
Glu
D
% M2 citrate from [U-13C6] Glucose
Vector
VHL
E
% 13C enrichment from [U-13C5] Glutamine
UMRC2 vector
UMRC2 VHL
M3 Fum
M3 Mal
M3 Asp
M5 Cit
F
Palmitate MID from [5-13C1] Glutamine
UMRC2 vector
UMRC2 VHL
M0 M1 M2 M3 M4 M5 M6 M7 M8
Palmitate MID from [U-13C6] Glucose
UMRC2 vector
UMRC2 VHL
M0 M2 M4 M6 M8 M10 M12 M14 M16
G
Palmitate MID from [5-13C1] Glutamine
UMRC3 vector
UMRC3 VHL
M0 M1 M2 M3 M4 M5 M6 M7 M8
Palmitate MID from [U-13C6] Glucose
UMRC3 vector
UMRC3 VHL
M0 M2 M4 M6 M8 M10 M12 M14 M16
H
% Contribution to lipogenic AcCoA
Glucose Oxidation
Glutamine Reduction
UMRC2 vector
UMRC2 VHL
I
% Contribution to lipogenic AcCoA
Glucose Oxidation
Glutamine Reduction
UMRC3 vector
UMRC3 VHL

Supplementary Figure IV-S3. Evidence for Regulation of Reductive Lipogenesis by pVHL and HIF-2α P-A Mutant in RCC Cells, Related to Figure IV-3.

(A) mRNA expression level of HIF-2α target genes, normalized that of the beta2-microglobulin. (B) HIF-2α, pVHL and GLUT1 protein levels in VHL-deficient/VHL-reconstituted UMRC2 cells. (C-E) Regulation of glucose oxidation (C, D) and reductive carboxylation (E) by reintroduction of pVHL in VHL-deficient UMRC2 cells. (F-G) Mass isotopomer distributions (MIDs) of palmitate in UMRC2 (F) and UMRC3 cells (G) labeled with [5-$^{13}C_1$] glutamine or [U-$^{13}C_6$] glucose. (H-I) Specific contribution from glucose oxidation and glutamine reduction to lipogenic AcCoA in UMRC2 (H) and UMRC3 (I) cells, determined by the ISA method. Student's t-test compared wild type EE-VHL, mutant HIF-2α pa, or inducible HIF-1α/2α expressing cells to corresponding control cells. Error bars represent 95% confidence intervals in (H), (I).

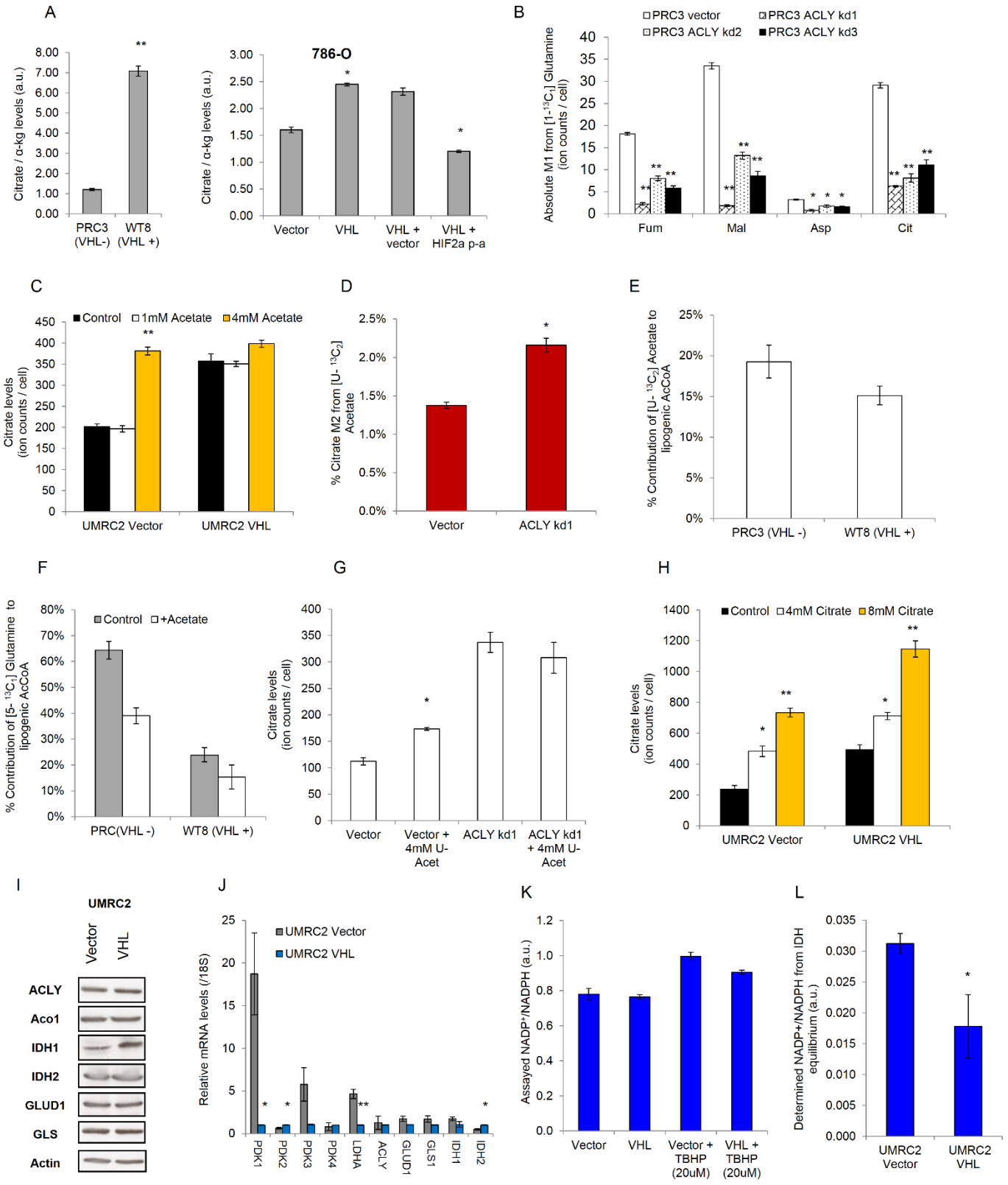
A
Citrate / α-kg levels (a.u.)
PRC3 (VHL-)
WT8 (VHL +)
786-O
Vector
VHL
VHL + vector
VHL + HIF2a p-a
B
PRC3 vector
PRC3 ACLY kd1
PRC3 ACLY kd2
PRC3 ACLY kd3
Absolute M1 from [1-13C1] Glutamine (ion counts / cell)
Fum
Mal
Asp
Cit
C
Control
1mM Acetate
4mM Acetate
Citrate levels (ion counts / cell)
UMRC2 Vector
UMRC2 VHL
D
% Citrate M2 from [U-13C2] Acetate
Vector
ACLY kd1
E
% Contribution of [U-13C2] Acetate to lipogenic AcCoA
PRC3 (VHL -)
WT8 (VHL +)
F
Control
+Acetate
% Contribution of [5-13C1] Glutamine to lipogenic AcCoA
PRC(VHL -)
WT8 (VHL +)
G
Citrate levels (ion counts / cell)
Vector
Vector + 4mM U-Acet
ACLY kd1
ACLY kd1 + 4mM U-Acet
H
Control
4mM Citrate
8mM Citrate
Citrate levels (ion counts / cell)
UMRC2 Vector
UMRC2 VHL
I
UMRC2
Vector
VHL
ACLY
Aco1
IDH1
IDH2
GLUD1
GLS
Actin
J
UMRC2 Vector
UMRC2 VHL
Relative mRNA levels (/18S)
PDK1
PDK2
PDK3
PDK4
LDHA
ACLY
GLUD1
GLS1
IDH1
IDH2
K
Assayed NADP+/NADPH (a.u.)
Vector
VHL
Vector + TBHP (20uM)
VHL + TBHP (20uM)
L
Determined NADP+/NADPH from IDH equilibrium (a.u.)
UMRC2 Vector
UMRC2 VHL

Supplementary Figure IV-S4. Evidence for Induction of Reductive Carboxylation by Citrate Levels in HIF--Expressing Cells, Related to Figure IV-5.

(A) Citrate to α-ketoglutarate ratio observed in PRC3/WT8 cells and in the panel of 786-O cell lines used in our isotopic studies. (B) Total contribution of reductive carboxylation in vector control/ACLY knocked-down PRC3 cells, determined by the total M1 counts of Krebs cycle metabolites. (C) Rescue of citrate levels by acetate addition in the panel of UMRC2 cells. (D) Contribution of [U-$^{13}C_2$] acetate to citrate production in vector control/ACLY knocked-down PRC3 cells. (E) Specific contribution of [U-$^{13}C_2$] acetate to lipid carbon and (F) the effect of naturally labeled acetate on the contribution of glutamine reduction to lipogenesis in PRC3/WT8 cells. (G) Rescue of citrate levels by acetate addition in control/ACLY knocked-down PRC3 cells. (H) Rescue of citrate levels by acetate addition in the panel of UMRC2 cells. (I) Immunoblot for glutaminase (GLS), glutamate dehydrogenase 1 (GLUD1), isocitrate dehydrogenase 2 (IDH2), isocitrate dehydrogenase 1 (IDH1), aconitase/IRP1 (Aco1), and ATPcitrate lyase (ACLY) in UMRC2 cells reconstituted with empty vector control (lane 1) or wild type EE-VHL (lane 2). (J) mRNA levels of pyruvate dehydrogeanse kinase 1 (PDK1), PDK2, PDK3, PDK4 and glutamine-metabolizing enzymes in the panel of UMRC2 cells. (K-L) NADP+/NADPH ratios in VHL-deficient/VHL-reconstituted UMRC2 cells assayed in the cell extract (K) and determined using the ratios of the oxidized and reduced metabolites of the NADPH-linked IDH equilibrium (L). tert-Butyl hydroperoxide (TBHP) was used as an oxidant control. Student's t-test compared: 1) VHL-reconstituted or mutant HIF-2α p-a to corresponding control cells (for panels A, J and L), 2) ACLY knocked-down to control PRC3 cells (for panels B and D), and 3) acetate or citrate-rescued cells to correspondent controls (for panels C, G and H).

This page was intentionally left blank

"Life is like riding a bicycle. To keep your balance you must keep moving".

Albert Einstein

This page was intentionally left blank

Chapter V

V. Cofactor Balance by Nicotinamide Nucleotide Transhydrogenase (NNT) Coordinates Reductive Carboxylation and Glucose Catabolism in the Krebs Cycle

Chapter V presents doctoral work published in a peer-reviewed scientific journal:

Gameiro, P.A., Laviolette, L. a., Kelleher, J.K., Iliopoulos, O., and Stephanopoulos, G. (2013b). Cofactor balance by nicotinamide nucleotide transhydrogenase (NNT) coordinates reductive carboxylation and glucose catabolism in the TCA cycle*. **The Journal of Biological Chemistry** *288*, 12967–12977.

* This article was selected as a Paper of the Week.

V.1. ABSTRACT

Cancer and proliferating cells exhibit an increased demand for glutamine-derived carbons to support anabolic processes. In addition, we have shown that reductive carboxylation (RC) of α-ketoglutarate by isocitrate dehydrogenase 1 (IDH1) and 2 (IDH2 is a major source of citrate synthesis from glutamine. The role of NAD(P)H/NAD(P)$^+$ cofactors in coordinating glucose and glutamine utilization in the Krebs cycle is not well understood, with the source(s) of NADPH for the RC reaction remaining unexplored. Nicotinamide nucleotide transhydrogenase (NNT) is a mitochondrial enzyme that transfers reducing equivalents from NADH to NADPH. Here, we show that knockdown of NNT inhibits the contribution of glutamine to the Krebs cycle and activates glucose catabolism in SkMel5 melanoma cells. The increase in glucose oxidation partially occurs through pyruvate carboxylase and renders NNT knockdown cells more sensitive to glucose deprivation. Importantly, knocking down NNT inhibits RC in SkMel5 and 786-O renal carcinoma cells. Overexpression of NNT is sufficient to stimulate glutamine oxidation and RC, whereas it inhibits glucose catabolism in the Krebs cycle. These observations are supported by an impairment of the NAD(P)H / NAD(P)$^+$ ratios. Our findings underscore the role of NNT in regulating central carbon metabolism via redox balance, calling for other mechanisms that coordinate substrate preference to maintain a functional Krebs cycle.

Cancer and proliferating cells largely depend on glycolysis but also switch to a glutamine-maintained Krebs cycle to meet the needs of accelerated growth and proliferation. Such metabolic reprogramming maximizes the utilization of glucose for glucose-specific anabolic processes, while ensuring a functional Krebs cycle for macromolecule synthesis (Dang, 2010; Wise and Thompson, 2010). As such, elucidating the signaling pathways and allosteric mechanisms that coordinate glucose and glutamine utilization is key to identify metabolic dependencies of cancer cells. In the previous chapters, we described the metabolic reprogramming of glutamine that occurs in hypoxia and *VHL*-deficient renal cell carcinoma (RCC) cells. Upon hypoxia, the reductive carboxylation (RC) of α-

ketoglutarate by isocitrate dehydrogenase 1 (IDH1) and/or 2 (IDH2) becomes the primary pathway of citrate and lipid synthesis. In Chapter IV, we showed that hypoxia inducible factors (HIFs) are necessary and sufficient to promote RC through a mass-action effect on citrate levels. In this context, the IDH1/IDH2 equilibrium is as follows:

$$\frac{[\alpha - \text{ketoglutarate}]\ [\text{NADPH}]\ [\text{CO2}]}{[\text{Isocitrate}][\text{NADP} +]} = \text{K (IDH)}$$

Therefore, the reverse IDH reaction (reductive carboxylation) is NADPH-dependent, whereby NADPH donates the hydride ion (H^-) that reduces α-ketoglutarate into isocitrate (Dalziel and Londesborough, 1968; Leonardi et al., 2012; Siebert et al., 1957). We observed that HIF expression did not increase NADPH levels, and the sources of this cofactor for the reverse reaction of IDH enzymes remain unexplored thus far.

In addition, it is recognized that the Krebs cycle is inherently an oxygen-dependent pathway that oxidizes metabolic intermediates to produce NADH, the reducing equivalents necessary for ATP production. Thus, the mitochondrial NADH/NAD^+ ratio is an allosteric regulator of the Krebs cycle activity via coupling to oxidative phosphorylation (Moreno-Sanchez et al., 1990), but its role in coordinating glucose and glutamine entry in the Krebs cycle is not well understood from a carbon flux distribution point of view. Given the requirement of a functional Krebs cycle for a cell to proliferate, it is possible that shifting the NADH/NAD^+ to a more oxidized or reduced state may differently affect glucose and glutamine utilization in the Krebs cycle.

Here, we investigate the role of cofactor balance by nicotinamide nucleotide transhydrogenase (NNT) in central carbon metabolism. Using ^{13}C isotopic tracers, we elucidate the function of NNT in regulating the Krebs cycle activity, in particular its contribution to glutamine-derived RC and glucose catabolism.

V.2. RESULTS

Knockdown of NNT Decreases the Contribution of Glutamine into the Krebs cycle

We hypothesized that disturbances in the mitochondrial NAD(P)H/NAD(P)$^+$ balance due to knockdown of NNT would affect glucose and glutamine utilization in the Krebs cycle. To investigate the role of NNT in intermediary central carbon metabolism, we knocked down its translation and employed different [^{13}C] glucose and [^{13}C] glutamine isotopic tracers to determine the enrichment of Krebs cycle metabolites by GC-MS analysis. We infected SkMel5 melanoma cell lines with lentiviruses containing NNT-targeting shRNA sequences and generated NNT knockdown polyclonal cell populations (Figure V-1A). The SkMel5 cell line highly expresses NNT at the RNA level, along with other melanomas, leukemia, and some renal cell carcinoma cells, according to the NCI-60 panel (dtp.nci.nih.gov/mtargets/mt_search.html). To trace the contribution of glutamine to the Krebs cycle, we cultured the SkMel5 cells in the presence of the [U-$^{13}C_5$] glutamine tracer. Knockdown of NNT decreased the contribution of glutamine oxidation to the Krebs cycle, as determined by the level of M4 enrichment of Krebs cycle metabolites (Figure V-1B, see Chapter II for atom transition map). We observed that the enrichment of M5 citrate, M3 fumarate, M3 malate, and M3 aspartate was also significantly decreased in NNT knockdown SkMel5 cells when compared with control cells infected with scramble vector shRNA (Figure V-1C), which indicates a decreased contribution of reductive carboxylation (RC) to the Krebs cycle. We also tested the effect of NNT knockdown on RC by culturing the cells with the [1-$^{13}C_1$] glutamine tracer, which specifically transfers the ^{13}Clabeled carbon to the Krebs cycle metabolites only through RC.

Knocking down NNT decreased the percentage of M1 Krebs cycle metabolites in SkMel5 cells (Figure V-1D). We observed that the anaplerotic contribution from glutamine was also reduced in NNT knockdown SkMel5 cells (Figure V-1E), suggesting a switch in substrate preference (from glutamine to glucose) for the production of α-ketoglutarate/glutamate. Nevertheless, we observed a specific inhibition of RC in SkMel5 cells under NNT knockdown conditions when accounting for the anaplerotic

contribution from glutamine (Figure V-1F). We also tested the role of NNT on RC activity in a *VHL*-deficient renal cell carcinoma cell line, which relies heavily on this reductive pathway (Gameiro et al., 2013a). To this end, we knocked down NNT in *VHL*-deficient 786-O cells (Figure V-1G) and cultured them in the presence of [1-$^{13}C_1$] glutamine. Scramble vector-infected 786O cells exhibited a high RC activity when compared with Sk-Mel5 cells (Figure V-1H). Knockdown of NNT decreased the enrichment of M1 citrate (Figure V-1H), whereas it only modestly affected glutamine-derived anaplerosis in 786-O cells (Figure V-1I), as determined by comparing the M1 enrichment between α-ketoglutarate and glutamate. This difference in the anaplerotic response to NNT knockdown may be due to the specific allosteric effects of NAD(P) on glutamate dehydrogenase (see "Discussion"). Interestingly, we did not observe changes in the M1 enrichment of fumarate, malate, and aspartate, downstream metabolites of the IDH2 reaction that are formed in the cytosol. Therefore, we cannot rule out a compensatory role of the cytosolic IDH1 reaction in cells that largely rely on this pathway and may require a constant supply of NADPH. Taken together, these data show that NNT, strictly involved in cofactor balance, contributes to glutamine oxidation and RC in the mitochondrion.

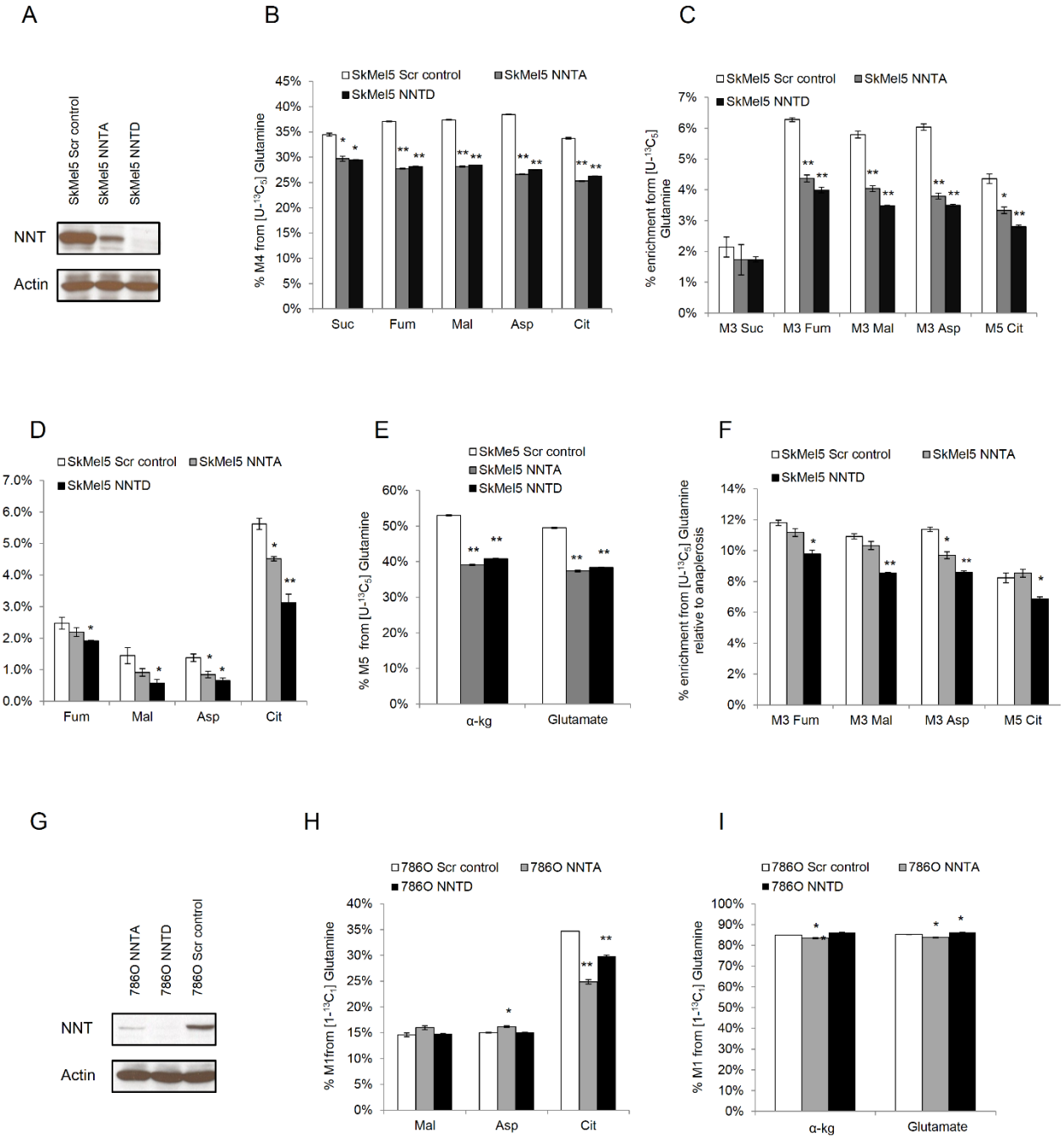
A
SkMel5 Scr control
SkMel5 NNTA
SkMel5 NNTD
NNT
Actin
B
SkMel5 Scr control
SkMel5 NNTA
SkMel5 NNTD
% M4 from [U-13C5] Glutamine
Suc
Fum
Mal
Asp
Cit
C
SkMel5 Scr control
SkMel5 NNTA
SkMel5 NNTD
% enrichment form [U-13C5] Glutamine
M3 Suc
M3 Fum
M3 Mal
M3 Asp
M5 Cit
D
SkMel5 Scr control
SkMel5 NNTA
SkMel5 NNTD
% M1 from [1-13C1] Glutamine
Fum
Mal
Asp
Cit
E
SkMe5 Scr control
SkMel5 NNTA
SkMel5 NNTD
% M5 from [U-13C5] Glutamine
α-kg
Glutamate
F
SkMel5 Scr control
SkMel5 NNTA
SkMel5 NNTD
% enrichment from [U-13C5] Glutamine relative to anaplerosis
M3 Fum
M3 Mal
M3 Asp
M5 Cit
G
786O NNTA
786O NNTD
786O Scr control
NNT
Actin
H
786O Scr control
786O NNTA
786O NNTD
% M1from [1-13C1] Glutamine
Mal
Asp
Cit
I
786O Scr control
786O NNTA
786O NNTD
% M1 from [1-13C1] Glutamine
α-kg
Glutamate

Figure V-1. Effect of NNT Knockdown on Glutamine Catabolism

(A) Validation of NNT knockdown in SkMel5 cells. (B–F) Effect of NNT knockdown on glutamine metabolism in SkMel5 cells. (B and C) Contribution of glutamine oxidation (B) and reductive carboxylation (C) to the Krebs cycle, from [U-$^{13}C_5$] glutamine. (D) Contribution of reductive carboxylation to the Krebs cycle using the [1-$^{13}C_1$] glutamine tracer. (E) Contribution of glutamine anaplerosis to α-ketoglutarate (α-kg) formation. (F) Normalized contribution of reductive carboxylation in the panel of SkMel5 cells, from [U-$^{13}C_5$] glutamine. (G) Validation of NNT knockdown in 786-O cells. (H) Contribution of reductive carboxylation to the Krebs cycle in NNT knockdown 786-O cells. (I) Contribution of glutamine anaplerosis to α-ketoglutarate (α-kg) formation in 786-O cells. Student's t test compares NNT knockdown cells to Scr control cells. Scr control, scramble control; Suc, succinate; Fum, fumarate; Mal, malate; Asp, aspartate; Cit, citrate.

Knockdown of NNT Stimulates Glucose Catabolism in the Krebs Cycle

To study the role of NNT in glucose metabolism, we labeled the SkMel5 cells with [U-$^{13}C_6$] glucose for 24hr and determined its contribution to the formation of Krebs cycle metabolites by GC-MS analysis. The [U-$^{13}C_6$] glucose tracer transfers *two* ^{13}C units to Krebs cycle metabolites via pyruvate dehydrogenase (PDH), whereas pyruvate carboxylase (PC) activity incorporates *three* ^{13}C atoms in oxaloacetate, which then propagate to other Krebs cycle metabolites (See atom transition map in Chapter II). As such, M3 mass isotopomers of Krebs cycle metabolites are associated with PC activity, whereas M5 citrate, M4 α-ketoglutarate, and M4 glutamate reflect the overall contribution of glucose carbons via pyruvate dehydrogenase and PC. Although knockdown of NNT decreased glutamine oxidation in SkMel5 cells, it concurrently activated glucose catabolism in the Krebs cycle, as seen by the level of enriched Krebs cycle metabolites from [U-$^{13}C_6$] glucose (Figure V-2A and V-2B), suggesting that knockdown of NNT switches substrate preference to a glucose-derived Krebs cycle. We did not observe changes in the M2 isotopomers of these metabolites, indicating that the specific contribution of PDH (relative to PC-derived anaplerosis) was not significantly affected under NNT knockdown conditions (data not shown). Because M3 mass isotopomers can also be formed by continued Krebs cycling, we cultured the SkMel5 cells with [3-$^{13}C_1$] glucose to trace the specific contribution of glucose-derived anaplerosis to the Krebs cycle, in which the labeled carbon in pyruvate is either retained in

oxaloacetate via PC or lost as CO_2 through PDH. PC activity was stimulated in NNT knockdown SkMel5 (Figure V-2C). Of note, the increase in the M1 enrichment of Krebs cycle metabolites in NNT knockdown cells was not as pronounced as that observed in the M3 and M5 isotopomers from [U-$^{13}C_6$] glucose. Because the M1 oxaloacetate (in the one-carbon form) from [3-$^{13}C_1$] glucose leads to M1 citrate (in the six-carbon form), the ^{13}C label is partially lost during oxidative Krebs cycle, possibly diluting the propagation of the PC-derived ^{13}C label during subsequent Krebs cycling. Similar results were obtained in 786-O cells (Figure V-2D and V-2E), although the effect was not as pronounced as that observed in SkMel5 cells. These observations support our results using [U-$^{13}C_5$] glutamine, which show that glutamine oxidation is decreased in SkMel5 cells but is not significantly affected in 786-O cells upon NNT knockdown.

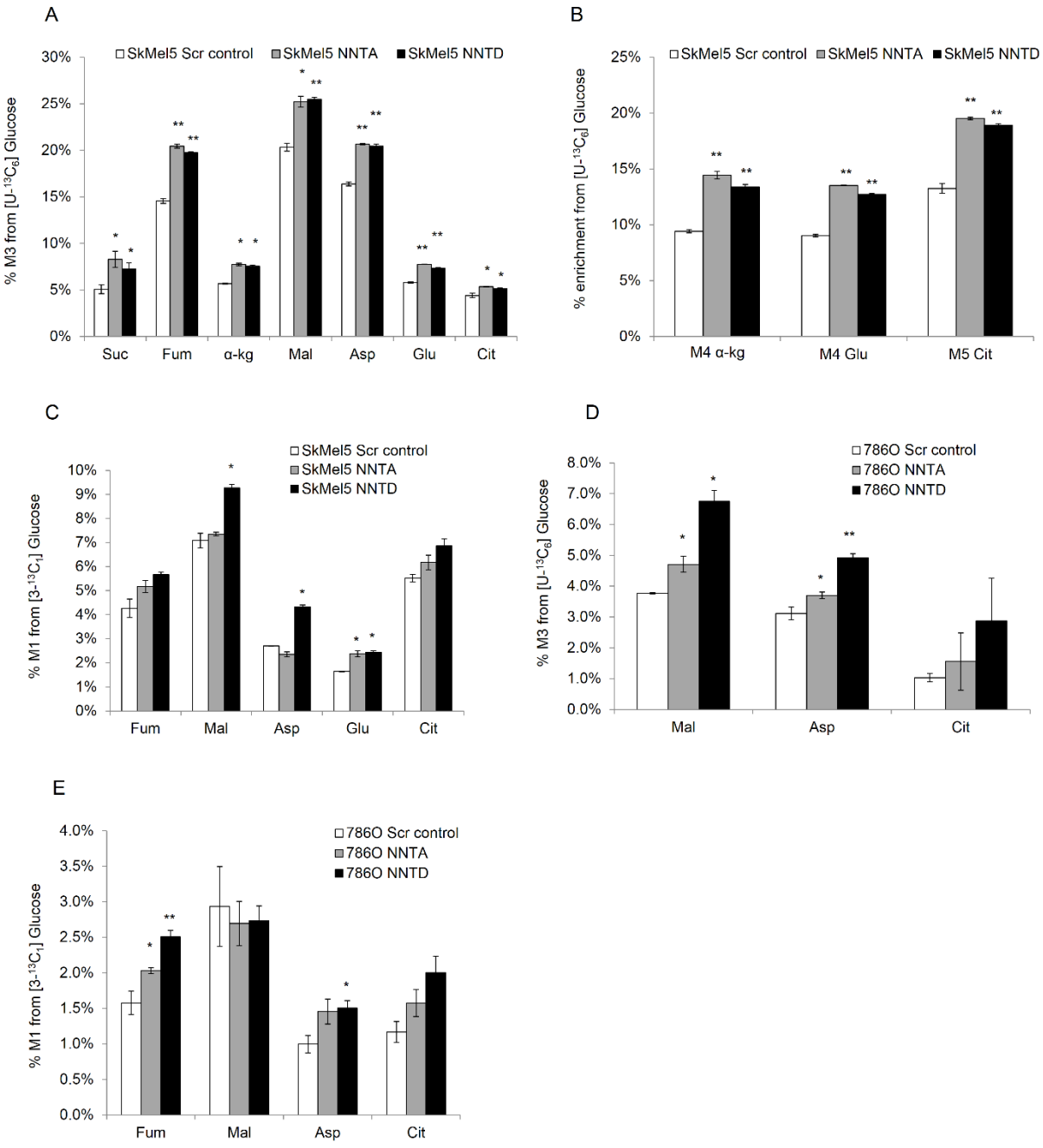

Figure V-2. Effect of NNT Knockdown on Glucose Catabolism

(A and B) Contribution of glucose oxidation to the Krebs cycle in the panel of SkMel5 cells, determined by the enrichment of M3 (A) and M4/M5 (B) Krebs cycle metabolites, from [U-$^{13}C_6$] glucose. (C) Specific contribution of pyruvate carboxylase to the formation of Krebs cycle metabolites in NNT knockdown and control SkMel5 cells, using the [3-$^{13}C_1$] glucose tracer. (D and E) Contribution of glucose oxidation to the Krebs cycle in the panel of 786-O cells, from [U-$^{13}C_6$] glucose (D) and [3-$^{13}C_1$] glucose (E). Student's t test compares NNT knockdown cells to Scr control cells. Scr control, scramble control; Suc, succinate; Fum, fumarate; α-kg, α-ketoglutarate; Mal, malate; Asp, aspartate; Glu, glutamate; Cit, citrate.

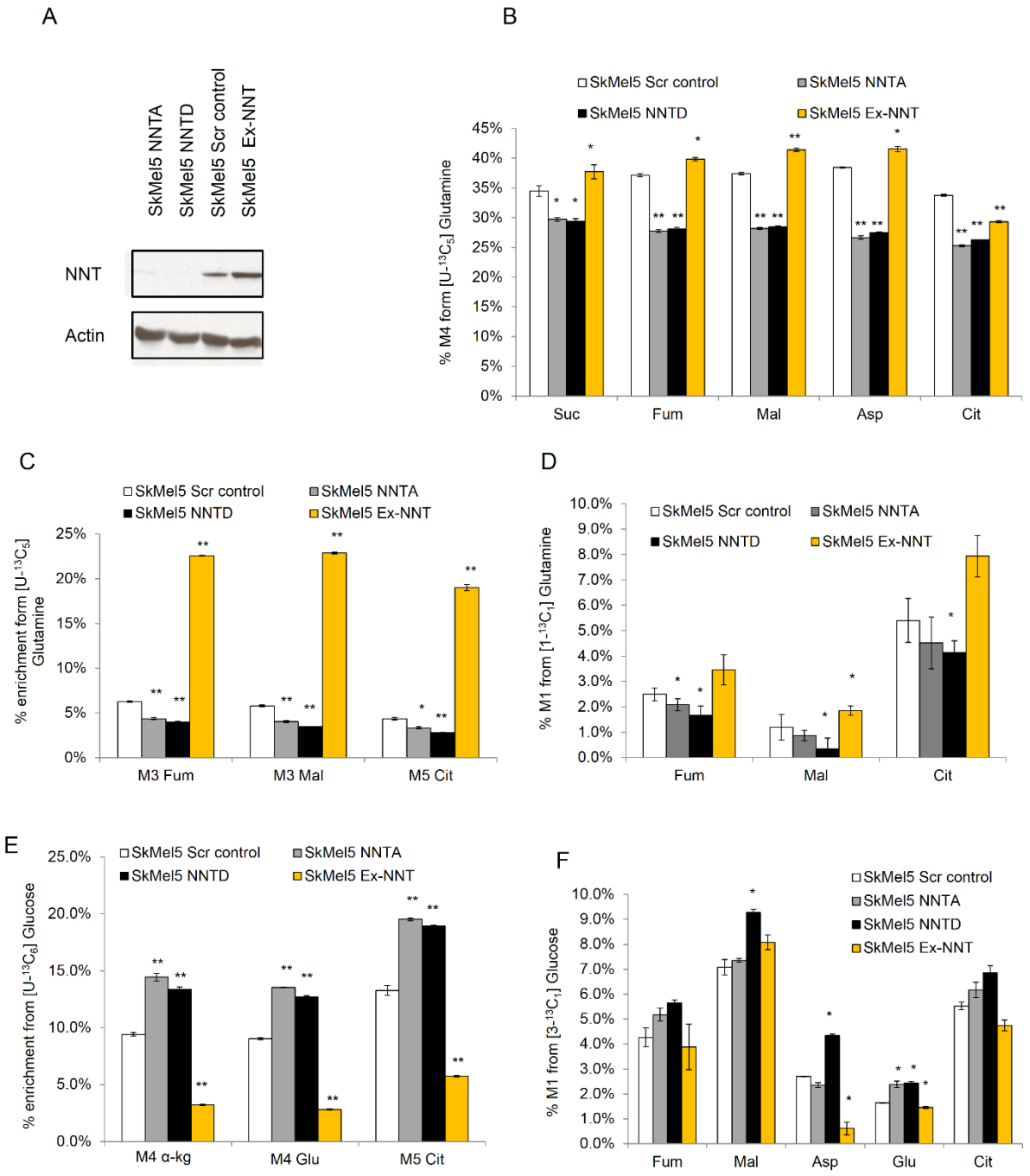
A
SkMel5 NNTA
SkMel5 NNTD
SkMel5 Scr control
SkMel5 Ex-NNT
NNT
Actin
B
SkMel5 Scr control
SkMel5 NNTA
SkMel5 NNTD
SkMel5 Ex-NNT
% M4 form [U-13C5] Glutamine
Suc
Fum
Mal
Asp
Cit
C
% enrichment form [U-13C5] Glutamine
M3 Fum
M3 Mal
M5 Cit
D
% M1 from [1-13C1] Glutamine
E
% enrichment from [U-13C6] Glucose
M4 α-kg
M4 Glu
M5 Cit
F
% M1 from [3-13C1] Glucose
Glu

Figure V-3. Metabolic Effects of NNT Overexpression in SkMel5 Cells

(A) NNT protein levels in the panel of SkMel5 cells (Ex-NNT, lane 4). (B–D) Effect of NNT overexpression on glutamine catabolism. (B and C) Contribution of glutamine oxidation (B) and reductive carboxylation (C) from [U-$^{13}C_5$] glutamine. (D) Effect of NNT overexpression on reductive carboxylation, using the [1-$^{13}C_1$] glutamine tracer. (E and F) Contribution of glucose oxidation to the Krebs cycle in the panel of SkMel5 cells, from [U-$^{13}C_6$] glucose (E) and [3-$^{13}C_1$] glucose (F). Student's t test compares NNT knockdown or NNT-overexpressing cells to Scr control cells. Scr control, scramble control; Suc, succinate; Fum, fumarate; Mal, malate; Asp, aspartate; Cit, citrate; α-kg, α-ketoglutarate.

NNT Is Sufficient to Stimulate RC and Suppress Glucose Catabolism in the Krebs Cycle

Because knockdown of NNT affected glucose and glutamine utilization in the Krebs cycle, we investigated whether overexpression of NNT could be sufficient to induce a complementary metabolic response, in particular in the contribution of reductive carboxylation (RC). To this end, we stably transfected SkMel5 cells with an NNT-coding cDNA plasmid and generated a polyclonal cell population that overexpressed NNT (Ex-NNT) when compared with their scramble vector counterparts (Figure V-3A). Overexpressing NNT simulated the contribution of glutamine oxidation (Figure V-3B) and RC (Figure V-3C and V-3D) to the Krebs cycle. Conversely, PC-derived anaplerosis was inhibited in NNT-overexpressing cells when compared with the scramble vector cells (Fig. 3, *E* and *F*). These data suggest that NNT is sufficient to coordinate glutamine and glucose utilization in the Krebs cycle.

Knockdown of NNT Decreases Cell Proliferation and Sensitizes SkMel5 Melanoma Cells to Glucose Deprivation

Because knockdown of NNT switched the substrate preference in the Krebs cycle from glutamine to glucose carbons, we hypothesized that NNT knockdown cells would be more dependent on glucose for proliferation. To test this, we first measured the specific glucose uptake and lactate secretion rates in the panel of SkMel5 cells over a period of 72hr. NNT knockdown SkMel5 cells exhibited higher glucose uptake and lactate secretion when compared with control cells (Figure V-4A). The net intake of

glucose was also higher in NNT knockdown cells when compared with control cells (Figure V-4B), compatible with an overall higher demand of glucose carbons to fuel the Krebs cycle. We did not observe significant differences in glutamine consumption and glutamate production rates in the panel of SkMel5 cells (data not shown). Next, to exploit the dependence on glucose carbons, we cultured the panel of SkMel5 cell lines for 24hr in low glucose medium. Loss of viability was more pronounced in NNT knockdown cells, with NNT-overexpressing cells being almost insensitive to low glucose concentrations (Figure V-4C). Conversely, NNT-overexpressing cells were more sensitive to glutamine deprivation when cultured in low glutamine-containing medium (Figure V-4D). We also observed that NNT knockdown SkMel5 cells exhibited decreased proliferation when compared with the control cells (Figure V-4E), with knockdown of

NNT partially suppressing the growth of SkMel5 cells growing as xenograft tumors in nu/nu mice (Figure V-4F). In agreement with the isotopic studies, these findings show that low expression of NNT partially rewires glucose and glutamine catabolism in the Krebs cycle, rendering cells sensitive to glucose deprivation.

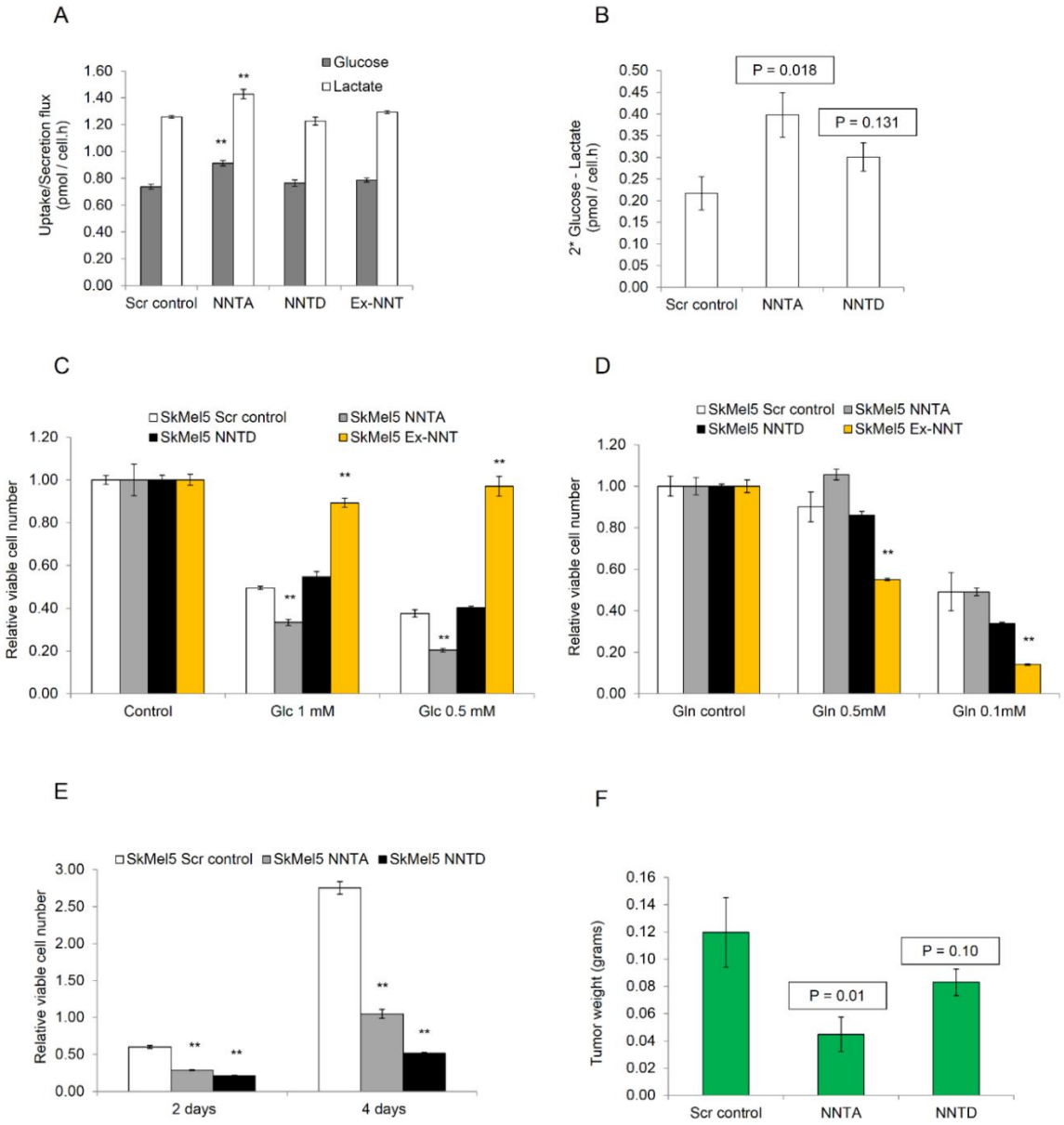

Figure V-4. Effect of NNT Knockdown on Cell Proliferation and Sensitivity to Glucose Carbons

(A) Glucose uptake and lactate secretion rates in the panel of SkMel5 cells used. (B) Net intake of glucose carbons as determined by the difference between twice the glucose consumption and lactate production rates. (C and D) Cell proliferation under low glucose (C) and low glutamine (D) conditions. Cell proliferation is normalized to the corresponding control cell type grown in 5mM glucose- and 1mM glutamine-containing medium. (E) Effect of NNT knockdown on the proliferation of SkMel5 cells. (F) Effect of NNT knockdown of the proliferation of SkMel5 cells growing as xenograft tumors in nu/nu mice. Student's t test compares NNT knockdown or NNT-overexpressing cells to Scr control cells in panels (A),(B), and the proliferation under low glucose- or glutamine-containing medium to correspondent controls in panels (C), (D). Statistical significance was determined using one-tailed Student's t test in (F). n=5 or more. Scr control, scramble control.

Effect of NNT Knockdown on Glucose and Glutamine Catabolism Is Mediated by a Distributed NAD(P)H/NAD(P)$^+$ Balance

Knockdown of NNT decreased the contribution of reductive carboxylation (RC) in the Krebs cycle, whereas NNT overexpression stimulated this pathway. To test whether the contribution of NNT to RC is related to its ability to produce NADPH, we quantified the cellular ratios of the NADP couple using a fluorescent enzymatic assay and LC-MS. As shown in Figure V-5A and V-5B, the cellular ratio of NADPH/NADP$^+$ was lower in NNT knockdown than in scramble control SkMel5 cells, whereas NNT-overexpressing cells exhibited a higher ratio (Figure V-5A). The NADPH and NADP$^+$ levels and the effect of each NNT knockdown construct on this ratio varied based on the quantification method, possibly reflecting the different extraction procedures. To examine the compensatory role of glucose in providing cytosolic NADPH, we assessed the activity of the pentose phosphate pathway (PPP) under NNT knockdown conditions. To this end, we labeled the panel of SkMel5 cells with [1,2-$^{13}C_2$] glucose, which transfers one labeled carbon to CO_2 through oxidative PPP but conserves both ^{13}C atoms via glycolysis (Vizan et al., 2005). Knocking down NNT mildly increased the PPP activity relative to glycolysis in SKMel5 cells, as determined by the ratio of labeled carbon (M1) to dually labeled (M2) carbons of pyruvate and lactate (Figure V-5C). This result indicates that the observed changes in the NADPH/NADP$^+$ ratio and RC in NNT knockdown cells are marginally compensated by PPP activity in the cytosol. The ratio of the mixed pool of isocitrate/citrate to α-ketoglutarate was not significantly affected in NNT knockdown cells (data not shown). This suggests that the IDH2 reaction may be at non equilibrium under NNT knockdown conditions, wherein changes in the NADPH/NADP$^+$ ratio are not accompanied by an altered ratio of the correspondent reduced (isocitrate/citrate) and oxidized (α-ketoglutarate) metabolites (Veech et al., 1969). Nevertheless, the citrate and isocitrate levels were elevated in NNT knockdown cells (Figure V-5D), suggesting that knockdown of NNT may indirectly affect the mass action kinetics of the IDH2 reaction by modulation of citrate levels. We observed a decreased cellular NADH/NAD$^+$ ratio in NNT knockdown cells (Figure V-5E and V-5F), in agreement

with the findings of Yin *et al.* (Yin et al., 2012), which showed that knockdown of NNT decreased the cellular NADH/NAD^+ ratio in PC12 cells. Nevertheless, this result is opposite to what would be expected based on the enzymatic reaction catalyzed by NNT. It is known that knockdown of NNT induces mitochondrial uncoupling and decreases the mitochondrial membrane potential (Freeman et al., 2006; Yin et al., 2012), which leads to a decreased mitochondrial NADH/NAD^+ ratio. Conversely, because the majority of mitochondrial NADH is in the bound form (Blinova et al., 2005) and mitochondria comprise up to 20% of the cellular volume (Alberts et al. 2002), the observed NADH/NAD^+ ratio represents mostly the ratio of the cytosolic compartment. To further examine the effect of NNT knockdown on the NADH/NAD^+ balance, we determined the levels of pyruvate and lactate, which reflect changes in the cytosolic NADH/NAD^+ ratio (Veech et al., 1969). NNT knockdown cells exhibited a higher pyruvate/ lactate ratio than control cells (Figure V-5G), which indicates a lower cytosolic NADH/NAD^+ ratio. The NADH/NAD^+ cofactor measurements support the model that knockdown of NNT stimulates the contribution of glucose oxidation to the Krebs cycle as a response to a lower NADH/NAD^+ ratio. Conversely, the NADPH/$NADP^+$ measurements corroborate our ^{13}C-labeled glutamine studies, showing that the role of NNT in contributing to RC lies in its ability to produce NADPH in the mitochondrion (Figure V-5H).

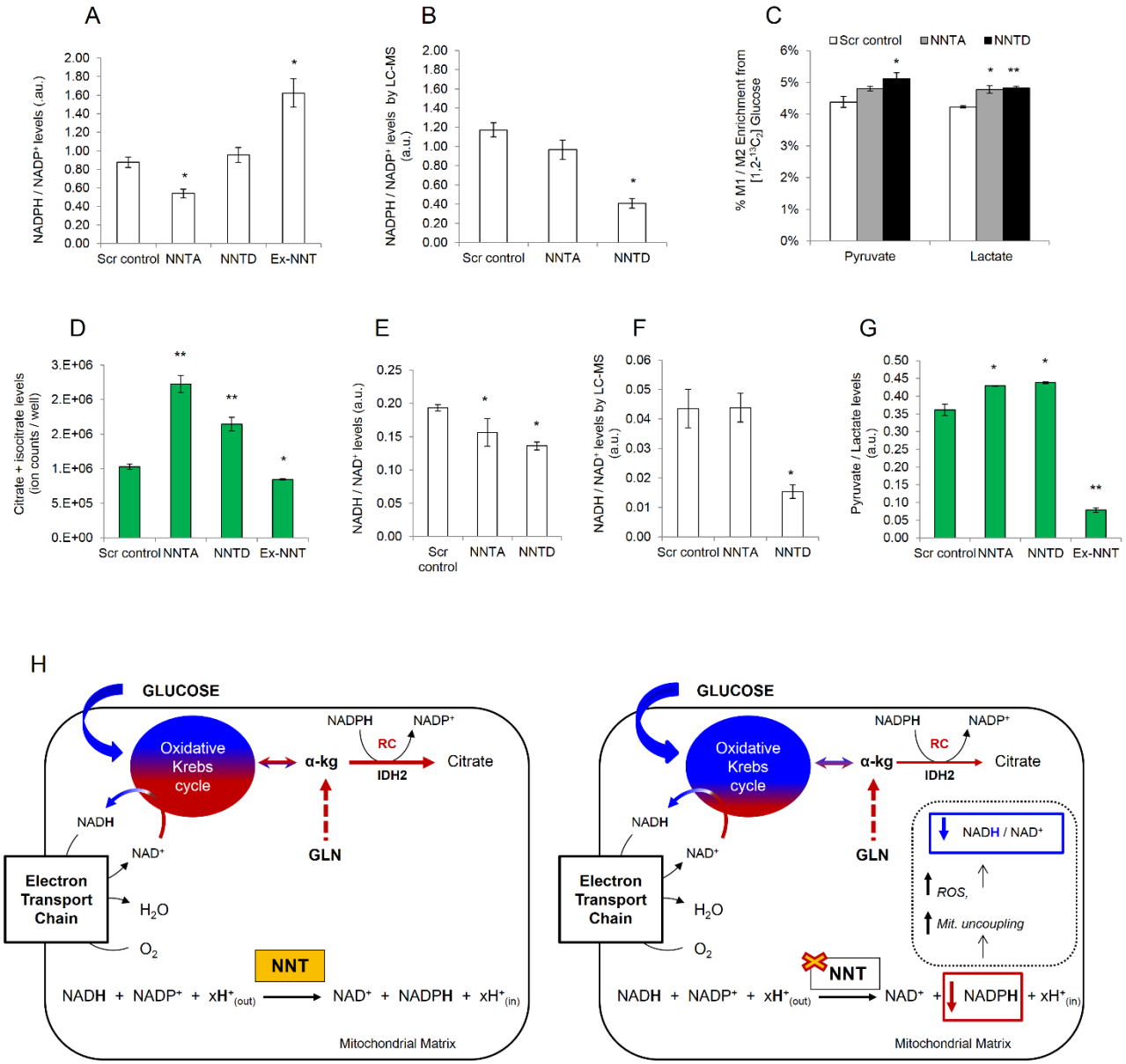

Figure V-5. Cofactor Levels in the Panel of SkMel5 Cells

(A) NADPH/NADP+ levels, assayed using an enzymatic kit according to the manufacturer's instructions. (B) NADPH/NADP+ levels, determined by LC-MS. (C) Contribution of PPP to pyruvate and lactate production, relative to glycolysis. (D) Citrate and isocitrate levels, determined by GC-MS analysis. (E) NADH/NAD+ levels assayed using an enzymatic kit according to the manufacturer's instructions. (F) NADH/NAD+ levels, determined by LC-MS. (G) Cellular pyruvate-to-lactate ratio, determined by GC-MS analysis. (H) Proposed model for the role of NNT in regulating the Krebs cycle activity. Left diagram, NNT catalysis contributes to reductive carboxylation (RC) in the mitochondrion via production of NADPH. Under NNT activated conditions, cells exhibit an adequate balance between the contribution of glucose (blue)- and glutamine (red)- derived carbons to the oxidative Krebs cycle. Right diagram, NNT loss of function decreases the NADPH/NADP+ ratio,

Figure V-5 (Cont.) which inhibits the formation of RC-derived citrate and increases reactive oxygen species (ROS) levels and mitochondrial uncoupling (Mit. uncoupling). This decreases the $NADH/NAD^+$ ratio thereby stimulating the contribution of glucose catabolism into the Krebs cycle, depicted as an increased percentage of the blue color in the oxidative Krebs cycle. Statistical significance compares NNT knockdown or NNT-overexpressing cells to Scr control cells. Error bars represent 95% confidence intervals in panels (A) and (E). Scr control, scramble control; AU, arbitrary units; α-kg, α-ketoglutarate.

V.3. DISCUSSION

NNT is recognized as a main generator of mitochondrial NADPH (Rydström, 2006). NNT has also been speculated to regulate insulin secretion and glucose homeostasis, and some studies show that NNT mutant C57BL/6J mice exhibit glucose intolerance and impaired insulin secretion (Freeman et al., 2006; Parker et al., 2009), whereas other studies have challenged this hypothesis (Nicholson et al., 2010; Wong et al., 2010). Being involved in NADPH production and proton translocation, NNT has been viewed mostly through the lens of reactive oxygen species detoxification and stress response (Rydström, 2006)(24), with mutations in NNT being reported in individuals with familial glucocorticoid deficiency (Meimaridou et al., 2012). NNT was also shown to modulate the inflammatory response of macrophages (Ripoll et al., 2012), again underscoring its role as a free radical detoxifier in the mitochondrion. NNT is strictly a cofactor-modulating enzyme, transferring the reducing equivalents (the hydride ion) from NADH to $NADP^+$, which produces the NADPH necessary to drive some anabolic reactions. In line with this perspective, the function of NNT in regard to central carbon metabolism has not been studied before. Our ^{13}C isotopic studies elucidated the outcome of a disturbed cofactor balance on the Krebs cycle activity.

Our work showed that RC by IDH2 can be modulated at the mass action level through the supply of NADPH. Knockdown of NNT inhibited the contribution of RC to the Krebs cycle in SkMel5 and 786-O cells, whereas overexpressing NNT was sufficient to stimulate this reaction. There are other candidate enzymes that may contribute to mitochondrial NADPH production. The malic enzyme 3 (ME3) is

localized in the mitochondrion and couples the production of pyruvate to reduction of $NADP^+$ (Sauer et al., 1980). We did not assess the expression levels of ME3 in SkMel5 cells or 786-O cells or its contribution to RC. However, ME3 is a carbon-metabolizing enzyme, and genetic approaches such as shRNA-mediated knockdown of overexpression will perturb not only cofactor balance but also carbon distribution. Thus, the delineation of the role of NADPH supply from that of carbon redistribution requires strategies to rule out metabolic effects that are NADPH-independent. The knockdown of NNT also inhibited glutamine oxidation in SkMel5 cells, which can be partially accounted for by a decreased anaplerosis from glutamine. Nevertheless, the contribution of RC was decreased in NNT knockdown SkMel5 cells when normalized to the anaplerotic contribution from glutamine. Conversely, the [U-$^{13}C_5$] glutamine and [1-$^{13}C_1$] glutamine studies in 786-O cells showed only a modest effect of NNT knockdown at the level of glutamine-derived anaplerosis. The conversion of glutamate into α-ketoglutarate (anaplerosis) can be mediated by glutamate dehydrogenase 1 (GLUD1) or aspartate transaminase (GOT1 and GOT2). In addition, the GLUD1 reaction can be $NADP^+$- or NAD^+-dependent toward the deamination of glutamate (Williamson et al., 1967). As such, it is conceivable that the different anaplerotic response of SkMel5 and 786-O cells to NNT knockdown may relate to the different activities of GLUD1 and GOT1/2 and/or specific requirements of GLUD1 for $NADP^+$ and NAD^+ in the different cell lines. Together, our findings highlight the role of NNT in contributing to RC via NADPH production.

We showed that knockdown of NNT concomitantly increases glucose catabolism in the Krebs cycle. The increase in glucose oxidation partially occurred via PC. This brings attention to the role of cofactors in coordinating glucose and glutamine utilization in the Krebs cycle and supports existing literature showing that PC activity is required for the growth of tumor cells in the absence of glutamine (Cheng et al., 2011). NNT knockdown SkMel5 cells exhibited a higher glucose uptake and appeared more sensitive to glucose deprivation than control cells, whereas NNT-overexpressing cells failed to do so and proliferated less under low glutamine conditions. Although the increased contribution of PC to

the Krebs cycle under NNT knockdown conditions was not as pronounced as that reported in "glutamine-independent cells" (Cheng et al., 2011), these observations shed light into the metabolic plasticity of cancer cells in response to a disturbed cofactor balance. Of note, although NNTD resulted in a better knockdown at the protein level and Krebs cycle response, we observed significant differences in the net intake of glucose, response to glucose deprivation, and *in vivo* proliferation only for NNTA (Figures V-4B, V-4C, and V-4F). This discrepancy may reflect the metabolic burden of NNTA knockdown SkMel5 cells that, even though they do not rewire their intracellular metabolism to the same extent as NNTD cells, are forced to increase their net glucose uptake to maintain an adequate flux of glucose carbons into the Krebs cycle.

It is of particular interest to discuss the observed changes in the $NADH/NAD^+$ ratio and the expected outcome in intermediary metabolism. The knowledge on the enzymatic reaction of NNT predicts that the mitochondrial $NADH/NAD^+$ ratio should be elevated under NNT knockdown conditions. We observed a decreased cellular $NADH/NAD^+$ ratio in NNT knockdown cells, which is in agreement with the findings of Yin *et al.* (Yin et al., 2012) and opposite to the predicted trend. In this context, it is reported that knockdown of NNT leads to mitochondrial uncoupling, low ATP levels, and decreased mitochondrial membrane potential (Rydström, 2006; Yin et al., 2012), which is mechanistically associated with a lower mitochondrial $NADH/NAD^+$ ratio. Therefore, the expected initial increase in mitochondrial $NADH/NAD^+$ ratio upon NNT knockdown is most likely offset by the indirect effect on mitochondrial coupling and activity of the electron transport chain. In fact, Yin *et al.* (Yin et al., 2012) noted that knockdown of NNT led to an initial increase in the cellular $NADH/NAD^+$ ratio followed by a decrease in this ratio. In addition, from the allosteric standpoint, a more reduced mitochondrion (higher $NADH/NAD^+$ ratio) should inhibit the Krebs cycle, which would be hard to reconcile with the increased glucose oxidation observed in NNT knockdown cells. However, because PC is an ATP-dependent enzyme, it is still conceivable that a higher mitochondrial $NADH/NAD^+$ may equally activate this reaction to maintain a functional Krebs cycle. The contribution of PC to the Krebs cycle in more

reduced or oxidized mitochondria is an open question. Overall, our isotopic studies showed that knockdown of NNT increased the contribution of glucose catabolism to the Krebs cycle partially through PC, as a response to a lower NADH/NAD^+ ratio.

Similarly to the study of Yin *et al.* (Yin et al., 2012), we measured the cellular NADH/NAD^+ ratio, which represents mostly the ratio of the cytosolic compartment. Indeed, the pyruvate/lactate ratio and pyruvate levels were higher in NNT knockdown cells when compared with control cells. In this context, the malate-aspartate shuttle (MAS) transfers reducing equivalents from the cytosol to the mitochondrion. The MAS activity is regulated by the mitochondrial redox state (Eto et al., 1999) and can be assessed by the pyruvate/lactate ratio (Cederbaum et al., 1973; Greenhouse and Lehninger, 1976; Kauppinen et al., 1987). Because MAS is expected to be activated by mitochondrial NADH oxidation, this raises the possibility that NNT knockdown may activate the MAS in response to a lower mitochondrial NADH/NAD^+ ratio. Conversely, MAS depends on the mitochondrial energetic state, with the addition of mitochondrial uncouplers inhibiting its activity (Cederbaum et al., 1973). Because NNT knockdown is known to increase mitochondrial uncoupling, it is unclear how NNT knockdown may impact on the MAS activity. The effect of NNT knockdown on the kinetics of reducing equivalents transport between cytosol and mitochondrion is open to debate and will require direct measurement of the compartmentalized pools of these cofactors.

Collectively, our results show the implications of a disturbed NAD(P)H/$NAD(P)^+$ balance in central carbon metabolism, highlighting the unexplored role of NNT in coordinating glucose and glutamine utilization in the Krebs cycle. These findings underline the need for cancer biologists to consider cofactors and allosterism when studying the metabolic outcomes of growth signals and transduction pathways.

"Unless you try to do something beyond what you have already mastered, you will never grow."

Ronald E. Osborn

This page was intentionally left blank

Chapter VI

VI. Loss of *VHL* Reprograms the *De Novo* and Salvage Pathways of Pyrimidine Biosynthesis in Renal Cancer Cells

Chapter VI presents doctoral work in preparation for publication in a peer-reviewed scientific journal:

Gameiro PA, Stephanopoulos G, Iliopoulos O. (2013). Loss of *VHL* Reprograms the *De Novo* and Salvage Pathways of Pyrimidine Biosynthesis Renal Cancer Cells. *(in preparation)*

VI.1. ABSTRACT

Hypoxia is a hallmark of solid tumors, and cancer cells adapt their metabolism for survival even under oxygen-limited conditions. The metabolic response to hypoxia largely relies on the transcriptional activity of hypoxia-inducible factors (HIFs), which stimulate glycolysis, lactate production, and biosynthesis from glutamine – via reductive carboxylation (RC) – to maintain *de novo* lipogenesis. The HIF-mediated metabolic program is necessary for cell survival under hypoxia, but how cancer cells regulate other anabolic processes under hypoxic or pseudohypoxic conditions is not characterized. Given the need of nucleotides for cellular growth, we sought to investigate how *VHL*-deficient RCC cells that constitutively express HIF utilize glucose and glutamine for DNA biosynthesis. In addition to being a source of lipogenic acetyl-CoA, glutamine can be used in the Krebs cycle to generate aspartate - the carbon source for pyrimidine synthesis. Here, using ^{13}C tracers, we showed that *VHL*-deficient RCC cells rely on RC-derived aspartate to maintain *de novo* pyrimidine synthesis. Pharmacological inhibition of glutaminase (GLS) depleted the levels of pyrimidine intermediates in *VHL*-deficient cells but not in *VHL*-reconstituted cells, which utilized glucose oxidation to fuel the aspartate pool. Moreover, *VHL*-deficient cells also required the salvage pathway to maintain adequate nucleotide biosynthesis. Inhibiting both the *de novo* and salvage pathways of pyrimidine synthesis selectively impaired the growth of *VHL*-deficient cells, whereas addition of nucleosides partially rescued the growth effect. Collectively, these findings add to the role of HIF in promoting metabolic adaptation to maintain macromolecule biosynthesis and viability in pseudohypoxic RCC cells.

Nucleotide availability plays a critical role in the regulation of cell-cycle and proliferation. Classical studies have shown the strong coupling of purine and pyrimidine nucleotide biosynthesis and their requirement for cell-cycle progression in normal cells (Burns, 1966; Cohen et al., 1983; Sigoillot et al., 2003). Importantly, it has been shown that *de novo* nucleotide biosynthesis is activated by oncogenes and growth signals in cancer cells (Ben-Sahra et al., 2013; Mannava et al., 2008; Robitaille et al.,

2013). Furthermore, recent studies have demonstrated that cellular nucleotide levels impinge on DNA repair and senescence (Aird et al., 2013; Hu et al., 2012; Pontarin et al., 2011). In particular, Aird *et al.,* showed that oncogene-induced repression of ribonucleotide redutase, a rate-limiting enzyme in deoxyribnonucleotide synthesis, triggers aberrant DNA replication, DNA damage and ultimately leads to senescence. The authors showed that exogenous deoxynucleosides were necessary and sufficient to suppress oncogene-induced senescence in established senescent cells, which promoted cell proliferation (Aird et al., 2013). Nucleotide insufficiency has also been implicated upon aberrant activation of the Rb-E2F pathway, which leads to genomic instability in newly transformed cells (Bester et al., 2011). Upon activation of the Rb-E2F pathway, the authors showed that expression of c-myc, a known transcriptional activator of nucleotide biosynthetic genes (Liu et al., 2008), rescues nucleotide levels and suppresses genomic instability. These studies demonstrate that importance of nucleotide availability for the proliferation of oncogene-activated cancer cells, and also suggest that nucleotide abundance or depletion may play cell-specific roles in cancer development.

Hypoxia is prevalent in many solid tumors and leads to a limited supply of nutrients to the tumor microenvironment. As a result, it selects for the survival of cells that can adapt their metabolism to oxygen- and nutrient-limited conditions, being associated with tumor chemoresistance, invasiveness, metastasis, and resistance to cell death (Gatenby and Gillies, 2004; Pouysségur et al., 2006; Wilson and Hay, 2011). As discussed in the previous chapters, hypoxia-inducible factors (HIFs) play a critical role in the cellular response to hypoxia, and mediate a transcriptional program that enforces anaerobic glucose metabolism, lactate production, and biosynthesis from glutamine (via reductive carboxylation). In addition, HIF-1α inhibits senescence (Welford et al., 2006) and, in somewhat contrast to its growth-promoting role (see Chapter I), it can also induce cell-cycle arrest at the G-1 phase, inhibition of DNA replication and reduced cell proliferation in normal and cancer cells (Goda et al., 2003; Hubbi et al., 2013; Koshiji et al., 2004a). In this context, there are evidences for a cell-specific and opposite role of the HIF-1α and HIF-2α paralogues in tumor growth (see Chapter IV - Discussion). Altogether, these

evidences underline the pleiotropic and complex role of HIF in cellular physiology, and suggest that HIF expression adapts cellular metabolism for survival under hypoxia, not only (aberrant) growth. Indeed, there is a growing interest to target hypoxia, HIF signaling and the hypoxic compartment of solid tumors (Moyer, 2012; Semenza, 2009; Wilson and Hay, 2011), but the knowledge on how HIF activation affects anabolic processes is limited. Given the role of HIF in suppressing senescence and promoting cell survival, there is an interest to investigate how oncogenic HIF activation, i.e., loss of *VHL*, redirects nutrients to maintain cell viability and growth.

Glutamine can be catabolized to aspartate in the Krebs cycle and therefore be used as carbon source for *de novo* pyrimidine synthesis (Tong et al., 2009). As introduced in chapter I, there is specific requirement for glutamine to progress through the S-phase of the cell cycle (Colombo et al., 2011; Gaglio et al., 2009). Give the role of HIF in regulating glutamine utilization in the Krebs cycle and that aspartate-carbons are necessary for *de novo* pyrimidine biosynthesis (Tong et al., 2009), we sought to investigate how *VHL* loss-of-function affects pyrimidine biosynthesis in RCC cells. Here, using ^{13}C tracers and employing a glutaminase (GLS) inhibitor as a tool compound, we show that *VHL*-deficient RCC cells depend on RC-derived aspartate to maintain *de novo* pyrimidine synthesis in a HIF-dependent manner. We provide evidences that HIF expression decreases the *de novo* flux of pyrimidines synthesis, rendering *VHL*-deficient cells more reliant on the salvage pathway to sustain nucleotide biosynthesis.

VI.2. RESULTS

Reductive Carboxylation Contributes to DNA Synthesis via Production of Aspartate in a HIF-Dependent Manner

In mammalian cells, uridine monophosphate (UMP) is the common precursor for pyrimidine-containing nucleotides, being synthesized *de novo* from 5-phosphoribosyl pyrophosphate (PRPP, produced from ribose 5-phosphate), glutamine-derived nitrogens, and aspartate. The pathway consists of six enzymatic steps; i.e., carbamoyl phosphate synthetase II (CPSII), aspartate transcarbamoylase (ACTase), dihydroorotase, dihydroorotate dehydrogenase, orotate phosphoribosyltransferase, and orotidine monophosphate decarboxylase (Shambaugh, 1979). CAD is the tri-functional enzyme that comprises the CPSII, ACTase and dehydroorotase steps of UMP synthesis, and its activity is allosterically regulated at multiple levels to mediate *de novo* pyrimidine biosynthesis in a cell cycle-dependent manner (Carrey, 1993; Rao and Church, 1988; Sigoillot et al., 2003). During the *de novo* pathway of pyrimidine synthesis in mammalian cells, glutamine donates the amide nitrogen to bicarbonate forming N-carbamoyl-phosphate via CPSII. In turn, N-carbamoyl-phosphate combines with aspartate to form N-carbamoyl-L-aspartate through ACTase, which is further modified and combined with PRPP to produce orotidine monophosphate and, after a decarboxylation step (which releases the one carbon of aspartate), uridine monophosphate (UMP) (Figure VI-1A). Therefore, aspartate contributes with three carbons for the synthesis of UMP and to the other pyrimidine nucleotides. Aspartate is produced from transaminated oxaloacetate, which can be generated from three distinct sources: i) glutamine-derived carbons only (through glutamine oxidation in the first round of the Krebs cycle), ii) reductive carboxylation, in which case it is also composed exclusively by glutamine-derived carbons, or iii) through several rounds of the Krebs cycle via the combined action of pyruvate dehydrogenase (PDH) and glutamine –anaplerosis, being formed from both glucose- and glutamine-carbons. We will refer to pathway iii) as glucose oxidation, since it requires the continuous supply of two glucose-carbons. To study pyrimidine synthesis in RCC cells, we utilized a system of isogenic RCC

UMRC2 cells that are *VHL*-deficient (HIF-expressing) and reconstituted with either a pBABE control vector (termed *VHL* $^{-/-}$) or with wild-type *VHL* (termed *VHL* $^{+/+}$), as previously described (Chapter IV). We cultured the pair of *VHL* $^{-/-}$ and *VHL* $^{+/+}$ cells in the presence of ^{13}C glucose and glutamine tracers and measured the ^{13}C isotopic enrichment of aspartate, intermediates in the pyrimidine synthesis pathway, and DNA. First, to quantify the contribution of the different pathways to aspartate synthesis in RCC cells, we cultured the pair of RCC cells with ^{13}C tracers that specifically trace the contribution of the aforementioned three routes, and observed that the contribution of these pathways is different between *VHL* $^{-/-}$ and *VHL* $^{+/+}$ UMRC2 cells (Figure VI-1B). While we acknowledge that most of the aspartate is formed from glutamine oxidation in both cell types (determined by the degree of M4 enrichment from [U-$^{13}C_5$] glutamine), there was a significant difference between the contribution of glucose oxidation (determined by the degree of M2 enrichment from [U-$^{13}C_6$] glucose), and reductive carboxylation (determined by the degree of M1 enrichment from [1-$^{13}C_1$] glutamine) between *VHL* $^{-/-}$ and *VHL* $^{+/+}$ UMRC2 cells (Figure VI-1B) – see Chapter II for atom transitions for these ^{13}C tracers. This observation primed us to hypothesize that HIF expression affects the substrate preference for *de novo* pyrimidine synthesis, and that this metabolic phenotype may be exploited to selectively inhibit pyrimidine synthesis in *VHL* $^{-/-}$ cells. To confirm the contribution of glutamine-carbons to DNA synthesis, we cultured the pair of UMRC2 cells in the presence of [U-$^{13}C_5$] glutamine for several days and monitored the ^{13}C label incorporation in thymine and cytosine using gas chromatography – mass spectrometry (GC-MS); the free bases were obtained from isolated and hydrolyzed DNA (see Chapter II for experimental procedures). [U-$^{13}C_5$] glutamine can contribute with three carbons to pyrimidine synthesis through the Krebs cycle (Figure VI-1A, either via glutamine oxidation or RC). As seen in Figures VI-1C, 1D, both *VHL* $^{-/-}$ and *VHL* $^{+/+}$ cells heavily rely on glutamine carbons to produce DNA bases with little difference observed between the two cell types, although *VHL* $^{+/+}$ cells appear to incorporate the ^{13}C tracer at a higher rate during the first 48hours. This is consistent with the notion that *de novo* DNA synthesis is a readout of cell proliferation rates (Macallan et al., 1998; Neese et al., 2002)

and, in actuality, *VHL* $^{+/+}$ UMRC2 cells grow slightly faster than their *VHL* $^{-/-}$ counterparts *in vitro* (although they do not form tumors *in vivo*). This indicates that glutamine oxidation is a major pathway for pyrimidine biosynthesis in both RCC cell, but this experiment does not distinguish the utilization of glutamine carbons via glutamine oxidation or RC. Furthermore, the fact that the ^{13}C incorporation is not higher in *VHL* $^{-/-}$ cells is not incompatible with the observed different contribution of glutamine-carbons for aspartate synthesis (Figure VI-1B), but rather raise the possibility that the *VHL* $^{+/+}$ counterparts may exhibit an overall higher flux of *de novo* pyrimidine synthesis (see later results and Discussion). Using a [^{15}N-amide] glutamine tracer, we observed a similar kinetic behavior of *de novo* DNA synthesis between *VHL* $^{-/-}$ and *VHL* $^{+/+}$ UMRC2 cells (Supplementary Figure VI-S1A, S1B), further supporting the positive correlation between DNA synthesis and cell proliferation rates. We also detected a similar ^{13}C labeling pattern in uracil albeit the lower signal (data not shown), possibly reflecting spontaneous deamination of cytosine during the experimental procedure (Duncan and Miller, 1980).

Next, to determine the contribution of RC for DNA synthesis, we labeled the pair of UMRC2 cells with [1-$^{13}C_1$] glutamine, which transfers the label to aspartate and pyrimidines specifically through RC. We observed that the ^{13}C enrichment of thymine and cytosine was higher in *VHL* $^{-/-}$ than *VHL* $^{+/+}$ UMRC2 cells, indicating that at least 10% of DNA was synthesized through RC during the course of eight days. Of note, the one carbon (C1) of aspartate is lost during *de novo* pyrimidine synthesis, but RC transfers the ^{13}C label to aspartate in the four carbon (C4). However, due to molecular symmetry of fumarate (Bernhard and Tompa, 1990) and reversibility of the malate dehydrogenase and fumarate hydratase reactions, C1 and C4 can interchange and lead to partial loss of ^{13}C incorporation in pyrimidines. Thus, the observed ^{13}C enrichment of DNA is an underestimation of the actual RC contribution to DNA synthesis due to the isotopic scrambling. Overall, these results indicate that reductive carboxylation can contribute to DNA synthesis in RCC cells in a HIF-dependent manner.

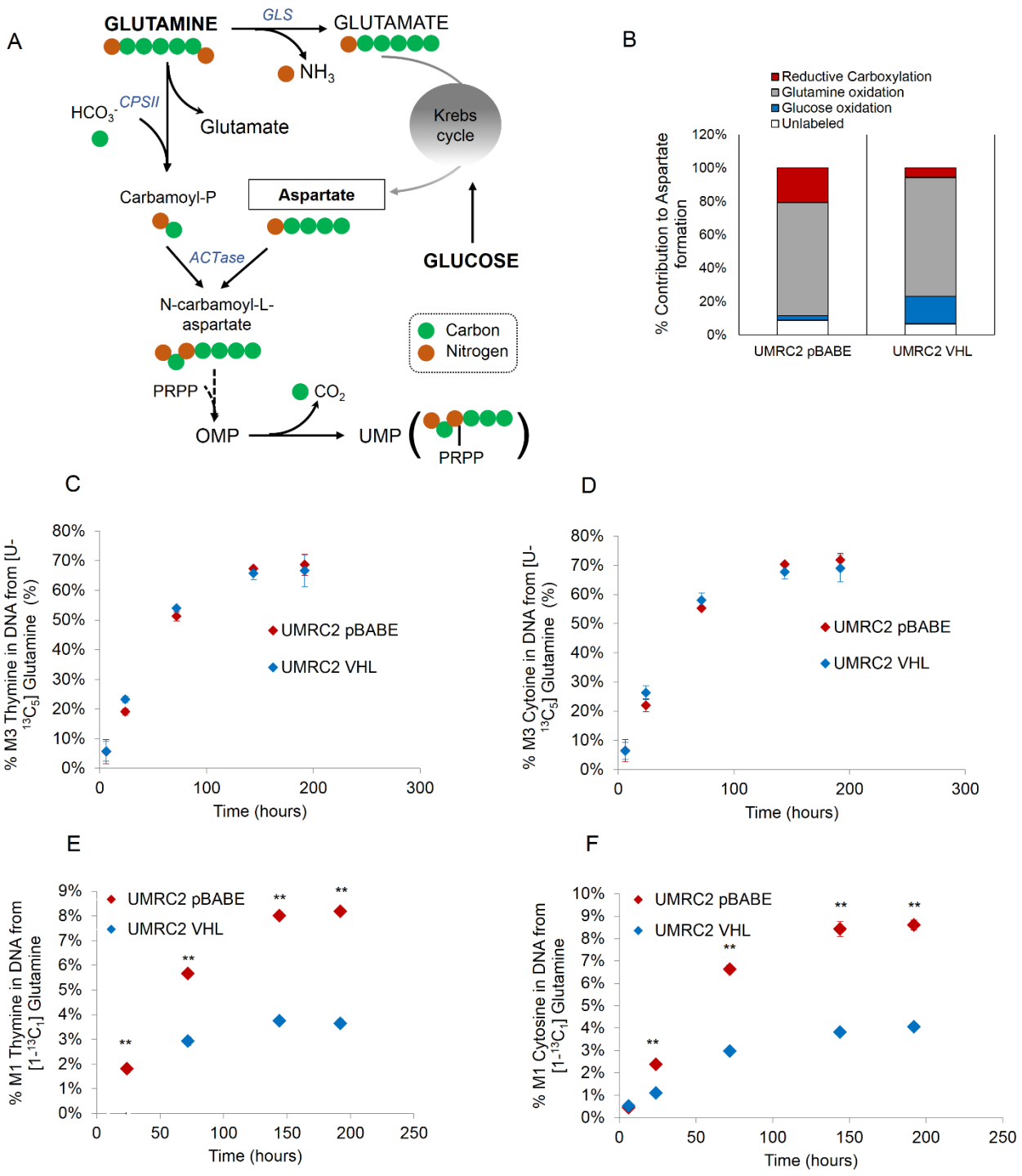
A
GLUTAMINE
GLS
GLUTAMATE
NH3
HCO3-
CPSII
Glutamate
Krebs cycle
Carbamoyl-P
Aspartate
ACTase
GLUCOSE
N-carbamoyl-L-aspartate
Carbon
Nitrogen
PRPP
CO2
OMP
UMP
PRPP
B
Reductive Carboxylation
Glutamine oxidation
Glucose oxidation
Unlabeled
% Contribution to Aspartate formation
120%
100%
80%
60%
40%
20%
0%
UMRC2 pBABE
UMRC2 VHL
C
% M3 Thymine in DNA from [U-13C5] Glutamine (%)
80%
70%
60%
50%
40%
30%
20%
10%
0%
0
100
200
300
Time (hours)
UMRC2 pBABE
UMRC2 VHL
D
% M3 Cytoine in DNA from [U-13C5] Glutamine (%)
80%
70%
60%
50%
40%
30%
20%
10%
0%
0
100
200
300
Time (hours)
UMRC2 pBABE
UMRC2 VHL
E
% M1 Thymine in DNA from [1-13C1] Glutamine
9%
8%
7%
6%
5%
4%
3%
2%
1%
0%
0
50
100
150
200
250
Time (hours)
UMRC2 pBABE
UMRC2 VHL
**
F
% M1 Cytosine in DNA from [1-13C1] Glutamine
10%
9%
8%
7%
6%
5%
4%
3%
2%
1%
0%
0
50
100
150
200
250
Time (hours)
UMRC2 pBABE
UMRC2 VHL
**

Figure VI-1. Biosynthesis of DNA Pyrimidines from Glutamine-Carbons in RCC Cells

(A) *De novo* pathway of pyrimidine biosynthesis in mammalian cells and the involved atom transitions. Green circles depict carbons, whereas orange circles depict nitrogens. For simplicity, only the linearized form of some intermediates is shown. (B) Contribution of the different source pathways for the formation of aspartate. One representative experiment in shown, in which the pair of UMRC2 cells was labeled with [U-$^{13}C_6$] glucose, [U-$^{13}C_5$] glutamine, or [1-$^{13}C_1$] glutamine for 24 hours; the M0 obtained using the [U-$^{13}C_5$] glutamine tracer was used to depict the "unlabeled" fraction of aspartate. (C-D) Using [U-$^{13}C_5$] glutamine, the time course (8 days) shows the ^{13}C enrichment of thymine (C), and cytosine (D), determined from column-purified and formic acid-hydrolyzed DNA. (E-F). Using [1-$^{13}C_1$] glutamine, the time course (8 days) shows the incorporation of the ^{13}C label on DNA-derived thymine (E) and cytosine (F). Student's t test compared *VHL*$^{-/-}$ to VHL $^{+/+}$ cells in (E) and (F). GLS, glutaminase; CPS-II, carbamoyl-phosphate synthetase II; ACTase, aspartate transcarbamoylase; OMP, orotidine monophosphate; UMP, uridine monophosphate; PRPP, 5-phosphoribosyl pyrophosphate.

Inhibition of Glutaminase Compromises *De Novo* Pyrimidine Biosynthesis in *VHL*-Deficient RCC Cells

N-carbamoyl-aspartate is formed via condensation of N-carbamoyl-phosphate with aspartate, the latter being produced from either glucose or glutamine (Figure VI-2A). Since glutamine-derived carbons contributed to a higher steady-state production of aspartate in *VHL* $^{-/-}$ than *VHL* $^{+/+}$ UMRC2 cells, we hypothesized that glutamine deprivation would impair pyrimidine synthesis selectively in HIF-expressing cells. To test this hypothesis, we cultured the pair of UMRC2 cells with the glutaminase (GLS) inhibitor BPTES for 48 hours and measured the levels of the pyrimidine intermediates using liquid-chromatography (LC) tandem mass spectrometry (MS/MS). Treatment with the BPTES significantly decreased the levels of N-carbamoyl-aspartate and UMP in *VHL* $^{-/-}$ UMRC2 cells (Figure VI-2B). Importantly, the levels of aspartate and N-carbamoyl-phopshate were also decreased and increased in *VHL* $^{-/-}$ cells, respectively, consistent with network topology and suggesting that loss of *VHL* limits RCC cells for the ability to produce aspartate under GLS-inhibited conditions, which leads to the accumulation of N-carbamoyl-phosphate (see Figure VI-2A). In contrast, the effect induced by

BPTES on metabolite pool sizes was overall less pronounced in *VHL* $^{+/+}$ cells (Figure VI-2B). The BPTES treatment increased the levels of glutamine and it did reduce glutamate levels in both UMRC2 cell types (Figure VI-2C), confirming the expected metabolic outcome of GLS-inhibition. Indeed, the effect was still less pronounced in *VHL* $^{+/+}$ UMRC2 cells at the level of glutamate, corroborating our previous observations that the expression of the wild-type pVHL protein in *VHL*-deficient RCC cells stimulates glucose oxidation in the Krebs cycle and enhances the production of glutamate from glucose-carbons (Chapter IV).

To test if the effect on pyrimidine synthesis induced by GLS inhibition is due to an impaired carbon flux to pyrimidine synthesis, we labeled the pair of UMRC2 cells with [U-$^{13}C_5$] glutamine for 48 hours, and measured the isotopic enrichment of N-carbamoyl-aspartate by LC-MS/MS under the presence of BPTES. The [U-$^{13}C_5$] glutamine tracer transfers ^{13}C label to N-carbamoyl-aspartate through both glutamine oxidation and RC. As expected, the ^{13}C enrichment of UMP and CMP was decreased in both *VHL* $^{-/-}$ and *VHL* $^{+/+}$ UMRC2 cells (Figure VI-2D, 2E). Interestingly, the BPTES effect on the ^{13}C enrichment of UMP and CMP was less pronounced in *VHL* $^{+/+}$ cells (See discussion). Of note, there was no ^{13}C incorporation in inosine monophosphate (IMP) – the precursor nucleotide for purines, whose synthesis does not require glutamine-carbons (Supplementary Figure VI-S2); the observed minimal M1 abundance (~5%) is most likely due to ^{13}C natural abundance (we did not correct for the natural abundance of isotopomer enrichments in our LC-MS/MS experiments). We also observed that levels of glutaminase are similar between *VHL* $^{-/-}$ and *VHL* $^{+/+}$ UMRC2 cells, as observed in Chapter IV (Supplementary Figure IV-S4E). These findings show that GLS inhibition compromises *de novo* pyrimidine biosynthesis selectively in *VHL* $^{-/-}$ cells because it limits aspartate production from glutamine-carbons.

VHL $^{+/+}$ RCC Cells Adapt to GLS Inhibition by Stimulating Glucose Oxidation in the Krebs Cycle

To investigate the metabolic mechanism by which *VHL* $^{+/+}$ RCC cells can tolerate GLS inhibition, we labeled the pair of UMRC2 RCC cells with [U-$^{13}C_6$] glucose and measured the ^{13}C enrichment of Krebs cycle intermediates by GS-MS, with and without BPTES. The BPTES treatment increased the enrichment of M2 and M3 intermediates in the Krebs cycle intermediates in *VHL* $^{+/+}$ and to a lesser extent in *VHL* $^{-/-}$ UMRC2 cells (Figures VI-3A, 3B, 3C), showing that GLS inhibition stimulates glucose oxidation in the Krebs cycle. Although *VHL* $^{-/-}$ UMRC2 cells responded to BPTES treatment, they exhibited increased glucose oxidation to a level which was, in most cases, lower or similar to that observed in BPTES-untreated *VHL* $^{+/+}$ cells, potentially underlying the depletion of pyrimidine intermediates observed in *VHL* $^{-/-}$ cells. This result was also corroborated in a pair of *VHL*-deficient / *VHL*-reconstituted UMRC3 cells (Figures VI-3D, 3E, 3F), indicating that the stimulation of glucose oxidation is not a cell line-specific phenomenon and reflects a metabolic response to GLS inhibition. These findings suggest that *VHL* $^{+/+}$ cells can adapt to GLS inhibition by upregulating glucose oxidation in the Krebs cycle more effectively than V*HL* $^{-/-}$ cells.

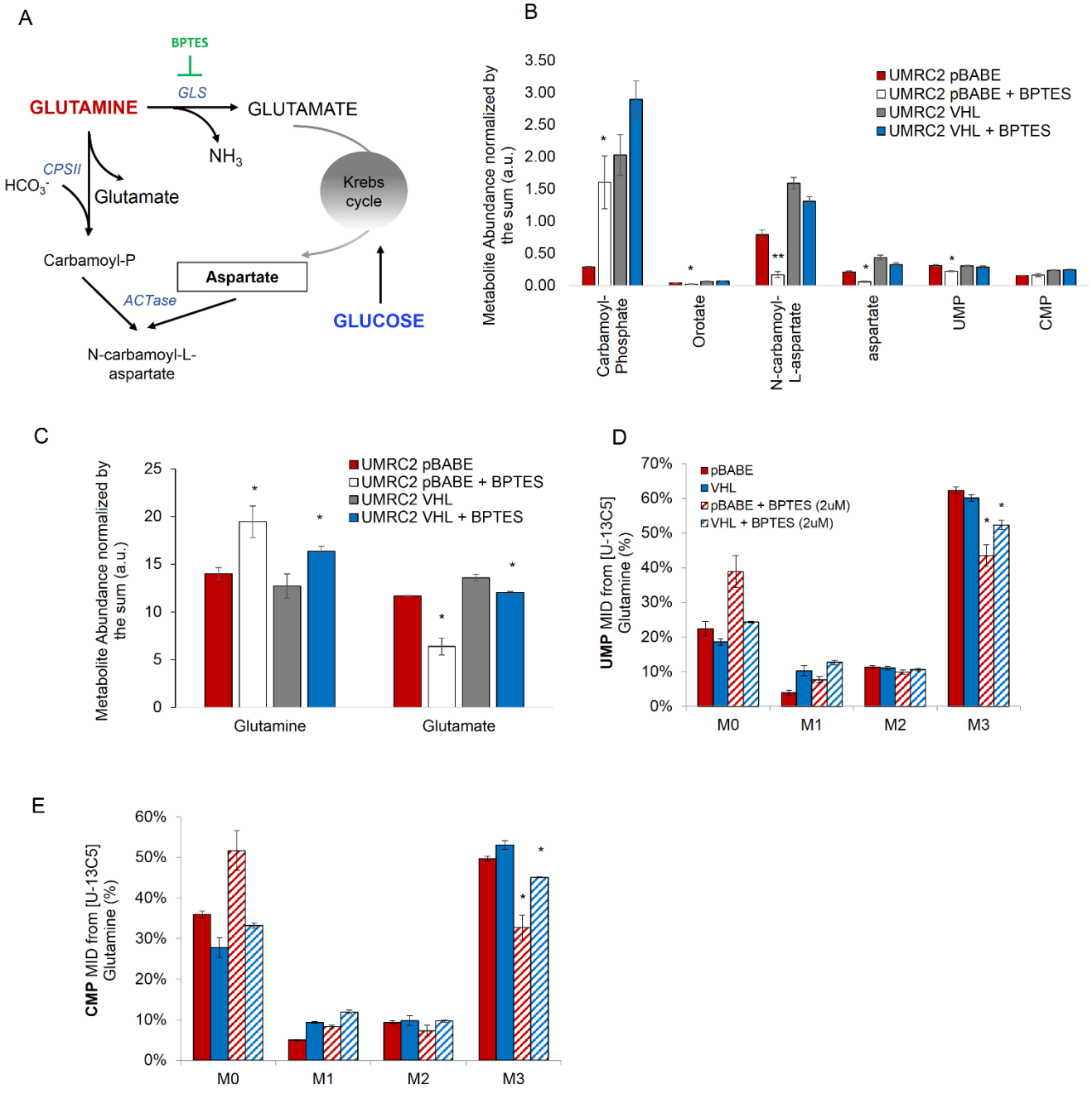
A
BPTES
GLS
GLUTAMINE
GLUTAMATE
NH3
CPSII
HCO3-
Glutamate
Krebs cycle
Carbamoyl-P
Aspartate
ACTase
GLUCOSE
N-carbamoyl-L-aspartate
B
Metabolite Abundance normalized by the sum (a.u.)
UMRC2 pBABE
UMRC2 pBABE + BPTES
UMRC2 VHL
UMRC2 VHL + BPTES
Carbamoyl-Phosphate
Orotate
N-carbamoyl-L-aspartate
aspartate
UMP
CMP
C
Metabolite Abundance normalized by the sum (a.u.)
Glutamine
Glutamate
D
UMP MID from [U-13C5] Glutamine (%)
pBABE
VHL
pBABE + BPTES (2uM)
VHL + BPTES (2uM)
M0
M1
M2
M3
E
CMP MID from [U-13C5] Glutamine (%)

Figure VI-2. Effect of Glutaminase Inhibition on the Production of Pyrimidines in RCC Cells

(A) Diagram depicting the contribution of glutamine and glucose to the formation of aspartate and downstream intermediates, and the inhibition of GLS by BPTES. (B-D) *VHL* $^{-/-}$ and *VHL* $^{+/+}$ UMRC2 cells were cultured in the absence or presence of BPTES for 48hours at 1.5μM and the metabolites analyzed by LC-MS/MS. (B) Effect of BPTES on the levels of pyrimidine/purine nucleotides and their intermediates. (C) Effect of BPTES on the levels of glutamine and glutamate in the pair of UMRC2 cells. Metabolite levels were normalized by the sum of 288 metabolites obtained from extracts in the corresponding cell type. (D-E) The pair of UMRC2 cells was labeled with [U-$^{13}C_5$] glutamine under the absence or presence of BPTES at 2μM (for 48 hours) and the metabolite enrichment measured by LC-MS/MS. Effect of BPTES on the ^{13}C enrichment of UMP (D) and CMP (E) is shown. Student's t test compared BPTES-treated to corresponding control cells in (B-E). GLS, glutaminase; CPS-II, carbamoyl-phosphate synthetase II; ACTase, aspartate transcarbamoylase.

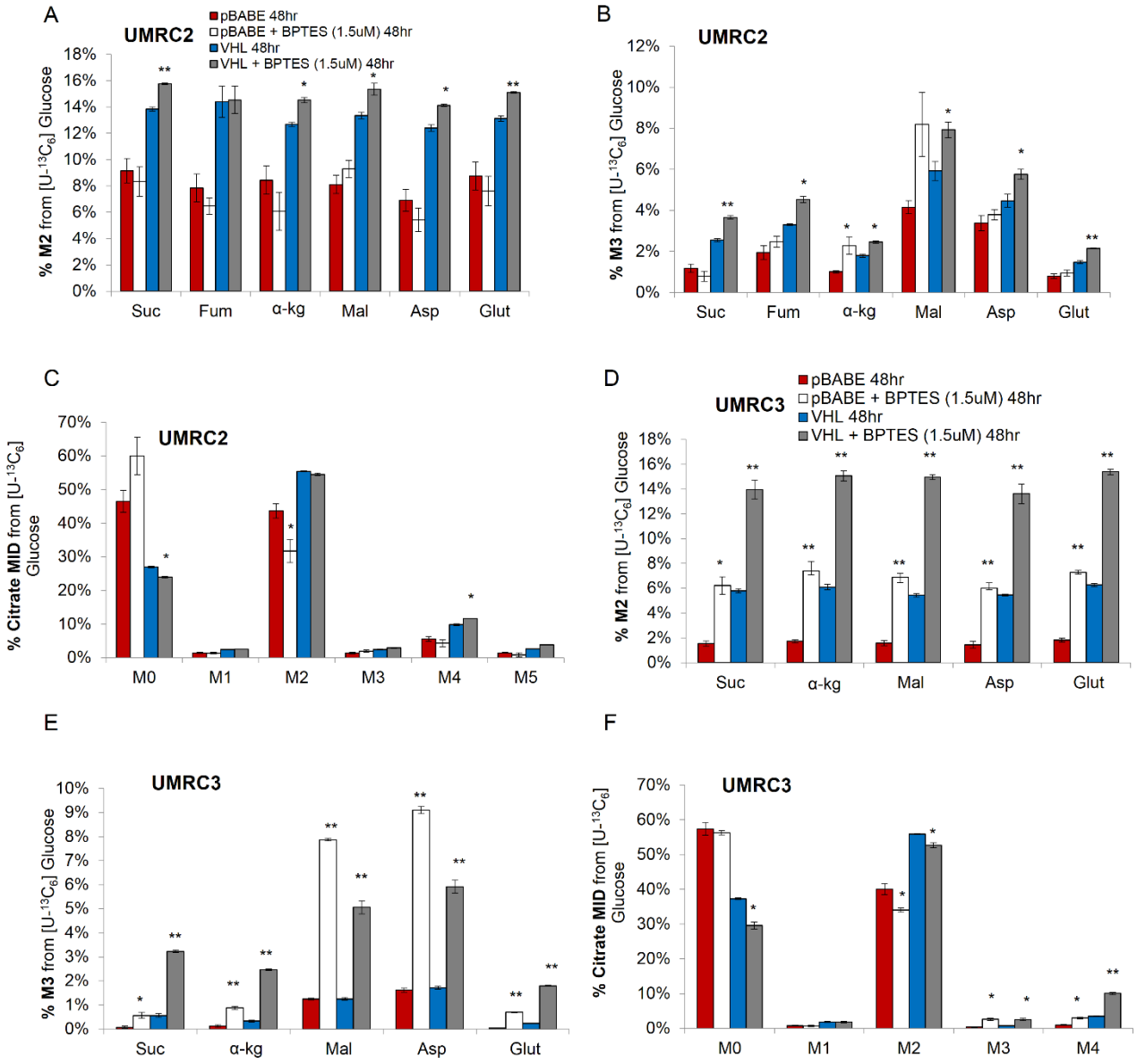

Figure VI-3. Evidence for Regulation of Glucose Oxidation in the Krebs cycle by BPTES

The pairs of UMRC2 and UMRC3 cells were labeled with [U-$^{13}C_6$] glucose with or without BPTES at the indicated concentrations (for 48 hours) and the metabolite enrichment measured by LC-MS/MS. (A-C) Effect of BPTES on the contribution of glucose oxidation, determined by the level of M2 (A) and M3 (B) enriched Krebs cycle intermediates, and of citrate enrichment (C) in UMRC2 cells. (D-F) Effect of BPTES on the contribution of glucose oxidation, determined by the level of M2 (A) and M3 (B) enriched Krebs cycle intermediates, and of citrate enrichment (C) in UMRC3 cells. Student's t test compared BPTES-treated to corresponding control cells. Suc, succinate; Fum, fumarate; α-kg, α-ketoglutarate; Mal, malate; Asp, aspartate; Glut, glutamate.

VHL-Deficient RCC Cells Utilize the Salvage Pathway to Maintain Pyrimidine Biosynthesis

Notwithstanding the glutamine addiction phenotype of *VHL* $^{-/-}$ RCC cells, some evidences suggested that *VHL* $^{-/-}$ RCC cells may rely on the salvage pathway to sustain nucleotide biosynthesis. First, we observed that both RCC cell types exhibited an overall similar incorporation of ^{13}C in DNA bases from [U-$^{13}C_5$] glutamine (Figure VI-1C, 1D), which is reconcilable with the dependence of *VHL* $^{-/-}$ cells on RC should the expression of wild-type *VHL* increase the *de novo* flux of pyrimidine biosynthesis. Second, we observed that the ratio of N-carbamoyl-aspartate to N-carbamoyl-phosphate is higher in *VHL* $^{-/-}$ than *VHL* $^{+/+}$ cells (Figure VI-4A, compare first and third bars). Since CAD is a major regulatory point of *de novo* pyrimidine synthesis (Carrey, 1993), this observation suggests from the thermodynamic standpoint that *VHL*$^{-/-}$ UMRC2 cells exhibit a lower driving force for *de novo* pyrimidine biosynthesis than their isogenic controls. The N-carbamoyl-aspartate to N-carbamoyl phosphate ratio was greatly reduced upon BPTES treatment (Figure VI-4A, compare second and fourth bars), indicating that GLS inhibition indirectly affects the kinetics of CAD. The effect on this ratio further suggests that differences in CAD activity may underlie the HIF-mediated regulation of pyrimidine biosynthesis in RCC cells. To this end, we measured the expression level of CAD in the pair of UMRC2 cells. Since CAD is reported to be regulated in a cell-cycle dependent manner (Rao and Church, 1988), we measured its levels in either unsynchronized or G1/S-phase synchronized RCC cells. While no difference was observed in the unsynchronized cultures, *VHL*$^{-/-}$ UMRC2 exhibited a slightly lower expression of CAD than *VHL*$^{+/+}$ cells (Figure VI-4D), which would be in agreement with the report showing that HIF-1α decreases the expression of CAD (Chen et al., 2005) (see Discussion). These evidences raise the possibility that *VHL*$^{-/-}$ RCC cells, albeit the requirement for glutamine-carbons to produce aspartate via RC, may exhibit an overall lower flux of *de novo* pyrimidine synthesis. We therefore hypothesized that *VHL*$^{-/-}$ RCC cells may require the salvage pathway to maintain nucleotide availability.

To test the hypothesis that the salvage pathway is utilized by *VHL*-deficient cells, we measured the ability of UMRC2 cells to uptake exogenous nucleosides. First, we cultured the pair of UMRC2 cells under the presence of [U-$^{13}C_5$] glutamine and different concentrations of exogenous deoxyadenosine (dA), deoxyguanosine (dG), deoxycytidine (dC), thymidine (T) and uridine (U), and determined the ^{13}C enrichment of pyrimidine nucleotides by LC-MS/MS. In mammalian cells, the uptake of extracellular nucleosides is mediated by the equilibrative nucleoside transporter (ENT) family (Baldwin et al., 2004). In turn, intracellular deoxyribonucleosides can be irreversibly phosphorylated to deoxyribonucleoside monophosphates (dAMP, dGMP, dCMP, TMP, and UMP) by four deoxyribonucleoside kinases (NKs): thymidine kinase 1, thymidine kinase 2, deoxycytidine kinase (dCK) and deoxyguanosine kinase (Johansson and Eriksson, 1996). Thus, the activity of ENT and NKs contribute to the salvage pathway of nucleotide synthesis. In our experiments, we observed that the ^{13}C enrichment of UMP and CMP from [U-$^{13}C_5$] glutamine was preferentially diluted in *VHL* $^{-/-}$ UMRC2 cells by the presence of unlabeled nucleosides in a dose-dependent manner (Figure VI-4B, 4C). To directly probe the salvage flux of pyrimidine synthesis and the effect of GLS inhibition on this pathway, we cultured the pair of UMRC2 cells under the presence of uniformly ^{13}C-labeled dC and ^{13}C-labeled dA at 5μM (together with unlabeled dG, and T) and determined the ^{13}C enrichment of intracellular nucleoside monophosphates. The ^{13}C-labeled dC and dA substrates will trace the salvage pathway of pyrimidine and purine nucleotides, respectively. Although not statistically significant for dCMP, we observed a trend increase in the ^{13}C enrichment of AMP in *VHL* $^{-/-}$ when compared to *VHL* $^{+/+}$ UMRC2 cells (Figures VI-4E, 4F). The ^{13}C enrichment of adenine monophosphate was shown for AMP (and not for dAMP) due to the low spectral intensity obtained for the deoxygenated version. Surprisingly, in these experimental setting, the BPTES appeared to increase the contribution of ^{13}C-labeled dA to AMP only, and one would expect it to be the case for dCMP from ^{13}C-labeled dC as well. Further experiments are necessary to determine putative differences in the basal utilization rate of the salvage pathway in RCC cells and the effect of GLS inhibition. Nevertheless, these isotopic studies show that *VHL* $^{-/-}$ RCC cells can utilize the salvage

pathway from exogenous nucleosides to produce pyrimidine nucleotides, and are suggestive that this pathway may be more active in VHL $^{-/-}$ cells. In support of our overall findings, addition of nucleosides at 5uM led to a partial rescue of cell proliferation by the BPTES treatment (Figure VI-4G). To exploit this HIF-dependent metabolic phenotype, we set out to block both the salvage and the *de novo* pathways of pyrimidine biosynthesis in RCC cells. To this end, we cultured the pair of UMRC2 cells in the presence of BPTES and a toxic nucleoside analog – 2-chlorodeoxyadenosine (or cladribine) – which is converted to cladribine-monophosphate by dCK and thereby contributes to the nucleotide pool through the salvage pathway. Combining both the GLS inhibitor and cladribine significantly decreased the proliferation of *VHL* $^{-/-}$ cells when compared to the *VHL* $^{+/+}$ controls (Figure VI-4H). Although not as pronounced, the pair of UMRC3 cells also exhibited a response to BPTES and cladribine treatments towards the selective killing of *VHL* $^{-/-}$ cells (Figure VI-4I). If the effect of GLS inhibition in RCC cells is due to a depletion of pyrimidine precursors, then the selective growth inhibition of *VHL* $^{-/-}$ cells when compared to *VHL* $^{+/+}$ cells should be abrogated by the inhibition of enzymes involved in the *de novo* pathway of pyrimidine biosynthesis. Thus, to further test our hypothesis, we treated the pair of UMRC2 cells with N-phosphonacetyl-L-aspartic acid (PALA), an inhibitor of aspartate transcarbamoylase (ACTase), alone or in combination with BPTES. As observed in Figure VI-4J, PALA inhibited the growth of both UMRC2 cell types. Importantly, we observed a strong growth inhibition of both UMRC2 cell types by the presence of PALA and BPTES (as expected), but there was no significant difference between *VHL* $^{-/-}$ and *VHL* $^{+/+}$ UMRC cells (Figure VI-4J). This result suggests that the selective growth phenotype of BPTES in *VHL* $^{-/-}$ cells is, at least in part, due to its ability to inhibit *de novo* pyrimidine biosynthesis. Interestingly, the PALA treatment inhibited the growth of *VHL* $^{+/+}$ cells to a slightly greater extent than the *VHL* $^{-/-}$ cells (Figure VI-4J), further suggesting that loss of *VHL* may decrease the rate of *de novo* pyrimidine biosynthesis. Collectively, these data indicate that RCC cells utilize the salvage pathway to maintain nucleotide biosynthesis, and that blocking both the glutamine-derived *de novo* and the salvage pathways selectively impairs the growth of *VHL* $^{-/-}$ cells.

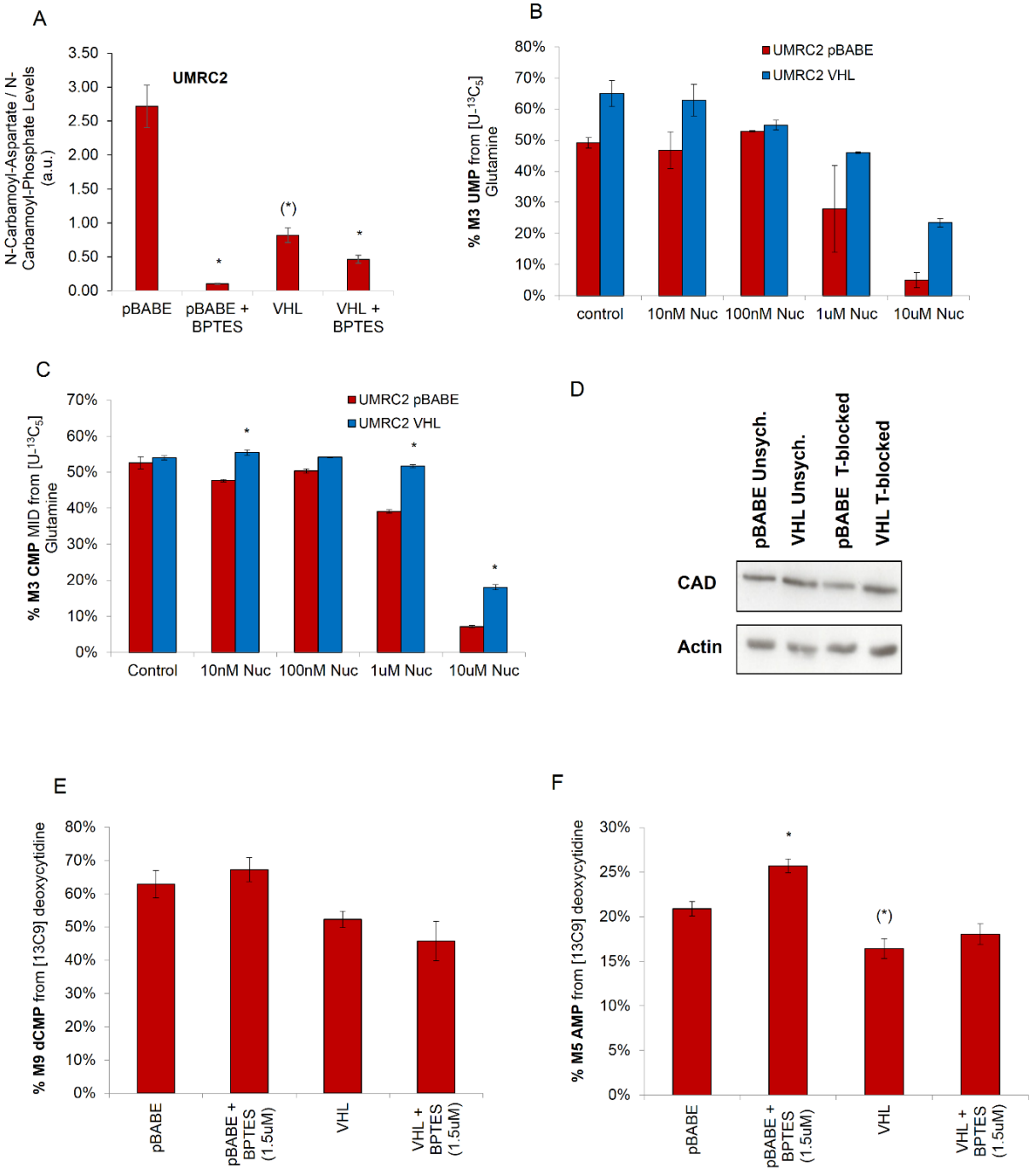
A
N-Carbamoyl-Aspartate / N-Carbamoyl-Phosphate Levels (a.u.)
UMRC2
3.50
3.00
2.50
2.00
1.50
1.00
0.50
0.00
(*)
*
*
pBABE
pBABE + BPTES
VHL
VHL + BPTES
B
% M3 UMP from [U-13C5] Glutamine
UMRC2 pBABE
UMRC2 VHL
80%
70%
60%
50%
40%
30%
20%
10%
0%
control
10nM Nuc
100nM Nuc
1uM Nuc
10uM Nuc
C
% M3 CMP MID from [U-13C5] Glutamine
UMRC2 pBABE
UMRC2 VHL
70%
60%
50%
40%
30%
20%
10%
0%
*
*
*
Control
10nM Nuc
100nM Nuc
1uM Nuc
10uM Nuc
D
pBABE Unsych.
VHL Unsych.
pBABE T-blocked
VHL T-blocked
CAD
Actin
E
% M9 dCMP from [13C9] deoxycytidine
80%
70%
60%
50%
40%
30%
20%
10%
0%
pBABE
pBABE + BPTES (1.5uM)
VHL
VHL + BPTES (1.5uM)
F
% M5 AMP from [13C9] deoxycytidine
30%
25%
20%
15%
10%
5%
0%
*
(*)
pBABE
pBABE + BPTES (1.5uM)
VHL
VHL + BPTES (1.5uM)

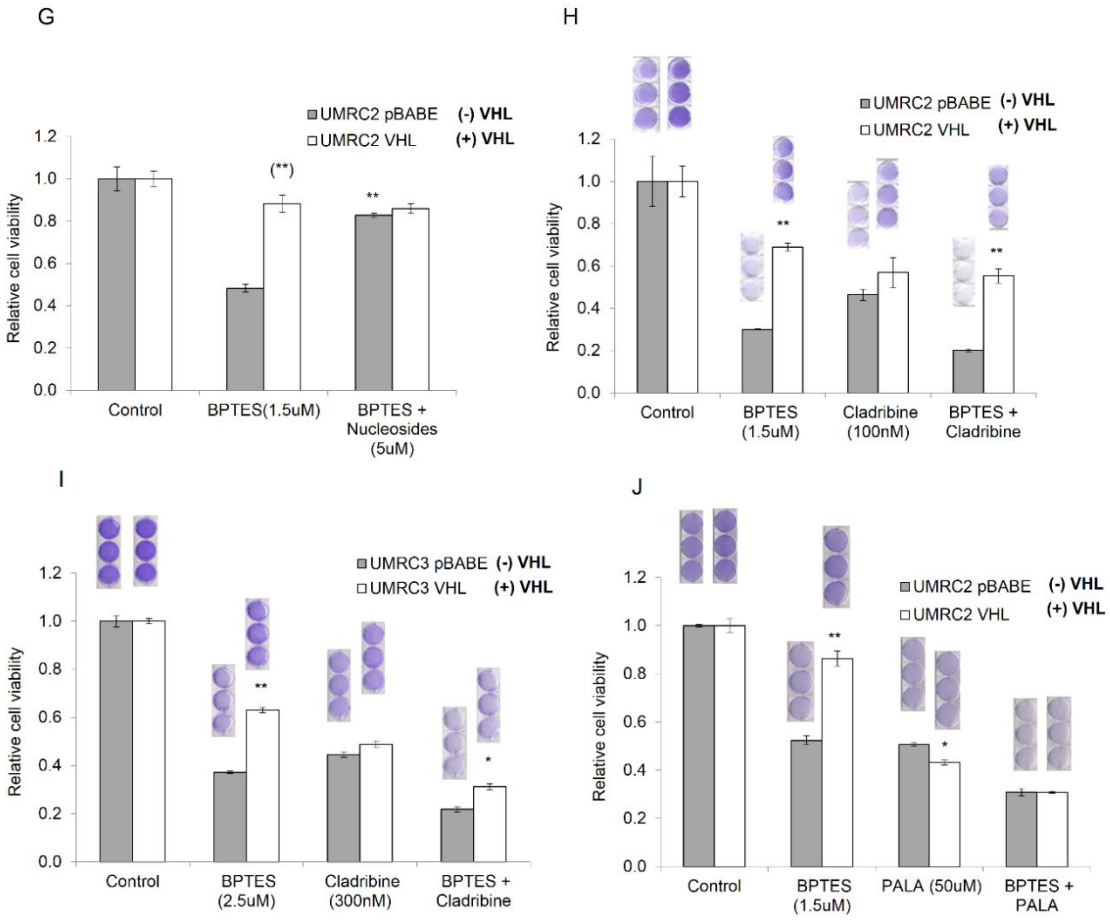

Figure VI-4. Evidence for Utilization of the Salvage Pathway of Pyrimidine Biosynthesis in RCC Cells

(A) Levels of N-carbamoyl-aspartate relative to its precursor N-carbamoyl-phosphate in control or BPTES-treated UMRC2 cells. (B-C) Effect of exogenous nucleosides on the contribution of [U-$^{13}C_5$] glutamine to UMP (B) and CMP (C) synthesis in UMRC2 cells. (D) UMRC2 cells were synchronized in S-phase by Thymidine double-block. CAD expression levels in unsynchronized ("Unsych.") and synchronized ("T-blocked") UMRC2 cells. (E-F) UMRC2 cells were cultured for 48hours in the presence of ^{13}C-labeled deoxyadenosine (^{13}C-dA), ^{13}C-labeled deoxycytidine (^{13}C-dA), unlabeled guanosine and unlabeled thymidine, at 5µM. Percent contribution of the salvage pathway from exogenous ^{13}C-dA and ^{13}C-dC to dCMP (E) and AMP (F) synthesis. (G) Effect of exogenous nucleosides on the proliferation of BPTES-treated *VHL* $^{-/-}$ and *VHL* $^{+/+}$ UMRC2 cells (H-I) Cell proliferation effect of targeting the *de novo* (using BPTES) and the salvage (using cladribine) pathways of pyrimidine biosynthesis in the pair of UMRC2 (H) and UMRC3 (I) cells. Cell proliferation effect of PTES and PALA (the *de novo* pyrimidines inhibitor) in UMRC2 cells. Student's t test compared BPTES-treated to corresponding control cells in (A) and (E-F) *VHL*-reconstituted to *VHL*-deficient cells in (B-C) and (H-J), and nucleosides-rescued cells to correspondent controls in (G). Asterisk in parenthesis indicates comparison between *VHL* $^{-/-}$ and *VHL* $^{+/+}$ cells in (A), (F), (G).

VI.3. DISCUSSION

Here, we showed that oncogenic activation of HIF through loss of *VHL* changes nucleotide metabolism in renal carcinoma cancer (RCC) cells. By tracing the fate of glucose and glutamine in central carbon metabolism, we demonstrated that loss of *VHL* redirects glutamine carbons for pyrimidine biosynthesis in RCC cells, via reductive carboxylation (RC). Inhibition of glutaminase (GLS) decreased the levels of aspartate and pyrimidine intermediates preferentially in VHL $^{-/-}$ cells, suggesting that RC-derived aspartate is required to maintain pyrimidine biosynthesis in RCC cells. By synchronizing the pair of isogenic RCC cells at the G1/S-phase of the cell-cycle, we revealed that VHL $^{-/-}$ cells appear to exhibit a lower expression level of the CAD enzyme, raising the possibility that HIF expression decreases *de novo* pyrimidine biosynthesis. Concordantly, we observed that RCC cells utilize exogenous nucleosides to fuel the nucleotide pool, and this salvage pathway appeared to be more active in VHL $^{-/-}$ cells. These results underline the importance of cellular nucleotide levels for cell viability. This was supported by the experiment in which inhibiting both the *de novo* and the salvage pathways of pyrimidine biosynthesis led to a selective growth inhibition of *VHL* $^{-/-}$ RCC cells. In the next paragraphs, I will interpret our findings under the light of the HIF literature and taking into consideration the concepts of cell survival versus cell growth. I will also discuss experiments that shall be conducted to support the present conclusion of this chapter.

Our metabolomics studies showed that GLS inhibition depleted the levels of aspartate and pyrimidine intermediates selectively in *VHL* $^{-/-}$ UMRC2 cells. In addition, we showed that the rate-limiting enzyme CAD was expressed at lower levels in G1/S-phase - synchronized *VHL* $^{-/-}$ UMRC2 cells when compared to their isogenic controls. Although this is in agreement with the report showing that HIF-1α decreases CAD expression (Chen et al., 2005), there was no difference in the unsynchronized cultures, as it would be expected if CAD is transcriptionally repressed by HIF. We did not access the transcript levels of CAD in unsynchronized/synchronized RCC cells, and this experiment is warranted. Nevertheless, we showed that the ratio of the N-carbamoyl-aspartate (the enzymatic product of CAD)

relative to N-carbamoyl-phosphate (the CAD substrate) is elevated in *VHL* $^{-/-}$ when compared to *VHL* $^{+/+}$ cells. These two observations suggest that HIF activation may decrease the *de novo* flux of pyrimidine biosynthesis, but it simultaneously renders RCC cells dependent on glutamine-carbons to maintain this anabolic flux. The observation of a similar incorporation from [U-$^{13}C_5$] glutamine into the DNA between *VHL* $^{-/-}$ and *VHL* $^{+/+}$ RCC cells (Figure VI-1A) furthers suggests that loss of *VHL* decreases the *de novo* flux of DNA biosynthesis, which is a readout of cell proliferation (Macallan et al., 1998). Although this interpretation would support the reported role of HIF-1α in inhibiting DNA replication and cell proliferation (Hubbi et al., 2013; Koshiji et al., 2004b), we did not provide direct evidences that the *de novo* flux of pyrimidine biosynthesis is affected in RCC cells. To directly measure DNA synthesis, one can monitor the incorporation of bromodeoxyuridine (BrdU) in the newly synthesized DNA of replicating cells. However, since BrdU is a nucleoside, it probes the salvage pathway and this experiment would not be suitable to determine the total the flux of the *novo* nucleotide biosynthesis in *VHL* $^{-/-}$ versus *VHL* $^{+/+}$ cells. Therefore, to investigate the role of glutamine and CAD activity during the cell cycle, it is a key experiment to determine the contribution of ^{13}C glutamine tracers (tracing RC or oxidative Krebs cycle) to pyrimidine biosynthesis in S-phase - synchronized and unsynchronized RCC cells. By combining such tracer data with extracellular flux measurements and employing MFA (see Chapter II), one can determine whether the total *de novo* flux is different between *VHL*-deficient and *VHL*-reconstituted cells.

Our ^{13}C tracer studies using [U-$^{13}C_5$] glutamine showed that glutaminase inhibition decreased the formation of ^{13}C-labeled UMP and CMP in both *VHL* $^{-/-}$ and *VHL* $^{+/+}$ UMRC2 cells (Figure VI-2D, 2E), but the effect was more pronounced in the VHL $^{-/-}$ negative background. One may expect the BPTES treatment to inhibit the ^{13}C enrichment of pyrimidines to the same degree in both RCC cell types, as GLS inhibition should equally decrease the conversion of glutamine into glutamate. However, the transfer of the glutamine amide nitrogen to N-carbamoyl-phosphate via CAD releases glutamate as by-product in the cytosol (Figure VI-1A). The CAD-derived glutamate can be potentially used as carbon

source for pyrimidine synthesis even under the presence of BPTES. On one hand, GLS inhibition did result in increased glutamine and decreased glutamate levels in both cell types (Figure VI-2C), ruling out the possibility that the BPTES does not act in *VHL* $^{+/+}$ cells. The observation that the BPTES treatment inhibited the contribution of [U-$^{13}C_5$] glutamine to pyrimidines preferentially in the *VHL* $^{-/-}$ background suggest these cells cannot reroute glutamine towards cytosolic the CAD reaction as efficiently. To further investigate the effect of GLS inhibition on the kinetics of CAD and glutamine-to-pyrimidine flux, one can label the pair of RCC cells with [^{15}N-Amide] glutamine and evaluate the effect of BPTES. The contribution of glutamine-derived nitrogens to N-carbamoyl-aspartate is independent from GLS inhibition (see Figure VI-1A), unless the production of aspartate is compromised, as one would expect in BPTES-treated VHL$^{-/-}$ cells. Thus, to perform the ^{15}N labeling experiments will be crucial to dissect the flux of glutamine-carbons from that of glutamine-nitrogens to pyrimidines. This experiment will also be important to better interpret the different BPTES-induced effect on the production of UMP and CMP from [U-$^{13}C_5$] glutamine in each RCC cell type.

It is relevant to discuss the role of the pentose phosphate pathway (PPP) in the production of ribose 5-phosphate, the sugar precursor used in the *de novo* synthesis of purine and pyrimidine nucleotides (Tong et al., 2009). As reviewed in (Tong et al., 2009), HIF appears to reduce activity of oxidative PPP but, in contrast, it induces the expression of transketolase, thereby maintaining the levels of ribose 5-phosphate through the non-oxidative arm of PPP. In our RCC cell lines, we did not observe significant changes in the oxidative PPP activity, as determined using the [1, 2 - $^{13}C_2$] glucose tracer (data not shown). Although the network topology of *de novo* pyrimidine biosynthesis does require the condensation of 5-phosphoribosyl-phosphate with orotate, we assessed the effect of BPTES at the level of N-carbamoyl-aspartate and N-carbamoyl-phosphate, which lie upstream of this reaction. Yet, we cannot rule out the possibility that indirect effects on the PPP activity by HIF expression do not indirectly affect the observed metabolic phenotype upon GLS inhibition. This may actually explain the modest changes observed in the levels of UMP and downstream nucleotides under GLS inhibition.

Further experiments are necessary to test the role of HIF in regulating PPP and the effect of glutaminase inhibition on the contribution of PPP to *de novo* pathway of pyrimidine biosynthesis in RCC cells.

An additional limitation of the experimental approach in this study was the use of a GLS inhibitor to evaluate the role of glutamine metabolism in pyrimidine biosynthesis. As mentioned in previous chapters, GLS inhibition blocks both glutamine oxidation and RC in the Krebs cycle. Since the contribution of glutamine oxidation to aspartate synthesis is similar between *VHL* $^{-/-}$ and *VHL* $^{+/+}$ cells, it will be critical to interrogate the metabolic outcomes of inhibiting one pathway versus the other. Thus, to directly study the role of reductive carboxylation, it would be informative to induce a genetic deletion or a knockdown of IDH1 and/or IDH2 in our RCC cell lines. Supplying IDH knocked-down or knockout RCC cell lines with glutamate or a cell-permeable version of α-ketoglutarate can in principle compensate for the inhibition of the forward IDH reaction and allow one to specifically assess the contribution of reductive carboxylation to pyrimidine biosynthesis.

Finally, we did not address the biological mechanism by which GLS inhibition affects the proliferation of *VHL*-deficient cells. Whether GLS inhibition slows down cell growth due to reduced macromolecule biosynthesis, or it instead promotes cell-cycle arrest and/or cell death was not investigated. Understanding how the proliferation of *VHL*-deficient cells is affected under glutamine deprivation will shed light into the metabolic adaptation of HIF signaling and how it may suppress senescence.

A recent study analyzing the genomic alterations, DNA methylation and RNA expression profiles of a comprehensive cohort of clear cell renal cell carcinomas (ccRCC) indicated a significant correlation between a worsened prognosis in cc RCC patients and increased glutamine transporters (Creighton et al., 2013). This recent advance indeed correlates avid glutamine metabolism with kidney cancer, and the biosynthetic fates of glutamine must be revealed to fully understand the necessity for this nutrient by RCC tumors. In keeping with the established role of HIF and the findings of the previous chapters,

we conclude that reductive carboxylation in the Krebs cycle is a maintenance mechanism to avoid lipid and nucleotide insufficiency in hypoxic and *VHL*-deficient cancer cells.

VI.4. Supplemental Information

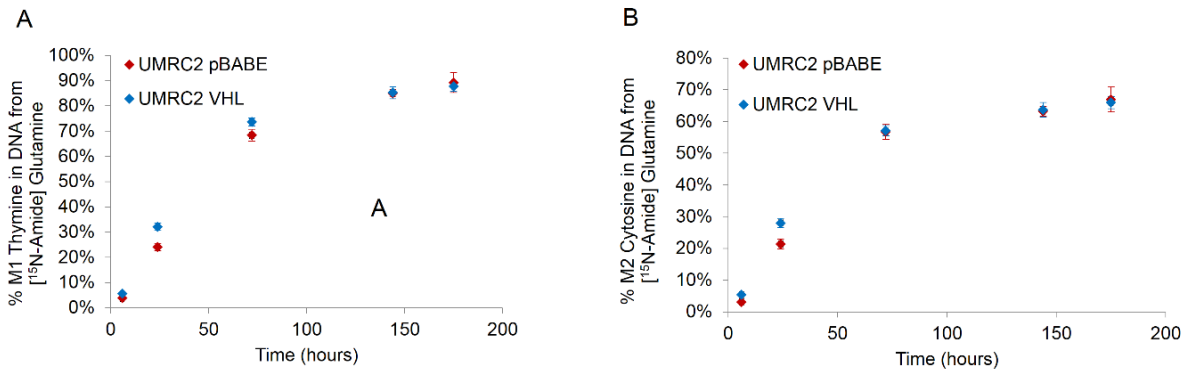

Supplementary Figure VI-S1. Biosynthesis of DNA-Isolated Pyrimidine Bases from Glutamine-Nitrogens in RCC Cells, Related to Figure VI-1

(A) VHL $^{-/-}$ and VHL $^{+/+}$ UMRC2 cells were labeled with [^{15}N-amide] glutamine for eight days. The time course shows the enrichment of M1 thymine (A), and M2 cytosine (B) from [^{15}N-amide] glutamine, determined from column-purified and formic acid-hydrolyzed DNA.

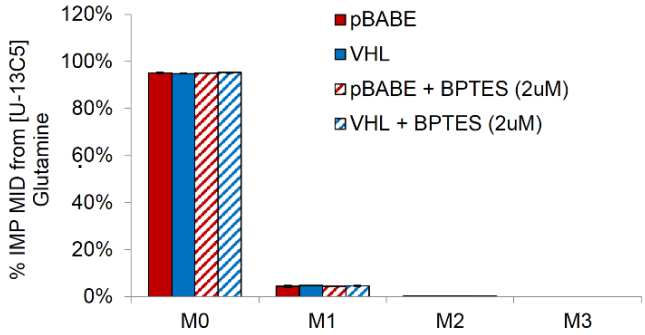

Supplementary Figure VI-S2. Effect of BPTES on the Mass Isotopomer Distribution of IMP from [U-$^{13}C_5$] Glutamine in RCC Cells, Related to Figure VI-2

The pair of UMRC2 cells was labeled with [U-$^{13}C_5$] glutamine under the absence or presence of BPTES at 2μM (for 48 hours) and the enrichment of the purine precursor inosine monophosphate (IMP) was determined by LC-MS/MS.

This page was intentionally left blank

CONCLUDING REMARKS

There has been an astonishing reawakening of the role of metabolism and its alterations in cancer. Appreciating that cellular metabolism can be regulated by oncogenes/tumor suppressors to promote i) macromolecule biosynthesis and ii) adaptation to nutrient-limited conditions has been a great progress towards understanding the behavior of cancer cells. Such efforts in understanding cancer cell metabolism have led to the identification of new metabolic targets for cancer therapy, and some of them are being tested in pre-clinical and clinical trials (Locasale, 2013; Zhao et al., 2013). From the biological standpoint, this thesis identified metabolic vulnerabilities of hypoxic and pseudohypoxic cancer cells. Using isotopic tracing and mass spectrometry analyses, this work studied the hypoxia-induced alterations in the Krebs cycle and elucidated the role of reductive carboxylation in supporting lipid and pyrimidine biosynthesis in *VHL*-deficient RCC cells. We propose that targeting reductive glutamine utilization may be effective to treat HIF-expressing tumors.

Targeting cancer cell metabolism is not a new idea. In actuality, one of oldest anti-cancer strategies is the targeting of one-carbon metabolism using folate antagonists that block DNA synthesis [reviewed in (Vander Heiden, 2011; Locasale, 2013)]. One example of an anti-folate drug is 5-fluoroacil (5-FU), which is clinically used to treat many cancers and acts by inhibiting thymidylate synthase, an enzyme required for the synthesis of deoxythymidine monophosphate (dTMP) for DNA synthesis (Locasale, 2013). Although successful for the treatment of certain malignancies, anti-folate drugs may not be an ideal anti-cancer strategy because their mechanism of action appears to be the inhibition of rapidly proliferating cells, not cancer cells in specific. The apparent non-selective and growth-coupled nature of 5-FU and similar anti-metabolites underlies the toxicity of many conventional chemotherapies, and it is one of arguments against targeting the metabolism of cancer cells. The argument – metabolic pathways promoting growth of cancer cells are also required for the growth of normal cells – is true to the extent that some metabolic pathways are essential and cannot be bypassed or replaced. However,

this being said, the clinical success of old-standing anti-metabolite drugs such as 5-FU, methotrexate, hydroxyurea and others signifies that a therapeutic window exists for these apparent non-selective chemotherapies. This window cannot be entirely explained based on differences in growth rate between normal and cancer proliferating cells (Vander Heiden, 2011), and rather suggests that unknown metabolic dependences underlie the therapeutic effect of these drugs. Elucidating these cancer-specific metabolic alterations is a challenge that will better tailor current anti-metabolites and aid in novel drug design against cancer.

There is a second argument that distrusts the idea of targeting cancer cell metabolism and this one is more thoughtful - causality. It has been often argued that altered metabolism *accompanies* carcinogenesis, but it does not drive the transformation of normal cell into cancer cells. The causality argument has been supported by the first efforts in cancer genome sequencing, which showed a repertoire of genetic mutations that affected core signaling pathways of cell growth and survival but not in metabolic enzymes (Vogelstein et al., 2013). However, recent advances have shown that genetic lesions in metabolic enzymes such as IDH1, IDH2, fumarate hydratase and succinate dehydrogenase are frequent in different types of cancer (see Chapter I). In addition, there are functional evidences showing necessity and/or sufficiency of specific enzyme isoforms, fluxes or metabolites to support the malignancy of specific tumors (See Chapter I). These discoveries support the paradigm of a metabolic reprogramming as essential for tumor growth and malignancy, and are fostering pharmaceutical endeavors to target recently identified metabolic targets in cancer ([No authors Listed], 2010).

There is an emerging link between metabolism and cancer that circles the causality discussion into a chicken and egg problem. Growing evidences have demonstrated how metabolic signals can affect chromatin structure and epigenetic programs [see the following reviews (Kaelin and McKnight, 2013; Lu and Thompson, 2012)]. Some of these recent studies have implied metabolites themselves as proto-oncogenes, showing that modulations of metabolite levels cause chemical modifications of histones and DNA, which in turn affect gene expression and may contribute to cancer development [See

comments by (Kim and DeBerardinis, 2013; Sassone-Corsi, 2013)]. Given the established role of epigenetic changes in carcinogenesis (Dawson and Kouzarides, 2012), the molecular connection between metabolites and gene expression is indeed a strong evidence for the critical role of metabolism in cell physiology and cancer development. The large-scale understanding of changes in gene expression in response to environmental inputs will certainly uncover mechanisms of cell plasticity, survival and growth. In turn, elucidating how genetic lesions and environmental insults cooperate with metabolism to hijack gene expression in favor of malignancy will lead to a new era of cancer biology. But before, we are yet to satisfactorily characterize the metabolic alterations that affect energy and biomass production in cancer cells.

In this thesis, we revisited the role of the Krebs cycle in central carbon metabolism and investigated its biological significance in hypoxic and *VHL*-deficient cancer cells. These results illustrated that the metabolic plasticity and substrate preference can be remarkably different in cancer cells. I hope this work be actively kept in reasoning for future studies, and that it be a step closer towards targeting the metabolic abnormalities of renal cell carcinomas, perhaps with glutaminase inhibitors. That understanding of cellular bioenergetics and the regulation of Krebs cycle will help us solve clinical problems is evident, and this conclusion would most likely not be a surprise if Krebs himself witnessed the recent discoveries on cancer metabolism:

"The research I have been doing - studying how foodstuffs yield energy in living cells - does not lead to the kind of knowledge that can be expected to give immediate practical benefits to mankind. If I have chosen this field of study, it was because I believed in its importance in spite of its theoretical character. My reason for this belief was that all living things must be continuously fed with energy and I am convinced that an understanding of the process of energy production will eventually help us in solving some of the practical problems of medicine." – Hans Krebs, Banquet Speech at the Nobel Prize Ceremony, 1953.

This page was intentionally left blank

"You have achieved success if you have lived well, laughed often and loved much."

Author Unknown

This page was intentionally left blank

REFERENCES

[No authors Listed] (2010). Targeting tumour metabolism. Nature Reviews. Drug Discovery *9*, 503–504.

Aird, K.M., Zhang, G., Li, H., Tu, Z., Bitler, B.G., Garipov, A., Wu, H., Wei, Z., Wagner, S.N., Herlyn, M., et al. (2013). Suppression of nucleotide metabolism underlies the establishment and maintenance of oncogene-induced senescence. Cell Reports *3*, 1252–1265.

Alberts, B., et al. Johnson, A., Lewis, J., Raff, M., Roberts, K., and Walter, P. (2002). Energy Conversion: Mitochondria and Chloroplasts. In Molecular Bology of the Cell, (Garland Science, New York),.

Antoniewicz, J.K.K.M.R., Antoniewicz, M.R., Kelleher, J.K., Stephanopoulos, G., and Maciek R. Antoniewicz, J.K.K. (2007). Elementary metabolite units (EMU) - A novel framework for modeling isotopic distributions. Metabolic Engineering *9*, 19.

Antoniewicz, M.R., Kelleher, J.K., Stephanopoulos, G., and Maciek R. Antoniewicz, J.K.K. (2006). Determination of confidence intervals of metabolic fluxes estimated from stable isotope measurements. Metabolic Engineering *8*, 14.

Baldwin, S. a, Beal, P.R., Yao, S.Y.M., King, A.E., Cass, C.E., and Young, J.D. (2004). The equilibrative nucleoside transporter family, SLC29. Pflügers Archiv : European Journal of Physiology *447*, 735–743.

Baysal, B.E., Ferrell, R.E., Willett-Brozick, J.E., Lawrence, E.C., Myssiorek, D., Bosch, A., van der Mey, A., Taschner, P.E., Rubinstein, W.S., Myers, E.N., et al. (2000). Mutations in SDHD, a mitochondrial complex II gene, in hereditary paraganglioma. Science (New York, N.Y.) *287*, 848–851.

Ben-Haim, S., and Ell, P. (2009). 18F-FDG PET and PET/CT in the Evaluation of Cancer Treatment Response. Journal of Nuclear Medicine *50*, 88–99.

Ben-Sahra, I., Howell, J.J., Asara, J.M., and Manning, B.D. (2013). Stimulation of de Novo Pyrimidine Synthesis by Growth Signaling Through mTOR and S6K1. Science *339*, 1323–1328.

Bernhard, S. a, and Tompa, P. (1990). The mechanism of succinate or fumarate transfer in the tricarboxylic acid cycle allows molecular rotation of the intermediate. Archives of Biochemistry and Biophysics *276*, 191–198.

Bester, A.C., Roniger, M., Oren, Y.S., Im, M.M., Sarni, D., Chaoat, M., Bensimon, A., Zamir, G., Shewach, D.S., and Kerem, B. (2011). Nucleotide Deficiency Promotes Genomic Instability in Early Stages of Cancer Development. Cell *145*, 435–446.

Blinova, K., Carroll, S., Bose, S., Smirnov, A. V, Harvey, J.J., Knutson, J.R., and Balaban, R.S. (2005). Distribution of Mitochondrial NADH Fluorescence Lifetimes: Steady-State Kinetics of Matrix NADH Interactions. Biochemistry *44*, 2585–2594.

Boiteux, A., and Hess, B. (1981). Design of Glycolysis. Philosophical Transactions of the Royal Society B: Biological Sciences *293*, 5–22.

Bonnet, S., Archer, S.L., Allalunis-Turner, J., Haromy, A., Beaulieu, C., Thompson, R., Lee, C.T., Lopaschuk, G.D., Puttagunta, L., Harry, G., et al. (2007). A Mitochondria-K+ Channel Axis Is Suppressed in Cancer and Its Normalization Promotes Apoptosis and Inhibits Cancer Growth. Cancer Cell *11*, 37–51.

Brand, K. (1985). Glutamine and glucose metabolism during thymocyte proliferation. Biochem J. *228*, 353–361.

Brand, M.D., and Murphy, M.P. (1987). Control of electron flux through the respiratory chain in mitochondria and cells. Biological Reviews of the Cambridge Philosophical Society *62*, 141–193.

Brugarolas, J., Lei, K., Hurley, R.L., Manning, B.D., Reiling, J.H., Hafen, E., Witters, L.A., Ellisen, L.W., and Kaelin, W.G. (2004). Regulation of mTOR function in response to hypoxia by REDD1 and the TSC1/TSC2 tumor suppressor complex. Genes & Development *18*, 2893–2904.

Brugarolas, J.B., Vazquez, F., Reddy, A., Sellers, W.R., and Kaelin, W.G. (2003). TSC2 regulates VEGF through mTOR-dependent and -independent pathways. Cancer Cell *4*, 147–158.

Burns, V.W. (1966). Regulation of pyrimidine biosynthesis and its strong coupling to the purine system. Biophysical Journal *6*, 787–800.

Cairns, R.A., Harris, I.S., and Mak, T.W. (2011). Regulation of cancer cell metabolism. Nat Rev Cancer *11*, 85–95.

Carrey, E.A. (1993). Phosphorylation, allosteric effectors and inter-domain contacts in CAD; their role in regulation of early steps of pyrimidine biosynthesis. Biochemical Society Transactions *21*, 191–195.

Cederbaum, A.I., Lieber, C.S., Beattie, D.S., and Rubin, E. (1973). Characterization of shuttle mechanisms for the transport of reducing equivalents into mitochondria. Archives of Biochemistry and Biophysics *158*, 763–781.

Cerdan, S., Kunnecke, B., Seelig, J., and Künnecke, B. (1990). Cerebral metabolism of [1,2-13C2]acetate as detected by in vivo and in vitro 13C NMR. The Journal of Biological Chemistry *265*, 12916–12926.

Chan, S.Y., Zhang, Y.Y., Hemann, C., Mahoney, C.E., Zweier, J.L., and Loscalzo, J. (2009). MicroRNA-210 controls mitochondrial metabolism during hypoxia by repressing the iron-sulfur cluster assembly proteins ISCU1/2. Cell Metab *10*, 273–284.

Chaneton, B., Hillmann, P., Zheng, L., Martin, A.C.L., Maddocks, O.D.K., Chokkathukalam, A., Coyle, J.E., Jankevics, A., Holding, F.P., Vousden, K.H., et al. (2012). Serine is a natural ligand and allosteric activator of pyruvate kinase M2. Nature.

Chen, K.-F., Lai, Y.-Y., Sun, H.S., and Tsai, S.-J. (2005). Transcriptional repression of human cad gene by hypoxia inducible factor-1alpha. Nucleic Acids Research *33*, 5190–5198.

Cheng, T., Sudderth, J., Yang, C., Mullen, A.R., Jin, E.S., Mates, J.M., and DeBerardinis, R.J. (2011). Pyruvate carboxylase is required for glutamine-independent growth of tumor cells. Proc Natl Acad Sci U S A *108*, 8674–8679.

Chitalia, V.C., Foy, R.L., Bachschmid, M.M., Zeng, L., Panchenko, M. V, Zhou, M.I., Bharti, A., Seldin, D.C., Lecker, S.H., Dominguez, I., et al. (2008). Jade-1 inhibits Wnt signalling by ubiquitylating beta-catenin and mediates Wnt pathway inhibition by pVHL. Nat Cell Biol *10*, 1208–1216.

Christensen, B., and Nielsen, J. (1999). Isotopomer analysis using GC-MS. Metabolic Engineering *1*, 282–290.

Christofk, H.R., Vander Heiden, M.G., Wu, N., Asara, J.M., Cantley, L.C., and Heather R. Christofk, M.G.V.H. (2008a). Pyruvate kinase M2 is a phosphotyrosine-binding protein. Nature *452*, 181–186.

Christofk, M.G.V.H.H.R., Christofk, H.R., Vander Heiden, M.G., Harris, M.H., Ramanathan, A., Gerszten, R.E., Wei, R., Fleming, M.D., Schreiber, S.L., Cantley, L.C., et al. (2008b). The M2 splice isoform of pyruvate kinase is important for cancer metabolism and tumour growth. Nature Letters *452*, 5.

Cohen, A., Barankiewicz, J., Lederman, H.M., and Gelfand, E.W. (1983). Purine and pyrimidine metabolism in human T lymphocytes. Regulation of deoxyribonucleotide metabolism. The Journal of Biological Chemistry *258*, 12334–12340.

Colombo, S.L., Palacios-Callender, M., Frakich, N., Carcamo, S., Kovacs, I., Tudzarova, S., and Moncada, S. (2011). Molecular basis for the differential use of glucose and glutamine in cell proliferation as revealed by synchronized HeLa cells. Proceedings of the National Academy of Sciences of the United States of America *108*, 21069–21074.

Cooper, J.A., Esch, F.S., Taylor, S.S., and Hunter, T. (1984). Phosphorylation sites in enolase and lactate dehydrogenase utilized by tyrosine protein kinases in vivo and in vitro. The Journal of Biological Chemistry *259*, 7835–7841.

Creighton, C.J., Morgan, M., Gunaratne, P.H., Wheeler, D.A., Gibbs, R.A., Gordon Robertson, A., Chu, A., Beroukhim, R., Cibulskis, K., Signoretti, S., et al. (2013). Comprehensive molecular characterization of clear cell renal cell carcinoma. Nature *499*, 43–49.

Dalziel, K., and Londesborough, J.C. (1968). The mechanisms of reductive carboxylation reactions. Carbon dioxide or bicarbonate as substrate of nicotinamide-adenine dinucleotide phosphate-linked isocitrate dehydrogenase and malic enzyme. The Biochemical Journal *110*, 223–230.

Dandekar, T., Schuster, S., Snel, B., Huynen, M., and Bork, P. (1999). Pathway alignment: application to the comparative analysis of glycolytic enzymes. The Biochemical Journal *343 Pt 1*, 115–124.

Dang, C. V (2009a). PKM2 Tyrosine Phosphorylation and Glutamine Metabolism Signal a Different View of the Warburg Effect. Sci. Signal. *2*, pe75.

Dang, C. V (2009b). MYC, microRNAs and glutamine addiction in cancers. Cell Cycle *8*, 3243–3245.

Dang, C. V. (2010). Glutaminolysis: Supplying carbon or nitrogen, or both for cancer cells? Cell Cycle *9*, 3884–3886.

Dang, L., White, D.W., Gross, S., Bennett, B.D., Bittinger, M.A., Driggers, E.M., Fantin, V.R., Jang, H.G., Jin, S., Keenan, M.C., et al. (2010). Cancer-associated IDH1 mutations produce 2-hydroxyglutarate. Nature *465*, 966.

Dauner, M., and Sauer, U. (2000). GC-MS analysis of amino acids rapidly provides rich information for isotopomer balancing. Biotechnology Progress *16*, 642–649.

David, C.J., Chen, M., Assanah, M., Canoll, P., and Manley, J.L. (2010). HnRNP proteins controlled by c-Myc deregulate pyruvate kinase mRNA splicing in cancer. Nature *463*, 364–368.

Dawson, M.A., and Kouzarides, T. (2012). Cancer epigenetics: from mechanism to therapy. Cell *150*, 12–27.

DeBerardinis, R.J., and Cheng, T. (2009). Q's next: the diverse functions of glutamine in metabolism, cell biology and cancer. Oncogene *29*, 313–324.

DeBerardinis, R.J., and Thompson, C.B. (2012). Cellular Metabolism and Disease: What Do Metabolic Outliers Teach Us? Cell *148*, 1132–1144.

DeBerardinis, R.J., Mancuso, A., Daikhin, E., Nissim, I., Yudkoff, M., Wehrli, S., and Thompson, C.B. (2007). Beyond aerobic glycolysis: transformed cells can engage in glutamine metabolism that exceeds the requirement for protein and nucleotide synthesis. Proceedings of the National Academy of Sciences of the United States of America *104*, 19345–19350.

DeBerardinis, R.J., Lum, J.J., Hatzivassiliou, G., and Thompson, C.B. (2008). The biology of cancer: metabolic reprogramming fuels cell growth and proliferation. Cell Metabolism *7*, 11–20.

Denko, N.C. (2008). Hypoxia, HIF1 and glucose metabolism in the solid tumour. Nature Reviews Cancer *8*, 705–713.

Diebold, I., Petry, A., Hess, J., Görlach, A., and Gorlach, A. (2010). The NADPH oxidase subunit NOX4 is a new target gene of the hypoxia-inducible factor-1. Molecular Biology of the Cell *21*, 2087–2096.

Duncan, B.K., and Miller, J.H. (1980). Mutagenic deamination of cytosine residues in DNA. Nature *287*, 560–561.

Ebert, B.L., Gleadle, J.M., O'Rourke, J.F., Bartlett, S.M., Poulton, J., and Ratcliffe, P.J. (1996). Isoenzyme-specific regulation of genes involved in energy metabolism by hypoxia: similarities with the regulation of erythropoietin. The Biochemical Journal *313 (Pt 3*, 809–814.

Elstrom, R.L., Bauer, D.E., Buzzai, M., Karnauskas, R., Harris, M.H., Plas, D.R., Zhuang, H., Cinalli, R.M., Alavi, A., Rudin, C.M., et al. (2004). Akt stimulates aerobic glycolysis in cancer cells. Cancer Res *64*, 3892–3899.

Eto, K., Tsubamoto, Y., Terauchi, Y., Sugiyama, T., Kishimoto, T., Takahashi, N., Yamauchi, N., Kubota, N., Murayama, S., Aizawa, T., et al. (1999). Role of NADH Shuttle System in Glucose-Induced Activation of Mitochondrial Metabolism and Insulin Secretion. Science *283*, 981–985.

Fernandez, C.A., Rosiers, C. Des, Previs, S.F., David, F., Brunengraber, H., and Des Rosiers, C. (1996). Correction of 13C Mass Isotopomer Distributions for Natural Stable Isotope Abundance. Journal of Mass Spectrometry *31*, 255–262.

Firth, J.D., Ebert, B.L., Pugh, C.W., and Ratcliffe, P.J. (1994). Oxygen-regulated control elements in the phosphoglycerate kinase 1 and lactate dehydrogenase A genes: similarities with the erythropoietin 3' enhancer. Proceedings of the National Academy of Sciences of the United States of America *91*, 6496–6500.

Flier, J.S., Mueckler, M.M., Usher, P., and Lodish, H.F. (1987). Elevated levels of glucose transport and transporter messenger RNA are induced by ras or src oncogenes. Science (New York, N.Y.) *235*, 1492–1495.

Freeman, H., Shimomura, K., Horner, E., Cox, R.D., and Ashcroft, F.M. (2006). Nicotinamide nucleotide transhydrogenase: A key role in insulin secretion. Cell Metabolism *3*, 35–45.

Gaglio, D., Soldati, C., Vanoni, M., Alberghina, L., and Chiaradonna, F. (2009). Glutamine Deprivation Induces Abortive S-Phase Rescued by Deoxyribonucleotides in K-Ras Transformed Fibroblasts. PLoS ONE *4*.

Gaglio, D., Metallo, C., Gameiro, P.A., Hiller, K., Danna, L.S., Balestrieri, C., Alberghina, L., Stephanopoulos*, G.N., and Chiaradonna, F. (2011). Oncogenic K-Ras decouples glucose and glutamine metabolism to support cancer cell growth. Mol Syst Biol *7*, 523.

Gameiro, P.A., Yang, J., Metelo, A.M., Pérez-Carro, R., Baker, R., Wang, Z., Arreola, A., Rathmell, W.K., Olumi, A., López-Larrubia, P., et al. (2013a). In vivo HIF-mediated reductive carboxylation is regulated by citrate levels and sensitizes VHL-deficient cells to glutamine deprivation. Cell Metabolism *17*, 372–385.

Gameiro, P.A., Laviolette, L. a., Kelleher, J.K., Iliopoulos, O., and Stephanopoulos, G. (2013b). Cofactor balance by nicotinamide nucleotide transhydrogenase (NNT) coordinates reductive carboxylation and glucose catabolism in the TCA cycle. The Journal of Biological Chemistry *288*, 12967–12977.

Gatenby, R.A., and Gillies, R.J. (2004). Why do cancers have high aerobic glycolysis? Nature Reviews. Cancer *4*, 891–899.

Goda, N., Ryan, H.E., Khadivi, B., McNulty, W., Rickert, R.C., and Johnson, R.S. (2003). Hypoxia-inducible factor 1alpha is essential for cell cycle arrest during hypoxia. Molecular and Cellular Biology *23*, 359–369.

Gordan, J.D., and Simon, M.C. (2007). Hypoxia-inducible factors: central regulators of the tumor phenotype. Current Opinion in Genetics & Development *17*, 71–77.

Gordan, J.D., Thompson, C.B., and Simon, M.C. (2007). HIF and c-Myc: Sibling Rivals for Control of Cancer Cell Metabolism and Proliferation. Cancer Cell *12*, 108–113.

Greenhouse, W.V. V, and Lehninger, A.L. (1976). Occurrence of the Malate-Aspartate Shuttle in Various Tumor Types Occurrence of the Malate-Aspartate Shuttle in Various Tumor. 1392–1396.

Griffin, J.L., and Shockcor, J.P. (2004). Metabolic profiles of cancer cells. Nat Rev Cancer *4*, 551–561.

Guzy, R.D., Sharma, B., Bell, E., Chandel, N.S., and Schumacker, P.T. (2008). Loss of the SdhB, but Not the SdhA, Subunit of Complex II Triggers Reactive Oxygen Species-Dependent Hypoxia-Inducible Factor Activation and Tumorigenesis. Mol. Cell. Biol. *28*, 718–731.

Halket, J.M., Waterman, D., Przyborowska, A.M., Patel, R.K.P., Fraser, P.D., and Bramley, P.M. (2005). Chemical derivatization and mass spectral libraries in metabolic profiling by GC/MS and LC/MS/MS. Journal of Experimental Botany *56*, 219–243.

Hardie, D.G. (2000). Metabolic control: A new solution to an old problem. Current Biology *10*, R757–R759.

Hartong, D.T., Dange, M., McGee, T.L., Berson, E.L., Dryja, T.P., and Colman, R.F. (2008). Insights from retinitis pigmentosa into the roles of isocitrate dehydrogenases in the Krebs cycle. Nature Genetics *40*, 1230–1234.

Hatzivassiliou, G., Zhao, F., Bauer, D.E., Andreadis, C., Shaw, A.N., Dhanak, D., Hingorani, S.R., Tuveson, D.A., and Thompson, C.B. (2005). ATP citrate lyase inhibition can suppress tumor cell growth. Cancer Cell *8*, 311–321.

Hitosugi, T., Kang, S., Vander Heiden, M.G., Chung, T.-W., Elf, S., Lythgoe, K., Dong, S., Lonial, S., Wang, X., Chen, G.Z., et al. (2009). Tyrosine Phosphorylation Inhibits PKM2 to Promote the Warburg Effect and Tumor Growth. Sci. Signal. *2*, ra73–ra73.

Hu, C.-J., Wang, L.-Y., Chodosh, L.A., Keith, B., and Simon, M.C. (2003). Differential Roles of Hypoxia-Inducible Factor 1{alpha} (HIF-1{alpha}) and HIF-2{alpha} in Hypoxic Gene Regulation. Mol. Cell. Biol. *23*, 9361–9374.

Hu, C.-M., Yeh, M.-T., Tsao, N., Chen, C.-W., Gao, Q.-Z., Chang, C.-Y., Lee, M.-H., Fang, J.-M., Sheu, S.-Y., Lin, C.-J., et al. (2012). Tumor Cells Require Thymidylate Kinase to Prevent dUTP Incorporation during DNA Repair. Cancer Cell *22*, 36–50.

Hubbi, M.E., Kshitiz, Gilkes, D.M., Rey, S., Wong, C.C., Luo, W., Kim, D.-H., Dang, C. V, Levchenko, A., and Semenza, G.L. (2013). A nontranscriptional role for HIF-1α as a direct inhibitor of DNA replication. Science Signaling *6*, ra10.

Iliopoulos, O. (2006). Molecular Biology of Renal Cell Cancer and the Identification of Therapeutic Targets. Journal of Clinical Oncology *24*, 5593 –5600.

Iliopoulos, O., Kibel, A., Gray, S., and Kaelin, W.G. (1995). Tumour suppression by the human von Hippel-Lindau gene product. Nature Medicine *1*, 822–826.

Isaacs, J.S., Jung, Y.J., Mole, D.R., Lee, S., Torres-Cabala, C., Chung, Y.L., Merino, M., Trepel, J., Zbar, B., Toro, J., et al. (2005). HIF overexpression correlates with biallelic loss of fumarate hydratase in renal cancer: novel role of fumarate in regulation of HIF stability. Cancer Cell *8*, 143–153.

Ivan, M., Kondo, K., Yang, H., Kim, W., Valiando, J., Ohh, M., Salic, A., Asara, J.M., Lane, W.S., and Kaelin Jr, W.G. (2001). HIFalpha targeted for VHL-mediated destruction by proline hydroxylation: implications for O2 sensing. Science *292*, 464–468.

Iyer, N. V, Kotch, L.E., Agani, F., Leung, S.W., Laughner, E., Wenger, R.H., Gassmann, M., Gearhart, J.D., Lawler, A.M., Yu, A.Y., et al. (1998). Cellular and developmental control of O2 homeostasis by hypoxia-inducible factor 1 alpha. Genes & Development *12*, 149–162.

Jaakkola, P., Mole, D.R., Tian, Y.M., Wilson, M.I., Gielbert, J., Gaskell, S.J., von Kriegsheim, A., Hebestreit, H.F., Mukherji, M., Schofield, C.J., et al. (2001). Targeting of HIF-alpha to the von Hippel-Lindau ubiquitylation complex by O2-regulated prolyl hydroxylation. Science (New York, N.Y.) *292*, 468–472.

Jain, M., Nilsson, R., Sharma, S., Madhusudhan, N., Kitami, T., Souza, A.L., Kafri, R., Kirschner, M.W., Clish, C.B., and Mootha, V.K. (2012). Metabolite Profiling Identifies a Key Role for Glycine in Rapid Cancer Cell Proliferation. Science *336*, 1040–1044.

Johansson, N.G., and Eriksson, S. (1996). Structure-activity relationships for phosphorylation of nucleoside analogs to monophosphates by nucleoside kinases. Acta Biochimica Polonica *43*, 143–160.

Kaadige, M.R., Looper, R.E., Kamalanaadhan, S., and Ayer, D.E. (2009). Glutamine-dependent anapleurosis dictates glucose uptake and cell growth by regulating MondoA transcriptional activity. Proceedings of the National Academy of Sciences *106*, 14878–14883.

Kaelin, W.G., and McKnight, S.L. (2013). Influence of Metabolism on Epigenetics and Disease. Cell *153*, 56–69.

Kaelin, W.G., Thompson, C.B., and Jr, W.G.K. (2010). Q&A: Cancer: Clues from cell metabolism. Nature *465*, 562–564.

Kaelin Jr., W.G. (2009). SDH5 Mutations and Familial Paraganglioma: Somewhere Warburg is Smiling. Cancer Cell *16*, 180–182.

Kauppinen, R.A., Sihra, T.S., and Nicholls, D.G. (1987). Aminooxyacetic acid inhibits the malate-aspartate shuttle in isolated nerve terminals and prevents the mitochondria from utilizing glycolytic substrates. Biochimica et Biophysica Acta *930*, 173–178.

Keith, B., Johnson, R.S., and Simon, M.C. (2012). HIF1α and HIF2α: sibling rivalry in hypoxic tumour growth and progression. Nat Rev Cancer *12*, 9–22.

Kelleher, J.K., and Masterson, T.M. (1992). Model equations for condensation biosynthesis using stable isotopes and radioisotopes. The American Journal of Physiology *262*, E118–125.

Kharroubi, A.T., Masterson, T.M., Aldaghlas, T.A., Kennedy, K.A., and Kelleher, J.K. (1992). Isotopomer spectral analysis of triglyceride fatty acid synthesis in 3T3-L1 cells. The American Journal of Physiology *263*, E667–75.

Kim, J., and DeBerardinis, R.J. (2013). Cancer. Silencing a metabolic oncogene. Science (New York, N.Y.) *340*, 558–559.

Kim, J.W., Tchernyshyov, I., Semenza, G.L., and Dang, C. V (2006). HIF-1-mediated expression of pyruvate dehydrogenase kinase: A metabolic switch required for cellular adaptation to hypoxia. Cell Metabolism *3*, 177–185.

Kim, W., Kaelin, W.G., and Jr (2003). The von Hippel–Lindau tumor suppressor protein: new insights into oxygen sensing and cancer. Current Opinion in Genetics & Development *13*, 55–60.

Kondo, K., Klco, J., Nakamura, E., Lechpammer, M., and Kaelin Jr., W.G. (2002). Inhibition of HIF is necessary for tumor suppression by the von Hippel-Lindau protein. Cancer Cell *1*, 237–246.

Koppenol, W.H., Bounds, P.L., and Dang, C. V (2011). Otto Warburg's contributions to current concepts of cancer metabolism. Nat Rev Cancer *11*, 325–337.

Koshiji, M., Kageyama, Y., Pete, E.A., Horikawa, I., Barrett, J.C., and Huang, L.E. (2004a). HIF-1alpha induces cell cycle arrest by functionally counteracting Myc. The EMBO Journal *23*, 1949–1956.

Koshiji, M., Kageyama, Y., Pete, E.A., Horikawa, I., Barrett, J.C., and Huang, L.E. (2004b). HIF-1alpha induces cell cycle arrest by functionally counteracting Myc. The EMBO Journal *23*, 1949–1956.

Kulshreshtha, R., Ferracin, M., Wojcik, S.E., Garzon, R., Alder, H., Agosto-Perez, F.J., Davuluri, R., Liu, C.-G., Croce, C.M., Negrini, M., et al. (2007). A microRNA signature of hypoxia. Molecular and Cellular Biology *27*, 1859–1867.

Laplante, M., and Sabatini, D.M.M. (2012). mTOR Signaling in Growth Control and Disease. Cell *149*, 274–293.

Le, A., Lane, A.N., Hamaker, M., Bose, S., Gouw, A., Barbi, J., Tsukamoto, T., Rojas, C.J., Slusher, B.S., Zhang, H., et al. (2012). Glucose-independent glutamine metabolism via TCA cycling for proliferation and survival in B cells. Cell Metabolism *15*, 110–121.

Leonardi, R., Subramanian, C., Jackowski, S., and Rock, C.O. (2012). Cancer-associated isocitrate dehydrogenase mutations inactivate NADPH-dependent reductive carboxylation. J Biol Chem *287*, 14615–14620.

Levine, A.J., and Puzio-Kuter, A.M. (2010). The control of the metabolic switch in cancers by oncogenes and tumor suppressor genes. Science (New York, N.Y.) *330*, 1340–1344.

Li, L., Zhang, L., Zhang, X., Yan, Q., Minamishima, Y.A., Olumi, A.F., Mao, M., Bartz, S., and Kaelin Jr., W.G. (2007). Hypoxia-inducible factor linked to differential kidney cancer risk seen with type 2A and type 2B VHL mutations. Mol Cell Biol *27*, 5381–5392.

Liu, Y.-C., Li, F., Handler, J., Huang, C.R.L., Xiang, Y., Neretti, N., Sedivy, J.M., Zeller, K.I., and Dang, C. V (2008). Global regulation of nucleotide biosynthetic genes by c-Myc. PloS One *3*, e2722.

Locasale, J.W. (2013). Serine, glycine and one-carbon units: cancer metabolism in full circle. Nature Reviews. Cancer *13*, 572–583.

Lu, C., and Thompson, C.B. (2012). Metabolic Regulation of Epigenetics. Cell Metabolism *16*, 9–17.

Lum, J.J., Bui, T., Gruber, M., Gordan, J.D., DeBerardinis, R.J., Covello, K.L., Simon, M.C., and Thompson, C.B. (2007). The transcription factor HIF-1α plays a critical role in the growth factor-dependent regulation of both aerobic and anaerobic glycolysis. Genes & Development *21*, 1037–1049.

Luo, W., Hu, H., Chang, R., Zhong, J., Knabel, M., O'Meally, R., Cole, R.N., Pandey, A., and Semenza, G.L. (2011). Pyruvate kinase M2 is a PHD3-stimulated coactivator for hypoxia-inducible factor 1. Cell *145*, 732–744.

Macallan, D.C., Fullerton, C.A., Neese, R. a, Haddock, K., Park, S.S., and Hellerstein, M.K. (1998). Measurement of cell proliferation by labeling of DNA with stable isotope-labeled glucose: Studies in vitro, in animals, and in humans. Proceedings of the National Academy of Sciences of the United States of America *95*, 708–713.

Mannava, S., Grachtchouk, V., Wheeler, L.J., Im, M., Zhuang, D., Slavina, E.G., Mathews, C.K., Shewach, D.S., and Nikiforov, M.A. (2008). Direct role of nucleotide metabolism in C-MYC-dependent proliferation of melanoma cells. Cell Cycle (Georgetown, Tex.) *7*, 2392–2400.

Maranchie, J.K., Vasselli, J.R., Riss, J., Bonifacino, J.S., Linehan, W.M., and Klausner, R.D. (2002). The contribution of VHL substrate binding and HIF1-alpha to the phenotype of VHL loss in renal cell carcinoma. Cancer Cell *1*, 247–255.

Marin-Valencia, I., Yang, C., Mashimo, T., Cho, S., Baek, H., Yang, X., Kartik, N., Maddie, M., Vemireddy, V., Zhao, Z., et al. (2012). Analysis of tumor metabolism reveals mitochondrial glucose oxidation in genetically diverse human glioblastomas in the mouse brain in vivo. Cell Metabolism *15*, 827–837.

McKnight, S.L. (2010). On getting there from here. Science (New York, N.Y.) *330*, 1338–1339.

Meimaridou, E., Kowalczyk, J., Guasti, L., Hughes, C.R., Wagner, F., Frommolt, P., Nurnberg, P., Mann, N.P., Banerjee, R., Saka, H.N., et al. (2012). Mutations in NNT encoding nicotinamide nucleotide transhydrogenase cause familial glucocorticoid deficiency. Nat Genet *44*, 740–742.

Melvin, A., and Rocha, S. (2012). Chromatin as an oxygen sensor and active player in the hypoxia response. Cell Signal *24*, 35–43.

Metallo, C.M., Walther, J.L., and Stephanopoulos, G. (2009). Evaluation of 13C isotopic tracers for metabolic flux analysis in mammalian cells. Journal of Biotechnology *144*, 167–174.

Metallo, C.M., Gameiro, P.A., Bell, E.L., Mattaini, K.R., Yang, J., Hiller, K., Jewell, C.M., Johnson, Z.R., Irvine, D.J., Guarente, L., et al. (2012). Reductive glutamine metabolism by IDH1 mediates lipogenesis under hypoxia. Nature *481*, 380–384.

Mikhaylova, O., Ignacak, M.L., Barankiewicz, T.J., Harbaugh, S. V, Yi, Y., Maxwell, P.H., Schneider, M., Van Geyte, K., Carmeliet, P., Revelo, M.P., et al. (2008). The von Hippel-Lindau tumor suppressor protein and Egl-9-Type proline hydroxylases regulate the large subunit of RNA polymerase II in response to oxidative stress. Mol Cell Biol *28*, 2701–2717.

Mitchell, P. (1979). Keilin's respiratory chain concept and its chemiosmotic consequences. Science *206*, 1148–1159.

Mitsuishi, Y., Taguchi, K., Kawatani, Y., Shibata, T., Nukiwa, T., Aburatani, H., Yamamoto, M., and Motohashi, H. (2012). Nrf2 Redirects Glucose and Glutamine into Anabolic Pathways in Metabolic Reprogramming. Cancer Cell *22*, 66–79.

Mole, D.R., Blancher, C., Copley, R.R., Pollard, P.J., Gleadle, J.M., Ragoussis, J., and Ratcliffe, P.J. (2009). Genome-wide association of hypoxia-inducible factor (HIF)-1alpha and HIF-2alpha DNA binding with expression profiling of hypoxia-inducible transcripts. J Biol Chem *284*, 16767–16775.

Moreno-Sanchez, R., Hogue, B.A., Hansford, R.G., and Moreno-Sánchez, R. (1990). Influence of NAD-linked dehydrogenase activity on flux through oxidative phosphorylation. Biochemical Journal *268*, 421–428.

Moyer, M.W. (2012). Targeting hypoxia brings breath of fresh air to cancer therapy. Nature Medicine *18*, 636–637.

Mullen, A.R., Wheaton, W.W., Jin, E.S., Chen, P.-H., Sullivan, L.B., Cheng, T., Yang, Y., Linehan, W.M., Chandel, N.S., and DeBerardinis, R.J. (2011). Reductive carboxylation supports growth in tumour cells with defective mitochondria. Nature *advance on*.

Neermann, J., and Wagner, R. (1996). Comparative analysis of glucose and glutamine metabolism in transformed mammalian cell lines, insect and primary liver cells. Journal of Cellular Physiology *166*, 152–169.

Neese, R.A., Misell, L.M., Turner, S., Chu, A., Kim, J., Cesar, D., Hoh, R., Antelo, F., Strawford, A., McCune, J.M., et al. (2002). Measurement in vivo of proliferation rates of slow turnover cells by 2H2O labeling of the deoxyribose moiety of DNA. Proceedings of the National Academy of Sciences of the United States of America *99*, 15345–15350.

Newsholme, E.A., Crabtree, B., and Ardawi, M.S. (1985a). Glutamine metabolism in lymphocytes: its biochemical, physiological and clinical importance. Quarterly Journal of Experimental Physiology (Cambridge, England) *70*, 473–489.

Newsholme, E.A.A., Crabtree, B., and Ardawi, M.S.M.S. (1985b). The role of high rates of glycolysis and glutamine utilization in rapidly dividing cells. Bioscience Reports *5*, 393–400.

Nicholson, A., Reifsnyder, P.C., Malcolm, R.D., Lucas, C.A., MacGregor, G.R., Zhang, W., and Leiter, E.H. (2010). Diet-induced obesity in two C57BL/6 substrains with intact or mutant nicotinamide nucleotide transhydrogenase (Nnt) gene. Obesity (Silver Spring) *18*, 1902–1905.

Nicolay, B.N., Gameiro, P.A., Tschöp, K., Korenjak, M., Heilmann, A.M., Asara, J.M., Stephanopoulos, G., Iliopoulos, O., and Dyson, N.J. (2013). Loss of RBF1 changes glutamine catabolism. Genes & Development *27*, 182–196.

O'Donoghue, K., Brown, T.A., Carter, J.F., and Evershed, R.P. (1994). Detection of nucleotide bases in ancient seeds using gas chromatography/mass spectrometry and gas chromatography/mass spectrometry/mass spectrometry. Rapid Communications in Mass Spectrometry *8*, 503–508.

Ohh, M., Yauch, R.L., Lonergan, K.M., Whaley, J.M., Stemmer-Rachamimov, A.O., Louis, D.N., Gavin, B.J., Kley, N., Kaelin Jr., W.G., and Iliopoulos, O. (1998). The von Hippel-Lindau tumor suppressor protein is required for proper assembly of an extracellular fibronectin matrix. Mol Cell *1*, 959–968.

Ortiz-Barahona, A., Villar, D., Pescador, N., Amigo, J., and del Peso, L. (2010). Genome-wide identification of hypoxia-inducible factor binding sites and target genes by a probabilistic model integrating transcription-profiling data and in silico binding site prediction. Nucleic Acids Res *38*, 2332–2345.

Papandreou, I., Cairns, R.A., Fontana, L., Lim, A.L., and Denko, N.C. (2006). HIF-1 mediates adaptation to hypoxia by actively downregulating mitochondrial oxygen consumption. Cell Metabolism *3*, 187–197.

Parker, N., Vidal-Puig, A.J., Azzu, V., and Brand, M.D. (2009). Dysregulation of glucose homeostasis in nicotinamide nucleotide transhydrogenase knockout mice is independent of uncoupling protein 2. Biochim Biophys Acta *1787*, 1451–1457.

Pollard, P.J., Brière, J.J., Alam, N.A., Barwell, J., Barclay, E., Wortham, N.C., Hunt, T., Mitchell, M., Olpin, S., Moat, S.J., et al. (2005). Accumulation of Krebs cycle intermediates and over-expression of HIF1alpha in tumours which result from germline FH and SDH mutations. Human Molecular Genetics *14*, 2231–2239.

Pontarin, G., Ferraro, P., Rampazzo, C., Kollberg, G., Holme, E., Reichard, P., and Bianchi, V. (2011). Deoxyribonucleotide Metabolism in Cycling and Resting Human Fibroblasts with a Missense Mutation in p53R2, a Subunit of Ribonucleotide Reductase. Journal of Biological Chemistry *286*, 11132 –11140.

Possemato, R., Marks, K.M., Shaul, Y.D., Pacold, M.E., Kim, D., Birsoy, K., Sethumadhavan, S., Woo, H.-K., Jang, H.G., Jha, A.K., et al. (2011). Functional genomics reveal that the serine synthesis pathway is essential in breast cancer. Nature *476*, 346–350.

Pouysségur, J., Dayan, F.F., Mazure, N.M., and Pouyssegur, J. (2006). Hypoxia signalling in cancer and approaches to enforce tumour regression. Nature *441*, 437–443.

Rao, G.N., and Church, R.L. (1988). Regulation of CAD gene expression in mouse fibroblasts during the transition from the resting to the growing state. Experimental Cell Research *178*, 449–456.

Raval, R.R., Lau, K.W., Tran, M.G.B., Sowter, H.M., Mandriota, S.J., Li, J.-L., Pugh, C.W., Maxwell, P.H., Harris, A.L., and Ratcliffe, P.J. (2005). Contrasting properties of hypoxia-inducible factor 1 (HIF-1) and HIF-2 in von Hippel-Lindau-associated renal cell carcinoma. Molecular and Cellular Biology *25*, 5675–5686.

Ripoll, V.M., Meadows, N.A., Bangert, M., Lee, A.W., Kadioglu, A., and Cox, R.D. (2012). Nicotinamide nucleotide transhydrogenase (NNT) acts as a novel modulator of macrophage inflammatory responses. FASEB J *26*, 3550–3562.

Robitaille, A.M., Christen, S., Shimobayashi, M., Cornu, M., Fava, L.L., Moes, S., Prescianotto-Baschong, C., Sauer, U., Jenoe, P., and Hall, M.N. (2013). Quantitative Phosphoproteomics Reveal mTORC1 Activates de Novo Pyrimidine Synthesis. Science *339*, 1320–1323.

Roe, J.S., Kim, H., Lee, S.M., Kim, S.T., Cho, E.J., and Youn, H.D. (2006). p53 stabilization and transactivation by a von Hippel-Lindau protein. Mol Cell *22*, 395–405.

Rouault, T.A. (2006). The role of iron regulatory proteins in mammalian iron homeostasis and disease. Nat Chem Biol *2*, 406–414.

Rydström, J. (2006). Mitochondrial NADPH, transhydrogenase and disease. Biochimica et Biophysica Acta (BBA) - Bioenergetics *1757*, 721–726.

Sassone-Corsi, P. (2013). When Metabolism and Epigenetics Converge. Science *339*, 148–150.

Sauer, L.A., Dauchy, R.T., Nagel, W.O., and Morris, H.P. (1980). Mitochondrial malic enzymes. Mitochondrial NAD(P)+-dependent malic enzyme activity and malate-dependent pyruvate formation are progression-linked in Morris hepatomas. The Journal of Biological Chemistry *255*, 3844–3848.

Sazanov, L.A., and Jackson, J.B. (1994). Proton-translocating transhydrogenase and NAD- and NADP-linked isocitrate dehydrogenases operate in a substrate cycle which contributes to fine regulation of the tricarboxylic acid cycle activity in mitochondria. FEBS Letters *344*, 109–116.

Schödel, J., Oikonomopoulos, S., Ragoussis, J., Pugh, C.W., Ratcliffe, P.J., and Mole, D.R. (2011). High-resolution genome-wide mapping of HIF-binding sites by ChIP-seq. Blood *117*, e207–217.

Scott, D.A., Richardson, A.D., Filipp, F. V, Knutzen, C.A., Chiang, G.G., Ronai, Z.A., Osterman, A.L., and Smith, J.W. (2011). Comparative metabolic flux profiling of melanoma cell lines: beyond the Warburg effect. J Biol Chem *286*, 42626–42634.

Selak, M.A., Armour, S.M., MacKenzie, E.D., Boulahbel, H., Watson, D.G., Mansfield, K.D., Pan, Y., Simon, M.C.C., Thompson, C.B., and Gottlieb, E. (2005). Succinate links TCA cycle dysfunction to oncogenesis by inhibiting HIF-α prolyl hydroxylase. Cancer Cell *7*, 77–85.

Semenza, G.L. (2007). HIF-1 mediates the Warburg effect in clear cell renal carcinoma. Journal of Bioenergetics and Biomembranes *39*, 231–234.

Semenza, G.L. (2009). Defining the role of hypoxia-inducible factor 1 in cancer biology and therapeutics. Oncogene *29*, 625–634.

Semenza, G.L. (2010). HIF-1: upstream and downstream of cancer metabolism. Current Opinion in Genetics & Development *20*, 51–56.

Shackelford, D.B., Vasquez, D.S., Corbeil, J., Wu, S., Leblanc, M., Wu, C.-L., Vera, D.R., and Shaw, R.J. (2009). mTOR and HIF-1alpha-mediated tumor metabolism in an LKB1 mouse model of Peutz-Jeghers syndrome. Proceedings of the National Academy of Sciences of the United States of America *106*, 11137–11142.

Shambaugh, G. (1979). Pyrimidine biosynthesis. The American Journal of Clinical Nutrition *32*, 1290 –1297.

Shaw, R.J., and Cantley, L.C. (2006). Ras, PI(3)K and mTOR signalling controls tumour cell growth. Nature *441*, 424–430.

Sheeran, F.L., Rydström, J., Shakhparonov, M.I., Pestov, N.B., and Pepe, S. (2010). Diminished NADPH transhydrogenase activity and mitochondrial redox regulation in human failing myocardium. Biochimica et Biophysica Acta (BBA) - Bioenergetics *1797*, 1138–1148.

Shim, H., Dolde, C., Lewis, B.C., Wu, C.S., Dang, G., Jungmann, R.A., Dalla-Favera, R., and Dang, C. V (1997). c-Myc transactivation of LDH-A: implications for tumor metabolism and growth. Proceedings of the National Academy of Sciences of the United States of America *94*, 6658–6663.

Siebert, G., Carsiotis, M., and Plaut, G.W. (1957). [The enzymatic properties of isocitric dehydrogenase]. J Biol Chem *226*, 977–991.

Sigoillot, F.D., Berkowski, J.A., Sigoillot, S.M., Kotsis, D.H., and Guy, H.I. (2003). Cell cycle-dependent regulation of pyrimidine biosynthesis. The Journal of Biological Chemistry *278*, 3403–3409.

Son, J., Lyssiotis, C.A., Ying, H., Wang, X., Hua, S., Ligorio, M., Perera, R.M., Ferrone, C.R., Mullarky, E., Shyh-Chang, N., et al. (2013). Glutamine supports pancreatic cancer growth through a KRAS-regulated metabolic pathway. Nature *496*, 101–105.

Sonveaux, P., Végran, F., Schroeder, T., Wergin, M.C., Verrax, J., Rabbani, Z.N., De Saedeleer, C.J., Kennedy, K.M., Diepart, C., Jordan, B.F., et al. (2008). Targeting lactate-fueled respiration selectively kills hypoxic tumor cells in mice. The Journal of Clinical Investigation *118*, 3930–3942.

Sybille Mazurek, C.B.B., Mazurek, S., Boschek, C.B., Hugo, F., and Eigenbrodt, E. (2005). Pyruvate kinase type M2 and its role in tumor growth and spreading. Seminars in Cancer Biology *15*, 9.

Thoma, C.R., Frew, I.J., Hoerner, C.R., Montani, M., Moch, H., and Krek, W. (2007). pVHL and GSK3beta are components of a primary cilium-maintenance signalling network. Nat Cell Biol *9*, 588–595.

Tong, X., Zhao, F., and Thompson, C.B. (2009). The molecular determinants of de novo nucleotide biosynthesis in cancer cells. Curr Opin Genet Dev *19*, 32–37.

Tribble, D.L., and Jones, D.P. (1990). Oxygen dependence of oxidative stress. Rate of NADPH supply for maintaining the GSH pool during hypoxia. Biochemical Pharmacology *39*, 729–736.

Vander Heiden, M.G. (2011). Targeting cancer metabolism: a therapeutic window opens. Nature Reviews. Drug Discovery *10*, 671–684.

Vander Heiden, M.G., Locasale, J.W., Swanson, K.D., Sharfi, H., Heffron, G.J., Amador-Noguez, D., Christofk, H.R., Wagner, G., Rabinowitz, J.D., Asara, J.M., et al. (2010). Evidence for an alternative glycolytic pathway in rapidly proliferating cells. Science (New York, N.Y.) *329*, 1492–1499.

Veech, R.L., Eggleston, L. V, and Krebs, H.A. (1969). The redox state of free nicotinamide-adenine dinucleotide phosphate in the cytoplasm of rat liver. Biochem J *115*, 609–619.

Vizan, P., Boros, L.G., Figueras, A., Capella, G., Mangues, R., Bassilian, S., Lim, S., Lee, W.-N.P., and Cascante, M. (2005). K-ras codon-specific mutations produce distinctive metabolic phenotypes in NIH3T3 mice [corrected] fibroblasts. Cancer Research *65*, 5512–5515.

Vogelstein, B., Papadopoulos, N., Velculescu, V.E., Zhou, S., Diaz, L.A., and Kinzler, K.W. (2013). Cancer Genome Landscapes. Science *339*, 1546–1558.

Wallace, D.C. (2012). Mitochondria and cancer. Nature Reviews Cancer *12*, 685–698.

Walther, J.L., Metallo, C.M., Zhang, J., and Stephanopoulos, G. (2012). Optimization of 13C isotopic tracers for metabolic flux analysis in mammalian cells. Metabolic Engineering *14*, 162–171.

Wang, J.B., Erickson, J.W., Fuji, R., Ramachandran, S., Gao, P., Dinavahi, R., Wilson, K.F., Ambrosio, A.L., Dias, S.M., Dang, C. V, et al. (2010a). Targeting mitochondrial glutaminase activity inhibits oncogenic transformation. Cancer Cell *18*, 207–219.

Wang, Q., Zhang, Y., Yang, C., Xiong, H., Lin, Y., Yao, J., Li, H., Xie, L., Zhao, W., Yao, Y., et al. (2010b). Acetylation of metabolic enzymes coordinates carbon source utilization and metabolic flux. Science *327*, 1004–1007.

Warburg, O. (1956). The Prime Cause and Prevention of Cancer. Science *124*, 269–270.

Warburg, O., Wind, F., and Negelein, E. (1927). THE METABOLISM OF TUMORS IN THE BODY. The Journal of General Physiology *8*, 519–530.

Ward, P.S., Patel, J., Wise, D.R., Abdel-Wahab, O., Bennett, B.D., Coller, H.A., Cross, J.R., Fantin, V.R., Hedvat, C. V, Perl, A.E., et al. (2010). The common feature of leukemia-associated IDH1 and IDH2 mutations is a neomorphic enzyme activity converting alpha-ketoglutarate to 2-hydroxyglutarate. Cancer Cell *17*, 225–234.

Welford, S.M., Bedogni, B., Gradin, K., Poellinger, L., Broome Powell, M., and Giaccia, A.J. (2006). HIF1alpha delays premature senescence through the activation of MIF. Genes & Development *20*, 3366–3371.

Wellen, K.E., Hatzivassiliou, G., Sachdeva, U.M., Bui, T. V, Cross, J.R., and Thompson, C.B. (2009). ATP-Citrate Lyase Links Cellular Metabolism to Histone Acetylation. Science *324*, 1076–1080.

Wellen, K.E., Lu, C., Mancuso, A., Lemons, J.M.S., Ryczko, M., Dennis, J.W., Rabinowitz, J.D., Coller, H. a, and Thompson, C.B. (2010). The hexosamine biosynthetic pathway couples growth factor-induced glutamine uptake to glucose metabolism. Genes & Development *24*, 2784–2799.

Wenger, R.H., Stiehl, D.P., and Camenisch, G. (2005). Integration of oxygen signaling at the consensus HRE. Sci STKE *2005*, re12.

Williamson, J.R., and Cooper, R.H. (1980). Regulation of the citric acid cycle in mammalian systems. FEBS Letters *117 Suppl*, K73–85.

Williamson, D.H., Lund, P., and Krebs, H.A. (1967). The redox state of free nicotinamide-adenine dinucleotide in the cytoplasm and mitochondria of rat liver. Biochem J *103*, 514–527.

Wilson, W.R., and Hay, M.P. (2011). Targeting hypoxia in cancer therapy. Nature Reviews Cancer *11*, 393–410.

Wise, D.R., and Thompson, C.B. (2010). Glutamine addiction: a new therapeutic target in cancer. Trends Biochem Sci *35*, 427–433.

Wise, D.R., DeBerardinis, R.J., Mancuso, A., Sayed, N., Zhang, X.-Y., Pfeiffer, H.K., Nissim, I., Daikhin, E., Yudkoff, M., McMahon, S.B., et al. (2008). Myc regulates a transcriptional program that stimulates mitochondrial glutaminolysis and leads to glutamine addiction. Proceedings of the National Academy of Sciences *105*, 18782–18787.

Wise, D.R., Ward, P.S., Shay, J.E., Cross, J.R., Gruber, J.J., Sachdeva, U.M., Platt, J.M., DeMatteo, R.G., Simon, M.C., and Thompson, C.B. (2011). Hypoxia promotes isocitrate dehydrogenase-dependent carboxylation of alpha-ketoglutarate to citrate to support cell growth and viability. Proc Natl Acad Sci U S A *108*, 19611–19616.

Wong, N., Blair, A.R., Morahan, G., and Andrikopoulos, S. (2010). The Deletion Variant of Nicotinamide Nucleotide Transhydrogenase (Nnt) Does Not Affect Insulin Secretion or Glucose Tolerance. Endocrinology *151*, 96–102.

Wouters, B.G., and Koritzinsky, M. (2008). Hypoxia signalling through mTOR and the unfolded protein response in cancer. Nature Reviews. Cancer *8*, 851–864.

Wu, H., Southam, A.D., Hines, A., and Viant, M.R. (2008). High-throughput tissue extraction protocol for NMR- and MS-based metabolomics. Analytical Biochemistry *372*, 204–212.

Yan, H., Parsons, D.W., Jin, G., McLendon, R., Rasheed, B.A., Yuan, W., Kos, I., Batinic-Haberle, I., Jones, S., Riggins, G.J., et al. (2009). IDH1 and IDH2 Mutations in Gliomas. N Engl J Med *360*, 765–773.

Yang, C., Sudderth, J., Dang, T., Bachoo, R.G., McDonald, J.G., and DeBerardinis, R.J. (2009). Glioblastoma Cells Require Glutamate Dehydrogenase to Survive Impairments of Glucose Metabolism or Akt Signaling. Cancer Research *69*, 7986 –7993.

Yang, H., Minamishima, Y.A., Yan, Q., Schlisio, S., Ebert, B.L., Zhang, X., Zhang, L., Kim, W.Y., Olumi, A.F., and Kaelin Jr., W.G. (2007). pVHL acts as an adaptor to promote the inhibitory phosphorylation of the NF-kappaB agonist Card9 by CK2. Mol Cell *28*, 15–27.

Ye, J., Mancuso, A., Tong, X., Ward, P.S., Fan, J., Rabinowitz, J.D., and Thompson, C.B. (2012). Pyruvate kinase M2 promotes de novo serine synthesis to sustain mTORC1 activity and cell proliferation. Proceedings of the National Academy of Sciences *109*, 6904–6909.

Yin, F., Sancheti, H., and Cadenas, E. (2012). Silencing of nicotinamide nucleotide transhydrogenase impairs cellular redox homeostasis and energy metabolism in PC12 cells. Biochim Biophys Acta *1817*, 401–409.

Yoo, H., Stephanopoulos, G., Kelleher, J.K., Yoo, G.S.H., and Hyuntae Yoo, G.S. (2004). Quantifying carbon sources for de novo lipogenesis in wild-type and IRS-1 knockout brown adipocytes. Journal of Lipid Research *45*, 1324–1332.

Yoo, H., Antoniewicz, M.R., Stephanopoulos, G., and Kelleher, J.K. (2008). Quantifying reductive carboxylation flux of glutamine to lipid in a brown adipocyte cell line. The Journal of Biological Chemistry *283*, 20621–20627.

Yuan, M., Breitkopf, S.B., Yang, X., and Asara, J.M. (2012). A positive/negative ion-switching, targeted mass spectrometry-based metabolomics platform for bodily fluids, cells, and fresh and fixed tissue. Nature Protocols *7*, 872–881.

Zhang, W.C., Shyh-Chang, N., Yang, H., Rai, A., Umashankar, S., Ma, S., Soh, B.S., Sun, L.L., Tai, B.C., Nga, M.E., et al. (2012). Glycine Decarboxylase Activity Drives Non-Small Cell Lung Cancer Tumor-Initiating Cells and Tumorigenesis. Cell.

Zhao, S., Xu, W., Jiang, W., Yu, W., Lin, Y., Zhang, T., Yao, J., Zhou, L., Zeng, Y., Li, H., et al. (2010). Regulation of cellular metabolism by protein lysine acetylation. Science (New York, N.Y.) *327*, 1000–1004.

Zhao, Y., Butler, E.B., and Tan, M. (2013). Targeting cellular metabolism to improve cancer therapeutics. Cell Death & Disease *4*, e532.

Zhong, Z., Arteel, G.E., Connor, H.D., Yin, M., Frankenberg, M. V, Stachlewitz, R.F., Raleigh, J.A., Mason, R.P., and Thurman, R.G. (1998). Cyclosporin A increases hypoxia and free radical production in rat kidneys: prevention by dietary glycine. The American Journal of Physiology *275*, F595–604.

Zimmer, M., Ebert, B.L., Neil, C., Brenner, K., Papaioannou, I., Melas, A., Tolliday, N., Lamb, J., Pantopoulos, K., Golub, T., et al. (2008). Small-Molecule Inhibitors of HIF-2a Translation Link Its 5'UTR Iron-Responsive Element to Oxygen Sensing. Molecular Cell *32*, 838–848.